Durham E-Theses

Perturbative integrability in 1+1 dimensions and affine Toda theories

POLVARA, DAVIDE

How to cite:

POLVARA, DAVIDE (2022) *Perturbative integrability in 1+1 dimensions and affine Toda theories*, Durham theses, Durham University. Available at Durham E-Theses Online: http://etheses.dur.ac.uk/14416/

Use policy

The full-text may be used and/or reproduced, and given to third parties in any format or medium, without prior permission or charge, for personal research or study, educational, or not-for-profit purposes provided that:

- a full bibliographic reference is made to the original source
- a link is made to the metadata record in Durham E-Theses
- the full-text is not changed in any way

The full-text must not be sold in any format or medium without the formal permission of the copyright holders.

Please consult the full Durham E-Theses policy for further details.

Academic Support Office, Durham University, University Office, Old Elvet, Durham DH1 3HP
e-mail: e-theses.admin@dur.ac.uk Tel: +44 0191 334 6107
http://etheses.dur.ac.uk

Perturbative integrability in 1+1 dimensions and affine Toda theories

Davide Polvara

A Thesis presented for the degree of
Doctor of Philosophy

Centre for Particle Theory
Department of Mathematical Sciences
Durham University
United Kingdom

May 2022

Perturbative integrability in 1+1 dimensions and affine Toda theories

Davide Polvara

Submitted for the degree of Doctor of Philosophy
May 2022

Abstract: In this thesis, the perturbative integrability of 1+1 dimensional bosonic massive quantum field theories is investigated. Starting from a theory with a generic polynomial-like potential, the constraints on the masses and Lagrangian couplings emerging by requiring purely elastic amplitudes at the tree level are obtained. It is observed that theories satisfying these constraints are completely determined by their mass ratios and 3-point couplings, while all the higher-order couplings can be obtained recursively in terms of them by imposing the absence of production for higher numbers of external legs. By exploiting different root system properties, it is shown that all the bosonic affine Toda field theories universally satisfy the constraints of purely elasticity at the tree level: a complete proof of their tree-level integrability is therefore provided. Subsequently, the higher-order poles observed in the bootstrapped S-matrices of the ADE series of affine Toda models are studied in perturbation theory. These singular points have been explained in the past in terms of anomalous threshold singularities in certain Feynman diagrams, where multiple propagators go on-shell simultaneously in loop integrations. Networks of Feynman diagrams contributing to these higher-order poles are found and residues at the poles are obtained through perturbation theory, showing agreement with the bootstrapped results. We show that the residues are generated by suitably cutting the loop diagrams into products of tree-level graphs, which will be called 'atoms'. Most of these atoms simplify between one another and only a small number of them survive matching the bootstrapped results. The simplification mechanism between atoms inside networks is reminiscent of Gauss's theorem in the space of Feynman diagrams.

Declaration

The work in this thesis is based on research carried out in the Department of Mathematical Sciences at Durham University under the supervision of Prof. Patrick Dorey.

Chapters 2 and 5 are two reviews focused on the S-matrix bootstrap approach in 1+1 dimensions and on geometrical aspects of affine Toda field theories. These chapters are necessary to introduce the reader to the topic of quantum integrability and to set the conventions used in the other chapters.

The remaining part of the thesis is based on results obtained in a number of joint papers and drafts in collaboration with Patrick Dorey [1–3]. Chapters 3, 4 and 6 cover the results of [1]: after having found the constraints imposed by having purely elastic S-matrices at zero loops in perturbation theory, in chapters 3 and 4, the tree-level integrability of affine Toda quantum field theories is proved in chapter 6. However, section 4.5 is due solely to the author and has not been presented elsewhere; in that section, it is shown how the bootstrap fusing relations and the S-matrix factorization emerge by imposing the cancellation of certain non-diagonal processes in perturbation theory. Chapter 7 contains results that will appear in [2, 3], currently in preparation, and covers an analysis of Landau poles in ADE series of affine Toda models.

No part of this thesis has been submitted elsewhere for any degree or qualification.

Copyright © 2022 Davide Polvara.
"The copyright of this thesis rests with the author. No quotation from it should be published without the author's prior written consent and information derived from it should be acknowledged."

Acknowledgements

First of all, I would like to express my gratitude to my supervisor Patrick Dorey to have allowed me to start this adventure as a PhD student at Durham University and a member of SAGEX, a European network that put me in contact with many beautiful people. I want to thank him to have guided me into the beautiful research area of integrability, sharing with me his knowledge, insights and ideas. Patrick has always left to me the freedom to follow my interests, leaving me the time I needed to learn and encouraging my ideas. Together with Patrick, I desire to thank all the colleagues and professors that during this PhD shared with me their knowledge and nourished my research interest; they include Edgardo Cheb-Terrab, Mario De Marco, Gabriele Dian, Paul Heslop, Ben Hoare, Arthur Lipstein and Silvia Penati. I especially desire to thank Gabriele for our many blackboard discussions and exciting conversations in our office. I think I did not really know what was the meaning of 'doing something with enthusiasm' before knowing you.

There are many other people I would like to thank that took a fundamental part in this period of my life: I wish to thank the other SAGEX ESRs and all my friends in Durham. With particular care, I remember my flatmates: Carlotta and Eilish. Thank you both to have made this last year a funny period of my life. Thanks also to Dario, Guido and Matilda for their friendship.

Finally, I wish to thank my family, to have always supported and encouraged me to follow my dreams, and to Alessandra that, despite my continuous absence, never stops loving me.

Dedicated to

Alessandra

Contents

Chapter 1

Introduction

1.1 A historical overview

Although the topic of this thesis is the integrability of certain 1+1 dimensional massive quantum field theories, we present here a broader historical overview of the subject starting from the study of critical phenomena and conformal field theories. In theoretical physics, exactly solvable theories have always been of great interest for their fundamental role in increasing our understanding of nature. The Ising model [4] is probably the best-known example of an exactly solvable statistical system. Its importance became clear when Onsager, by computing the free energy on a two-dimensional lattice with a zero magnetic field, provided the first exact description of a second-order phase transition [5]. In [6] Alexander Polyakov showed that the correlation functions at the transition point are invariant under conformal transformations suggesting that all critical phenomena in the scaling limit could be described by conformal field theories (CFTs). Among all the conformal transformations, the dilatation is of particular interest since the associated anomalous dimensions of the local fields determine the critical exponents at the transition point. These dimensions can in principle be computed by exploiting the *conformal bootstrap* approach. This method, initially proposed by Polyakov [7], is based on axiomatic properties. The most important requirement is the associativity of the algebra of operators comprising the CFT from which crossing symmetry is derived: this leads to an infinite set of dynamical equations for the structure constants of the operator product expansions. The structure constants are fixed by the conformal symmetry up to certain parameters: the anomalous dimensions and numerical factors. Therefore the solutions of crossing equations allow us to find the values of the anomalous dimensions.

The conformal bootstrap is formulated for an arbitrary number d of dimensions, but for $d > 2$ the system has proved too complicated to be solved and the problem remained untouched for decades. If $d = 2$ something special happens: the conformal group becomes infinite-dimensional, being the direct product of the analytic and anti-analytic transformations on the variables z and $\bar{z}$ in the complex plane. The algebra associated with these transformations is called the *Virasoro* algebra and

its representations can be organized into conformal families: each one of these families is defined by a state annihilated by all the lowering operators of the Virasoro algebra, the so-called highest-weight vector (HWV) or primary state, plus all its descendants. It was proved by Kac [8] that for particular values of the weights of the primary operators the conformal families contain 'null states' that can be consistently regarded as zero; as a consequence of this fact, the associated conformal families become degenerate in the sense that they contain fewer fields than usual. Focusing on the domain of the Virasoro central charge $0 < c \leq 1$, where the conformal weights are all real and positive, Belavin, Polyakov and Zamolodchikov [9] determined the values of c at which all the conformal families were degenerate. The infinite set of values they found for the central charge define the so-called *minimal models* having many interesting properties. Most importantly, the fact that all the conformal families of minimal models were degenerate, with the additional assumption of the existence of an associative algebra of local operators, allowed Belavin, Polyakov and Zamolodchikov to formulate linear differential equations for the correlation functions. They explained how to solve the conformal bootstrap exactly by solving these differential equations; moreover, they claimed that the minimal models could be identified with statistical systems at the critical points. Further effort was subsequently done to check this conjecture. In [10] Friedan, Qiu and Shenker showed that a necessary requirement for unitarity in the domain $0 < c \leq 1$ restricts the possible values of the central charge to

$$c = 1 - \frac{6}{(k+2)(k+3)} \quad , \quad k = 1, 2, 3 \ldots \tag{1.1.1}$$

They noted that these conditions were satisfied by particular minimal models found in [9]. By a matching between the scaling dimensions the values $k = 1$, $k = 2$, $k = 3$ and $k = 4$ have been identified in [10] with the Ising model, the tricritical Ising model, the three-state Potts model and the tricritical three-state Potts model respectively. This exact comparison has been made possible by simultaneous progress carried out in the exact resolution of statistical systems (see [11] and references therein).

In their work [9] Belavin, Polyakov and Zamolodchikov assumed that all the holomorphic and anti-holomorphic conserved currents, having conformal dimensions $(s, 0)$ and $(0, s)$ under the Virasoro dilatation generators on z and $\bar{z}$, were descendants of the identity operator through the action of the Virasoro lowering operators. The simplest examples were the holomorphic and anti-holomorphic components of the stress-energy tensor, with conformal dimensions $(2, 0)$ and $(0, 2)$ respectively. This assumption was later relaxed [12], allowing for the existence of additional conserved currents that are not Virasoro descendants of the identity. Any time this happens the symmetry group is enlarged. For example, the presence of operators of dimensions $(3/2, 0)$ and $(0, 3/2)$ generate the superconformal group [13], while conserved currents of dimensions $(1, 0)$ and $(0, 1)$ enlarge the symmetry to that of a Kac-Moody algebra [14]. In a pair of remarkable papers [15, 16] Goddard, Kent and Olive showed that the representations of the Virasoro algebra could be constructed out of representations of the Kac-Moody algebras. All the minimal models with central charges (1.1.1) were obtained from coset theories defined as quotients of Kac-Moody

algebras:[1]

$$\frac{su(2)_k \times su(2)_1}{su(2)_{k+1}}. \tag{1.1.2}$$

Through this construction Goddard, Kent and Olive were able to prove that the condition (1.1.1) is not only necessary but also sufficient to have unitary conformal field theories.

The *S-matrix bootstrap* program is even older than the conformal bootstrap and was a philosophy very famous in the sixties: it was based on the idea that the S-matrix elements could be derived directly, without the use of Lagrangians or fields, by imposing certain symmetries and universal properties. In this way, infrared and ultraviolet divergences encountered in the computation of amplitudes through the usual Lagrangian formalism could have been completely avoided. One of the most important requirements of the S-matrix bootstrap is the analytical structure of the amplitudes, arising by requiring unitarity and causality. An important book on the subject is [17]. Due to the lack of symmetries, unfortunately, the initial S-matrix bootstrap was insufficient alone to uniquely define physical observables and interest in it was lost, partially due to the emergence of quantum chromodynamics and the improvement of perturbative techniques. However, once again a special consideration has to be given to two-dimensional quantum field theories: in 1978 Alexander and Alexei Zamolodchikov published a paper [18] in which they explained how the presence of higher spin commuting conserved charges, in addition to unitarity, crossing symmetry and analyticity, could be used to fix the S-matrix elements of certain massive quantum field theories in 1+1 dimensions almost completely. The theories considered in [18], characterised by having an infinite tower of conserved charges, are called 'integrable' and the S-matrix bootstrap resulted extremely fruitful in the computation of their S-matrices.

Even though the conformal and the S-matrix bootstrap approaches in 1+1 dimensions being formulated in different contexts, the former to compute correlation functions and the latter to evaluate S-matrices, they have a remarkable connection. For a given CFT, all the composite fields made up of the analytic and anti-analytic components of the stress-energy tensor define an infinite set of local integrals of motion (the descendants of other analytic and anti-analytic primaries can also be considered if a larger symmetry is involved than Virasoro). In [19, 20] Alexander Zamolodchikov showed that certain deformations of minimal models by some of their spinless relevant primary fields lead to renormalization group trajectories which conserve a subset of the integrals of motion of the unperturbed CFT. As an example, in [19, 20] the Ising model (in the scaling limit) was considered at the critical temperature in the presence of a magnetic field and it was proved that higher-spin integrals of motion exist other than energy and momentum. The existence of even one of these higher-spin charges, together with its parity-symmetric partner, is enough to prove that the S-matrix factorises and particle production is forbidden [21]. These considerations allowed Zamolodchikov to implement the S-matrix bootstrap approach earlier defined in [18] to solve the Ising model at the critical point in the presence of a magnetic field: the

[1] The subscript letters represent the grading of the Kac-Moody algebras.

solution consisted of a list of S-matrix elements describing the interactions of eight different types of relativistic particles. The results of Alexander Zamolodchikov were then used as a starting example to study many other universality classes of critical phenomena in two dimensions: while critical points can be described by conformal field theories [9], some of their deformations by suitable relevant operators induce renormalization group trajectories that are exactly solvable.

In 1990 Alexei Zamolodchikov introduced the Thermodynamic Bethe Ansatz (TBA) in the context of two-dimensional relativistic quantum field theories [22]. This is a method to compute the ground state energy and effective central charge of two dimensional integrable systems on a finite volume in terms of their S-matrix elements. The effective central charge $\tilde{c}(R)$ can be numerically determined as a function of the spatial volume R, interpolating between an ultraviolet- and an infrared-value in the limits $R \to 0$ and $R \to +\infty$. In [23], by means of the TBA, Klassen and Melzer were able to evaluate the effective central charges of different integrable theories that were thought to be obtained as deformations of CFTs through a relevant operator. In all the considered cases they obtained the expected values of the CFT central charge in the ultraviolet limit. In particular, the central charges of the minimal models with $k = 1$, $k = 2$ and $k = 4$ in the series (1.1.1) were recovered starting from the minimal S-matrices associated with the exceptional Lie algebras $e_8^{(1)}$, $e_7^{(1)}$ and $e_6^{(1)}$ respectively, confirming results earlier conjectured in [20, 24, 25] through the S-matrix bootstrap.

In more recent years both the conformal and the S-matrix bootstrap approaches have been revived. In [26], starting from Polyakov's idea of crossing symmetry [7], together with general considerations on the conformal block decomposition, it was explained how to determine rigorous bounds on the anomalous dimensions of the operators comprising a generic CFT. The study initiated in [26] opened the door to numerical solutions of the conformal bootstrap in more than two dimensions and was continued in a series of papers. Defining the continuum space version of the spin by σ and the energy density by ϵ in the 3-dimensional Ising model, in [27] the crossing symmetry was imposed on $\langle\sigma\sigma\sigma\sigma\rangle$ and from it the space of allowed dimensions $(\Delta_\sigma, \Delta_\epsilon)$ was carved out: surprisingly the 3-dimensional Ising model was identified at a corner point on the boundary of this space. By performing a similar study on mixed correlators, involving both σ and ϵ, further information was later obtained [29], allowing the 3-dimensional Ising model to be isolated in a small closed region in the $(\Delta_\sigma, \Delta_\epsilon)$ parameter space. The little island identifying the 3-dimensional Ising model in the parameter space was later determined with extremely high numerical precision in [30]. The Ising model is just an example of how the conformal bootstrap can be used to numerically classify conformal quantum field theories. Encouraged and inspired by the promising results obtained in the study of CFTs, in the last few years many people revisited the S-matrix bootstrap as well: the general philosophy is to use optimization algorithms to carve out the space of scattering amplitudes numerically by the imposition of global symmetries, unitarity, crossing and analyticity. The numerical S-matrix bootstrap has been studied in a large number of papers touching many different models, from two-dimensional theories [31] to gravitational amplitudes [32] (we point at [33] for a fresh overview of the subject). More related to the topic of this thesis is the numerical

S-matrix bootstrap in 1+1 dimensions introduced in [31]; in that paper and several following publications it has been tried to carve out the space of scattering amplitudes numerically by solving certain optimization problems. Particular points on the boundary of such a space, on which the unitarity is saturated, have then been identified with known integrable theories. If, on one hand, the optimization problem developed in [31] is extremely interesting, being able to characterize the space of S-matrices saturating unitarity, which therefore are suitable candidates to represent integrable theories, a direct connection with standard perturbation theory is still not completely understood and will be the focus of this thesis.

1.2 About perturbation theory

Examples of two-dimensional integrable models are in general hard to find, even at the classical level. One of the main reasons is that the integrability of a given theory is proven by finding the so-called Lax connection, from which an infinite set of conserved charges can be generated. However, finding a Lax connection is in general a difficult task; indeed only in recent years it has been argued how to extract such a connection in a more systematic way making use of a correspondence with 4-dimensional Chern-Simons theories [34]. Different approaches have been developed to generate integrable models to avoid the problem of finding a Lax connection; one way is to deform known integrable theories through solvable deformations: this is the method used by Zamolodchikov in [19, 20] to study integrable trajectories of the renormalization group flow away from the critical points. In that case, the undeformed starting theory was not just integrable but also conformal. More recently, deformations have played an important role in the study of integrable sigma models (see [35] and references therein) from which examples of solvable string theories can be generated. The optimization techniques developed in [31] also provide useful tools to classify integrable theories.

In this thesis, we will discuss a different approach to understanding the integrability of a given theory pointed out in a review article [36]. In that review, it was shown how the Lagrangian couplings of certain bosonic massive quantum field theories can be constructed iteratively by imposing the absence of production in perturbation theory. This imposition, already at the tree level, extremely constrains the possible masses and Lagrangian couplings and can be used to define the space of massive integrable quantum field theories having a Lagrangian construction. If on one hand this approach can be used to classify integrable models, on the other hand, the way in which integrability manifests itself in perturbation theory is interesting to understand in its own right. Well-known integrable models, for which the S-matrix elements have been conjectured through the bootstrap approach [18], when studied perturbatively, manifest cancellations and simplifications in sums of Feynman diagrams that are often ill-understood. This thesis will look at these cancellations in some detail: the first part of the thesis is focused on general quantum field theories, while the second part is devoted to the perturbative study of bosonic affine Toda models, a famous class of integrable theories. More precisely the two parts of the thesis are structured

as follows.

First part

In chapter 2 the S-matrix bootstrap program introduced in [18] will be reviewed and the conventions used along with all the thesis will be set. The discussion includes the Parke argument [21] to prove the absence of production in theories with higher spin conserved charges and part of the Zamolodchikov computations presented in [19, 20] to solve the Ising model deformed by a magnetic field. In chapters 3 and 4 the constraints on the masses and couplings obtained by imposing purely elastic amplitudes at the tree level in bosonic Lagrangian theories with polynomial-like potentials are derived. Following the discussion of [1], it is shown that the masses and 3-point couplings, tuned by imposing pure elasticity in 4- and 5-point processes at the tree level, are sufficient to classify integrable models while all the higher-order couplings can be obtained through certain recursion relations introduced in [37]. By adding the extra requirements that poles in elastic two-to-two processes are due to only one on-shell propagating particle at a time and poles cancel between pairs of Feynman diagrams in inelastic two-to-two processes, it is shown that the imposition of pure elasticity in tree-level amplitudes implies the so-called 'area rule'. This rule was derived in [1] and connects the 3-point couplings $C^{(3)}_{abc}$ to the areas Δ_{abc} of the triangles composed of the masses m_a, m_b and m_c of the coupled particles in a universal way. The bootstrap fusing relations and the factorisation properties at all orders of loops are shown to be implied by the absence of production in perturbation theory.

Second part

The second part of the thesis is focused on affine Toda field theories. Chapter 5 is a review of these models: we define their Lagrangian and a Lax pair construction of their equations of motion showing proof of their classical integrability following the lines of [38]. The results are presented making use of universal geometrical properties of root systems and following conventions that will be useful also for chapter 6. In chapter 6 we provide proof of the absence of production at the tree level valid for all the affine Toda field theories. The proof, taken from [1], uses the Lie algebra properties reviewed in chapter 5 to prove the scattering constraints discussed in the first part of the thesis. Finally in chapter 7 certain loop features of simply-laced affine Toda theories are investigated. Higher-order poles in amplitudes predicted by the bootstrap are explained in perturbation theory in terms of anomalous threshold singularities in certain Feynman diagrams according to the Coleman-Thun mechanism [39]: these singularities are generated by collections of diagrams that can be arranged inside networks. We show that residues of amplitudes at higher-order poles are obtained by cutting the diagrams into products of tree-level graphs, the so-called atoms. In each network, most of the atoms cancel between one another in a way that can be explained using the tree-level properties of these models. In the end, the only contributing cuts are located on the boundary of the network. The results in this chapter will appear in papers [2, 3] currently in preparation

Part I

Axiomatic and Perturbative Integrability in 1+1 Dimensions

Chapter 2

The S-matrix bootstrap in 1+1 dimensions

Integrable quantum field theories in 1+1 dimensions provide a fantastic playground where non-perturbative techniques can be explored. This chapter aims to be a short review of the topic; more extended pedagogical lectures can be found for example in [36, 40]. Part of the study carried out in [18] will be reviewed together with the argument presented in [21]: this argument shows how the absence of production and the factorization of multiple-point S-matrices emerge by the action of the higher-spin conserved operators on the wave packets. The concepts of unitarity, crossing symmetry and bootstrap fusing relations will also be reviewed and used to revisit the Zamolodchikov construction [19, 20] of the Ising model deformed by a magnetic field.

2.1 Conserved charges and absence of production

The focus of this thesis will be on massive theories with possibly-different types of scalar particles, each one coming with its own mass m_j, in 1+1 dimensions. A convenient choice to represent momenta is to use light-cone components, p_j and $\bar{p}_j$, with respect to which the energy and the spatial momentum are given by

$$E_j = \frac{p_j + \bar{p}_j}{2} \quad , \quad P_j = \frac{p_j - \bar{p}_j}{2}. \tag{2.1.1}$$

A particle of mass m_j is on-shell if $p_j \bar{p}_j = E_j^2 - P_j^2 = m_j^2$. If this constraint is satisfied then a single particle state can be parametrised by

$$p_j = m_j a_j = m_j e^{\theta_j} \quad , \quad \bar{p}_j = m_j \frac{1}{a_j} = m_j e^{-\theta_j}, \tag{2.1.2}$$

where $a_j \equiv e^{\theta_j}$ is a certain number and θ_j is called the 'rapidity'. Physical states are characterized by real values of θ_j (or equivalently by positive values of a_j); in particular a single particle moving to the right has a positive rapidity, while a particle

moving to the left has a negative rapidity. A state corresponding to a particle of type j will be indicated by $A_j(\theta)$. It is possible to define an n-particle state

$$|A_{a_1}(\theta_1)A_{a_2}(\theta_2)\dots A_{a_n}(\theta_n)\rangle \tag{2.1.3}$$

composed by a set of n possibly-different particles of types $a_1,\dots,a_n$, carrying respectively rapidities $\theta_1,\dots,\theta_n$. Each particle has to be imagined to be spread around a certain time-dependent position, with a momentum smeared around the central value given by the corresponding rapidity. The state is therefore a collection of wave packets. As long as the distance between the different wave packets is much bigger than the interaction scale of the model it makes sense to think of the state in (2.1.3) as a free state. Because the theory is massive, the interaction has indeed a finite range[1].

In the following the problem of computing the amplitude that a state subject to no interaction in the far past ($t\to-\infty$), evolves into a certain free-state in the far future ($t\to+\infty$) will be addressed. Since for $t\to-\infty$ it is required that the particles do not interact, they have to be located from the left to the right on the spatial line following the increasing order of their rapidities $\theta_1>\theta_2>\ldots>\theta_n$; the 'incoming state' can therefore unambiguously be written, removing the ket, as

$$|A_{a_1}(\theta_1)A_{a_2}(\theta_2)\dots A_{a_n}(\theta_n)\rangle_{in} = A_{a_1}(\theta_1)A_{a_2}(\theta_2)\dots A_{a_n}(\theta_n), \tag{2.1.4}$$

with the fastest particle on the left and the slowest particle on the right. We define a particle with rapidity θ_i to be faster than a particle with rapidity θ_j if $\theta_i>\theta_j$, with both the rapidities considered with the respective signs. Analogously, for $t\to+\infty$, the outgoing state has also to be free of further interactions; therefore, in the far future, the particles need to be ordered on the spatial line from the left to the right following the increasing order of their rapidities. If the state is composed by m particles of types $b_1,\dots,b_m$ carrying rapidities $\theta'_1>\theta'_2>\ldots>\theta'_m$, the state can be written as

$$|A_{b_1}(\theta'_1)A_{b_2}(\theta'_2)\dots A_{b_m}(\theta'_m)\rangle_{out} = A_{b_m}(\theta'_m)\dots A_{b_2}(\theta'_2)A_{b_1}(\theta'_1). \tag{2.1.5}$$

The order of the elements on the RHS of (2.1.4) and (2.1.5) is meaningful; the operators $A_{a_j}(\theta_j)$ are elements of the so-called Zamolodchikov-Faddeev (ZF) algebra [18, 43], which is an associative non-commutative algebra. Assuming asymptotic completeness, any intermediate state can equivalently be expanded in the in- or out-basis. Moreover, there exists a change of basis through which it is possible to write each element of the basis of in-states as a linear combination of out-states (and vice-versa). Usually, a state taking a simple form when is written on the in-basis becomes a very complicated object after it is written on the basis of out-states. This reflects the fact that eigenstates of the free Hamiltonian in the far past become, in the far future, complicated superpositions of out-states; contrarily, simple eigenstates of the

[1]Some results that will be presented in this chapter can be carefully extended to the massless case. See for example [41] for an old review of the massless integrability and [42] for a more recent one in the context of integrability in AdS/CFT.

free Hamiltonian in the far future were complicated superpositions of in-states in the far past. The matrix of the change of basis, describing the evolution between incoming- and outgoing-states, is called the 'S-matrix'. Given an incoming state defined in (2.1.4), with rapidities $\theta_1 > \theta_2 > \ldots > \theta_n$, it can be written on the basis of the out-states (2.1.5) as

$$A_{a_1}(\theta_1)\ldots A_{a_n}(\theta_n) = \sum_{m=2}^{+\infty} \int_{\theta'_m<\ldots<\theta'_1} d\theta'_m \ldots d\theta'_1 S^{b_1,\ldots,b_m}_{a_1,\ldots,a_n}(\theta_1,\ldots,\theta_n;\theta'_1,\ldots,\theta'_m) A_{b_m}(\theta'_m)\ldots A_{b_1}(\theta'_1). \tag{2.1.6}$$

The absolute values squared of the different S-matrix elements

$$S^{b_1,\ldots,b_m}_{a_1,\ldots,a_n}(\theta_1,\ldots,\theta_n;\theta'_1,\ldots,\theta'_m)$$

correspond to the probabilities that the initial state $A_{a_1}(\theta_1)\ldots A_{a_n}(\theta_n)$ evolves, after the interaction, into the different final states $A_{b_m}(\theta'_m)\ldots A_{b_1}(\theta'_1)$. Not all the final states $A_{b_m}(\theta'_m)\ldots A_{b_1}(\theta'_1)$ are kinematically allowed. Usually, conserved quantities constrain the space of possible nonzero S-matrix elements. For example, the outcomes that do not satisfy energy and momentum conservation have zero S-matrix elements. Let Q_1 and Q_{-1} be the light-cone operators of the momentum. These operators act on single-particle states as

$$Q_1|A_a(\theta)\rangle = m_a e^{\theta}|A_a(\theta)\rangle \quad , \quad Q_{-1}|A_a(\theta)\rangle = m_a e^{-\theta}|A_a(\theta)\rangle,$$

i.e. they are diagonal and have as eigenvalues the light-cone components (2.1.2). Since Q_1 and Q_{-1} are local charges, which means they can be written as integrals of local densities, their action on well-separated multi-particle wave packets behaves additively

$$Q_{\pm 1}|A_{a_1}(\theta_1)\ldots A_{a_n}(\theta_n)\rangle = \left(m_{a_1}e^{\pm\theta_1} + \ldots + m_{a_n}e^{\pm\theta_n}\right)|A_{a_1}(\theta_1)\ldots A_{a_n}(\theta_n)\rangle. \tag{2.1.7}$$

Such charges are conserved in all the translation-invariant theories, so that the corresponding eigenvalues cannot change during the collisions; therefore the only nonzero S-matrix elements $S^{b_1,\ldots,b_m}_{a_1,\ldots,a_n}(\theta_1,\ldots,\theta_n;\theta'_1,\ldots,\theta'_m)$ are those satisfying

$$m_{a_1}e^{\pm\theta_1} + \ldots + m_{a_n}e^{\pm\theta_n} = m_{b_1}e^{\pm\theta'_1} + \ldots + m_{b_m}e^{\pm\theta'_m}.$$

Beyond energy and momentum, certain theories possess an infinite tower of functionally-independent higher-spin conserved charges Q_s. If these charges are in involution, which means they all commute between one another (and with Q_1 and Q_{-1}), then they can be simultaneously diagonalized by a suitable basis of particle-states and the S-matrix can be exactly solved on this basis. In this sense, the theory is said to be 'integrable'. By 'higher-spin' we mean that the commutator between these

operators and the generator M of the Lorentz boosts[2] is

$$[M, Q_s] = sQ_s, \tag{2.1.8}$$

where the integer s is called the 'spin' of Q_s. As a consequence of this fact, the action of these charges on single particle states is determined by

$$Q_s|A_a(\theta)\rangle = \gamma_a^{(s)} e^{s\theta}|A_a(\theta)\rangle \quad , \quad Q_{-s}|A_a(\theta)\rangle = \gamma_a^{(s)} e^{-s\theta}|A_a(\theta)\rangle. \tag{2.1.9}$$

The reason why the eigenvalues of the charges Q_s take the simple form in equation (2.1.9) is the following. Let $w_a^{(s)}(\theta)$ be a function of the rapidity defined by

$$Q_s|A_a(\theta)\rangle = w_a^{(s)}(\theta)|A_a(\theta)\rangle. \tag{2.1.10}$$

Then, up to a normalization factor irrelevant to this discussion, it holds that

$$w_a^{(s)}(\theta) = \langle A_a(\theta)| \; Q_s \; |A_a(\theta)\rangle. \tag{2.1.11}$$

In 1+1 dimensions the action of the Lorentz group is very simple, being determined by rapidity translations: $\theta \to \theta + \lambda$. Under one of these transformations, the eigenvalue changes as follows

$$w_a^{(s)}(\theta + \lambda) = \langle A_a(\theta)|e^{\lambda M} \; Q_s \; e^{-\lambda M}|A_a(\theta)\rangle = e^{\lambda s} w_a^{(s)}(\theta),$$

where equations (2.1.8) and (2.1.11) have been used in the last equality. The equality above leaves as only option for $w_a^{(s)}(\theta)$ to be of the form in (2.1.9). We will deal with parity-symmetric models, in which the conserved charges always appear in pairs, Q_s and Q_{-s}.

Here we will just consider local charges, and their effect on the scattering, following the lines presented in [18]. If we label by V the Hilbert space of the single particle states, over which these charges act as shown in (2.1.9), then their action can be trivially extended to multi particle states in $V \otimes V \otimes \ldots \otimes V$. The action of a charge Q_s on multi particle states is usually referred to as the comultiplication $\Delta(Q_s)$. If Q_s is local then it is characterized by a trivial comultiplication:

$$\Delta(Q_s) = Q_s \otimes 1 \otimes \ldots \otimes 1 + 1 \otimes Q_s \otimes \ldots \otimes 1 + \ldots + 1 \otimes 1 \otimes \ldots \otimes Q_s$$

so that its action on a multiparticle state $A_{a_1}(\theta_1) \ldots A_{a_n}(\theta_n)$ is determined by

$$Q_s|A_{a_1}(\theta_1) \ldots A_{a_n}(\theta_n)\rangle = \left(\gamma_{a_1}^{(s)} e^{s\theta_1} + \ldots + \gamma_{a_n}^{(s)} e^{s\theta_n}\right)|A_{a_1}(\theta_1) \ldots A_{a_n}(\theta_n)\rangle. \tag{2.1.12}$$

The simplest examples of these charges are the light-cone components of the energy and momentum operators previously defined. The effect of non-local charges is also very important: they are symmetries of the theory acting with non-trivial comultiplication on multi particle states. Since the comultiplication is non-trivial, the 2-to-2 S-matrix elements can be directly constrained by requiring the vanishing of $[Q_s, \hat{S}]$

[2] In 1+1 dimensions the Lorentz group has a single generator, that in Euclidean signature becomes a rotation in a plane.

on two-particle states [44, 45]. The non-local charges belong to the mathematical framework of Hopf algebras, to which notably the Yangian group belongs. Although we will not go further into this topic, we refer the interested reader to [46] for a nice review on the subject.

The action of the local charges on multi-particle states behaves as in (2.1.12): since they are conserved during the scattering an infinite set of conservation equations

$$\gamma_{a_1}^{(s)} e^{s\theta_1} + \ldots + \gamma_{a_n}^{(s)} e^{s\theta_n} = \gamma_{b_1}^{(s)} e^{s\theta'_1} + \ldots + \gamma_{b_m}^{(s)} e^{s\theta'_m} \tag{2.1.13}$$

needs to be imposed. For $s = \pm 1$ we have the usual energy-momentum conservation, with $\gamma_a^{(\pm 1)} = m_a$. The existence of such conservation laws, for infinitely-many different values of s, suggests that there are only trivial solutions of the scattering: the number of particles has to be the same before and after the collision, $n = m$, and the sets of incoming- and outgoing-particles need to have the same quantum numbers. This is reasonable, even though the argumentation is not rigorous; indeed an infinite number of constraints does not automatically imply a trivial solution. For example, for purely imaginary rapidities, it is possible to find production processes conserving the infinite set of higher spin conserved charges. However, for real sets of rapidities, that is no more the case and actually (2.1.13) is only satisfied by elastic solutions. However, this requires some extra proof. A more rigorous argument was presented in [21]. In that paper Stephen Parke argued that the existence of a pair of higher-spin charges in (1+1)-dimensional theories is sufficient alone to ensure the absence of production and the factorization of the scattering. In other words, after having chosen a particular order of the rapidities, for any conserved charge of spin s the following relations need to hold

$$\theta_i = \theta'_i \quad \text{and} \quad \gamma_{a_i}^{(s)} = \gamma_{b_i}^{(s)} \ \forall \ i = 1, \ldots, n.$$

This does not imply that the initial and the final particles have to be the same (i.e. $a_i = b_i$); they just need to have the same sets of quantum numbers ($\gamma_{a_i}^{(s)} = \gamma_{b_i}^{(s)}$) under these higher-spin representations of the Lorentz group. In particular the following conditions are satisfied:

- the number of incoming particles has to be the same as the number of the outgoing ones;
- the sets of incoming and outgoing momenta are the same;
- any allowed $n \to n$ nonzero S-matrix factorises into the product of $2 \to 2$ S-matrices.

In the next section we will review the Parke argument, through which the bullet points above will be proved.

2.2 Factorisation and Yang-Baxter equation

Let $\psi(x)$ be the spatial part of a single-particle wave packet, propagating with momentum $\tilde{P}$ and located at the position $\tilde{x}$ at the starting time. It is described by

$$\psi(x) \propto \int_{-\infty}^{+\infty} dP\ e^{-a^2(P-\tilde{P})^2} e^{iP(x-\tilde{x})}, \tag{2.2.1}$$

where the overall normalization factor is omitted. We can introduce a phase in the Fourier transform of the wave function

$$\psi(x;\alpha) \propto \int_{-\infty}^{+\infty} dP\ e^{-a^2(P-\tilde{P})^2} e^{iP(x-\tilde{x})} e^{-i\alpha\phi(P)} \tag{2.2.2}$$

by acting on (2.2.1) with $e^{-i\alpha\hat{\Phi}}$ and assuming $\hat{\Phi}$ to be a diagonal operator on the eigenvectors of the momentum. Since the Gaussian is centred in $\tilde{P}$, most of the contribution to the integral comes from the region around $\tilde{P}$. Expanding ϕ at the first order around $P = \tilde{P}$, up to a constant overall multiplicative factor the wave packet is modified as

$$\psi(x;\alpha) \propto \int_{-\infty}^{+\infty} dP\ e^{-a^2(P-\tilde{P})^2} e^{iP[x-\tilde{x}-\alpha\phi'(\tilde{P})]}. \tag{2.2.3}$$

The starting position $\tilde{x}$ is translated by $\alpha\phi'(\tilde{P})$. By considering higher powers of the expansion in $P-\tilde{P}$, it would also be possible to compute the dependence of the width a as a function of α.

As a starting example, the action of the Hamiltonian on the packet (2.2.1) will be considered. In this case, assuming that the mass of the propagating particle is m, then $\phi(P) = \sqrt{P^2+m^2}$, and the centre of the wave function changes as

$$\tilde{x}(\alpha) = \tilde{x} + \alpha \frac{\tilde{P}}{\sqrt{\tilde{P}^2+m^2}}. \tag{2.2.4}$$

Parametrizing the spatial momentum in terms of the rapidity, according to (2.1.1) and (2.1.2), then $\tilde{P} = m\sinh\theta$ and

$$\tilde{x}(\alpha) = \tilde{x} + \alpha\tanh\theta. \tag{2.2.5}$$

In this case, α plays the role of the time, while the quantity $\tanh\theta$ is the velocity of the particle. Such a formula describes the motion of a single-particle wave-packet having a Gaussian distribution centered on the α-dependent position given in (2.2.5). In the non-relativistic limit $\theta \ll 1$ (or equivalently $\tilde{P}^2 \ll m^2$) the velocity can be approximated $\tanh\theta \sim \sinh\theta = \frac{\tilde{P}}{m}$, which is of course what we expect.

The next step is to consider a multi-particle state, describing n particles located at the starting time at the positions $\tilde{x}_1 < \ldots < \tilde{x}_n$, and carrying a set of rapidities $\theta_1 > \ldots > \theta_n$

$$\psi(x_1,\ldots,x_n) \propto \prod_{i=1}^{n} \int_{-\infty}^{+\infty} dP_i\ e^{-a^2(P_i-\tilde{P}_i)^2} e^{iP_i(x_i-\tilde{x}_i)}, \tag{2.2.6}$$

where the momenta are connected to the rapidities through $\tilde{P}_i = m_i \sinh\theta_i$ with $i = 1, \dots, n$. It is possible to modify such a state by acting, for example, with $e^{-i\alpha\hat{P}}$. The effect is to translate all the centres of the wave packets of the same quantity $\tilde{x}_i \to \tilde{x}_i + \alpha$. Since the physics is invariant under spatial translations, the S-matrix elements do not change under such transformations and for any final state $|f\rangle$ it holds that

$$\langle f|e^{i\alpha\hat{P}}\hat{S}e^{-i\alpha\hat{P}}|\psi\rangle = \langle f|\hat{S}|\psi\rangle.$$

Similarly the Hamiltonian $\hat{H}$ is the correct generator to describe time-translations. Acting by $e^{-i\alpha\hat{H}(P)}$, from the previous discussion, the particles are translated by rapidity dependent parameters $\tilde{x}_i(\alpha) = \tilde{x}_i + \alpha\tanh\theta_i$. This transformation makes sense while α is small enough that no particles cross each other during the transformation so that the state is free at all times between t_0 (the starting time) and $t_0 + \alpha$. If at $t = t_0$ the particles occupy certain space positions, at the time $t = t_0 + \alpha$ their positions are modified according to their velocities; for sure the action by $e^{-i\alpha\hat{H}(P)}$ does not modify the order in which the different particles collide since it is just a temporal translation. If the starting time is assumed to be t_0 or $t_0 + \alpha$, the same order of collisions between the different wave packets will be observed.

The situation is more interesting if additional higher-spin conserved charges, of the form in (2.1.9), exist. In the following, it will be shown that in the presence of such operators the scattering factorises. The proof was given in a paper by Stephen Parke [21] and it is based on the action of the 'light-cone' operators (2.1.9) on wave packets. However, it should be mentioned that elements of the argument used in [21] date back to [47, 48]. Below we explain this argument following the lines of the review [36]. We assume there exists a conserved operator $\hat{P}_s$ acting on single-particle states as $\hat{P}^s$, the power s of the spatial momentum ($s \geq 2$).[3] Acting with the exponential of such operator on (2.2.6) it follows that

$$\psi(x_1, \dots, x_n; \alpha) \propto \prod_{i=1}^{n} \int_{-\infty}^{+\infty} dP_i \; e^{-a^2(P_i - \tilde{P}_i)^2} e^{iP_i(x_i - \tilde{x}_i)} e^{-i\alpha P_i^s}. \tag{2.2.7}$$

According to the previous discussion, the centres of the different wave packets are translated by $\alpha s \tilde{P}_i^{s-1}$ so that each particle is smeared around an α-dependent position

$$\tilde{x}_i(\alpha) = \tilde{x}_i + \alpha s \cdot m_i^{s-1} \cdot (\sinh\theta_i)^{s-1}. \tag{2.2.8}$$

Differently from the action of the Hamiltonian, which translates the particle positions $\tilde{x}_i$ along space-time lines with gradients given by the velocities of the particles (i.e. $\frac{d\tilde{x}_i}{d\alpha} = v_i = \tanh\theta_i$), in this case the gradients are given by $s \cdot m_i^{s-1} \cdot (\sinh\theta_i)^{s-1}$ and can grow arbitrarily with the rapidity. While the first transformation is associated with a temporal translation, which preserves the order in which the different particles collide, the second one can alter such order. The operator $e^{-i\alpha\hat{P}_s}$ can be used to move the particles relative to each other, changing their spatial distances. The

[3] Note that the action of $\hat{P}_s$ is not the same as that one of Q_s; however assuming the conservation of $\hat{P}_s$ instead of Q_s does not modify the message of Parke's argument and at the same time allows to maintain simple mathematical expressions.

consequence is that the order in which the different particles interact during the temporal evolution of $e^{-i\alpha\hat{P}_s}|\psi\rangle$ can be different from the order in which they interact letting evolve in time the state $|\psi\rangle$. Nevertheless, if $\hat{P}_s$ is an operator associated with a conserved charge (commuting therefore with the Hamiltonian), it must be true that

$$\langle f|\hat{S}|\psi\rangle = \langle f|e^{i\alpha\hat{P}_s}\hat{S}e^{-i\alpha\hat{P}_s}|\psi\rangle. \tag{2.2.9}$$

The only possibility to have such equality valid for general sets of rapidities is that the initial number of particles is the same as the final one and that $\langle f|\hat{S}|\psi\rangle$ does not have to depend on the order in which the particles interact.

To give some more explanation let us consider a production process of the form

$$1 + 2 \to 3 + 4 + \ldots + M, \tag{2.2.10}$$

where the numbers $1, \ldots, M$ are labels for the particles involved in the collision and $M \geq 5$. If we consider 1 and 2 as asymptotic particles, nothing can happen before their wave packets overlap: this is a consequence of the macroscopic causal properties of space-time, usually named 'macrocausality'. We will return to this concept in one moment. The time t_{12}, at which the trajectories of 1 and 2 intersect, must precede the time of all the other interactions. After the first two particles collide a cascade of subsequent collisions can in principle happen. An example of possible subsequent collisions for $M = 5$ is shown in figure 2.1, where the vertical axis measures the time and the horizontal axis measures the space. Though the process in figure 2.1 cannot be identified with any integrable theory, due to the fact that there is a long-living bound state particle propagating, it is however consistent with 'macrocausality'. In the considered example, 2 is the slower incoming particle. If we take its trajectory and, at each collision, we follow the trajectory of the rightmost particle (the blue line in figure 2.1) we end up on the trajectory of the fastest outgoing particle, which we label by 3. By extending the trajectories of the particle 2 and 3, as is done in figure 2.1 through two dashed red lines, we can find the time t_{23} at which they would interact if they were freely propagating. Of course, it holds that

$$t_{12} < t_{23} \tag{2.2.11}$$

otherwise the particle 3 would be generated before the incoming particles collide. This is clear from figure 2.1 where the meeting point between the trajectories of 1 and 2 is below the meeting point of the trajectories associated with 2 and 3. This fact has to be true in general, indeed the generation of the particle 3 is an effect of the interaction of 1 and 2. If $t_{23} < t_{12}$ then cause and effect are temporally inverted and there is a violation of the macrocausality. The name macrocausality follows from the fact that the causality violation happens at finite time scales and not microscopically. The equality (2.2.11) may be violated at microscopic time scales but not macroscopically. If we label by 2 the slower incoming particle and by 3 the faster outgoing particle the same constraint $t_{12} < t_{23}$ has to hold in any process of the form in (2.2.10). An example of a production process (2.2.10) satisfying macrocausality is shown on the LHS of figure 2.2. However, if $\hat{P}_s$ is a conserved operator, by properly tuning α in (2.2.9), we can move the trajectory of the particle 3 so that the amplitude

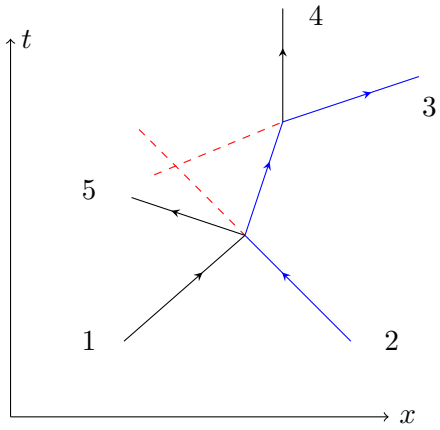

Figure 2.1: Example of production process $1+2 \to 3+4+5$.

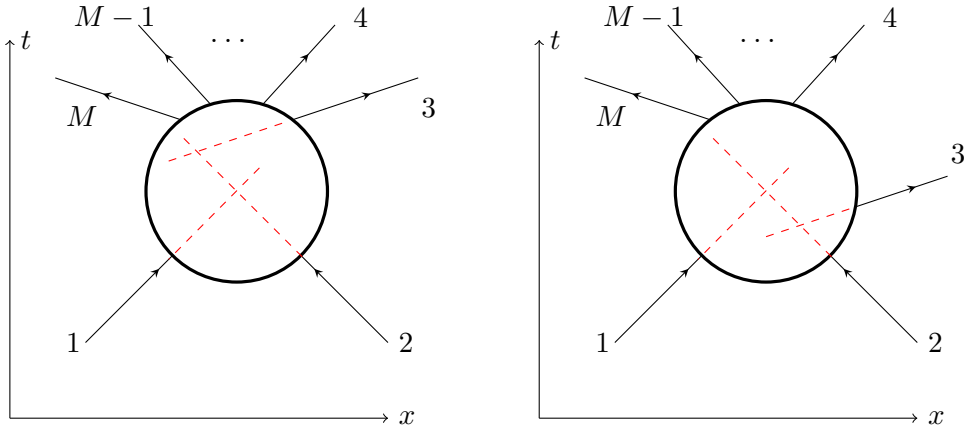

Figure 2.2: On the left is a scattering process preserving the macrocausality while on the right is a scattering process violating the macrocausality. If the theory is integrable, the two processes are related by the action of a higher-spin conserved charge and both need to vanish.

defined on the RHS of equation (2.2.9) satisfies $t_{23} < t_{12}$; its pictorial representation is shown on the RHS of figure (2.2). Since this amplitude violates macrocausality, it has to vanish and by (2.2.9) also the starting amplitude is zero. The reader is invited to look at the paper by Parke [21] for a detailed computation of the action of the higher-spin charges on the trajectories.

Due to this fact, the only processes having nonzero amplitudes are those in which the incoming and outgoing particles have the same sets of rapidities. In these situations, the S-matrix factorises into the product of 2-to-2 S-matrices and any scattering event can be determined in terms of 2-to-2 S-matrix elements of the form depicted in figure 2.3, where θ_{ij} is a label for the difference between the rapidities of the scattered particles, $\theta_i - \theta_j$. It will be always assumed that the 2-to-2 S-matrices depend on the rapidities through such difference; this is a feature of all Lorentz-invariant theories. The invariance under the order in which the collisions happen is then expressed in terms of the so-called Yang-Baxter equation (or factorisation equation); it states

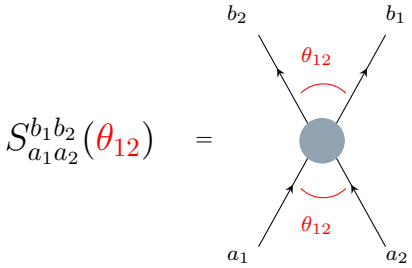

Figure 2.3: Pictorial representation of a 4-point S-matrix element.

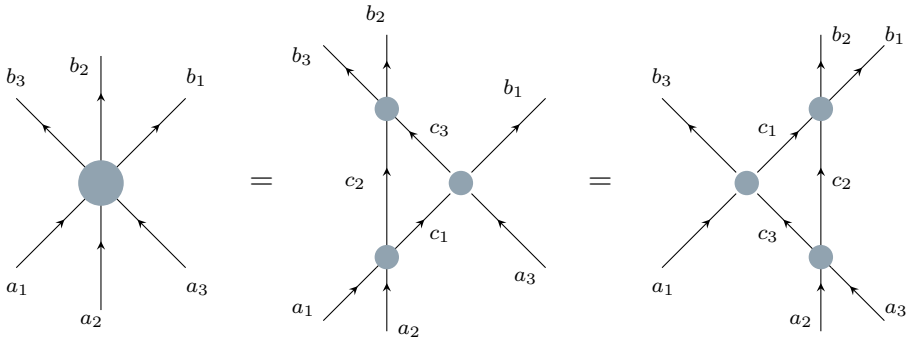

Figure 2.4: Pictorial representation of the Yang-Baxter equation.

that, in a 3-to-3 scattering process of the form

$$A_{a_1}(\theta_1)A_{a_2}(\theta_2)A_{a_3}(\theta_3) \to A_{b_3}(\theta_3)A_{b_2}(\theta_2)A_{b_1}(\theta_1),$$

where $\{a_1, a_2, a_3\}$ and $\{b_1, b_2, b_3\}$ represent respectively the types of the incoming- and outgoing-particles and $\theta_1 > \theta_2 > \theta_3$, the S-matrix can be written equivalently as

$$S^{b_1 b_2 b_3}_{a_1 a_2 a_3}(\theta_1, \theta_2, \theta_3) = S^{c_1 c_2}_{a_1 a_2}(\theta_{12}) S^{b_1 c_3}_{c_1 a_3}(\theta_{13}) S^{b_2 b_3}_{c_2 c_3}(\theta_{23}) = S^{c_2 c_3}_{a_2 a_3}(\theta_{23}) S^{c_1 b_3}_{a_1 c_3}(\theta_{13}) S^{b_1 b_2}_{c_1 c_2}(\theta_{12}). \tag{2.2.12}$$

In (2.2.12) there is an implicit sum over the repeated indices c_1, c_2 and c_3, corresponding to all possible intermediate propagating particles between the 2-to-2 collisions. Acting with $e^{-i\alpha \hat{P}_s}$ on the initial state we can move the trajectories of the particles as we wish, so to modify the points of interaction between pairs of particles. The three types of collision depicted in figure 2.4, each one corresponding to one term in the chain of equalities (2.2.12), are obtained by acting with $e^{-i\alpha \hat{P}_s}$ on the initial state for suitably chosen values of α. No matter the choice of α, the operator $e^{-i\alpha \hat{P}_s}$ commutes with the S-matrix and therefore the processes in figure 2.4 are physically equivalent. The pictorial representation of the Yang-Baxter equation is given in figure 2.4 and provides a restriction on the structure of the 4-point S-matrices.

Most of the following sections will be focused on integrable theories with purely elastic S-matrices, in which the initial and the final sets of particles involved in the scattering are identical. A legitimate question is then how we can distinguish such interaction processes from freely propagating particles. In the remaining part of this section, an answer to this question will be presented. Let $\psi_{in}(x_1, x_2)$ be a

two-particle state defined as

$$\psi_{in}(x_1,x_2) \propto \int_{-\infty}^{+\infty} dP_1 dP_2 \; e^{-a^2(P_1-\tilde{P}_1)^2} e^{iP_1(x_1-\tilde{x}_1)} e^{-a^2(P_2-\tilde{P}_2)^2} e^{iP_2(x_2-\tilde{x}_2)}. \tag{2.2.13}$$

It describes an initial set of particles located at the starting positions $x_1 < x_2$ and propagating with rapidities $\theta_1 > \theta_2$. If the distance between the two wave packets is much bigger than their width ($|x_2 - x_1| \gg a$) then it makes sense to consider such a state as a tensor product of two free single-particle states. If the particles are left to propagate in time, after the collision the final state will be described by

$$\psi_{out}(x_1,x_2) \propto \int_{-\infty}^{+\infty} dP_1 dP_2 \; e^{-a^2(P_1-\tilde{P}_1)^2} e^{iP_1(x_1-\tilde{x}_1)} e^{-a^2(P_2-\tilde{P}_2)^2} e^{iP_2(x_2-\tilde{x}_2)} e^{-i\phi(P_1,P_2)} \tag{2.2.14}$$

where the phase $\phi(P_1,P_2)$ contains a contribution coming from the energies of the two freely propagating particles ($t\sqrt{P_1^2+m_1^2} + t\sqrt{P_2^2+m_2^2}$), plus a phase inherited from the collision. If the 2-to-2 S-matrix is given by

$$S(\theta) = e^{-i\gamma(\theta)},$$

with $\theta \equiv \theta_1 - \theta_2$, then the phase in (2.2.14) can be written as

$$\phi(P_1,P_2) = t\sqrt{P_1^2+m_1^2} + t\sqrt{P_2^2+m_2^2} + \gamma(\theta). \tag{2.2.15}$$

As explained before, expanding (2.2.15) around the values $\tilde{P}_1 = m_1 \sinh\theta_1$ and $\tilde{P}_2 = m_2 \sinh\theta_2$ the propagation equations for the centres of the two wave packets are obtained

$$\begin{aligned} \tilde{x}_1(t) &= \tilde{x}_1 + \tanh\theta_1 \Big(t + \frac{1}{m_1 \sinh\theta_1} \frac{d}{d\theta}\gamma\Big) \\ \tilde{x}_2(t) &= \tilde{x}_2 + \tanh\theta_2 \Big(t - \frac{1}{m_2 \sinh\theta_2} \frac{d}{d\theta}\gamma\Big). \end{aligned} \tag{2.2.16}$$

If the centre of mass frame is assumed, where

$$m_1 \sinh\theta_1 = -m_2 \sinh\theta_2 = \tilde{P},$$

it holds

$$\tilde{x}_1(t) = \tilde{x}_1 + \tanh\theta_1 t' \quad , \quad \tilde{x}_2(t) = \tilde{x}_2 + \tanh\theta_2 t' \tag{2.2.17}$$

with

$$t' = t + \frac{i}{\tilde{P}} \frac{d}{d\theta} \log S. \tag{2.2.18}$$

In the absence of interactions the particle-positions would evolve in time according with (2.2.17) and $t' = t$. If instead the theory is integrable, with a purely elastic S-matrix, but it is not free, a time delay is observed; this delay can be written in terms of the S-matrix, as given in (2.2.18). Even though after the collision the two outgoing particles are the same as the initial ones, and do not modify their momenta, it is possible to note that indeed an interaction happened since a time delay in the motion of the wave packets is observed. We remark that the same behaviour is found

also in the scattering between solitons in classical physics.

2.3 The axiomatic S-matrix

It has just been discussed how, in all integrable theories, multi-particle scattering processes factorise into products of 2-to-2 interactions. Therefore any scattering event can be written in terms of 4-point S-matrix elements. For a process of the form

$$a(p_1) + b(p_2) \to c(p_3) + d(p_4), \tag{2.3.1}$$

where $\{a, b\}$ and $\{c, d\}$ represent respectively the types of the incoming and outgoing particles, such elements are defined, according to (2.1.6), as

$$A_a(\theta_1)A_b(\theta_2) = S_{ab}^{dc}(\theta)A_c(\theta_2)A_d(\theta_1), \tag{2.3.2}$$

where the integral has been removed and the initial and final rapidities have been set to be the same due to the conservation of the charges. As already mentioned in section 2.1, the order of the operators $A_j(\theta)$ in (2.3.2) is important since they are elements of the Zamolodchikov-Faddeev algebra. We also stress once again that the focus of this thesis will be on Lorentz invariant theories, where S_{ab}^{dc} depends on the external kinematics through the difference between rapidities, $\theta = \theta_1 - \theta_2$. Such S-matrices, whose pictorial representation is shown in figure 2.3, and their universal properties will be described in this section.

First of all $S_{ab}^{dc}(\theta)$ is nonzero only if the initial and the final states agree on all the eigenvalues of the conserved charges (2.1.9), for which $\gamma_a^{(s)} = \gamma_d^{(s)}$ and $\gamma_b^{(s)} = \gamma_c^{(s)}$. As a consequence of this fact, $(m_a, m_b) = (m_d, m_c)$, and therefore $(p_1, p_2) = (p_4, p_3)$. Moreover, the models that will be considered here are assumed to respect the following additional symmetries

- $S_{ab}^{dc}(\theta) = S_{ba}^{cd}(\theta)$ (invariance under *parity*);
- $S_{ab}^{dc}(\theta) = S_{\bar{a}\bar{b}}^{\bar{d}\bar{c}}(\theta)$ (invariance under *charge conjugation*);
- $S_{ab}^{dc}(\theta) = S_{cd}^{ba}(\theta)$ (invariance under *time reversal*).

For the process in (2.3.1) the Mandelstam variables (written in the light-cone components of momenta) can be defined as

$$\begin{aligned} s &= (p_1 + p_2)(\bar{p}_1 + \bar{p}_2) \\ t &= (p_1 - p_3)(\bar{p}_1 - \bar{p}_3) \\ u &= (p_1 - p_4)(\bar{p}_1 - \bar{p}_4). \end{aligned} \tag{2.3.3}$$

In two dimensions they can all be expressed as functions of a single parameter. For example, if the initial set of momenta is the same as the final one (i.e. $p_4 = p_1$, $p_3 = p_2$), then $u = 0$ and

$$\begin{aligned} s &= m_a^2 + m_b^2 + 2m_a m_b \cosh\theta \\ t &= m_a^2 + m_b^2 - 2m_a m_b \cosh\theta = 2m_a^2 + 2m_b^2 - s. \end{aligned} \tag{2.3.4}$$

As can be seen from (2.3.4), physical external momenta correspond to the kinematical region $s \geq (m_a + m_b)^2$, the equality being saturated when the incoming particles propagate with equal rapidities. In such a region a requirement to have a well-defined quantum field theory is that the S-matrix is unitary. For integrable models, in which all production processes are forbidden by the existence of higher-spin conserved charges, this requires

$$\sum_{ln} S_{ab}^{ln}(s)\bar{S}_{dc}^{ln}(s) = \delta_{ad}\delta_{bc} \;\forall\; s \geq (m_a + m_b)^2.$$

Combined with parity invariance and time reversal, the unitarity constraint can also be written as

$$S_{ab}^{ln}(s)\bar{S}_{ln}^{dc}(s) = \delta_a^d\delta_b^c \;\forall\; s \geq (m_a + m_b)^2, \tag{2.3.5}$$

where the sum over the intermediate particles l and n is understood. Although scattering processes are computed at physical values of the external momenta, where $s \geq (m_a + m_b)^2$, it is postulated that the S-matrix element S_{ab}^{dc} can be analytically continued above the physical region into the complex plane. The function defined in this way is single-valued after suitable cuts have been made. The properties of the analytic continuation of the S-matrix are explained below.

The unitarity constraint (2.3.5), that in integrable theories receives contributions only from 2-to-2 processes, would in a generic quantum field theory receive contributions also from higher-point production processes. Any time the Mandelstam variable s reaches a threshold value at which more particles can be generated on-shell (for example $a + b \to c_1 + \cdots + c_n$) the S-matrix element S_{ab}^{dc} receives a new contribution[4]. The value $s = (m_a + m_b)^2$ is the first of a series of branch points, each one corresponding to one of these thresholds; the others are distributed on the real axis at values $s > (m_a + m_b)^2$. A cut on the complex s plane can be attached to each branch point; by convention it is assumed to run to $s = +\infty$ on the real axis. In integrable theories, due to the absence of production, only the leading threshold $(m_a + m_b)^2$ is present, the least energy squared at which the two-particle state $A_a(\theta_1)A_b(\theta_2)$ can exist. So, for positive s, a single branch cut, connecting $s = (m_a + m_b)^2$ to $s = +\infty$ on the real axis, is present. However, this is not the end of the story. A universal property of a quantum field theory is the so-called *crossing symmetry*: given a generic process it is possible to convert an incoming particle into an outgoing particle (and vice-versa) by changing the sign of its momentum and transforming it into the corresponding anti-particle. Using this fact on the process (2.3.1), combined with (2.3.4), it is possible to write

$$S_{ab}^{dc}(s) = S_{a\bar{c}}^{d\bar{b}}(2m_a^2 + 2m_b^2 - s). \tag{2.3.6}$$

For the previous discussion the function $S_{a\bar{c}}^{d\bar{b}}$ has a branch cut starting at $(m_a + m_b)^2$ ($m_c = m_b$ is used, since the initial and final conserved charges have to be the same) and running to $+\infty$ on the real axis. This implies that the function $S_{ab}^{dc}(s)$ has

[4]Such discontinuities can be seen by expressing the S-matrix in the form $S = 1 + iT$, and writing the discontinuity of T through the optical theorem. See chapter one of [17] for a more detailed discussion.

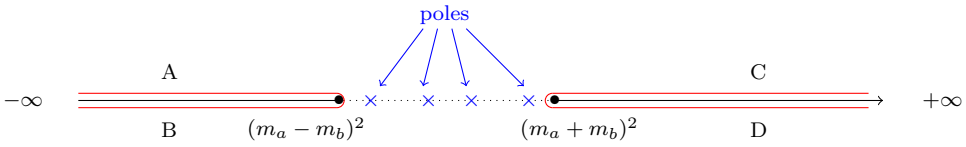

Figure 2.5: Complex s plane corresponding to the physical sheet.

another branch cut, this time connecting $s = (m_a - m_b)^2$ to $s = -\infty$. The two branch cuts are shown in figure 2.5, where they are surrounded by a red contour. On the real axis in the middle between the cuts, for $(m_a - m_b)^2 < s < (m_a + m_b)^2$, possible poles are present. They are due to intermediate bound state particles propagating on-shell.

Since it is postulated that the S-matrix can be analytically continued above the physical region into the complex plane, defining an analytic function, it follows that $S^-(s)$, defined by

$$S^-(s) \equiv \bar{S}(\bar{s}) \tag{2.3.7}$$

is also analytic. This follows from a theorem in complex analysis stating that given an analytic function $f(z)$ then $g(z) \equiv \bar{f}(\bar{z})$ is also analytic. While S is defined above the right cut, matching the values of physical scattering processes by approaching the cut from above (the C region in figure 2.5), S^- provides the analytic continuation of $\bar{S}(\bar{s})$ below the cut (having as boundary the region D in figure 2.5). It can be proven that on the region $(m_a - m_b)^2 < s < (m_a + m_b)^2$ of the real axis the S-matrix is real and $S^-(s) = \bar{S}(s) = S(s)$. A proof of this fact can be found in chapter 4 of [17]. Since S and S^- share the same analytic continuation on $(m_a - m_b)^2 < s < (m_a + m_b)^2$ it follows that they are the same on the full complex s plane. Due to this fact it follows that the S-matrix is *real-analytic*, i.e. it takes complex conjugate values at complex conjugate points

$$\bar{S}^{dc}_{ab}(s) = S^{dc}_{ab}(\bar{s}). \tag{2.3.8}$$

Consequently the unitarity constraint (2.3.5) can be written in the form

$$S^{ln}_{ab}(s^+) S^{dc}_{ln}(s^-) = \delta^d_a \delta^c_b \;\forall\; s \geq (m_a + m_b)^2, \tag{2.3.9}$$

being s^+ and s^- the values of the Mandelstam variable s approaching the cut from above and below, $s^\pm = s \pm i0$. Once the different S-matrix elements have been defined on the boundary regions C and D in figure 2.5, the values on the regions A and B, respectively above and below the left-hand side cut, are obtained using crossing symmetry. For example if s_1 is taken to be a point just above the left-cut on the region A, then $S^{dc}_{ab}(s_1) = S^{d\bar{b}}_{a\bar{c}}(s_2)$ with $s_2 = 2m_a^2 + 2m_b^2 - s_1$ defined on the region just below the right-cut.

It is then possible to prove that such cuts are both of square root type, by following the argument presented for example in [36]. The proof will be given for the right-cut; however for the one on the left the same argument applies. A function S_γ can be defined by circling one time around the branch point $s^* = (m_a + m_b)^2$ following the anticlockwise direction, so that $S_\gamma(s^* + \rho e^{i\delta}) = S(s^* + \rho e^{i(\delta + 2\pi)})$ with $\rho \in \mathbb{R}^+$ and

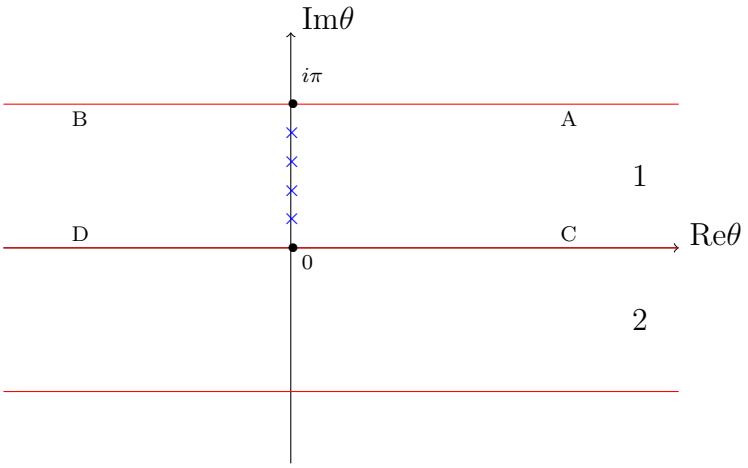

Figure 2.6: Complex θ plane. The region 1, corresponding to $0 <$ Im $\theta < \pi$, represents the physical strip.

$\delta \in (0, 2\pi)$. Unitarity is then given by $S_\gamma(s^+)S(s^+) = 1$. Such relation, defined on the region just above the cut, is written in a form that can be analytically continued to the entire s plane, so to obtain

$$S_\gamma(s)S(s) = 1. \tag{2.3.10}$$

In particular, if a point just below the cut is considered then it holds

$$S_\gamma(s^-) = S^{-1}(s^-) = S(s^+), \tag{2.3.11}$$

where the first equality comes from (2.3.10) and the second equality is the unitarity constraint on S. Since $S_\gamma(s^-)$ is the value of S after circling two times around the branch point, from (2.3.11) it is evident that after two anticlockwise circles we come back to the value $S(s^+)$. This implies that $s^* = (m_a + m_b)^2$ has to be a branch point of square root type. The same argument can be repeated almost identically for the other branch point, $s^{**} = (m_a - m_b)^2$. Despite the fact that s^* and s^{**} are both of square root type, the Riemann surface over which S_{ab}^{dc} is defined is not necessarily a double cover of the complex plane. By circling one branch point at a time, alternating between s^* and s^{**}, it is in principle possible to reach many different sheets. Figure 2.5 represents the 'physical sheet', containing on its boundary regions the physical values of the S-matrix; in particular, approaching the right-cut from above, on the region C, S_{ab}^{dc} makes physical sense as the S-matrix element describing the scattering of $\{a, b\}$ into $\{c, d\}$.

In terms of the variable s the story may look quite complicated, but everything becomes simpler if the functional dependence is expressed in terms of the rapidity, as discussed in [18]. By inverting the first equation in (2.3.4) the 'physical sheet' can be mapped into a region of the complex θ plane known as the 'physical strip'. It corresponds to the strip $0 <$ Im$\theta < \pi$ in figure 2.6 and it is labelled by the number 1. The region of the s plane near the branch cuts, indicated with letters A, B, C and D in figure 2.5 are mapped to the regions of the θ plane having imaginary part

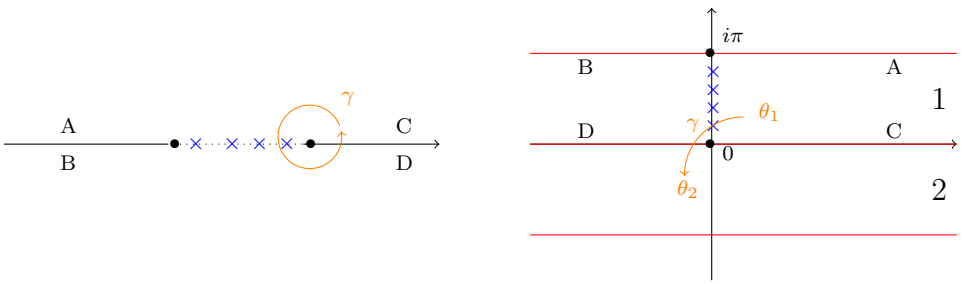

Figure 2.7: Map of a path γ from the physical sheet to the physical strip.

close to 0 and $i\pi$ inside the strip. Now let s_1 to be a point just above the right-cut of the physical sheet and to circle around s^* following the anticlockwise direction until, after a 2π angle, we return to the starting point; the situation is represented on the LHS part of figure 2.7. As previously explained the S-matrix, as a function of s, is not single-valued at the point s_1. After circling around the branch point we get the analytic continuation S_γ of the matrix S, so that $S_\gamma(s_1) \neq S(s_1)$, and it holds the matrix equation (2.3.10). Working in terms of the rapidity, by looking at the RHS part of figure 2.7, it is possible to observe that the path γ maps the point θ_1 into $\theta_2 = -\theta_1$. Of course due to the fact that $\cosh\theta$ is an even function, the Mandelstam variable s takes the same value both at θ_1 and at θ_2 and it is necessary to analytically continue S into S_γ to distinguish between the two points, which are defined on two different sheets of the complex s plane. However, if the S-matrix is written as a function of θ it comes out that it is single-valued in this variable and the unitarity matrix equation (2.3.10) becomes

$$S(-\theta)S(\theta) = 1, \tag{2.3.12}$$

which written making all the indices explicit is

$$S_{ab}^{ln}(-\theta)S_{ln}^{dc}(\theta) = \delta_a^d \delta_b^c. \tag{2.3.13}$$

Differently from (2.3.5), the formula in (2.3.13) is written in a form that can be analytically continued to the full θ plane and is therefore valid for any value of θ. Given a matrix S, defined on the physical strip, which is the region 1 in figure 2.6, its value on the region 2 is known from the analytic continuation of unitarity (2.3.13). It is possible to analytically continue the crossing constraint as well; in such case (2.3.6) becomes

$$S_{ab}^{dc}(\theta) = S_{a\bar{c}}^{d\bar{b}}(i\pi - \theta). \tag{2.3.14}$$

While the strip $0 < \text{Im}\ \theta < \pi$ is the most interesting region of the θ plane, since it contains on its boundary physical scattering processes, the S-matrix is defined on an infinite number of possibly-different strips, $n\pi < \text{Im}\ \theta < (n+1)\pi$, each one corresponding to a different cover of the complex s plane. In the remaining part of this thesis the focus will be just on models having purely elastic S-matrices, for which no degeneracies appear and the existence of higher-spin conserved charges is enough

to impose the equality between the incoming- and outgoing-particles. In one moment it will be shown that in these models there are only two different strips, 1 and 2 in figure 2.6, and that all the 2-to-2 S-matrix elements are periodic functions with periodicity $2\pi i$. If the process in (2.3.1) is elastic not only the incoming- and outgoing-momenta are the same (this is indeed a feature of all integrable theories), but also the types of particles do not change during the collision, i.e. $S_{ab}^{dc}(\theta) = S_{ab}(\theta)\delta_a^d\delta_b^c$. For real positive values of θ (i.e. on physical configurations) $S_{ab}(\theta)$ has to be a phase. Then the unitarity and crossing constraints, for these purely elastic models, become respectively

$$S_{ab}(-\theta)S_{ab}(\theta) = 1 \quad \text{(unitarity)}, \tag{2.3.15a}$$

$$S_{ab}(\theta) = S_{a\bar{b}}(i\pi - \theta) \text{ (crossing)}. \tag{2.3.15b}$$

Combining in sequence crossing and unitarity relations the following chain of equalities holds

$$S_{ab}(\theta) = S_{a\bar{b}}(i\pi - \theta) = \Big(S_{a\bar{b}}(\theta - i\pi)\Big)^{-1} = \Big(S_{ab}(2i\pi - \theta)\Big)^{-1} = S_{ab}(\theta - 2i\pi), \tag{2.3.16}$$

from which it is clear that the S-matrix has to be a $2\pi i$-periodic function.

2.4 Bound states and bootstrap equations

Since the S-matrices that will be considered are diagonal, the Yang-Baxter equation (2.2.12) is trivially satisfied and plays no role. Instead, a set of 'bootstrap relations', that will be defined in this section, are of great importance to construct consistent S-matrix elements. The bootstrap machinery to construct purely elastic S-matrices of integrable models from scratch was first developed by Alexander B. Zamolodchikov [19]; through it, he conjectured the S-matrix elements for the quantum field theory describing the scaling limit of the Ising model at the critical temperature perturbed by a magnetic field. Remarkably he found out from completely axiomatic principles the particles comprising the theory and their masses. These masses have been more recently confirmed experimentally [49] in the laboratory. Before moving to discuss the axiomatic approach implemented by Zamolodchikov, some more information about the poles lying on the imaginary axis of the physical strip (see the blue marks in figure 2.6) have to be given. They are not necessarily all simple. Higher-order singularities can be present and explained in terms of Coleman-Thun type diagrams [39]. These are Feynman diagrams in which the internal propagators go all on-shell simultaneously for particular values of the loop integration variables and external momenta. These diagrams will be discussed in some detail in the final chapter of this thesis in the context of affine Toda field theories, while the focus here will be only on the simple poles, due to intermediate bound states propagating on-shell in tree-level Feynman diagrams.

All the particles are assumed to be possible asymptotic states of the theory; this implies, to prevent decay processes, that any time a 3-point coupling $C_{ijk}^{(3)}$ is nonzero the mass of each particle appearing in the vertex should be smaller than the sum of

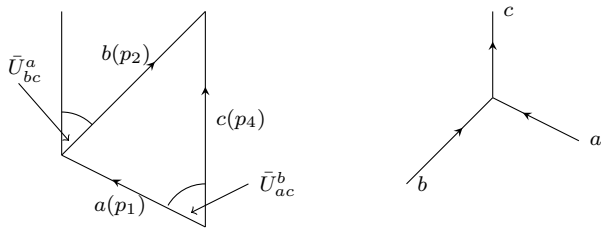

Figure 2.8: On-shell vertex on the right and its dual description on the left.

the other two. As a consequence of this, the masses of three particles admitting a nonzero 3-point coupling can be drawn in Euclidean space as the sides of a triangle. To find the poles it is necessary to study the region in which the external momenta are complex and the a_j factors in (2.1.2) are phases (i.e. the rapidities θ_j are imaginary).

If there exists a nonzero coupling $C^{(3)}_{ab\bar{c}}$ mediating the interaction between three on-shell particles a, b and c [5], then the momenta p_1, p_2 and p_4 making the process

$$a(p_1) + b(p_2) \to c(p_4)$$

on-shell are complex numbers satisfying

$$p_1 + p_2 = p_4 \tag{2.4.1}$$

and having absolute values equal respectively to m_a, m_b and m_c. By considering the first equality in (2.1.2) then (2.4.1) can be written as

$$m_a e^{iU_1} + m_b e^{iU_2} = m_c e^{iU_4} \tag{2.4.2}$$

where the imaginary values of the rapidities of the different particles have been labelled by iU. A similar equality is obtained for the other light-cone components of the momenta, $\bar{p}_1 + \bar{p}_2 = \bar{p}_4$, corresponding to substitute U with $-U$ for all the rapidities in (2.4.2). The three complex numbers in (2.4.2) close a mass-triangle corresponding to the 3-point vertex $C^{(3)}_{ab\bar{c}}$. By looking at the triangle in figure 2.8, assuming the direction of p_4 to be the axis respect to which the angles are measured in counterclockwise way, it holds $p_1 = m_a e^{i\bar{U}^b_{ac}}$, $p_2 = m_b e^{-i\bar{U}^a_{bc}}$ and $p_4 = m_c$; the conservation equations for the light-cone components of the momentum can therefore be written as

$$m_a e^{i\bar{U}^b_{ac}} + m_b e^{-i\bar{U}^a_{bc}} = m_c \quad \text{(conservation of } Q_1\text{)}, \tag{2.4.3a}$$

$$m_a e^{-i\bar{U}^b_{ac}} + m_b e^{i\bar{U}^a_{bc}} = m_c \quad \text{(conservation of } Q_{-1}\text{)}. \tag{2.4.3b}$$

Such triangular relations can be combined to construct Feynman diagrams with

[5] For a given index c representing a particle of type c, it is adopted the convention to use $\bar{c}$ to represent the respective antiparticle. While a particle of type c is annihilated by the index c and it is created by the index $\bar{c}$, the respective antiparticle is respectively annihilated/created by the index $\bar{c}/c$.

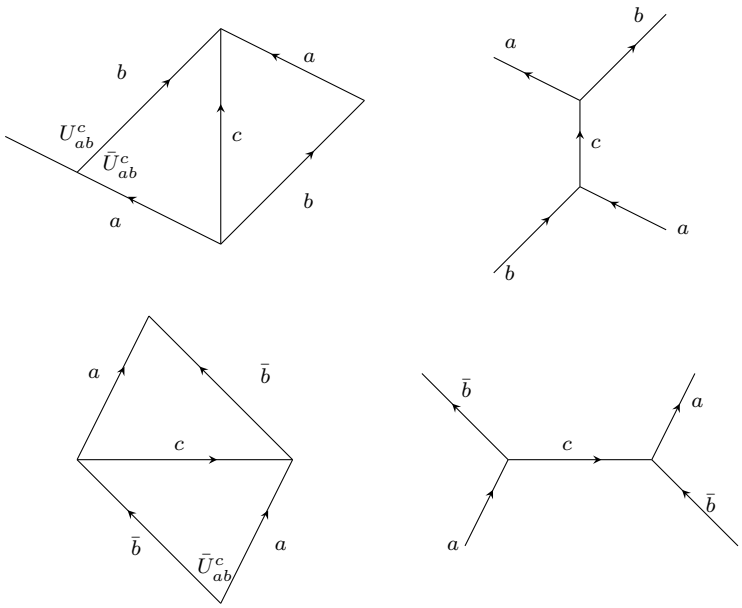

Figure 2.9: On-shell singular Feynman diagram (on the first row) and its crossed symmetric version (on the second row).

internal propagators on-shell as shown in figure 2.9. The conventions to label by $\bar{U}^c_{ab}$ the angle opposite to the side c in the mass-triangle Δ_{abc}, and to set $U^c_{ab} \equiv \pi - \bar{U}^c_{ab}$, are used. Following such conventions the square of the mass of the particle c is given by

$$m_c^2 = m_a^2 + m_b^2 + 2m_a m_b \cos U^c_{ab}. \tag{2.4.4}$$

In an elastic process

$$a + b \to a + b,$$

with $C^{(3)}_{ab\bar{c}} \neq 0$, the pole at $s = m_c^2$ can then be written in terms of θ (the difference between the rapidities of the incoming particles)

$$S_{ab}(\theta) \sim \frac{|C^{(3)}_{ab\bar{c}}|^2}{s - m_c^2} = \frac{|C^{(3)}_{ab\bar{c}}|^2}{2m_a m_b(\cosh\theta - \cos U^c_{ab})}.$$

Equation (2.4.4) and the first relation in (2.3.4) have been used in the second equality above. It is immediate to see that the pole is located at the position $\theta = iU^c_{ab}$, the external angle obtained by extending the side a in the triangle composed by the masses m_a, m_b and m_c (as indicated in figure 2.9). If now the 'crossed symmetric' process

$$a + \bar{b} \to a + \bar{b}$$

is considered, by writing the Mandelstam variable t as in the second row of (2.3.4) it holds that

$$S_{a\bar{b}}(\theta) \sim \frac{|C^{(3)}_{ab\bar{c}}|^2}{t - m_c^2} = \frac{-|C^{(3)}_{ab\bar{c}}|^2}{2m_a m_b(\cosh\theta + \cos U^c_{ab})}.$$

This time the pole is located at $\theta = i\bar{U}^c_{ab} = i(\pi - U^c_{ab})$, as shown in the second line of figure 2.9; this is exactly what is expected from crossing symmetry, since due

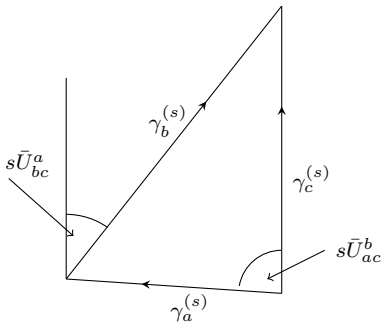

Figure 2.10: Closure relation associated to the conservation of Q_s when $C_{ab\bar{c}\neq 0}$.

to (2.3.15b) any time S_{ab} has a pole, say at $\theta = i\theta_0$ (with $0 < \theta_0 < \pi$), then $S_{a\bar{b}}$ has a pole at $\theta = i(\pi - \theta_0)$ with opposite residue compared to S_{ab}.

The conservation of the light-cone components of the momentum (2.4.3) can be extended to all the higher-spin conserved charges in a natural way. The idea is that the particle c, propagating with rapidity θ_4 in figure 2.8, can be seen as a superposition of two bound particles a and b, propagating with rapidities $\theta_1 = \theta_4 + i\bar{U}_{ac}^b$ and $\theta_2 = \theta_4 - i\bar{U}_{bc}^a$ respectively

$$A_a(\theta_1)A_b(\theta_2) = A_c(\theta_4). \tag{2.4.5}$$

Acting on such a state with any pairs of higher spin conserved charges, Q_s and Q_{-s}, and comparing the eigenvalues obtained on the two sides of (2.4.5) we obtain

$$\gamma_a^{(s)} e^{is\bar{U}_{ac}^b} + \gamma_b^{(s)} e^{-is\bar{U}_{bc}^a} = \gamma_c^{(s)} \quad \text{(conservation of } Q_s\text{)}, \tag{2.4.6a}$$

$$\gamma_a^{(s)} e^{-is\bar{U}_{ac}^b} + \gamma_b^{(s)} e^{is\bar{U}_{bc}^a} = \gamma_c^{(s)} \quad \text{(conservation of } Q_{-s}\text{)}. \tag{2.4.6b}$$

Such 'fusing relations' provide a generalization of (2.4.3) to the higher-spin conserved charges of the model. As happens for the momenta, the fusing relations of higher-spin charges can also be drawn in the complex plane as closure conditions of triangles (this time having sides of length $\gamma_a^{(s)}$, $\gamma_b^{(s)}$ and $\gamma_c^{(s)}$); the pictorial representation of (2.4.6a) is given in figure 2.10. The set of relations (2.4.6) is known as the 'conserved charge bootstrap'. Starting with a set of masses and 3-point couplings all the angles of the mass fusing triangles are determined. From them, the angles of the higher spin triangles are fixed, being just the angles of the mass-triangles multiplied by s, the spin of the charges (as shown in figure 2.10). This returns an overdetermined set of constraints for $\gamma_j^{(s)}$, the eigenvalues of the higher-spin charges: for a given s, if the only solution to such constraints is the trivial one $\boldsymbol{\gamma}^{(s)} = \mathbf{0}$ then there is no conserved charge of that spin. Given the masses and the 3-point couplings, the infinite tower of higher-spin conserved charges is therefore determined. The eigenvalues of such charges are then defined up to overall multiplicative factors, one for each s, that do not modify the fusing angles of the triangles in figure 2.10.

The argument can be repeated similarly for the S-matrix and leads to a set of algebraic bootstrap relations [50] connecting the S-matrix elements to one another.

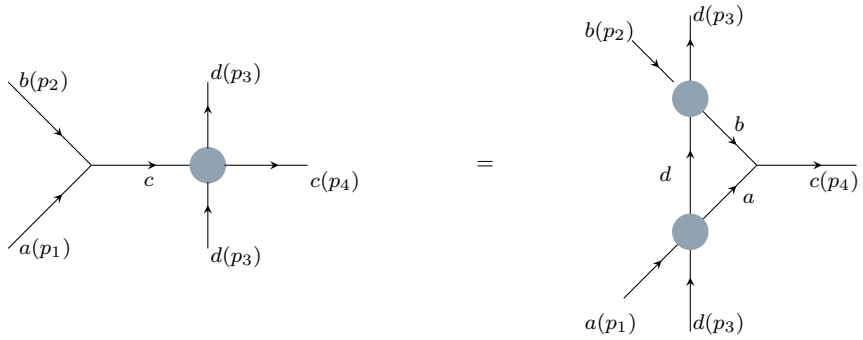

Figure 2.11: Pictorial representation of an S-matrix bootstrap constraint.

Such equations emerge from the following fusing idea: suppose that c is a bound state of two elementary particles a and b. Then consider a particle of type d; it can interact before or after the particles a and b fuse together to generate c. Through the action of the higher-spin conserved charges it is possible to move from the LHS to the RHS picture in figure 2.11. By equating the two expressions, the S-matrix element S_{dc} can be obtained as the product of the elements S_{da} and S_{db} shifted by the proper fusing angles:

$$S_{dc}(\theta_{34}) = S_{da}(\theta_{31})S_{db}(\theta_{32}),$$

where $\theta_{ij} \equiv \theta_i - \theta_j$. Defining $\theta \equiv \theta_{34}$ and substituting the values of the fusing angles given in figure 2.8 the following algebraic equation must hold

$$C^{(3)}_{ab\bar{c}} \neq 0 \implies S_{dc}(\theta) = S_{da}(\theta - i\bar{U}^b_{ac})S_{db}(\theta + i\bar{U}^a_{bc}). \tag{2.4.7}$$

Of course if (2.4.7) is valid for any θ it also holds that

$$S_{dc}(-\theta) = S_{da}(-\theta - i\bar{U}^b_{ac})S_{db}(-\theta + i\bar{U}^a_{bc}).$$

Using the unitarity condition (2.3.15a) we conclude that

$$C^{(3)}_{ab\bar{c}} \neq 0 \implies S_{dc}(\theta) = S_{da}(\theta + i\bar{U}^b_{ac})S_{db}(\theta - i\bar{U}^a_{bc}). \tag{2.4.8}$$

The two constraints (2.4.7) and (2.4.8), similarly to the charge conservation equations (2.4.6a) and (2.4.6b), are therefore equivalent. If the nonzero 3-point couplings and a single S-matrix element, say S_{11}[6], of a given integrable theory are known, then it is possible to construct all the other S-matrix elements by using one of the two bootstrap conditions, (2.4.7) or (2.4.8). The approach, that was used by A. B. Zamolodchikov in his seminal works [19, 20] on perturbed conformal field theories, is to make an ansatz for a single S-matrix element and from that apply the bootstrap to generate new S-matrix elements iteratively. The process should close on a finite number of S-matrix elements reproducing through their poles a particular set of

[6]In this regard the particle 1 has to be 'fundamental' in the sense that we will be discussed in the next section.

particles. In the next section it will be shown how the 'bootstrap philosophy' works for the example first studied in [19].

2.5 Building blocks and minimal S-matrices

The scaling limit of the Ising model taken at the critical temperature $T = T_c$ and zero magnetic field is probably the best-known example of a conformal field theory. It is the $c = 1/2$ conformal field theory ($k = 1$ in the series of minimal models (1.1.1)) describing the propagation of free massless Majorana fermions. Defining by $H_{1/2}$ the action of this theory, it is then possible to perturb it by switching on a magnetic field:

$$H = H_{1/2} + \lambda \int d^2x \sigma(x). \tag{2.5.1}$$

In (2.5.1) σ is the local magnetisation (or spin density) in the scaling limit, while λ is a magnetic field. The renormalization group flow induced by the presence of such a perturbation drags the theory out from the conformal point. The c theorem [51] teaches us that the effective central charge has to decrease along with the RG flow and reaches its minimal value in the infrared limit. Since there is no unitary CFT with $c < 1/2$, the perturbation has to introduce a mass gap and the perturbed theory has to be massive. Even though the conformal symmetry is broken, the trajectory of the renormalization group induced by λ is integrable. In [19, 20] Zamolodchikov argued, based on the counting of dimensions in Virasoro representations, that the perturbed action (2.5.1) supported integrals of motion with (at least) spins

$$s = 1, 7, 11, 13, 17, 19 \tag{2.5.2}$$

(and their negatives $s = -1, -7, -11, -13, -17, -19$), a remnant of the conformal symmetry.

Even though the counting argument implemented by Zamolodchikov is not sufficient to verify the existence of conserved charges for infinitely many spins, it provides enough spins to implement the Parke argument discussed in section 2.2 (which makes complete sense since the deformed theory has to be massive, due to the c theorem). So the factorisation of the S-matrix is ensured. With the additional assumption that all the masses of the deformed theory are different, and the associated S-matrix is therefore purely elastic, Zamolodchikov was able to implement the bootstrap technology previously explained to derive a proposal for the S-matrix and the mass spectrum of the model. This is incredibly surprising since he started only from the knowledge of the existence of conserved charges with spins (2.5.2). In the following we will revisit the steps of [19, 20] that made this construction possible.

Let us start assuming the existence of a massive real particle, that we label by 1 with associated mass m_1 and with a nonzero 3-point coupling $C_{111}^{(3)}$. In this case there is a fusing relation leading to an equilateral triangle in figure 2.8, for which the conservation equation (2.4.6a) becomes

$$\gamma_1^{(s)} e^{is\frac{\pi}{3}} + \gamma_1^{(s)} e^{-is\frac{\pi}{3}} = \gamma_1^{(s)}. \tag{2.5.3}$$

Zamolodchikov worked with the assumption that the particle 1 is 'fundamental', by which we mean that all the other particles can be obtained by initial fusions of 1. This implies that $\gamma_1^{(s)} \neq 0$ for all the conserved charges Q_s that the theory possesses. Indeed, if we suppose that there exists a particular $\tilde{s}$ such that $\gamma_1^{(\tilde{s})} = 0$, then all the particles a propagating in one of the direct or crossed channels of S_{11} need to have $\gamma_a^{(\tilde{s})} = 0$ or the fusing relations (2.4.6) associated with $\tilde{s}$ cannot be satisfied. We can then apply the fusion on the particles a so generated: since 1 is fundamental we can continue fusing generating the eigenvalues of all the other particles. In the end, we would obtain that $\gamma_a^{(\tilde{s})} = 0$ for any particle a of the model. Since by asymptotic completeness any state $|\psi\rangle$ can be written as a superposition of multi-particle states in the in- or out-basis and Q_s acts additively on these states we have

$$Q_{\tilde{s}}|\psi\rangle = 0 \quad \forall \quad |\psi\rangle,$$

having as only solution $Q_{\tilde{s}} = 0$. Therefore $\tilde{s}$ cannot be the spin of a conserved charge. This implies $\gamma_1^{(s)} \neq 0$ for all the spins s of the conserved charges and equation (2.5.3) becomes

$$2\cos\Big(\frac{\pi s}{3}\Big) = 1.$$

It admits as solutions all integers s with no common divisor with 6. These are

$$s = 1, 5, 7, 11, 13, 17, 19, 23, 25, 29 \ldots \tag{2.5.4}$$

and their negatives. We note that the spins found in (2.5.4) are more than is expected from the counting argument in (2.5.2). In particular $s = 5$ has to be excluded since is not present in (2.5.2). This induced Zamolodchikov to enlarge the starting spectrum by adding a further particle with mass $m_2 > m_1$, and to assume two other nonzero couplings: $C_{112}^{(3)}$ and $C_{221}^{(3)}$. If that is the case then the following fusion relations have to hold:

$$\begin{aligned} C_{112}^{(3)} \neq 0 \implies \gamma_1^{(s)} e^{is\bar{U}_{12}^1} + \gamma_1^{(s)} e^{-is\bar{U}_{12}^1} = \gamma_2^{(s)} \\ C_{221}^{(3)} \neq 0 \implies \gamma_2^{(s)} e^{is\bar{U}_{21}^2} + \gamma_2^{(s)} e^{-is\bar{U}_{21}^2} = \gamma_1^{(s)} \end{aligned} \tag{2.5.5}$$

Dividing the first equation by $\gamma_1^{(s)}$ and the second equation by $\gamma_2^{(s)}$ respectively, and multiplying the two we obtain

$$4\cos s\bar{U}_{12}^1 \cos s\bar{U}_{21}^2 = 1. \tag{2.5.6}$$

If we have more than two conserved charges (2.5.6) provides an overdetermined system of equations in $\bar{U}_{12}^1$ and $\bar{U}_{21}^2$. However, for all values of s in (2.5.4) that are not multiples of of 5, it admits the solution

$$\bar{U}_{12}^1 = \frac{\pi}{5} \quad , \quad \bar{U}_{21}^2 = \frac{2\pi}{5}.$$

The remaining angles $\bar{U}_{11}^2$ and $\bar{U}_{22}^1$ (obtained by imposing the sum of the internal

angles of triangles equal to π) are $\frac{3\pi}{5}$ and $\frac{\pi}{5}$ respectively. Then m_2 is determined by

$$m_2^2 = 2m_1^2 - 2m_1^2 \cos(\bar{U}_{11}^2).$$

leading to the 'golden' mass ratio

$$\frac{m_2}{m_1} = 2\cos\frac{\pi}{5}.$$

This is a promising result, that removes all multiples of 5 from the allowed spins; the list (2.5.4) is therefore further reduced to

$$s = 1, 7, 11, 13, 17, 19, 23, 29\ldots \tag{2.5.7}$$

This is now a set that looks in agreement with what we expect from the lower-order spins of the surviving Virasoro currents (2.5.2).

Having imposed the fusing relations on the charges, we now study their effect on the S-matrix. In that regard, a convenient choice of building blocks from which to construct the S-matrix elements is given by

$$(x)_\theta = \frac{\sinh\left(\frac{\theta}{2} + \frac{i\pi x}{2h}\right)}{\sinh\left(\frac{\theta}{2} - \frac{i\pi x}{2h}\right)}, \tag{2.5.8}$$

where h is an integer depending on the theory under consideration. In this case, because we know in advance the final result, we adopt the choice $h = 30$; this is the minimum number making all the arguments x of the building blocks integers. The building blocks (2.5.8) are $2\pi i$-periodic functions that by construction satisfy

$$(x)_{-\theta} = (2h - x)_\theta = (x)_\theta^{-1}.$$

Each S-matrix element S_{ab} constructed as a product over these fundamental blocks is therefore meromorphic on the complex θ plane, $2\pi i$-periodic and unitary, in agreement with (2.3.16) and (2.3.15a). Crossing symmetry is less straightforward and has to be imposed. For each building block $(x)_\theta$ its crossed symmetric partner is $(h - x)_\theta$ for which

$$(x)_{i\pi-\theta} = -(h - x)_\theta. \tag{2.5.9}$$

An S-matrix element S_{ab}, describing the interactions of two particles of types a and b, will be written (up to an overall sign) as the product over certain building blocks

$$S_{ab}(\theta) = \prod_{x\in\Lambda} (x)_\theta, \tag{2.5.10}$$

where Λ is a set of possibly-repeated integers in $[0, h]$. Imposing crossing symmetry (2.3.15b) and making use of (2.5.9) the element $S_{a\bar{b}}$ has then to be

$$S_{a\bar{b}}(\theta) = \prod_{x\in\Lambda} -(h - x)_\theta. \tag{2.5.11}$$

In the special situation in which the particle b is real (i.e. $\bar{b} = b$) the two S-matrices

Figure 2.12: Picture of the building block $(x)_\theta$. For purely imaginary rapidities the sign of $(x)_\theta$ is negative for $\mathrm{Im}\theta < \frac{\pi x}{h}$ and is positive for $\mathrm{Im}\theta > \frac{\pi x}{h}$. The pole region of the physical strip has been represented in units of $\frac{\pi}{h}$ with increasing angles from the left to the right.

in (2.5.10) and (2.5.11) have to be the same, implying that for each $x \in \Lambda$ then $h - x$ has also to be in Λ. In other words S-matrices involving real particles always have blocks coming in pairs $(x)(h-x)$[7]. The overall sign is then fixed in such a way that the residues at the poles come with the correct sign according to their being generated by bound states propagating in the forward or crossed channels. Note that each building block, for purely imaginary rapidity $\theta = iu$ ($u \in [0, \pi]$), is negative if $u < \frac{\pi x}{h}$ and positive if $u > \frac{\pi x}{h}$ as shown in figure 2.12. At the pole the residue is therefore positive and we have

$$(x)_{iu} \sim \frac{2 \sin \frac{\pi x}{h}}{u - \frac{\pi x}{h}}.$$

If there is no more than one building block in the S-matrix, then we expect it corresponds to a particle propagating in the forward (or s) channel, its residue being positive[8]. For multiple building blocks the situation is more complicated: the sign changes each time we cross a building block in the way shown in figure 2.13. The requirement is that poles dividing a negative (on the left) and a positive (on the right) region of the S-matrix correspond to bound states propagating in the forward channel while poles dividing a positive region from a negative one correspond to bound states propagating in the crossed channel. In certain cases blocks appear with even multiplicity, as happens in (2.5.17), where two blocks (at positions 11 and 19) are of type $(x)^2$. In this case, the sign does not change when we cross the block and they do not have an explanation in terms of particles propagating in one of the direct or crossed channels. Their origin is due to certain threshold singularities in loop level Feynman diagrams [39], but we will not go further into that discussion here. We will return to this issue in chapter 7.

Let us now move on with our original discussion. We have indeed defined all the necessary ingredients to start constructing the S-matrix elements of the model described by (2.5.1). We note that $C^{(3)}_{111}$ and $C^{(3)}_{112}$ are both nonzero implying that S_{11} has two poles at $iU^1_{11} = i\frac{2\pi}{3}$ and $iU^2_{11} = i\frac{2\pi}{5}$ corresponding to the propagation in the forward channel of the particles 1 and 2 previously found. Since all the particles are real, the same bound states have also to propagate in the crossed channel, and other two poles are present at $i\bar{U}^1_{11} = i\frac{\pi}{3}$ and $i\bar{U}^2_{11} = i\frac{3\pi}{5}$. Having set $h = 30$

[7]The product between crossed symmetric building blocks $(x)(h-x)$ is often found in literature in the more compact notation $-\frac{\sinh\theta + i\sin(\pi x/h)}{\sinh\theta - i\sin(\pi x/h)}$ or $-\frac{\tanh(\theta/2 + i\pi x/2h)}{\tanh(\theta/2 - i\pi x/2h)}$.

[8]This requirement can fail if the theory is not unitary, but it is not our case. See for example [52].

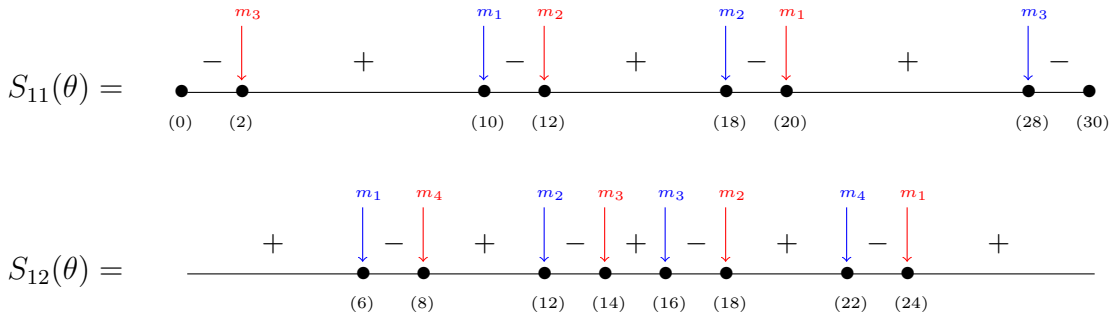

Figure 2.13: Pole structure of S_{11} and S_{12}. Each nontrivial building block corresponds to the propagation of a bound state in the forward (red) or crossed (blue) channel. The masses of the intermediate propagators are indicated above the poles.

then the arguments of the building blocks (corresponding to the pole positions) are represented in units of $\frac{\pi}{30}$ and a reasonable guess for S_{11} is

$$S_{11}(\theta) = (10)(12)(18)(20).$$

However, it turns out that the bootstrap equation

$$S_{11}(\theta) = S_{11}(\theta - i\frac{\pi}{3})S_{11}(\theta + i\frac{\pi}{3}), \tag{2.5.12}$$

coming from setting $a = b = c = d = 1$ in (2.4.7), is not satisfied by this guess. The minimal way to satisfy (2.5.12) is to add a pair of building blocks, (2) and (28), to S_{11} corresponding to the propagation of a further particle. The minimal solution to (2.5.12) is then given by

$$S_{11}(\theta) = -(2)(10)(12)(18)(20)(28). \tag{2.5.13}$$

The overall sign has been set to make all the poles appear with the correct sign of the residues, in agreement with the expected channels of the propagating bound states. Noting that

$$(0) = 1 \quad \text{and} \quad (h) = -1$$

the element in (2.5.13) can also be written as

$$S_{11}(\theta) = (0)(2)(10)(12)(18)(20)(28)(30). \tag{2.5.14}$$

Its pictorial representation is shown in the first line in figure 2.13. The pole at $i\frac{2\pi}{30}$ has to correspond to a particle, say 3 (with $m_3 > m_1$), propagating in the s-channel, for which it holds $U_{11}^3 = i\frac{2\pi}{30}$ and $\bar{U}_{11}^3 = i\frac{28\pi}{30}$. From the presence of this new pole, obtained by requiring the bootstrap relation (2.5.12), the spectrum has to be enlarged so to contain a new particle with mass

$$m_3^2 = 2m_1^2(1 + \cos U_{11}^3)$$

from which we obtain

$$\frac{m_3}{m_1} = 2\cos\frac{\pi}{30}.$$

Having found the masses m_1, m_2 and m_3 (which are defined up to an overall scale) the angles of the triangle Δ_{123}, having as sides m_1, m_2 and m_3, can be determined. They are

$$\bar{U}_{12}^3 = \frac{16\pi}{30} \quad , \quad \bar{U}_{13}^2 = \frac{9\pi}{30} \quad , \quad \bar{U}_{23}^1 = \frac{5\pi}{30}. \tag{2.5.15}$$

Moreover we can now going forward applying the bootstrap. Since $C_{112}^{(3)} \neq 0$ the S-matrix element S_{12} is obtained from (2.5.14) by using (2.4.7) with $a = b = d = 1$ and $c = 2$

$$S_{12}(\theta) = S_{11}(\theta - i\frac{\pi}{5})S_{11}(\theta + i\frac{\pi}{5}) = (6)(8)(12)(14)(16)(18)(22)(24). \tag{2.5.16}$$

Most of the poles of S_{12} are expected. The pair of blocks (6)(24) and (12)(18) corresponds to the propagation of 1 and 2. Similarly the pair (14)(16) corresponds to the propagation of the particle 3 in agreement with the fusing angle $\bar{U}_{12}^3$ found in (2.5.15). This confirms that the coupling $C_{123}^{(3)}$ is not zero and can be used to introduce additional fusing relations between different S-matrix elements. There is just one pair of building blocks that could not have been predicted. It is (8)(22) which introduces an additional particle, that we label by 4. The interested reader can try to go forward and generate new S-matrix elements by applying the fusing relations (2.4.7) inserting from time to time as input the masses and fusing angles obtained from the pole structure predicted by the S-matrices previously generated. For example, it can be checked that

$$S_{13}(\theta) = (1)(3)(9)(11)^2(13)(17)(19)^2(21)(27)(29). \tag{2.5.17}$$

Incredibly in [19, 20] Zamolodchikov discovered that the bootstrap closed within exactly eight particles with the following masses:

$$\begin{aligned} &m_1 && m_5 = 2m_2\cos\frac{2\pi}{15} \\ &m_2 = 2m_1\cos\frac{\pi}{5} && m_6 = \frac{m_2}{m_1}m_3 \\ &m_3 = 2m_1\cos\frac{\pi}{30} && m_7 = \frac{m_2}{m_1}m_4 \\ &m_4 = 2m_2\cos\frac{7\pi}{30} && m_8 = \frac{m_2}{m_1}m_5 \end{aligned} \tag{2.5.18}$$

One of the strongest pieces of evidence that the S-matrix conjectured by Zamolodchikov was the correct one to describe the system in (2.5.1) comes from [23]. In that paper, Klassen and Melzer, by using the thermodynamic Bethe ansatz (TBA) [22][9], recovered the central charge of the unperturbed model $H_{1/2}$ starting from the S-matrix elements described above. Indeed, by putting the theory on a ring of finite length R and taking the ultraviolet limit $R \to 0$, they observed that $\tilde{c}(R) \to 1/2$.

[9] We refer to [53] for a pedagogical introduction to the TBA.

The final set of masses and S-matrix elements obtained by closing the bootstrap have many interesting features. The masses (2.5.18) correspond to the components of the lowest eigenvalue eigenvector of the Cartan matrix of E_8, that we label by $C^{[E_8]}$. This means that, if we define $\boldsymbol{\gamma}^{(1)} = (m_1, \dots, m_8)$, then

$$C^{[E_8]}\boldsymbol{\gamma}^{(1)} = 4\sin^2\frac{\pi}{60}\boldsymbol{\gamma}^{(1)}.$$

Surprisingly the first eight spins (2.5.7) correspond to the exponents of the Lie algebra E_8. For each of them there is an eigenvector of $C^{[E_8]}$ defined by

$$\boldsymbol{\gamma}^{(s)} = (\gamma_1^{(s)}, \dots, \gamma_8^{(s)}),$$

where $\gamma_a^{(s)}$ are the sides of the higher-spin fusing triangles (see figure 2.10), satisfying

$$C^{[E_8]}\boldsymbol{\gamma}^{(s)} = 4\sin^2\frac{\pi s}{60}\boldsymbol{\gamma}^{(s)}.$$

This observation suggests that a generalization should be possible also for other Lie algebras that therefore have to be in correspondence with certain integrable theories. We will return to the deep mathematical aspects of this topic in chapter 5. S-matrices of this type, which do not show any further poles or zeros in addition to those demanded by the bootstrap fusing relations, have been linked in literature with perturbations of certain conformal field theories; a representative example is the one just discussed. These S-matrices are called 'minimal' since they contain only the minimal requirements imposed by the bootstrap, with no additional zeros or poles.

A reason why the mass ratios and the spins (2.5.7) of the theory just discussed might be related to the root system of E_8 can be traced back to the fact that the Ising model at the critical point can be realized in terms of the coset [15, 16]

$$\frac{(E_8)_1 \times (E_8)_1}{(E_8)_2}.$$

Similar constructions are verified for different statistical systems, which have a realization in terms of cosets of the form

$$\frac{\mathcal{G}_1 \times \mathcal{G}_1}{\mathcal{G}_2}, \tag{2.5.19}$$

where $\mathcal{G}$ is a simply-laced Lie algebra. Examples can be found for example in appendices B and C of [54]. The central charge of the CFT constructed from the coset (2.5.19) is given by

$$c = r\left(1 - \frac{h}{(h+2)}\right) \tag{2.5.20}$$

where r and h are the rank and the Coxeter number of the simply-laced Lie algebra $\mathcal{G}$ respectively. Integrable deformations of these CFTs by a suitable operator generate massive theories with minimal S-matrices encoding properties of the Lie algebra $\mathcal{G}$.

More generally in [55, 56] the discussion was extended to cosets of the form

$$\frac{\mathcal{G}_n \times \mathcal{G}_1}{\mathcal{G}_{n+1}} \tag{2.5.21}$$

with central charges given by

$$c = r\Big(1 - \frac{h(h+1)}{(n+h)(n+h+1)}\Big). \tag{2.5.22}$$

In [56] it was argued that integrable deformations of these cosets could be described by affine Toda field theories with imaginary coupling and with underlying Lie algebra $\mathcal{G}$, but for $n > 1$ the associated S-matrices are expected to be non-diagonal.

2.6 Introducing coupling-dependent factors

The minimal S-matrices discussed in the previous section cannot be derived from a Lagrangian using standard Feynman diagram techniques. If that were the case, they should contain a coupling constant g inherited from the interacting part of the Lagrangian: in this way the S-matrices could be perturbatively expanded for small values of g and would reproduce a free theory at the value $g = 0$. However, such a parameter is missing and the minimal S-matrices do not have a perturbative interpretation. A natural question is then how we can introduce a coupling g into these models so that in the limit $g \to 0$ it holds that $S_{ab} = 1$ ($\forall$ types of particles a and b). This can be done by multiplying each building block $(x)_\theta$ of the minimal S-matrices by a factor $(x + B_x)_\theta^{-1}$, where $B_x(g)$ is a certain (in principle x-dependent) function of g satisfying $B_x(0) = 0$. For a certain minimal S-matrix of the form in (2.5.10), its perturbed version will be

$$S_{ab}(\theta; g) = \prod_{x \in \Lambda} \frac{(x)_\theta}{(x + B_x(g))_\theta}. \tag{2.6.1}$$

Each factor $(x + B_x)^{-1}$ introduces a zero at the position $\theta = \frac{i\pi(x+B_x)}{h}$; in the limit $g \to 0$ all the $B_x(g)$ go to zero and the positions of the zeros overlap the positions of the poles so to return a trivial S-matrix. We should now find the set of B_x, one for each building block, that allow for the closure of the bootstrap fusing relations, satisfy crossing symmetry and do not alter the signs of the residues at the poles. In [57] it was discovered that the imposition of such constraints leaves very little freedom on the possible values of B_x which can differ one from another just by a multiplicative sign.

Let $B(g)$ be a function of the coupling, positive for small g, describing the displacement of the zeros from the poles. Below we show how such a displacement-function has to enter into the S-matrix element S_{12} in (2.5.16). Starting with the first building block on the right, which in this case is (24), we need to introduce the zero so that the pole residue at $\theta = i\pi 24/30$ does not change sign. As it happens for the poles, a zero at the position $i\pi x/h$ divides the imaginary axis of the physical strip into

Right Wrong

Figure 2.14: Right and wrong way to introduce the zero (depicted in red) overlapping the pole (depicted in black) of S_{12} in the limit $g \to 0$.

Figure 2.15: Correct way to introduce zeros in S_{12} so that the signs of the residues are left unchanged.

a left region where $(x)^{-1}$ is negative and a right region where $(x)^{-1}$ is positive; its behaviour is the same as that reported in figure 2.12, with the only difference that now $i\pi x/h$ represents the position of a zero. By using this consideration, the zero associated with the pole at $\theta = i\pi 24/30$ needs to approach the pole from the left, as shown on the LHS of figure 2.14 where it is depicted in red; this is the only way to maintain the same ordering of signs as in the minimal S-matrix element S_{12} in figure 2.13. Indeed, approaching the pole from the right we would change the signs around the pole, introducing a forward channel with negative residue. The zero has therefore to be introduced through $(24-B)^{-1}$. On the left of the zero, the sign of the S-matrix becomes positive again (see the LHS of figure 2.14). To avoid changing the sign of the residue of the next pole, located at $i\pi 22/30$, the zero associated with it has to approach $i\pi 22/30$ from the right. In figure 2.15 the positions of the first few zeros are shown. Comparing it with the minimal S-matrix element S_{12} we see that the residues of the poles do not change signs. If we go forward introducing the zeros so to do not alter the sign order around the poles we discover that the non-minimal S-matrix element S_{12} can be written in the form

$$S_{12}(\theta; g) = \{7\}\{13\}\{17\}\{23\}, \tag{2.6.2}$$

where we have introduced the new notation for the building blocks

$$\{x\}_\theta = \frac{(x-1)_\theta (x+1)_\theta}{(x-1+B)_\theta (x+1-B)_\theta} \tag{2.6.3}$$

following the lines of [57]. In that paper, it was observed that all the S-matrices obtained from introducing a coupling dependence in the minimal S-matrices associated with simply-laced Dynkin diagrams (the case discussed in section 2.5 is a particular example where the Dynkin diagram is that of the E_8 Lie algebra) can be written as

$$S_{ab}(\theta; g) = \prod_{\substack{x=1 \\ \text{step } 2}}^{h-1} \{x\}_\theta^{N_{ab}(x)}, \tag{2.6.4}$$

where the non-negative integer coefficients $N_{ab}(x)$ depend on x and on the types of particles $\{a, b\}$. They correspond to the multiplicities of the building blocks $\{x\}$. It is worth saying that the bootstrap constraints, together with the request of preserving the signs of residues at the poles, force these new S-matrices to be written in the form (2.6.4), as noted in [57]. Surprisingly the displacement between poles and zeros is described by a single function $B(g)$, which is the same for all the building blocks. This is a consequence of requiring the closure of the bootstrap fusing relations. These theories enter the class of the so-called affine Toda models and we will discuss them in detail in the second half of this thesis, where we will introduce them through their Lagrangian description.

The new building blocks (2.6.3) have many important properties inherited from the minimal building blocks (2.5.8). They are meromorphic in θ, $2\pi i$-periodic and satisfy

$$\{x\}_{-\theta} = \{2h - x\}_\theta = \{x\}_\theta^{-1}. \tag{2.6.5}$$

Similarly to what happens for the minimal cases the S-matrices constructed using the building blocks (2.6.3) are therefore automatically $2\pi i$-periodic and unitary. The crossing symmetry is satisfied by noting that

$$\{x\}_{i\pi-\theta} = \{h - x\}_\theta.$$

If a building block $\{x\}$ appears in S_{ab} then it can be checked that $\{h-x\}$ is contained in $S_{a\bar{b}}$ so that these modifications of minimal S-matrices are again crossing symmetric. Figure 2.16 shows the first eight S-matrix elements obtained by introducing the required zeros in the E_8 minimal model. Each building block $\{x\}$ is represented by a brick, with vertical faces located at $x-1$ and $x+1$ respectively, the pole positions. The zeros of $\{x\}$ are both in the region inside the brick, indeed for small g it holds that

$$x - 1 < x - 1 + B < x + 1 - B < x + 1.$$

While the zeros can cross one another without changing the sign of the residues at $\theta = i\pi(x \pm 1)/h$, they cannot intersect the poles. In this second case, we would obtain bound state particles generating pole residues with wrong signs. To avoid this situation we require

$$0 < B(g) < 2. \tag{2.6.6}$$

In addition, the same constraint avoids that additional unwanted poles are introduced inside the physical strip [57]. Note also that each building block is invariant by sending B into $2 - B$:

$$\{x\}_{2-B} = \{x\}_B. \tag{2.6.7}$$

Such a property is of course reflected on the S-matrix that becomes trivial not only when $B = 0$ but also when $B = 2$ (in this second case the zero located at $x + 1 - B$ overlaps the pole located on $x - 1$). This property is universally satisfied in all the self-dual affine Toda theories [57]. The dependence of B in terms of the coupling g will be given in section 6.4, where g will be a specific coupling in the Lagrangian.

With the axiomatic construction of S-matrices explained above we conclude this chapter. In the rest of the thesis, the focus will be on Lagrangian aspects of integ-

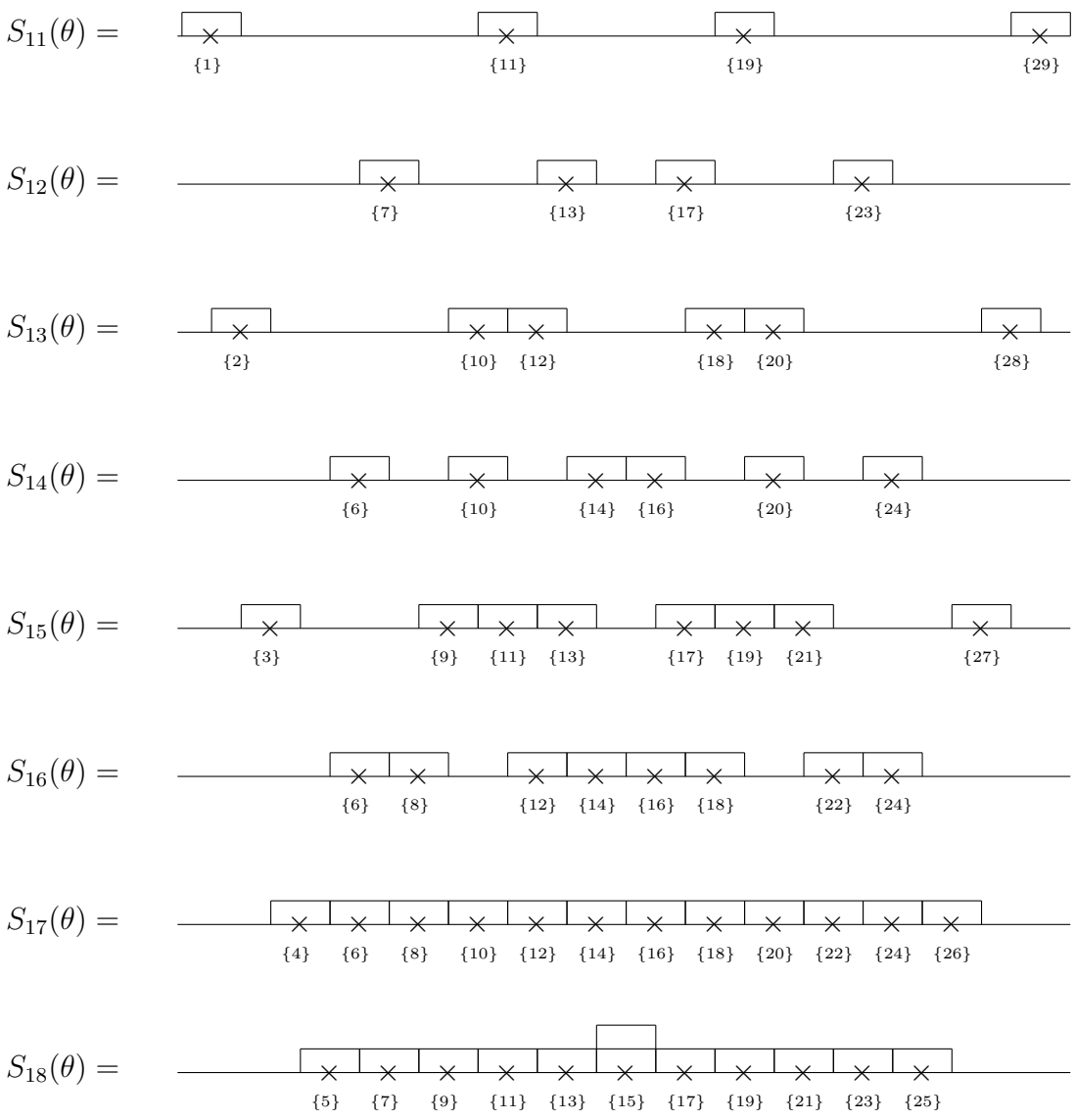

Figure 2.16: First eight S-matrix elements of the $e_8^{(1)}$ affine Toda theory.

rability, from which we will try to rediscover many of the properties presented in the previous sections.

Chapter 3

Perturbative S-matrices and no particle production

3.1 Perturbative simplicity in 1+1 dimensions

The existence of an infinite tower of higher spin conserved charges, responsible for the Yang-Baxter and bootstrap equations, combined with the constraints of crossing and unitarity has led in the past to proposals for the exact S-matrices of many integrable theories in 1+1 dimensions. In the previous sections, some examples of constructions of these S-matrices have been reviewed. The results obtained through this axiomatic procedure can then be checked further using standard perturbation theory, from whose perspective integrability reveals itself in cancellations of sums of Feynman diagrams contributing to production processes. This is what in this thesis will be referred to as 'perturbative integrability', by which is meant the vanishing of all such sums, both at tree level or including all loop diagrams as well. Despite these cancellations being expected in all the massive quantum field theories possessing higher spin conserved charges, their explanation in perturbation theory is mathematically intricate and interesting to understand in its own right. The Lagrangian requirements to make these cancellations possible are generally ill-understood and will be a matter of discussion in the remaining part of this thesis.

The topic can be introduced along the lines of [36], by looking at the simplest example of interacting theory in 1+1 dimensions, $\lambda\phi^4$ [1]. The Lagrangian of the model is

$$\mathcal{L} = \frac{1}{2}\partial_\mu\phi\partial^\mu\phi - \frac{m^2}{2}\phi^2 - \frac{\lambda}{4!}\phi^4 \tag{3.1.1}$$

from which the following Feynman rules can be derived

[1] Early studies of the absence of production in integrable models include [58, 59], which discuss the cancellation mechanism of Feynman diagrams contributing to production processes in the sine-Gordon theory at tree level and at one loop.

Figure 3.1: Different sets of Feynman diagrams in a production process $2\phi \to 4\phi$, depending on if the incoming particles (in red) are directed to the same vertex or different vertices.

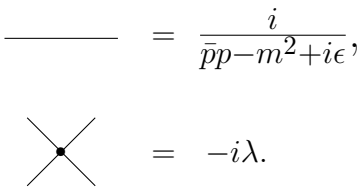

The task is to compute the connected part of the amplitude for the production process $2\phi \to 4\phi$ at the tree level. If the momenta are parametrized using their light-cone components (2.1.2) (where in the present case all the masses are the same), by labelling with a_1 and a_2 the components of the incoming particles and with a_3, a_4, a_5, a_6 the components of the outgoing ones, it is clear that for physical external momenta it needs to be true that $a_i > 0 \ \forall \ i \in \{1, 2, 3, 4, 5, 6\}$. This is a requirement to have all particles with positive energies. For these physical kinematic configurations, the production process $2\phi \to 4\phi$ cannot have internal momenta on-shell. This is easily verified if we split the Feynman diagrams contributing to the process into two different sets characterised as follows: the first set contains Feynman diagrams having both the incoming particles directed to the same vertex, as shown in the first picture in figure 3.1. Contrarily, the second set contains diagrams with the two incoming particles directed to different vertices. This second configuration is shown in the second picture in figure 3.1. Let us suppose that, in a Feynman diagram belonging to the first set, the momentum of the internal propagator is on-shell. In this case, the propagating particle can be directed from left to right or from right to left in the first diagram in figure 3.1. In both cases we end up with a contradiction: if the momentum is directed to the right then the RHS vertex, on the pole, would correspond to a tree-level process $1\phi \to 3\phi$ where all the particles involved are physical and on-shell. Similarly, if the momentum is directed to the left, on the pole we would obtain a tree-level process $3\phi \to 1\phi$ on the LHS vertex. Both of these processes are kinematically forbidden since they do not conserve energy. It is therefore impossible, for any physical choice of the external momenta, to make the internal propagator on-shell in diagrams belonging to the first set in figure 3.1. An analogous discussion can be repeated for the Feynman diagrams in the second configuration implying the impossibility to have, for physical values of the external momenta, poles in a production process $2\phi \to 4\phi$.

To obtain a more symmetric expression for the amplitude, it is convenient to look at the annihilation process $6\phi \to 0$ instead of $2\phi \to 4\phi$. In the end it is clear that

it is possible to generate the amplitude $M_{2\phi\to 4\phi}$ by crossing 4 incoming momenta to outgoing momenta in $M_{6\phi\to 0}$, indeed it holds that $M_{2\phi\to 4\phi}(a_1,a_2,a_3,a_4,a_5,a_6) = M_{6\phi\to 0}(a_1,a_2,-a_3,-a_4,-a_5,-a_6)$. With this in mind, we perform the sum over all the Feynman diagrams with six incoming momenta at the tree level. Since in the production process $2\phi \to 4\phi$ there is no choice of physical external momenta for which internal bound states can go on-shell we can set $i\epsilon = 0$ in all the denominators of propagators so that the amplitude $M_{6\phi\to 0}(a_1,\dots,a_6)$ (in the physical region of external kinematics of $M_{2\phi\to 4\phi}$: $a_1>0, a_2>0, a_3<0, a_4<0, a_5<0, a_6<0$) is given by

$$\sum_\sigma \quad = \frac{-i\lambda^2}{m^2} \sum_\sigma \frac{1}{(a_{\sigma(1)}+a_{\sigma(2)}+a_{\sigma(3)})(a_{\sigma(1)}^{-1}+a_{\sigma(2)}^{-1}+a_{\sigma(3)}^{-1})-1}$$

$$= \frac{-i\lambda^2}{m^2} \sum_\sigma \frac{a_{\sigma(1)}a_{\sigma(2)}a_{\sigma(3)}}{(a_{\sigma(1)}+a_{\sigma(2)})(a_{\sigma(2)}+a_{\sigma(3)})(a_{\sigma(3)}+a_{\sigma(1)})}$$

There is a single master topology, into which the momenta can enter in $\frac{6!}{3!3!2!} = 10$ different ways, each one labelled by a suitable permutation σ and corresponding to a different Feynman diagram.

Note that there are many manners to write the amplitude as a function of $a_1,\dots,a_6$, each one corresponding to a choice of variables used to write the momenta flowing in the intermediate propagators. For a given permutation σ, the propagator connecting the two vertices with incoming momenta $(a_{\sigma(1)},a_{\sigma(2)},a_{\sigma(3)})$ on the left and $(a_{\sigma(4)},a_{\sigma(5)},a_{\sigma(6)})$ on the right can be written both as

$$\frac{a_{\sigma(1)}a_{\sigma(2)}a_{\sigma(3)}}{(a_{\sigma(1)}+a_{\sigma(2)})(a_{\sigma(2)}+a_{\sigma(3)})(a_{\sigma(3)}+a_{\sigma(1)})} \tag{3.1.2}$$

or

$$\frac{a_{\sigma(4)}a_{\sigma(5)}a_{\sigma(6)}}{(a_{\sigma(4)}+a_{\sigma(5)})(a_{\sigma(5)}+a_{\sigma(6)})(a_{\sigma(6)}+a_{\sigma(4)})}. \tag{3.1.3}$$

After imposing the overall conservation of the light-cone components of the momenta

$$\sum_{i=1}^{6} a_i = 0 \quad , \quad \sum_{i=1}^{6} \frac{1}{a_i} = 0 \tag{3.1.4}$$

the two quantities (3.1.2) and (3.1.3) become the same so that the choice adopted to write the propagator in each Feynman diagram is irrelevant. A convenient convention is to do not privilege any of the two choices and to write each propagator as the average of the two. With this prescription, the amplitude is given by

$$M_{6\phi\to 0}(a_1,\dots,a_6) = \frac{-i\lambda^2}{m^2} H(a_1,\dots,a_6) \tag{3.1.5}$$

where

$$H(a_1,\dots,a_6)=\frac{1}{2}\sum_{\sigma}\left(\frac{a_{\sigma(1)}a_{\sigma(2)}a_{\sigma(3)}}{(a_{\sigma(1)}+a_{\sigma(2)})(a_{\sigma(2)}+a_{\sigma(3)})(a_{\sigma(3)}+a_{\sigma(1)})}\right.\\ \left.+\frac{a_{\sigma(4)}a_{\sigma(5)}a_{\sigma(6)}}{(a_{\sigma(4)}+a_{\sigma(5)})(a_{\sigma(5)}+a_{\sigma(6)})(a_{\sigma(6)}+a_{\sigma(4)})}\right). \tag{3.1.6}$$

Remarkably the expression in (3.1.6) is symmetric under any permutation of the variables a_j, and the same property applies separately to its numerator and denominator, defined by

$$H(a_1,\dots,a_6)=\frac{1}{2}\frac{N(a_1,\dots,a_6)}{D(a_1,\dots,a_6)}.$$

This symmetry is manifest in the sum of pictures of the Feynman diagrams. However, it is in general broken once we adopt a particular choice of momenta to write the algebraic expressions of the graphs and is restored only on the kinematical surface conserving the overall energy and momentum. The advantage of using the prescription (3.1.6) is that this symmetry is maintained also if (3.1.4) is not satisfied. This allows us, following the same method of [60], to apply the fundamental theorem of symmetric polynomials on (3.1.6). This theorem states that any symmetric polynomial in n variables $a_1,\dots,a_n$ can be written as a polynomial expression in terms of the elementary symmetric polynomials defined by

$$s_k\equiv\begin{cases}1 & \text{if } k=0\\ \sum_{1\le i_1<\dots<i_k\le n} a_{i_1}\dots a_{i_k} & \text{if } k=1,\dots,n.\end{cases} \tag{3.1.7}$$

In the considered case $n=6$ and with some manipulations it can be shown that

$$N=-2s_3^3s_6+s_3^2s_4s_5+s_1^2s_4^2s_5+s_1s_2^2s_5^2-2s_2s_3s_5^2-6s_1s_4s_5^2+5s_5^3\\ +s_1s_2s_3^2s_6-2s_1^2s_3s_4s_6-6s_1^2s_2s_5s_6+12s_1s_3s_5s_6+5s_1^3s_6^2 \tag{3.1.8}$$

and

$$D=s_3^3s_6+s_1s_2s_3s_4s_5-s_3^2s_4s_5-s_1^2s_4^2s_5-s_1s_2^2s_5^2+s_2s_3s_5^2-s_5^3+\\ 2s_1s_4s_5^2-s_1s_2s_3^2s_6+s_1^2s_3s_4s_6+2s_1^2s_2s_5s_6-3s_1s_3s_5s_6-s_1^3s_6^2. \tag{3.1.9}$$

Despite the expressions (3.1.8) and (3.1.9) are quite complicated, on the kinematical surface satisfying (3.1.4) it holds that $s_1=s_5=0$ and they drastically simplify. Indeed, the only combination of symmetric polynomials different from zero in ((3.1.8),(3.1.9)) is $s_3^3s_6$ so that

$$H(a_1,a_2,a_3,a_4,a_5,a_6)=-1.$$

This implies, in two dimensions, that provided the overall energy and momentum are conserved the amplitude $M_{6\phi\to 0}$, and therefore also $M_{2\phi\to 4\phi}$, is a constant which does not depend on the particular configuration of the external momenta. At this

point, it is tempting to cancel such a constant by adding a properly tuned coupling

$$-\frac{1}{6!}\frac{\lambda^2}{m^2}\phi^6$$

to the starting Lagrangian (3.1.1). In this manner, after such a coupling is introduced, the tree-level production amplitude $M_{2\phi\to 4\phi}$ is identically zero. By defining $g^2 \equiv \frac{\lambda}{m^2}$ the new Lagrangian with both the ϕ^4- and the ϕ^6-interaction is

$$\mathcal{L} = \frac{1}{2}\partial_\mu\phi\partial^\mu\phi - \frac{m^2}{g^2}\left(\frac{g^2}{2}\phi^2 + \frac{g^4}{4!}\phi^4 + \frac{g^6}{6!}\phi^6\right).$$

It is also possible to go forward and calculate the amplitude for the process $2\phi \to 6\phi$. Once again, after a challenging computation, it will be discovered that $M_{2\phi\to 6\phi}$ is a constant that can be cancelled by introducing a proper 8-point coupling. By continuing without stopping to cancel higher- and higher-point processes by introducing new couplings we end up with a well-known integrable Lagrangian, that one of the sinh-Gordon model

$$\mathcal{L}_{ShG} = \frac{1}{2}\partial_\mu\phi\partial^\mu\phi - \frac{m^2}{g^2}\left(\cosh g\phi - 1\right). \tag{3.1.10}$$

The analysis can be repeated in a similar fashion by starting assuming the existence of a cubic interaction. In this case, though the problem is a bit harder, by imposing the absence of production for all processes with even and odd numbers of external legs (note that in the previous case all the processes with odd external legs were automatically zero due to the symmetry $\phi \to -\phi$ of the Lagrangian), the following Bullough–Dodd Lagrangian

$$\mathcal{L}_{BD} = \frac{1}{2}\partial_\mu\phi\partial^\mu\phi - \frac{m^2}{6g^2}\left(e^{2g\phi} + 2e^{-g\phi} - 3\right). \tag{3.1.11}$$

would be obtained. The fact that (3.1.10) and (3.1.11) are the only two possible options arising from imposing absence of production at all orders of external legs for Lagrangians with a single scalar field was already remarked in [36].

One fact deserves a little attention at this point. Previously it was mentioned that the two amplitudes $M_{6\phi\to 0}$ and $M_{2\phi\to 4\phi}$ can be mapped one into the other by just changing the signs of the light-cone components $a_4, \ldots, a_6$. This may sounds a bit suspect in general, since then it needs also to be true that $M_{2\phi\to 4\phi}(a_1, a_2, a_3, a_4, a_5, a_6) = M_{3\phi\to 3\phi}(a_1, a_2, -a_3, a_4, a_5, a_6)$ and therefore the cancellation of $M_{2\phi\to 4\phi}$ should also imply the cancellation of $M_{3\phi\to 3\phi}$. This is actually in contradiction with what is expected in an integrable theory, where a 3-to-3 process should not be zero, but instead it should factorize into the product of 2-to-2 S-matrices as discussed in section 2.2. Where is the mistake? The answer comes from the $i\epsilon$ factors in the denominators of the propagators. In a generic production process, such as $2\phi \to 4\phi$, there is no way for physical external momenta to make the internal propagators on-shell. This implies that the amplitude $M_{2\phi\to 4\phi}(\epsilon)$, with all the ϵ-parameters in place, on the physical external configurations of momenta is equivalent to $M_{2\phi\to 4\phi}(0)$,

the same amplitude obtained by summing Feynman diagrams having set $\epsilon = 0$ in all propagators. Then it is possible to verify that $M_{2\phi\to 4\phi}(0)$ is a function identically zero on all the complex domain of $a_1, \dots, a_6$ (as far as the energy and momentum are conserved), implying that $M_{2\phi\to 4\phi}(\epsilon) = 0$ for any choice of physical external momenta. On the other hand, $M_{3\phi\to 3\phi}(\epsilon)$ can develop poles in its propagators for physical values of the external momenta, and it is not true that ϵ can be set to zero in the Feynman diagrams or infinities in physical processes would be observed. Instead, all propagators have to be considered with the respective $i\epsilon$ factor. After summing over all diagrams, the limit $\epsilon \to 0$ has to be taken. In this limit, the connected part of the 3-to-3 amplitude decomposes into two pieces

$$\lim_{\epsilon\to 0^+} M_{3\phi\to 3\phi}(\epsilon) = M^{fact}_{3\phi\to 3\phi} + M^{prod}_{3\phi\to 3\phi}$$

of which the first corresponds to factorized scattering, and contains additional delta functions of the momenta that force the incoming and outgoing particles to carry the same set of momenta. Instead $M^{prod}_{3\phi\to 3\phi}$ contributes to production processes. This second term is exactly the contribution satisfying the crossing symmetry equality previously discussed: $M^{prod}_{2\phi\to 4\phi}(a_1, a_2, a_3, a_4, a_5, a_6) = M^{prod}_{3\phi\to 3\phi}(a_1, a_2, -a_3, a_4, a_5, a_6)$. At the tree level, such a term is not affected by ϵ and can be obtained by summing all the different Feynman diagrams, imposing $\epsilon = 0$ in all the propagators from the beginning. In a generic quantum field theory M^{prod} can contain singularities for complex kinematics, arising from on-shell propagating particles in internal lines; however, in an integrable model, all such infinities must cancel each other, since otherwise the production amplitude would not vanish[2]. This means that if a certain Feynman diagram is singular for particular values of the external momenta, at least one other diagram is expected to become singular for the same choice of the external momenta in such a way that the infinities cancel, making the total M^{prod} free of singularities. This has to hold at any number of external particles.

In this chapter and the next one, such a problem will be rigorously defined by searching for the necessary and sufficient conditions that have to hold to make these cancellations possible at the tree level. Some of the results covered here have been studied in other literature. The way to constrain the structure of higher-point couplings of general massive two-dimensional quantum field theories by imposing the absence of particle production at the tree level has been studied for example in [37, 63, 64]. In particular, in [37], adopting a particular multi-Regge limit, an explicit condition determining higher-point couplings in integrable theories of multiple massive bosonic fields in terms of the masses and lower-order couplings was found; such condition was then solved for Lagrangians with a single scalar field, leading to the 'rediscovery' of the sinh-Gordon and Bullough-Dodd theories. Such results will be revisited in the next sections. Different open problems, left uncovered in [37], have then been studied in [1] and will be mentioned along with the next sections. Most importantly for this chapter, in [1] is shown that the absence of singularities

[2] An exception happens in massless theories where an expansion around a trivial vacuum generally leads in two dimensions to an IR catastrophe. This generates ambiguities in perturbation theory, and integrable Lagrangians can manifest production at the tree level [61, 62].

in amplitudes imply that they are constant. It is worth also mentioning that the presence of production in the world-sheet scattering has been used to rule out the tree-level integrability for different string theories [60, 65, 66].

The problem that will be addressed can be defined as follows. Let

$$\mathcal{L} = \sum_{a=1}^{r}\left(\frac{1}{2}\partial_\mu\phi_a\partial^\mu\phi_{\bar{a}} - \frac{1}{2}m_a^2\phi_a\phi_{\bar{a}}\right) - \sum_{n=3}^{+\infty}\sum_{a_1,\dots,a_n=1}^{r}\frac{1}{n!}C^{(n)}_{a_1\dots a_n}\phi_{a_1}\dots\phi_{a_n} \tag{3.1.12}$$

be a general Lagrangian for a quantum field theory of r interacting massive scalar fields, possibly with different masses, in two dimensions. The index a in (3.1.12) is a label for the possible types of particles in the model, which correspond to the possible asymptotic states of the theory. The convention $\phi_{\bar{a}} = \phi_a^*$ is adopted. If the component ϕ_a is real, it is assumed $a = \bar{a}$, while if ϕ_a is a complex field $\bar{a}$ represents an index $\in \{1,\dots,r\}$ different from a.[3] In this way, it is taken into account both the case in which the fields in (3.1.12) are real and the one in which they are complex. By assuming the Lagrangian (3.1.12) as a starting point, in the next sections it will be explained how to find the possible sets of masses and couplings for which the theory defined by (3.1.12) is perturbatively integrable at tree level, with a purely elastic S-matrix for 2-to-2 processes.

Before going on, for the sake of clarity, is appropriate to comment a bit more on the conventions adopted. A generic n-point amplitude will be labelled by $M^{(n)}$, which corresponds to the sum over all relevant connected Feynman diagrams without inserting additional normalization factors. Contrarily it will be referred to the S-matrix as the amplitude properly normalized and multiplied by the Dirac delta function of overall energy-momentum conservation. In 2-to-2 elastic processes it holds

$$S_{ab}(p_1,p_2,p_1',p_2') = M^{(4)}_{ab}(p_1,p_2,p_1',p_2')(2\pi)^2\delta^{(2)}(p_1+p_2-p_1'-p_2')A_{legs} \tag{3.1.13}$$

where A_{legs} contains external leg normalization factors; it can be checked that each external particle carries a factor $(\sqrt{4\pi})^{-1}$ so that in this case $A_{legs} = (4\pi)^{-2}$. Then the Dirac delta function of the overall energy-momentum conservation can be expressed in terms of the rapidities; by considering only the kinematical configuration in which the outgoing momenta are equal to the incoming ones then

$$\delta^{(2)}\big(p_1+p_2-p_1'-p_2'\big) = \frac{\delta(\theta_1-\theta_1')\delta(\theta_2-\theta_2')}{m_a m_b\sinh\theta_{12}}. \tag{3.1.14}$$

An additional contribution corresponding to the reflection kinematical configuration is present on the RHS of (3.1.14) but it is omitted here, since $M^{(4)}_{ab}$ is zero on such configurations in purely elastic models. Plugging A_{legs} and (3.1.14) inside (3.1.13)

[3] For example if a theory of two real fields ϕ_1 and ϕ_2 is given, then it has to be considered $\bar{1}=1$ and $\bar{2}=2$ so that the non-interacting part of the Lagrangian is $\frac{1}{2}\partial_\mu\phi_1\partial^\mu\phi_1 + \frac{1}{2}\partial_\mu\phi_2\partial^\mu\phi_2 - \frac{1}{2}m_1^2\phi_1\phi_1 - \frac{1}{2}m_2^2\phi_2\phi_2$. On the other hand if the fields are one the complex conjugate of the other it is assumed $\bar{1}=2$ and $\bar{2}=1$, so that the free Lagrangian is given by $\partial_\mu\phi_1\partial^\mu\phi_{\bar{1}} - m_1^2\phi_1\phi_{\bar{1}}$.

the value of the elastic S-matrix is

$$S_{ab}(\theta) = \frac{M_{ab}^{(4)}(\theta)}{4m_a m_b \sinh\theta}, \tag{3.1.15}$$

where as usual $\theta \equiv \theta_1 - \theta_2$ and the product of Dirac delta functions $\delta(\theta_1 - \theta_1')\delta(\theta_2 - \theta_2')$ has been omitted.

3.2 The logic step by step

Below the steps followed to find the set of masses and couplings making sums of Feynman diagrams contributing to inelastic processes equal to zero are summarized. Here is the logic:

(i) A generic n-point on-shell tree-level amplitude $M^{(n)}$ (by it we mean the production part of the amplitude, which is the sum over Feynman diagrams having set $\epsilon = 0$ in the propagators) is assumed as a starting point; it depends on $n-2$ momentum parameters $a_1, \ldots, a_{n-2}$ (a_{n-1} and a_n are fixed by imposing the momentum conservation constraints), defined as in (2.1.2). By exploiting some universal properties of the amplitude it will be proved that the absence of poles in $M^{(n)}$ (including poles at infinity) implies that such a function is a constant, not depending on the particular choice of $a_1, \ldots, a_{n-2}$. This fact is rather easily-seen if the scattering involves particles with the same mass, since in this case $M^{(n)}$ is a rational function of $a_1, \ldots, a_{n-2}$ and by Liouville's theorem the fact that such a function is bounded implies that it is a constant. This is the case considered in [37]. More work is required if $M^{(n)}$ involves particles with different masses, since after imposing momentum conservation square roots in $M^{(n)}$ are introduced. This second situation was covered later in [1] and will be discussed in section 3.3.

(ii) Then it is possible to proceed inductively by supposing that $M^{(j)}$ is not just constant but zero for $j \in \{5, 6, 7, \ldots, n-1\}$ with $n - 1 \geq 6$; in this case $M^{(n)}$ has to be a constant. Indeed suppose that $M^{(n)}$ has a pole. This corresponds to putting a propagator on-shell as shown in figure 3.2 and factorising the amplitude into two on-shell sub-amplitudes $M^{(m+1)}$ and $M^{(n+1-m)}$. Since $n - 1 \geq 6$, at least one of $M^{(m+1)}$ and $M^{(n+1-m)}$ involves a scattering process of five or more particles and therefore it is equal to zero by the induction hypothesis. Since the residue at the pole is proportional to the product of $M^{(m+1)}$ and $M^{(n+1-m)}$ in the limit in which the k-particle in figure 3.2 goes on shell, the residue goes to zero and no singularity arises. Due to the previous point, the fact that $M^{(n)}$ is free of any singularities implies that such an amplitude is a constant.

(iii) The next step is to determine what constant such an n-point amplitude is equal to, and subsequently tune the next higher point coupling $C^{(n)}_{a_1,\ldots,a_n}$ in (3.1.12) in such a way to cancel that constant. To achieve this the multi-Regge limit defined in [37] should be adopted; it corresponds to a particular kinematical configuration in which most of the Feynman diagrams are suppressed, making the computation of the amplitude particularly simple. In this manner, by imposing that $M^{(n)}$ has to

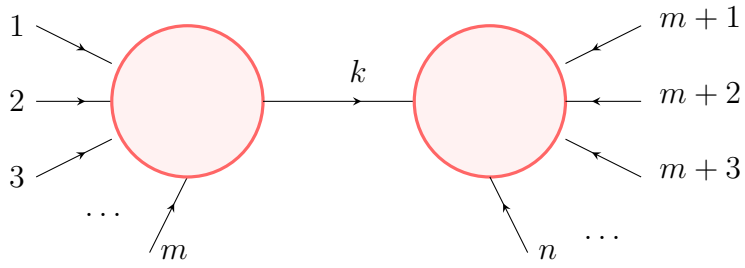

Figure 3.2: The residue of $M^{(n)}$ in the limit in which the k-propagator is on-shell factorises into the product of two amplitudes involving scattering processes of less particles. Since at least one of them is equal to zero for the induction procedure the full amplitude does not present singularities.

vanish, the n-point coupling can be obtained in terms of the masses and the lower point couplings. The method is described in detail in section 3.5 where the technique used in [37] is reviewed. For the sake of clarity it is important to emphasise once again how the induction procedure explained in (ii) and (iii) works in a step by step way. Suppose that the absence of production in 5- and 6-point processes has been proved, which corresponds to have $M^{(5)} = M^{(6)} = 0$. Then as explained above the amplitude $M^{(7)}$ cannot have any poles and, by point (i), is a constant, not depending on the particular choice of the external momenta. Since the choice of the kinematics does not affect the value of the 7-point amplitude it is not restrictive at this point to adopt a particularly simple kinematical configuration to tune the value of the 7-point couplings. In this manner a new amplitude, $M^{(7)}$, can be added to the set of null processes and it holds that $M^{(5)} = M^{(6)} = M^{(7)} = 0$. It is then possible to proceed inductively to all the higher point amplitudes. The relation allowing all the n-point couplings to be found (with $n \geq 5$) in terms of the masses, 3- and 4-point couplings is given in equation (3.5.7), and was first obtained in [37].

(iv) Finally and most importantly the sets of masses, and 3- and 4-point couplings, that ensure the absence of particle production in 5- and 6-point processes, have to be found. They will provide the basis for the induction procedure.

In the rest of this chapter first point (i) is proved (in section 3.3), and then the multi-Regge limit mentioned in (iii) to obtain the recursion relation for higher point couplings is reviewed. This is done in section 3.5. Point (iv), which provides the basis of the entire induction hypothesis, will be covered in chapter 4; that chapter contains part of the results presented in [1]. Defining the set of allowed masses, 3- and 4-point couplings making the induction possible corresponds of defining the space of tree-level integrable theories with a Lagrangian of type (3.1.12). This opens the door to the possibility of classifying integrable models by imposing the absence of production.

3.3 Constant amplitudes from the absence of singularities

Let us consider the scattering of n particles that by convention we assume to be all incoming, with possibly-different masses. Written in the light cone components (2.1.2), the constraints of overall energy-momentum conservation are

$$\sum_{i=1}^{n} m_i a_i = 0, \tag{3.3.1a}$$

$$\sum_{i=1}^{n} \frac{m_i}{a_i} = 0. \tag{3.3.1b}$$

In the following, $a_1, \ldots, a_{n-2}$ are kept as independent variables, while a_{n-1} and a_n are written as functions of them by using (3.3.1). The constraint (3.3.1a) can be used to write a_{n-1} as a negative linear combination of the other light cone components; therefore by substituting its expression into (3.3.1b) a quadratic equation for a_n is generated. If we solve this equation two different solutions for a_n are obtained, differing from one another for a square root quantity coming with opposite sign in the two solutions. Due to the structure of the constraints (3.3.1), it is not difficult to check that the argument of the square root is a homogeneous polynomial, that will be called $S^{(2n-4)}$, of order $2n-4$ in the variables $a_1, \ldots, a_{n-2}$, where n is the number of scattered particles. Moreover $S^{(2n-4)}$ is a polynomial of order four in each one of the a_j, with $j \in \{1, \ldots, n-2\}$. Let us consider for example the scattering of 5 particles. In that case $S^{(2n-4)} = S^{(6)}$ is a homogeneous polynomial of order six in a_1, a_2, a_3; possible terms of order six admitted in $S^{(6)}$ are $a_1^2 a_2^2 a_3^2$ or $a_1^4 a_2 a_3$ while $a_1^5 a_2$, though it is of order six, is not an admitted term since it is of order 5 in a_1; indeed, for any n, $S^{(2n-4)}$ is a polynomial of order four in each one of its variables, so that powers of the a_js bigger than four are not admitted.

Without imposing the overall energy-momentum conservation there are many different ways to write an n-point amplitude, corresponding to different rational functions in $a_1, \ldots, a_n$. However, no matter the initial rational function in $a_1, \ldots, a_n$ is chosen, on the kinematical surface conserving the total energy and momentum the amplitude becomes a uniquely defined function of the form

$$M^{(n)}(a_1, \ldots, a_{n-2}) = \frac{Q_1^{(N)} + Q_2^{(N+2-n)} \sqrt{S^{(2n-4)}}}{Q_3^{(N)} + Q_4^{(N+2-n)} \sqrt{S^{(2n-4)}}}. \tag{3.3.2}$$

The different quantities in the numerator and denominator on the RHS of (3.3.2) are homogeneous polynomials in the variables $a_1, \ldots, a_{n-2}$ of degree indicated in their superscripts. For example, $S^{(2n-4)}(\lambda a_1, \ldots, \lambda a_{n-2}) = \lambda^{2n-4} S^{(2n-4)}(a_1, \ldots, a_{n-2})$. The number of particles involved in the scattering is indicated by the lowercase letter n, while the capital letter N depends on n and the number of Feynman diagrams contributing to the process and it is a generic positive integer. It is worth mentioning that the total amplitude, due to the Lorentz invariance of the Lagrangian (3.1.12), does not scale under a global transformation $a_j \to \lambda a_j$. This fact is guaranteed by

the matching between the degrees of the different polynomials in (3.3.2). Note also that in principle the amplitude is not a single-valued function for a particular choice of $a_1, \ldots, a_{n-2}$, but instead has two branches of solutions that correspond to taking the positive or negative sign in front of the square root term $\sqrt{S^{(2n-4)}}$. The two signs correspond to the two possible kinematical configurations obtained solving the constraints (3.3.1) in terms of a_{n-1} and a_n.

In the special situation in which the n- and $(n-1)$-particle are of the same type, a symmetry is present in the two solutions obtained by imposing energy-momentum conservation; they can be mapped one into the other by exchanging a_n and a_{n-1}. Since the amplitude is also symmetric under this transformation, it has to be invariant by mapping one branch into the other. The effect of this is that the two polynomials $Q_2^{(N+2-n)}$ and $Q_4^{(N+2-n)}$ in front of the square root terms in (3.3.2) have to be zero. Such situation, in which the amplitude continues to be rational also on the kinematical region satisfying the conservation constraints, has been analysed in [37]. In that paper, the authors discussed how proving the absence of poles in $M^{(n)}$ is equivalent to proving that it is a constant. Indeed the only rational function without any poles is a polynomial; moreover, the only polynomial in $a_1, \ldots, a_{n-2}$ invariant under a scaling $a_j \to \lambda a_j$ is a constant. A bit more tricky is the case in which the masses are different. In this case the square root could actually be present in (3.3.2) and Liouville's theorem cannot be directly applied to show that $M^{(n)}$ is a constant. In this more general scenario, a further step is required to prove the triviality of the amplitude and it is explained below following the argumentation of [1].

Let $a_1 = z$ be an independent free parameter and $a_2, \ldots, a_{n-2}$ be fixed in (3.3.2). For fixed values of $a_2, \ldots, a_{n-2}$, the term $S^{(2n-4)}(z, a_2, \ldots, a_{n-2})$ appearing in the square root, as previously mentioned, is a polynomial of order four in z; it is therefore proportional to

$$S(z) = (z - z_1)(z - z_2)(z - z_3)(z - z_4), \tag{3.3.3}$$

where z_1, z_2, z_3 and z_4 are four branch points depending on the particular values of $a_2, \ldots, a_{n-2}$. This makes $M^{(n)}$ a rational function of the two arguments z and $\sqrt{S(z)}$. The branch cuts of $\sqrt{S(z)}$ can be chosen to be any copy of non-intersecting segments connecting the branch points in pairs. For example, one branch cut can be set by connecting z_1 with z_2 and the other one by connecting z_3 with z_4. If we circle around the branch points we move from one cover of the complex plane, corresponding to one kinematical solution of the energy-momentum conservation (3.3.1), to a second one on which the sign of $\sqrt{S(z)}$ is flipped. The domain of the amplitude is therefore a two-sheeted covering of $\mathbb{C}$, Σ_1 and Σ_2, each one corresponding to one of the two kinematical configurations obtained by solving (3.3.1). If now the cuts are opened and the point at infinity is added it is possible to see that the double cover of the complex plane is homeomorphic to a torus, with Σ_1 and Σ_2 corresponding to the two halves of the doughnut. All this comes from standard considerations on Riemann surfaces as described for example in [67]. In appendix A a detailed map from such double cover of the complex plane to the torus is reported; the derivation follows an argument that can be found in [68].

In conclusion, if the amplitude does not have any singularities in a_1 in both the

Riemann sheets, no matter the choice of $a_2, \ldots, a_{n-2}$, then Liouville's theorem applies on the torus and the amplitude has to be a constant in the variable a_1. Repeating the previous analysis one variable at a time we conclude that if $M^{(n)}$ is completely free of singularities, both at finite values of the momenta and at infinity, then

$$\frac{\partial}{\partial a_1} M^{(n)}(a_1, \ldots, a_{n-2}) = \frac{\partial}{\partial a_2} M^{(n)}(a_1, \ldots, a_{n-2}) = \ldots = \frac{\partial}{\partial a_{n-2}} M^{(n)}(a_1, \ldots, a_{n-2}) = 0.$$

Therefore a necessary and sufficient condition an amplitude has to satisfy to be constant is to have a bounded absolute value. In this way point (i) is proved.

The fact that the Riemann surface Λ over which the amplitude is defined has the topology of a torus ensures that there exists a map between such a torus to Λ making the amplitude single-valued on the doughnut. In appendix A a parametrization on the torus is explicitly written using the Weierstrass $\wp$ elliptic function; it is possible applying this map by using other elliptic functions. In the next section, it will be explained how this map can be realised in a simple example using the Jacobi function sn. From it, we derive the elastic scattering as the limiting case in which the torus becomes degenerate.

3.4 Elastic scattering from degenerate doughnuts

A useful exercise to check that things go as expected is to parameterize a four-point inelastic scattering on a torus and recover the case in which the initial and final masses are equal in a second time. In the limit in which the initial and final particles are equal, we find that the torus over which the amplitude is a single-valued meromorphic function becomes degenerate. In such a limit it splits into two separate regions, over which the amplitude is still meromorphic, but cannot anymore be analytically continued from one region to the other by circling around the branch points. The two values of the amplitude over these two separate regions correspond to two distinct functions that represent respectively a transmission and a reflection process.

The scattering process (2.3.1) is now considered, assuming that the initial and final states are different: $\{a, b\} \neq \{c, d\}$. Using the already-defined Mandelstam variables in (2.3.3) and considering the external particles on-shell, in two dimensions the values of t and u can be completely fixed in terms of s

$$\begin{aligned} t &= \frac{m_a^2 + m_b^2 + m_c^2 + m_d^2 - s}{2} + \frac{(m_a^2 - m_b^2)(m_d^2 - m_c^2) - \Sigma(s)}{2s} \\ u &= \frac{m_a^2 + m_b^2 + m_c^2 + m_d^2 - s}{2} + \frac{(m_a^2 - m_b^2)(m_c^2 - m_d^2) + \Sigma(s)}{2s}. \end{aligned} \tag{3.4.1}$$

In the expressions above Σ is a double-valued function of s

$$\Sigma(s) = \sqrt{(s - s_1)(s - s_2)(s - s_3)(s - s_4)} \tag{3.4.2}$$

presenting two Riemann sheets. The branch point positions are given by

$$s_1 = (m_a + m_b)^2 \ , \ s_2 = (m_a - m_b)^2 \ , \ s_3 = (m_c + m_d)^2 \ , \ s_4 = (m_c - m_d)^2.$$

The branch cuts can be fixed along the two segments on the real axis of the s plane connecting s_1 with s_3 and s_2 with s_4. Then Σ is defined over a double cover of the complex plane and we can move from one to the other sheet over which Σ takes values by rotating by 2π around the branch points. To study an elastic process the limit in which the lengths of the branch cuts shrink to zero is taken; it corresponds to $m_d \to m_a$ and $m_c \to m_b$, in such a way as to close the tunnels between the two Riemann sheets. To this end, it is helpful adopting the following values of the masses given by

$$m_a = \mu \cos\alpha \quad , \quad m_b = \mu \sin\alpha$$

and

$$m_c = \mu \sin\beta \quad , \quad m_d = \mu \cos\beta.$$

In the limit $\beta \to \alpha$, the same values for the initial and final masses are obtained, moreover, with these special values of the masses, it holds $m_a^2 + m_b^2 = m_c^2 + m_d^2 = \mu^2$. Therefore if the change of variable

$$s = m_a^2 + m_b^2 + 2m_a m_b y,$$

is made then, by defining $\lambda = \frac{m_a m_b}{m_c m_d}$, the relation (3.4.2) can be expressed in terms of y

$$\Sigma(y) = 4m_a m_b m_c m_d \sqrt{(1-y^2)(1-\lambda^2 y^2)}. \tag{3.4.3}$$

By looking at (3.4.3) the argument under square root should be recognized as a known expression appearing in Jacobi elliptic functions. Using a Schwarz–Christoffel transformation defined by

$$\xi(y) = \int_0^y \frac{dt}{\sqrt{(1-t^2)(1-\lambda^2 t^2)}}. \tag{3.4.4}$$

the entire complex plane, over which y takes values, can be mapped into a rectangle composed of points ξ. For each $y \in \mathbb{C}$ there are two possible values for $\xi(y)$ depending on the Riemann sheet over which the function $w(y) = \frac{1}{\sqrt{(1-y^2)(1-\lambda^2 y^2)}}$ is integrated over. Integrating over the sheet where $w(0) = 1$ the entire complex plane is mapped into the red rectangle in figure 3.3. The branch points, corresponding to the values of y at which w is singular, are mapped into the bullets located on the frame of the red rectangle. Similarly by performing the integration (3.4.4) over the surface on which $w(0) = -1$ and translating by a λ dependent parameter $2\omega_1$ we map the second cover of $\mathbb{C}$ into the blue rectangle in figure 3.3. The union of the red and blue rectangles corresponds to a torus having periodicity along the real and imaginary axes given by $4\omega_1$ and $2\omega_2$ respectively, where the quantities ω_1, ω_2 depend on the ratio λ between the masses. The function Σ is not single-valued on $\mathbb{C}$, but is a meromorphic function on the torus. If we want to map back to the double cover of the complex plane from the torus we need to invert the integral expression (3.4.4).

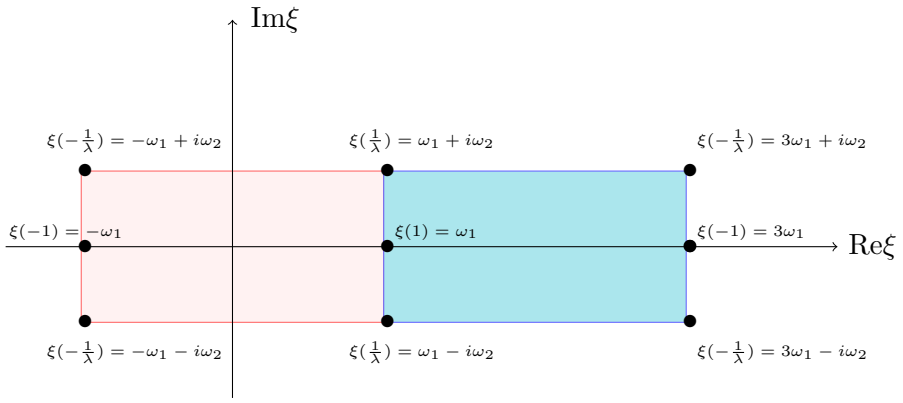

Figure 3.3: Torus surface over which the 4-point amplitude takes values. The red and blue regions correspond to the two different kinematical configurations obtained by solving the momentum conservation constraints and are the two halves of the torus.

This generates a known function in complex analysis known as Jacobi elliptic sine $\mathrm{sn}(x, \lambda^2)$. We can parametrize $y = \mathrm{sn}(x, \lambda^2)$, then for each $y \in \mathbb{C}$ there are two values of x, x_r taking value on the red rectangle, and x_b lying on on the blue rectangle, such that $\mathrm{sn}(x_r, \lambda^2) = \mathrm{sn}(x_b, \lambda^2) = y$. On the other hand, the Jacobi sine satisfies the following differential equation

$$(y')^2 = (1 - y^2)(1 - \lambda^2 y^2).$$

so that at the point x_r and x_b at which y takes the same value it holds $y'(x_r) = -y'(x_b)$. It is clear now why Σ is meromorphic on the torus; up to the multiplicative factor $4m_a m_b m_c m_d$ it is exactly the derivative of the Jacobi sine function, so that the Mandelstam variables can be entirely parametrized in terms of $\mathrm{sn}(x, \lambda^2)$ and $\mathrm{sn}'(x, \lambda^2)$, with x taking values on the two halved of the torus in figure 3.3, each one corresponding to a cover of $\mathbb{C}$.

To obtain the degenerate limit in which the initial and final masses are the same, the parameter λ is sent to one from the left, $\lambda \to 1^-$. In this limit, the quantity ω_1 tends to infinity and the red and blue regions in figure 3.3 become infinite far away from one another. This is the case in which the branch points collide in pairs $s_3 = s_1$, $s_4 = s_2$ and Σ reduces to

$$\Sigma(s) = \pm(s - s_1)(s - s_2). \tag{3.4.5}$$

The two disjoint red and blue regions on the torus correspond to the different choices of sign in (3.4.5); once a sign is chosen, it is not possible to move to the region with the opposite sign since the branch cuts have collapsed to points and the torus has become degenerate. The limit $\lambda \to 1$ corresponds to the special case in which Jacobi elliptic functions reduce to hyperbolic functions. In this situation, one of the

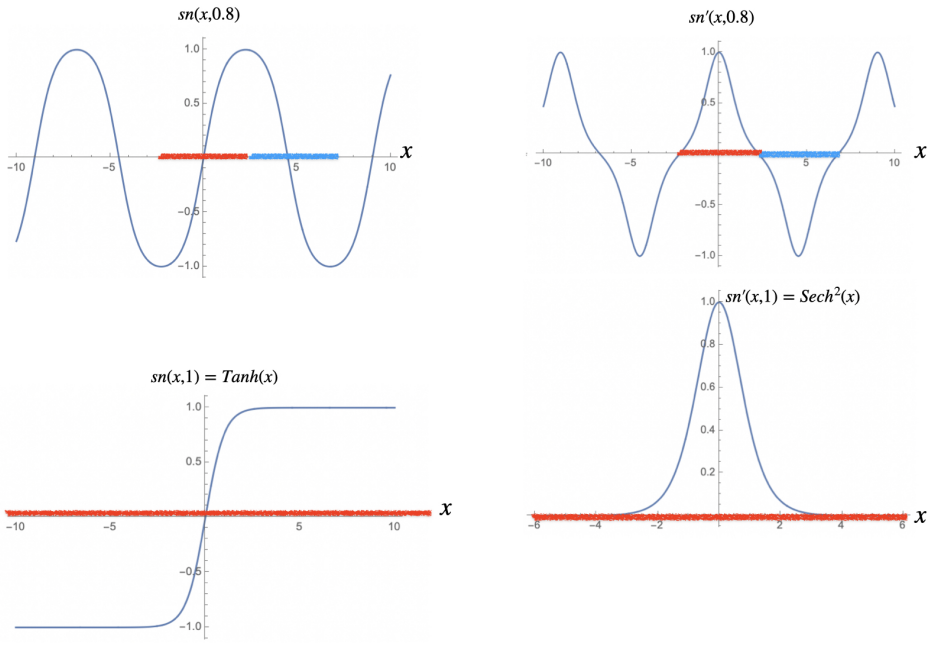

Figure 3.4: Example of Jacobi elliptic function $\mathrm{sn}(x, \lambda^2)$ and its derivative, plotted for real values of x. In the first row, the red and blue segments correspond to the intersection of the red and blue regions of the torus in figure 3.3 with the real axis. Approaching λ^2 to one, as shown in the second row, we push the blue part infinitely far away, and the Jacobi elliptic functions become hyperbolic functions defined over half of the torus.

two doughnut periodicities (that one along the imaginary axis) is preserved while the other one becomes infinite. In figure 3.4 an example of degeneracy is shown by plotting the functions $\mathrm{sn}(x,\lambda^2)$ and $\mathrm{sn}'(x,\lambda^2)$ for real values of x. It is possible to see that in the particular situation in which $\lambda = 1$ the red half part of the torus occupies the entire x axis not leaving the possibility to pass in a continuous way to the blue part of the doughnut. To do that it would be necessary to flip the sign in (3.4.5) which corresponds of sending $\mathrm{sn}'(x,1) = \mathrm{Sech}^2(x) \to -\mathrm{Sech}^2(x)$.

The red and the blue regions correspond to the two kinematical configurations in which transmission and reflection occur. In the first situation the scattering is elastic; it is the case in which the initial and final sets, (a,b) and (d,c), are the same and both carry the same momenta ($p_4 = p_1, p_3 = p_2$). In this configuration the Mandelstam variable u is equal to zero while $t = 2m_a^2 + 2m_b^2 - s$, reducing to the limiting case in (2.3.4). If the theory is integrable, the amplitude in this region does not have to be zero since the scattering conserves all the quantum numbers. Contrarily the blue half part of the degenerate torus corresponds to a reflection process in which the incoming and outgoing particles have different momenta. This is the region in which the amplitude (that is not the same function defined on the red cover, since we cannot analytically continue from one domain to the other) is expected to be zero and where all the singularities coming from different Feynman diagrams should cancel.

Having proved that the absence of poles implies a constant amplitude, it is possible now to move on to find the constraints on the masses and couplings leading to perturbative integrability at tree level. Point (ii) in section 3.2 was already discussed and does not need further study. It is based on the consideration that once a certain number of zero amplitudes $M^{(5)} = M^{(6)} = \cdots = M^{(n-1)} = 0$ has been set by having properly tuned the masses and the couplings $(C^{(3)}, C^{(4)}, \ldots, C^{(n-1)})$ in (3.1.12), the next n-point coupling is uniquely fixed by requiring the corresponding n-point scattering process to be zero. This mechanism and its first steps were discussed in [36] but it was only in [37] that it was explained how to handle the problem to all orders, making use of a particular multi-Regge limit of the amplitude. In the next section, a review of the analysis carried out in [37] will be performed, through which the higher point couplings will be found one by one; this is the content of point (iii) in the logic summarized in section 3.2.

3.5 The multi-Regge limit

To find a condition on the n-point coupling a particular multi-Regge limit has to be adopted; in such limit, one particle is assumed to be at rest while $n-3$ particles are taken to be extremely energetic with increasing energies

$$a_1 = 1 \quad \text{and} \quad a_j = -x^{j-2} \quad \text{for} \quad j = 3, \ldots, n-1 \tag{3.5.1}$$

where $x \gg 1$. By convention, it will be assumed that all the momenta are incoming. Imposing momentum conservation, the remaining two momenta, on one of the two

branches of solutions, are

$$a_2 = -\frac{m_2}{m_1} + o(x^{-1}) \quad \text{and} \quad a_n = \frac{m_{n-1}}{m_n} x^{n-3} + \frac{m_{n-2}}{m_n} x^{n-4} + \ldots + \frac{m_3}{m_n} x + o(x^0). \tag{3.5.2}$$

In a tree-level scattering process, any internal propagator inside a Feynman diagram splits the external particles into two subsets. On one side there is a subset $\alpha \subset \{1, \ldots, n\}$ while on the other side is its complement. If the a_j are chosen as in (3.5.1), (3.5.2), the only nonzero propagators in the limit $x \to \infty$ are those that divide the diagram into subsets $\{1, 2, \ldots, k\}$ and $\{k+1, \ldots, n-1, n\}$, since in all other cases the momentum transferred diverges. In particular if a propagator $G_a(\alpha)$ of a particle of type a, splitting a diagram into a subset α and its complement, is considered, then it holds

$$\begin{aligned} G_a(\alpha) &= \frac{i}{(\sum_{j\in\alpha} m_j a_j)(\sum_{j\in\alpha} \frac{m_j}{a_j}) - m_a^2 + i\epsilon} \\ &\to \begin{cases} -\frac{i}{m_a^2} & \text{if } \alpha = \{k+1, \ldots, n-1, n\} \quad (\text{or equivalently } \alpha = \{1, 2, \ldots, k\}), \\ 0 & \text{otherwise.} \end{cases} \end{aligned} \tag{3.5.3}$$

Therefore in this limit, the only surviving tree-level diagrams are chains with all the particles ordered from left to right as shown in figure 3.5 . Any nonzero diagram contributes with a factor $(-i)^{V+P}$ where V is the number of vertices and P is the number of propagators; moreover any time a propagator connects two vertices a sum over all the possible propagating particles has to be taken.

The scattering of 5 particles in this limit is discussed as a starting example. The types of the particles are labelled with the letters $b_1, \ldots, b_5$, and the parameters of the light cone components of their momenta are defined as in (2.1.2) with the letters $a_1, \ldots, a_5$. Proving that such an amplitude is a constant is not trivial, and finding the conditions on the masses, 3- and 4-point couplings making this possible will be the concern of the next chapter. But if it is assumed that they have been tuned in such a way that the conditions hold, and therefore $M^{(5)}_{b_1 b_2 b_3 b_4 b_5}$ is a constant not depending on the external momenta, then the multi-Regge limit (3.5.1), (3.5.2) can be used to find the value of this constant. As already explained, in this limit only Feynman diagrams corresponding to ordered chains survive, and the value of the amplitude can be read from the first (blue) row in figure 3.5

$$M^{(5)}_{b_1 b_2 b_3 b_4 b_5} \simeq \sum_i \frac{C^{(4)}_{b_1 b_2 b_3 \bar{i}} C^{(3)}_{i b_4 b_5}}{m_i^2} - \sum_{i,j} \frac{C^{(3)}_{b_1 b_2 \bar{i}} C^{(3)}_{i b_3 \bar{j}} C^{(3)}_{j b_4 b_5}}{m_i^2 m_j^2} + \sum_i \frac{C^{(3)}_{b_1 b_2 \bar{i}} C^{(4)}_{i b_3 b_4 b_5}}{m_i^2} - C^{(5)}_{b_1 b_2 b_3 b_4 b_5}. \tag{3.5.4}$$

The equality (3.5.4) is valid up to an overall multiplicative factor containing a power of the imaginary unit coming from vertices and propagators. By requiring that the 5-point process (3.5.4) is zero, for any choice of types $\{b_1, b_2, b_3, b_4, b_5\}$, the values of the 5-point couplings $C^{(5)}_{b_1 b_2 b_3 b_4 b_5}$ are fixed in terms of the masses and the 3- and 4-point couplings. Once it has been proved that all 5-point processes are null one can move to $M^{(6)}$. Once again the six-point amplitudes could in principle depend

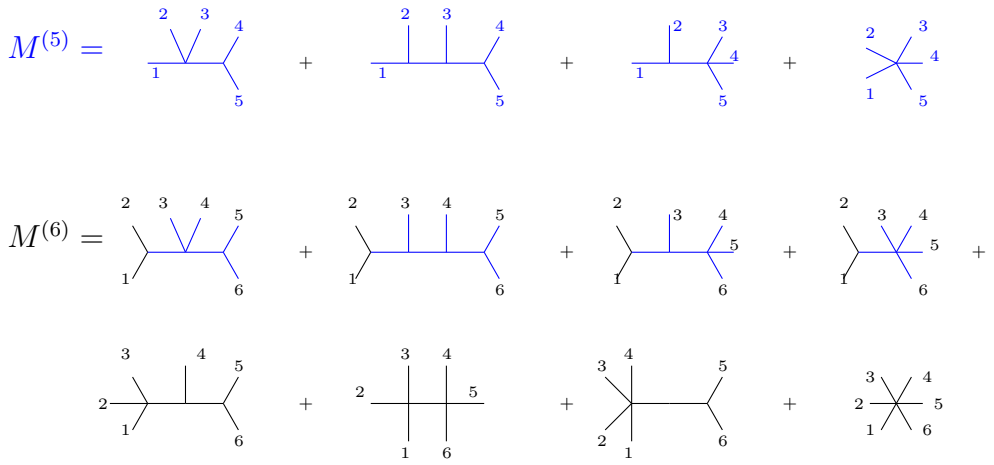

Figure 3.5: Nonzero diagrams contributing to a 5- and a 6-point process in the multi-Regge limit. In the result for $M^{(6)}$ it is contained the amplitude $M^{(5)}$; such amplitude is depicted in blue.

on the external kinematics adopted and it will be a matter of the next chapter to check the conditions for a six-point amplitude to be a constant. However if $M^{(6)}$ is assumed to be independent on the external momenta, then the values of 6-point couplings can be fixed by making these amplitudes equal to zero. Let $b_1, \dots, b_6$ be the labels for the external particles and $a_1, \dots, a_6$ be their momentum-parameters, defined as in (3.5.1), (3.5.2). Then the value of $M^{(6)}_{b_1 b_2 b_3 b_4 b_5 b_6}$ is given by summing over all the Feynman diagrams in which the external legs are ordered, as recorded in the second and third rows in figure 3.5. The algebraic expression for this sum is

$$M^{(6)}_{b_1 b_2 b_3 b_4 b_5 b_6} \simeq \sum_a \frac{C^{(3)}_{b_1 b_2 \bar{a}}}{m_a^2}\left[\sum_i \frac{C^{(4)}_{ab_3 b_4 \bar{i}} C^{(3)}_{ib_5 b_6}}{m_i^2} - \sum_{i,j} \frac{C^{(3)}_{ab_3 \bar{i}} C^{(3)}_{ib_4 \bar{j}} C^{(3)}_{jb_5 b_6}}{m_i^2 m_j^2} + \sum_i \frac{C^{(3)}_{ab_3 \bar{i}} C^{(4)}_{ib_4 b_5 b_6}}{m_i^2} - C^{(5)}_{ab_3 b_4 b_5 b_6}\right]$$
$$+ \sum_{i,j} \frac{C^{(4)}_{b_1 b_2 b_3 \bar{i}} C^{(3)}_{ib_4 \bar{j}} C^{(3)}_{jb_5 b_6}}{m_i^2 m_j^2} - \sum_i \frac{C^{(4)}_{b_1 b_2 b_3 \bar{i}} C^{(4)}_{ib_4 b_5 b_6}}{m_i^2} - \sum_i \frac{C^{(5)}_{b_1 b_2 b_3 b_4 \bar{i}} C^{(3)}_{ib_5 b_6}}{m_i^2} + C^{(6)}_{b_1 b_2 b_3 b_4 b_5 b_6}. \tag{3.5.5}$$

We note that the expression returned in (3.5.5) is not completely new. Indeed the blue part in (3.5.5), that matches the blue pictures in the second row of figure 3.5, is exactly the value of a 5-point amplitude in the multi-Regge limit. Since the 5-point couplings have already been tuned in such a way to make such part null, the blue terms in (3.5.5) can be ignored and the constraint on the six-point couplings to have a theory with null processes with six external legs can be obtained by imposing that the second row in (3.5.5) is equal to zero.

It is worth mentioning that the values of momenta entering into the 5-point process in the first row in figure 3.5 are all on-shell since all the momenta are associated with external particles. On the other hand, the amplitude $M^{(5)}$ that can be read as the blue expression in the second row of figure 3.5 is off-shell since one of the momenta (let us call it P) is flowing in an internal propagator and satisfies $P^2 = 0$ due to the

multi-Regge limit with six external legs. Despite this fact, the value of the off-shell 5-point amplitude appearing inside $M^{(6)}$, where the external parameters have been fixed to be in the multi-Regge limit according with (3.5.1) with $n = 6$, is exactly the same as the value of the on-shell amplitude $M^{(5)}$ verifying the multi-Regge limit with $n = 5$. This consideration, deriving from the fact that for $x \gg 1$ the Minkowski norm of momenta flowing inside propagators can only be zero or infinity, allows us to identify in a generic n-point amplitude all the k-point amplitudes, with $k < n$, that have already been derived in the previous steps. In principle these amplitudes are off-shell, but as an effect of this multi-Regge limit, their values are the same as if they are on-shell in a multi-Regge limit with fewer external particles. For example, the value of a 7-point amplitude in this high energy limit, up to an overall factor, is

$$\begin{aligned} M^{(7)}_{b_1\dots b_7} \simeq & \sum_a \frac{C^{(3)}_{b_1 b_2 \bar{a}}}{m_a^2} M^{(6)}_{a b_3 \dots b_7} + \sum_a \frac{C^{(4)}_{b_1 b_2 b_3 \bar{a}}}{m_a^2} M^{(5)}_{a b_4 \dots b_7} \\ & + i \sum_{i,j} \frac{C^{(5)}_{b_1 b_2 b_3 b_4 \bar{i}} C^{(3)}_{i b_5 \bar{j}} C^{(3)}_{j b_6 b_7}}{m_i^2 m_j^2} - i \sum_i \frac{C^{(5)}_{b_1 b_2 b_3 b_4 \bar{i}} C^{(4)}_{i b_5 b_6 b_7}}{m_i^2} - i \sum_i \frac{C^{(6)}_{b_1 b_2 b_3 b_4 b_5 \bar{i}} C^{(3)}_{i b_6 b_7}}{m_i^2} + i C^{(7)}_{b_1 \dots b_7}. \end{aligned} \tag{3.5.6}$$

Once again the first two contributions on the RHS of (3.5.6) contain respectively a 6- and 5-point process in their multi-Regge limit and have to be zero by the previous analysis. The constraint on the 7-point coupling is therefore derived by setting to zero the second row of (3.5.6).

With these preliminaries over, the general Lagrangian in (3.1.12) can be constructed by induction. The couplings up to $C^{(n-1)}_{b_1 \dots b_{n-1}}$ are assumed to be known and are tuned so as to set the amplitudes $M^{(5)} = M^{(6)} = \dots = M^{(n-1)} = 0$. If now a scattering process involving n external legs is considered, the only Feynman diagrams surviving are those shown in figure 3.6. All the other diagrams involve processes contained in the amplitudes that have been fixed to zero by the induction hypothesis. Imposing that the n-point scattering is also null, from figure 3.6 the following equation for the n-point coupling has to hold:

$$\begin{aligned} & C^{(n)}_{b_1 \dots b_n} - \sum_l C^{(n-1)}_{b_1 \dots b_{n-2} \bar{l}} \frac{1}{m_l^2} C^{(3)}_{l b_{n-1} b_n} - \sum_s C^{(n-2)}_{b_1 \dots b_{n-3} \bar{s}} \frac{1}{m_s^2} C^{(4)}_{s b_{n-2} b_{n-1} b_n} \\ & \quad + \sum_l C^{(n-2)}_{b_1 \dots b_{n-3} \bar{s}} \frac{1}{m_s^2} C^{(3)}_{s b_{n-2} \bar{l}} \frac{1}{m_l^2} C^{(3)}_{l b_{n-1} b_n} = 0. \end{aligned} \tag{3.5.7}$$

This equation was found in [37] and allows the value of $C^{(n)}$ to be found given the values of the masses and the 3-, 4-, $(n-2)$- and $(n-1)$-point couplings.

The sinh-Gordon model discussed at the beginning of this chapter can be rediscovered by using (3.5.7). If (3.1.1) is assumed to be the starting Lagrangian from which constructing all the higher-order couplings iteratively then $C^{(3)} = 0$ and (3.5.7) reduces to

$$C^{(n)} = \frac{1}{m^2} C^{(n-2)} C^{(4)} \tag{3.5.8}$$

with driving coupling $C^{(4)} = \lambda$. The recursion can be easily solved and the following

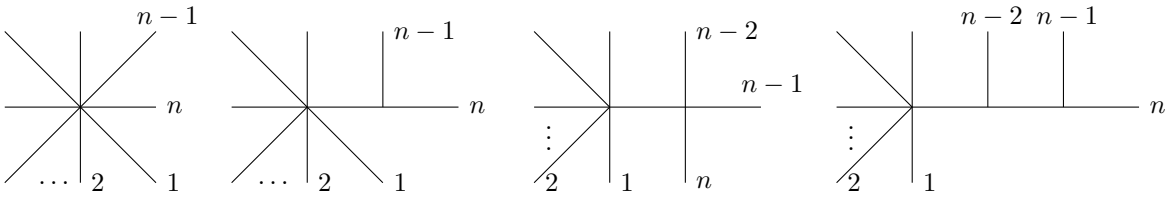

Figure 3.6: Diagrams surviving in an n-point scattering process in the multi-Regge limit having fixed $M^{(4)}$, $M^{(5)}$, ..., $M^{(n-1)}$ to be zero by tuning the vertices up to $C^{(n-1)}_{a_1 \dots a_{n-1}}$

closed expression

$$C^{(2n)} = \left(\frac{\lambda}{m^2}\right)^{n-2} \lambda \tag{3.5.9}$$

for the higher point couplings is obtained. By defining $g^2 \equiv \frac{\lambda}{m^2}$ the potential of the model can then be written as

$$V = \frac{m^2}{g^2} \sum_{n=1}^{+\infty} \frac{g^{2n}}{(2n)!} \phi^{2n}, \tag{3.5.10}$$

which is exactly the expansion of the sinh-Gordon potential in (3.1.10). Apart from this simple example, where the driving data are just composed of $(m_1, C^{(3)}_{111}, C^{(4)}_{1111}) = (m, 0, \lambda)$ (we label by 1 the single particle of the model), in all the other cases defining the set of masses, 3- and 4-point couplings allowing for integrable solutions of (3.5.7) is not an easy task. Equation (3.5.7) provides indeed a necessary condition for the absence of particle production at the tree level, but it is not a sufficient condition to ensure the tree-level integrability. Also in the simplest case of integrable theory, which is the sinh-Gordon model, (3.5.7) does not imply that the $2\phi \to 4\phi$ process studied at the beginning of this chapter is a constant.

With equation (3.5.7) the proof of points (i), (ii), (iii) from section 3.2 is concluded. What is still missing is point (iv), corresponding to the finding of possible sets of masses, 3- and 4-point couplings that make the induction possible. To find these values the cancellation of poles in 4-point inelastic processes[4] and in events involving production with 5 and 6 external legs has to be imposed. If suitable values for the masses and lower-order couplings can be found so to cancel such poles then the basis for the induction procedure is found and, by the analysis carried out in (i), (ii) and (iii), the relation in (3.5.7) becomes a sufficient condition to prove the absence of particle production in the theory. Since these lower point processes are the basis of the entire induction we call the masses and the 3/4-point couplings the 'seeds of integrability'.

[4] As already remarked more that one time in the present thesis we construct integrable Lagrangians of theories presenting purely elastic scattering, i.e. with a diagonal S-matrix in 2-to-2 interactions.

Chapter 4

Seeds of integrability

The purpose of this chapter is to figure out what constraints on masses, 3- and 4-point couplings need to be satisfied to allow only elastic tree-level scattering in 4-, 5- and 6-point interactions. The solutions to these constraints would define unambiguously integrable models, which therefore can be classified by imposing the absence of production at the tree level. The results presented in sections 4.1, 4.2 and 4.3 cover part of the content of a paper in collaboration with Patrick Dorey [1]. However, the full classification of possible sets of masses and lower-order couplings spanning the space of integrable theories with Lagrangians of the form in (3.1.12) is not addressed here. In section 4.4 some comments about this classification, also based on the discussion presented in [1], are reported. Section 4.5 is instead due solely to the author and is not presented in other literature; in such section, it is shown how the bootstrap and factorisation features at all orders follow by the cancellation of certain Landau poles in loop-level diagrams.

4.1 Simplification processes in 4-point non-diagonal scattering

We start by considering a 2-to-2 non-diagonal scattering amplitude; such amplitude is required to be null since the theories we are looking at are purely elastic. Let examine the case in which two incoming particles a and b evolve to two outgoing particles c and d of different types. The process, as well as the conventions for the Mandelstam variables, are those of section 2.3; they are respectively (2.3.1) and (2.3.3). In this case we assume $\{a, b\} \neq \{c, d\}$; in particular the masses of the incoming- and outgoing-particles are not necessarily the same.

If the theory is integrable such processes should be forbidden, a fact that should be visible perturbatively. This requires that a so-called flipping rule on the masses and couplings of the particles should exist, as introduced in the context of the perturbative study of higher poles in Toda theories in [69]. The idea is that any time a Feynman diagram contributing to a non-diagonal 2-to-2 process has a pole at a particular value of the external momenta, there must be a pole in at least one

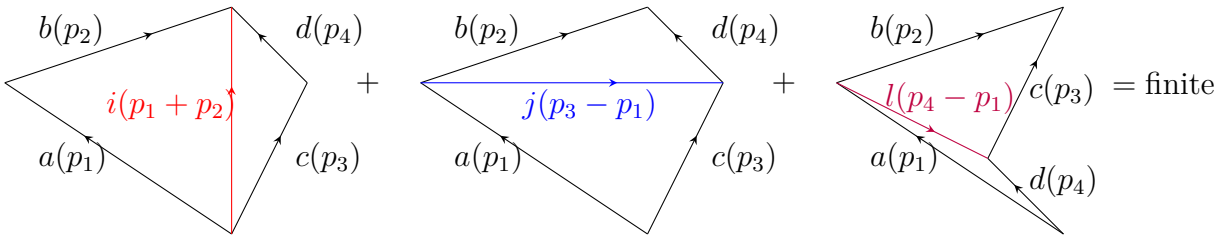

Figure 4.1: Poles in the s-, t- and u-channel in a 2-to-2 off-diagonal process. The poles cancel so that the total contribution is finite.

other diagram for the same value of the momenta, so as to obtain a finite (and therefore constant) overall result which can be cancelled by a suitably-chosen 4-point coupling. Note that this includes the possibility to have diagrams with on-shell bound state particles propagating in all three different s-, t- and u-channels, whose sum of residues is equal to zero.

Since by assumption all the fields contained in (3.1.12) are the creators and annihilators of asymptotic particles, as already explained in section 2.4, anytime a coupling $C^{(3)}_{abc}$ is nonzero the masses m_a, m_b and m_c can be drawn as sides of a fusing triangle Δ_{abc} (this would avoid decay processes at the tree level). The on-shell momenta entering the triangle are then complex numbers, having absolute values given by the respective masses, and with arguments given by their purely imaginary rapidities (see figure 2.9). Combining such fusing triangles in pairs it is then possible to draw Feynman diagrams with intermediate on-shell propagators. Such pictures do not restrict only to the diagonal processes depicted in figure 2.9 but extend also to the inelastic cases discussed in this section; for example, figure 4.1 shows three on-shell Feynman diagrams contributing to the inelastic process $a+b\to c+d$. It contains an example of flipping rule in a case for which poles appear simultaneously in three Feynman diagrams with three possibly-different particles i, j and l propagating on-shell in the s-, t- and u-channels respectively. As shown in the figure, while the diagrams having particles i and j propagating in the s- and t-channels are represented by convex quadrilaterals, the diagram with the l particle propagating in the u channel is concave. In such a situation on the pole position we have $s=m_i^2$, $t=m_j^2$ and $u=m_l^2$ for the same value of the external momenta. Remembering that in two dimensions only one Mandelstam variable is independent t and u can be Taylor expanded with respect to s as

$$\begin{aligned} t(s) &= t(m_i^2)+\left.\frac{dt}{ds}\right|_{m_i^2}(s-m_i^2)+\ldots = m_j^2+\left.\frac{dt}{ds}\right|_{m_i^2}(s-m_i^2)+\ldots \\ u(s) &= u(m_i^2)+\left.\frac{du}{ds}\right|_{m_i^2}(s-m_i^2)+\ldots = m_l^2+\left.\frac{du}{ds}\right|_{m_i^2}(s-m_i^2)+\ldots \end{aligned} \tag{4.1.1}$$

Summing the three diagrams in figure 4.1 the amplitude near the pole is

$$M^{(4)}_{ab\to cd} \sim C^{(3)}_{a\bar{i}b}\ \frac{1}{s-m_i^2}\ C^{(3)}_{\bar{c}i\bar{d}} + C^{(3)}_{aj\bar{c}}\ \frac{1}{\frac{dt}{ds}\Big|_{m_i^2}(s-m_i^2)}\ C^{(3)}_{b\bar{j}\bar{d}} + C^{(3)}_{al\bar{d}}\ \frac{1}{\frac{du}{ds}\Big|_{m_i^2}(s-m_i^2)}\ C^{(3)}_{bl\bar{c}}. \tag{4.1.2}$$

From a general property of the diagonals of quadrilaterals (in appendix B an explicit derivation is given) it is known that for the second diagram in figure 4.1,

$$\frac{dt}{ds}\Big|_{m_i^2} = -\frac{\Delta_{ajc}\Delta_{bjd}}{\Delta_{aib}\Delta_{cid}} \tag{4.1.3}$$

where Δ_{ABC} is the area of the triangle having for sides the masses m_A, m_B and m_C. The minus sign in (4.1.3) reflects the fact that the diagram is convex, so stretching the i diagonal keeping the lengths of the external sides fixed causes the j diagonal to get shorter. Contrarily for the concave quadrilateral (the last diagram in figure 4.1) increasing the i diagonal also increases the l diagonal too, and we have

$$\frac{du}{ds}\Big|_{m_i^2} = \frac{\Delta_{ald}\Delta_{blc}}{\Delta_{aib}\Delta_{cid}}. \tag{4.1.4}$$

Substituting (4.1.3) and (4.1.4) into (4.1.2) it holds

$$M^{(4)}_{ab\to cd} \sim \frac{\Delta_{aib}\Delta_{ci\bar{d}}}{s-m_i^2}\left[\ \frac{C^{(3)}_{a\bar{i}b}C^{(3)}_{\bar{c}i\bar{d}}}{\Delta_{aib}\Delta_{cid}} - \frac{C^{(3)}_{aj\bar{c}}C^{(3)}_{b\bar{j}\bar{d}}}{\Delta_{ajc}\Delta_{bjd}} + \frac{C^{(3)}_{al\bar{d}}C^{(3)}_{bl\bar{c}}}{\Delta_{ald}\Delta_{blc}}\ \right]. \tag{4.1.5}$$

The singular contribution to the amplitude in the neighbourhood of the pole $s \sim m_i^2$ is obtained; it corresponds to choosing a value of the red diagonal in figure 4.1 close to m_i with the external sides kept fixed at their mass-shell values. This formula makes it natural to incorporate the area of the corresponding mass triangles into the parametrisation of the 3-point couplings by setting

$$C^{(3)}_{ijk} = \ \Delta_{ijk}\ f_{ijk}. \tag{4.1.6}$$

While the area of the triangle does not distinguish particles from antiparticles, since their masses are equal, f_{ijk} needs to differentiate indices of particles from those of antiparticles that as usual are indicated respectively with i and $\bar{i}$. A first feature of these parameters, coming from the way in which the Lagrangian (3.1.12) was written, is that f_{ijk} has to be symmetric under exchange of any pair of indices. Moreover, the reality of the Lagrangian in (3.1.12) requires

$$f_{\bar{a}\bar{b}\bar{c}} = f^*_{abc}\,. \tag{4.1.7}$$

Substituting (4.1.6) into (4.1.5), the residue for a 2-to-2 inelastic amplitude is proportional to

$$Res(M^{(4)}_{ab\to cd}) \sim f_{a\bar{i}b}f_{\bar{c}i\bar{d}} - f_{aj\bar{c}}f_{b\bar{j}\bar{d}} + f_{al\bar{d}}f_{bl\bar{c}} \tag{4.1.8}$$

and the requirement that it be equal to zero implies the following constraint

$$f_{a\bar{i}b}f_{\bar{c}i\bar{d}} - f_{aj\bar{c}}f_{b\bar{j}\bar{d}} + f_{al\bar{d}}f_{b\bar{l}\bar{c}} = 0. \tag{4.1.9}$$

The situation can be generalized to the degenerate case in which more than a single particle propagates on-shell in each one of the channels. If for example there are different intermediate states, all with mass m_i, propagating on-shell in the s-channel we need to sum over all the possible particles i in (4.1.9) with that mass. The more general situation is therefore obtained by introducing in the relation (4.1.9) three different sums over all the possible particles i, j and l with respective masses m_i, m_j and m_l. Cases for which the cancellation of poles happens between pairs of Feynman diagrams with opposite residues, corresponding to particles propagating in just two different channels, are also contained in relation (4.1.9) by simply setting one of the terms to zero.

It is worth noting that the pole cancellation condition in inelastic 4-point processes not only relates the values of different 3-point couplings, but also gives strong constraints on the possible sets of masses. The requirement that poles always have to appear at least in pairs to cancel, as in figure 4.1, is highly non-trivial and leaves very little freedom on the possible masses of the theory. Moreover, the fact that the amplitude should not have any singularities, no matter which branch of the kinematics is considered in the solution of the energy-momentum constraints, together with the flipping move, allows for the construction of networks of Feynman diagrams related to each other. Below it is shown how this works in an example of the $e_8^{(1)}$ affine Toda theory. This model, like all the other affine Toda field theories constructed from simply-laced Dynkin diagrams, is characterised by satisfying the following 'simply-laced scattering conditions'

Property 4.1. *A theory respects 'simply-laced scattering conditions' if in* 2 *to* 2 *non-diagonal scattering the poles cancel in pairs (flip s/t, s/u or t/u) and in* 2 *to* 2 *diagonal interactions it presents only one on-shell propagating particle at a time.*

These conditions will be studied further in the analysis of 5-point interactions where they will play a crucial role in constraining the values of the couplings. If they are satisfied, the cancellation mechanism of the singularities happens between flipped copies of Feynman diagrams with particles propagating in a pair of channels: s/t, s/u or t/u. It never happens that three poles appear simultaneously in Feynman diagrams with on-shell bound states propagating in the three different channels. The two flipped diagonals correspond to the masses of two particles propagating in different channels cancelling each other. Three types of flip are distinguished depending on how a diagonal is replaced with its flipped version. Flips of type I are characterised by maintaining the external convex shape of the polygon during the replacement procedure (in figure 4.2 it is the flip connecting the s- to the t-channel). Contrarily flips of type II and type III change the order of the external particles in passing from one channel to its flip, obtaining in one case a concave polygon. These two kinds of flip are distinguished by the fact that in the former, one of the two points remains the same (in figure 4.2 we see indeed that both the j and l vectors

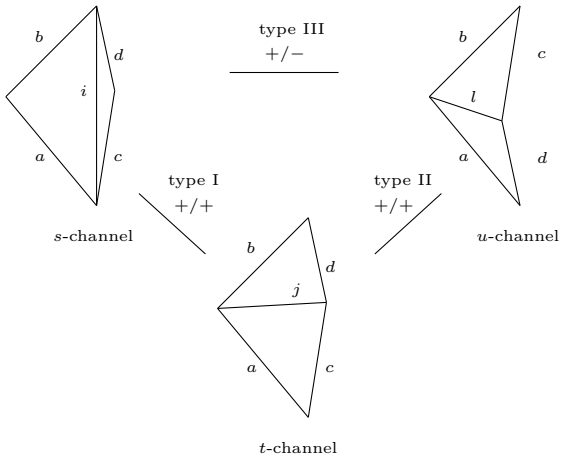

Figure 4.2: Possible simultaneous poles in a non-allowed four-point process. In theories satisfying simply-laced scattering conditions, only two among the three diagrams diverge simultaneously for a particular choice of the external kinematics. In this case the product of the three-point couplings changes sign flipping from the s- to the u-channel whereas it does not change sign flipping from the t- to the s-channel and flipping from the t- to the u-channel.

starts from the meeting point of the sides a and b) while in the latter both the starting and the ending point of the diagonal change. Depending on the type of flip connecting the cancelling diagrams, the product of the f-functions entering in the three-point vertices may or may not change sign. Assume for example to have a type I flip, connecting in our case the s- and the t-channels (which means the pair of cancelling singularities corresponds to a copy of diagrams with particles propagating in the s- and t-channels). In such a case only the first two terms in (4.1.9) are different from zero implying that the product of the corresponding f-functions, in order to avoid the singularity, does not change sign

$$f_{ab\bar{i}}f_{i\bar{c}\bar{d}} = f_{a\bar{c}\bar{j}}f_{jc\bar{d}}.$$

Using the same argument it is easy to see that the sign does not change in type II flips, while it does change with a flip of type III. These different situations are summarised in figure 4.2. This sign rule will return useful when loop diagrams will be studied in the final part of this thesis. It will allow us to understand the cancellation mechanism at the loop level and to compute sums of singular diagrams contributing to Landau poles. The original paper [69] differentiated between two different kinds of flips that were the two different types they encountered in the construction of loop networks of singular Feynman diagrams. We distinguish a third type of flip here in order to understand the sign rule connecting products of different 3-point couplings, as also shown in figure 4.2.

Below it is shown how to generate a network of Feynman diagrams entering into a

certain non-allowed process in the $e_8^{(1)}$ affine model. In the present case different colours are used to indicate the different masses of the theory, that are labelled following the increasing order $m_1 < \ldots < m_8$. Consider the inelastic process with external momenta

$$p_{\bullet} + p_{\bullet} \to p_{\bullet} + p_{\bullet}, \tag{4.1.10}$$

in which a 'blue'- and a 'black'-particle (with masses m_5 and m_3 respectively in $e_8^{(1)}$) evolve into a 'red'- and an 'orange'-particle (with masses m_1 and m_2). If the on-shell shape of a single Feynman diagram contributing to this scattering process is known, corresponding to a certain kinematical configuration of the external states at which an internal diagonal is on-shell, it is then possible to figure out from it all the remaining diagrams. In the following it is explained how all the on-shell graphs can be generated.

Suppose to know the quadrilateral number (1) in figure 4.3, with an on-shell green diagonal corresponding to a particle with mass m_4 propagating in the s channel. Starting from this configuration it is possible moving to the other two diagrams by applying two different moves. We can flip the green propagating particle finding what other diagonal is equal in length to one of the possible eight different values of masses in the theory. We find in this manner that a type III flip can be applied moving the diagram to the configuration (12), in which a 'black'-particle propagates in the crossed-channel. The two diagrams (1) and (12) are one the flipped of the other, and the associated poles, that appear for the same external kinematical configuration, cancel in the sum. On the other hand, it is also known that there is another choice of the external kinematics for which the 'green'-particle of diagram (1) is on-shell. Such a second choice corresponds to reflecting the outgoing 'red'- and 'orange'-particle with respect to this green segment, and represents the other solution of Σ in (3.4.2) satisfying energy-momentum conservation. This second move, which will be called a 'jump' in figure 4.3, corresponds to keeping the diagonal associated to the propagating bound state fixed and reflecting two external sides with respect to it. This move preserves the singular propagator while changing the external kinematical configuration at which this propagator diverges. Starting from the diagram (1), in figure 4.3, the two moves are applied, alternating 'jumps' and 'flips'. While the 'flip' changes the type of propagator entering into the diagram, connecting, therefore, two different Feynman diagrams contributing to the process, the 'jump' does not change the particles and the vertices of the diagram but only the values of the external momenta. In figure 4.3, (1) and (2) correspond to the same diagram with different choices of external kinematics, similarly (3) and (4) and so on. After a finite number of jumps and flips we return to the graph we started from. This generates in total six different Feynman diagrams contributing to the process, whose on-shell configurations are contained in the copies of pictures [(1),(2)], [(3),(4)], [(5),(6)], [(7),(8)], [(9),(10)] and [(11),(12)] (each pair of graphs contains two different kinematical configurations of the same diagram).

This discussion can be extended to models (such as the non simply-laced affine Toda theories) in which it is also possible to find 3 simultaneously on-shell propagating particles for a single kinematical configuration. Although figure 4.3 shows a particular scattering from the $e_8^{(1)}$ theory for which the flipping rule happens between pairs of

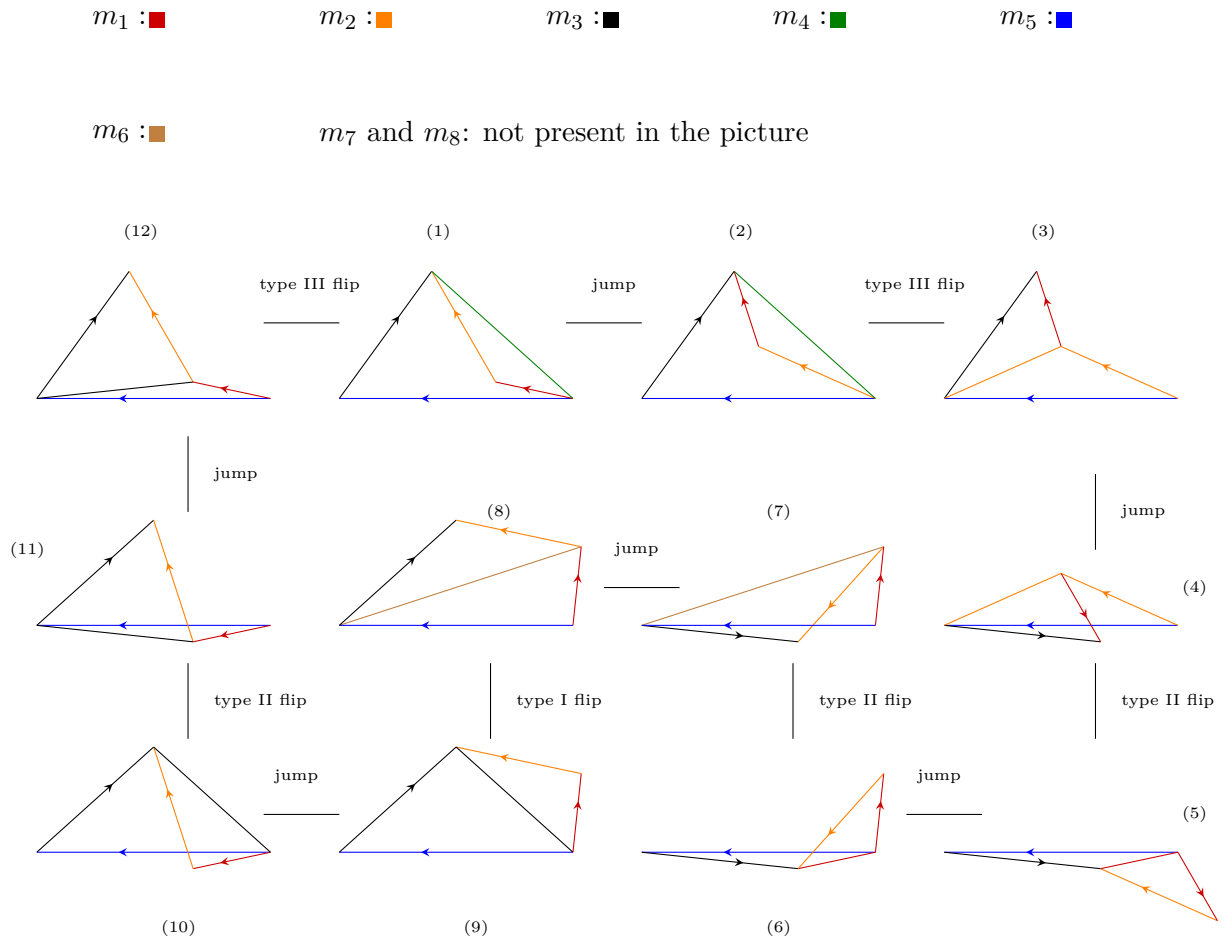

Figure 4.3: Network of Feynman diagrams with different on-shell configurations of external momenta contributing to an inelastic process in the $e_8^{(1)}$ affine Toda field theory. Segments depicted with different colours are equal in length to the different masses of the theory. By properly ordering the external lines it is possible, for each pair of diagrams connected by one flip, to recognize the corresponding flip shown in figure 4.2.

diagrams, similar networks need to be present in any integrable model constructed from a Lagrangian of the form in (3.1.12).

To any flip in a theory with simply-laced scattering conditions a constraint of the form (4.1.9) can be associated, where the contribution that is not present has to be set to zero. Since the network is closed in a circle this leads to a finite number of constraints on the functions f_{ijk}, that in the present case become

$$f_{\bullet\bullet\bullet}f_{\bullet\bullet\bullet} = -f_{\bullet\bullet\bullet}f_{\bullet\bullet\bullet} = -f_{\bullet\bullet\bullet}f_{\bullet\bullet\bullet} = -f_{\bullet\bullet\bullet}f_{\bullet\bullet\bullet} = -f_{\bullet\bullet\bullet}f_{\bullet\bullet\bullet} = -f_{\bullet\bullet\bullet}f_{\bullet\bullet\bullet}, \tag{4.1.11}$$

where different colours are used to label the different particles. The signs connecting the products of the different f-functions come from the sign rule (summarized in figure 4.2) for the different types of flip. By simplifying some of the equal terms in (4.1.11) it follows from these constraints that $f_{\bullet\bullet\bullet} = f_{\bullet\bullet\bullet}$ and $f_{\bullet\bullet\bullet} = f_{\bullet\bullet\bullet}$. It is interesting to note that the network of graphs in figure 4.3 includes all of the Feynman diagrams involving 3-point couplings contributing to the scattering (4.1.10), so, perhaps surprisingly, all these different graphs could be found starting from a single Feynman diagram. However the story is not quite over; indeed at this point a set of nonzero couplings is known and from them we can start studying further processes. For example both $f_{\bullet\bullet\bullet} \neq 0$ and $f_{\bullet\bullet\bullet} \neq 0$; this implies that a diagram in which a 'blue' and a 'black'-particle fuse into a 'red'-propagator, that then decays into a 'orange'- and a 'green'-state, can be drawn. Starting from this diagram, 'jumps' and 'flips' can be applied to obtain the different graphs contributing to the process

$$p_{\bullet} + p_{\bullet} \to p_{\bullet} + p_{\bullet}.$$

This would relate the 3-point couplings of this second process to the 3-point couplings entering into (4.1.10).

Only a few special sets of masses allow closed networks of diagrams to be obtained for all the different processes. If we instead start with a generic diagram, drawn as a quadrilateral having sides of random length, and start applying 'jumps' and 'flips' to it, we will go on adding more and more particles to the theory in order to make the singularity cancellations possible. In the end, the network will never close. To obtain a closed loop of graphs, we need to start with a special set of masses, corresponding to an integrable theory.

So far we have found the conditions under which the 2-to-2 non-diagonal scattering amplitude constructed using only 3-point vertices has no poles and is therefore a constant not depending on the choice of the momenta. Now the 4-point coupling has to be set to cancel this constant leading to a null process at the end. Focusing on the non-diagonal process having as incoming- and outgoing-particles respectively $\{a, b\}$ and $\{c, d\}$, the amplitude obtained using only 3-point vertices is given by summing over all the possible particles propagating in the s-, t- and u-channels

$$M^{(4)}_{ab\to cd} = -i\sum_s C^{(3)}_{ab\bar{s}}\,\frac{1}{s-m_s^2}\,C^{(3)}_{s\bar{c}\bar{d}} - i\sum_j C^{(3)}_{a\bar{c}\bar{j}}\,\frac{1}{t-m_j^2}\,C^{(3)}_{jb\bar{d}} - i\sum_l C^{(3)}_{a\bar{d}\bar{l}}\,\frac{1}{u-m_l^2}\,C^{(3)}_{lb\bar{c}}. \tag{4.1.12}$$

Since it has already been proved that after having properly tuned the masses and

3-point couplings such amplitude is a constant (for $\{c,d\} \neq \{a,b\}$) a particular choice of momenta that simplifies the computation can be taken. Two choices of multi-Regge limit can be adopted; we can set $s = +\infty$, $t = -\infty$ and $u = 0$ or $s = +\infty$, $t = 0$ and $u = -\infty$. This corresponds of solving the limit $s \to +\infty$ in the two different Riemann sheets over which Σ in (3.4.2) takes values. In both cases, the result needs to be the same, since in the absence of poles the amplitude is a constant, and the 4-point coupling cancelling the process is

$$C^{(4)}_{ab\bar{c}\bar{d}} = \sum_j C^{(3)}_{a\bar{c}\bar{j}} \frac{1}{m_j^2} C^{(3)}_{jb\bar{d}} = \sum_l C^{(3)}_{ad\bar{l}} \frac{1}{m_l^2} C^{(3)}_{lb\bar{c}}. \tag{4.1.13}$$

A similar result can be obtained in the case in which the particles in the initial and final state are equal, so that $\{c,d\} = \{a,b\}$. In this case, the 4-point coupling has to be set to cancel the reflection process, corresponding to the function defined over the blue half of the degenerate torus described in section 3.4; in this manner, only transmission is allowed. The only situation in which the 4-point coupling cannot be obtained from the masses and 3-point vertices is when it involves the scattering of 4 real equal particles. This is a situation in which the reflection cannot be distinguished from the transmission and the event is always allowed. In this case to tune the 4-point coupling correctly the interaction of five external states has to be studied.

4.2 No-particle production in 5-point processes

The cancellation of 4-point non-diagonal processes is made possible by the flipping rule, cancelling all the poles appearing in the sums of Feynman diagrams. We now study how the same rule permits the cancellation of all singularities in the 5-point scattering amplitudes, provided we impose extra constraints on the values of the f_{ijk} and the 4-point couplings.

We start with the case in which all the interacting particles are different. This is somewhat trivial, since whenever an internal propagator goes on-shell the amplitude is split into a 3-point vertex and an on-shell 4-point inelastic process. Since the inelastic 4-point processes are null, entering into the analysis previously performed, the residues of such scattering processes are all zero and no singularity appears. Even though this situation does not add any new constraints on the couplings, and these cancellations can be proved by using the flipping rule alone, it is anyway interesting to study in some more detail how these singular diagrams cancel. Since these diagrams will be also contained inside certain loop diagrams studied in chapter 7, we think is good to give some more detail on their cancellation and a discussion is reported in appendix C.

Here we move directly to a less trivial case, in which the scattering involves two equal particles as in the following 3-to-2 event:

$$a(p_1) + b(p_2) + d(p_3) \to c(p_4) + d(p_5). \tag{4.2.1}$$

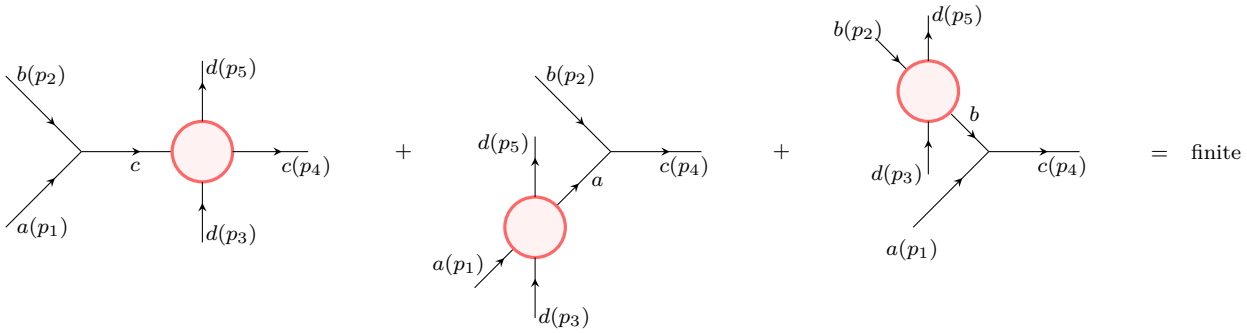

Figure 4.4: Divergent contributions to the process $a+b+d \to c+d$. We list the poles that have nonzero residues when the propagators connecting the 3-point vertices and the 4-point on-shell amplitudes are mass-shell. Despite the three contributions being separately divergent we prove that their sum is finite if additional constraints are imposed on the 3- and 4-point couplings.

We choose to study a process with 3 incoming and 2 outgoing particles, but of course particles can be brought from the left-hand side to the right-hand side of the arrow (and vice-versa) by changing the sign of the momenta and particles to antiparticles. This process represents the most general case of a 5-point scattering amplitude that could in principle contain poles. Such poles can appear when, as shown in figure 4.4, the propagator connecting the blobs[1] and the 3-point vertices is a particle of the same type as those present as external legs. This is indeed the only way to have a nonzero residue when the propagator diverges because the 2-to-2 scattering processes represented by the three blobs in figure 4.4 are diagonal. The three different combinations of Feynman diagrams in figure 4.4 are summed, choosing to write the momenta in light-cone components as in (2.1.2). By using Lorentz invariance and the conservation of the overall energy and momentum three parameters can be removed from the amplitude, so that it can be written as a function depending only on a_3 and a_5. Then we study its dependence on one parameter at a time, starting with a_5. Taking the limit $a_5 \to a_3$ (i.e. choosing the same momenta for the incoming and outgoing d particle in (4.2.1)) we can isolate the residue of the amplitude at the pole

$$M^{(5)}(a_3, a_5) \simeq \frac{1}{a_5 - a_3} \operatorname*{Res}_{a_5=a_3} M^{(5)}(a_3, a_5). \tag{4.2.2}$$

The residue in the expression above is a function of a single parameter a_3 and can be written as

$$\operatorname*{Res}_{a_5=a_3} M^{(5)}(a_3, a_5) = \\ -\frac{C^{(3)}_{ab\bar{c}}}{m_d} a_3 \left[\frac{1}{m_c} \frac{a_4 a_3}{a_4^2 - a_3^2} M^{(4)}_{cd}(a_4, a_3) - \frac{1}{m_a} \frac{a_1 a_3}{a_1^2 - a_3^2} M^{(4)}_{ad}(a_1, a_3) - \frac{1}{m_b} \frac{a_2 a_3}{a_2^2 - a_3^2} M^{(4)}_{bd}(a_2, a_3) \right]. \tag{4.2.3}$$

[1] The blobs represent the sum of all tree-level Feynman diagrams having as external legs the types of particles entering into the blob.

The parameters a_1, a_2 and a_4 in (4.2.3) are fixed and on the pole satisfy a fusing relation of the form depicted in figure 2.8, so that the residue depends only on a_3. $M^{(4)}_{cd}$, $M^{(4)}_{ad}$ and $M^{(4)}_{bd}$ are the on-shell values of the 2-to-2 amplitudes in figure 4.4. This corresponds to taking the limit in which the blobs in figure 4.4 go on-shell and the intermediate propagators diverge. Since these blobs are allowed processes, the three terms in the square brackets in (4.2.3) do not vanish individually but must cancel between themselves. To prove this, it is sufficient to prove that the sum of these terms has no poles as a function of a_3. This is enough to show that it is a constant as a function of a_3, which can be seen to be zero by taking the limit $a_3 \to \infty$.

Before continuing the study of the singularities connected to 5-point interactions we show how the requirement that the expression in (4.2.2) has zero residue is equivalent to imposing tree-level bootstrap relations connecting the different S-matrix elements.

4.2.1 The tree-level bootstrap

The 2-to-2 S-matrix elements S_{ij} are given in terms of $M^{(4)}_{ij}$ by (3.1.15). Using this conversion and writing the a-variables as $a_i = e^{\theta_i}$ the requirement that the residue of (4.2.2) is equal to zero is equivalent to the following constraint on the tree-level S-matrix

$$S^{tree}_{cd}(\theta_{43}) = S^{tree}_{ad}(\theta_{13}) + S^{tree}_{bd}(\theta_{23}). \tag{4.2.4}$$

In this equality, the only free parameter is the rapidity θ_3 of the d-particle, since all the other rapidities are frozen on their on-shell values making the diagrams in figure 4.4 singular on the pole. Defining the difference between the c- and d-particle rapidities to be $\theta_{43} = \theta$, the relation in (4.2.4) can be written as

$$S^{tree}_{cd}(\theta) = S^{tree}_{ad}(\theta + \theta_{14}) + S^{tree}_{bd}(\theta + \theta_{24}) \tag{4.2.5}$$

The quantities θ_{14} and θ_{24} are the differences between the rapidities of the a- and the c-particles, and between the rapidities of the b- and the c-particles interacting in the vertex $C^{(3)}_{ab\bar{c}}$. These are imaginary angles that are frozen on the pole position, where the on-shell particles fuse in the 3-point vertex $C^{(3)}_{ab\bar{c}}$ satisfying the triangular relation in figure 2.8. Referring to figure 2.8 we label

$$\theta_{41} = -i\bar{U}^b_{ac} \quad , \quad \theta_{42} = i\bar{U}^a_{bc}.$$

Therefore we can write the constraint for the cancellation of the 5-point process as

$$C_{ab\bar{c}} \neq 0 \implies S^{tree}_{dc}(\theta) = S^{tree}_{da}(\theta - i\bar{U}^b_{ac}) + S^{tree}_{db}(\theta + i\bar{U}^a_{bc}) \tag{4.2.6}$$

where $\bar{U}^b_{ac}$ is the angle between sides m_a and m_c and $\bar{U}^a_{bc}$ is the angle between m_b and m_c in the mass triangle Δ_{abc}.

The relation in (4.2.6) connects all the 2-to-2 tree-level S-matrix elements of the theory together and represents the first order in perturbation theory of the bootstrap relation (2.4.7), that, if the integrability is preserved at quantum level, is valid order

by order in the loop expansion

$$S_{ij}(\theta) = 1 + S_{ij}^{tree}(\theta) + \dots \tag{4.2.7}$$

It is interesting to note how the bootstrap equations at the tree level completely emerge from the sole requirement that all the 5-point processes are equal to zero and their pictorial representation can be recognised in the sum of the singular diagrams in figure 4.4. Verifying the cancellation of the 5-point processes for a general theory requires to prove that the tree-level bootstrap relation (4.2.6) is satisfied between all the different S-matrix elements. Such a relation is converted into particular constraints on the 3- and 4-point couplings of the theory.

4.2.2 Pole cancellation and 'Simply-laced scattering conditions'

We now search for the additional constraints on the couplings necessary for the tree-level bootstrap relations to be satisfied, and therefore for the vanishing of all the 5-point processes, for models satisfying the 'simply-laced scattering conditions' defined in property 4.1. We show how in these theories a necessary condition for the absence of particle production in 5-point interactions is that the absolute values of the f-functions do not depend on the particular 3-point vertex we are considering and from the relation in (4.1.6) we can then deduce the following area rule

$$|C_{ijk}^{(3)}| = |f|\ \Delta_{ijk}, \tag{4.2.8}$$

where $|f|$ is the absolute value common to each f-function. We now proceed to prove this assertion, adopting the method already used for the 4-point off-diagonal processes and imposing the absence of singularities. The requirement that the residue of (4.2.2) does not have any singularities in the variable a_3 is equivalent to requiring that the LHS and the RHS terms of the relation (4.2.6) have the same pole structure.

To verify the cancellation between the different poles appearing in (4.2.3) we split the possible singularities of the residue into two kinds. The first type corresponds to singularities due to the possibility that some propagators go on-shell inside the 4-point amplitudes $M_{cd}^{(4)}$, $M_{ad}^{(4)}$ and $M_{bd}^{(4)}$, and will be called 'flipped singularities' (since they will cancel by just using the flipping rule) while the second type are 'collinear singularities'; this last kind happens when one of the denominators in (4.2.3) diverges, that is the situation in which $a_3^2 \to a_4^2$, $a_3^2 \to a_1^2$ or $a_3^2 \to a_2^2$. We study these two different situations separately and we show how, with a few additional constraints, the poles of (4.2.3) cancel in both cases.

Flipped singularities

We start describing the first kind of poles, those due to simultaneous singularities in $M_{cd}^{(4)}$, $M_{ad}^{(4)}$ and $M_{bd}^{(4)}$. An example of this situation is represented in figure 4.5 where both the Feynman diagrams (on the bottom) and their dual description in terms of vectors in the complex plane (on the top) are drawn. A propagating i-particle is supposed to go on-shell in $M_{cd}^{(4)}$ (it is represented by a red line in the

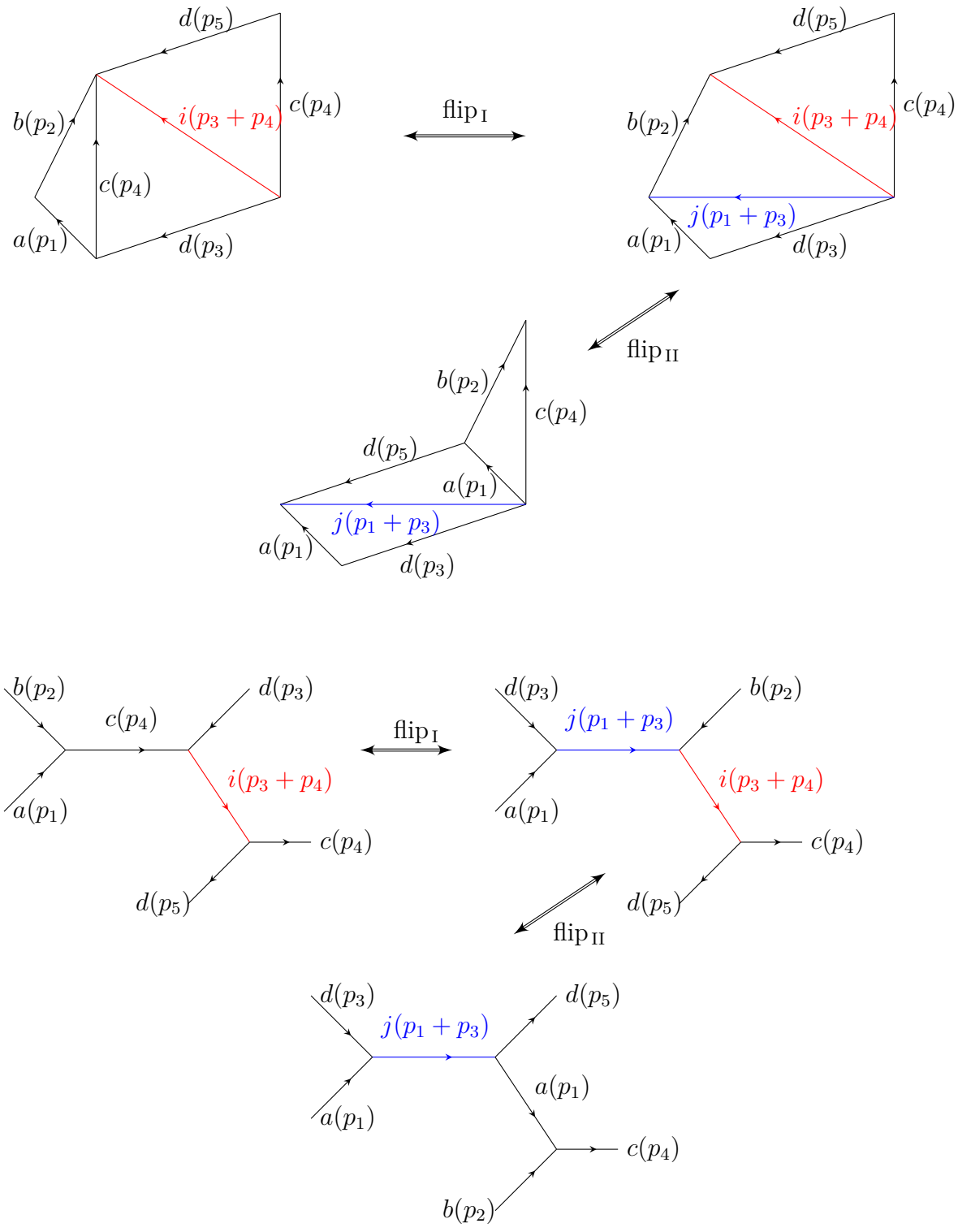

Figure 4.5: Pole structure in the process $a+b+d \to c+d$. On the bottom and the top are listed respectively the Feynman diagrams and their on-shell description.

first picture of figure 4.5). Looking at the quadrilateral defined by vectors $a(p_1)$, $b(p_2)$, $i(p_3+p_4)$ and $d(p_3)$ we note that the flipping rule can be applied on the propagating particle $c(p_4)$. As explained previously there are two possibilities for the flip, one case in which $a(p_1)+d(p_3)=i(p_3+p_4)-b(p_2)=j(p_1+p_3)$ where j is an on-shell propagating particle, and one in which the on-shell propagating particle is given by $b(p_2)+d(p_4)=i(p_1+p_3)-a(p_1)$. We are assuming that we cannot have both at the same time. In figure 4.5 the first situation is shown; it is evident how, after having applied two flips, the same values of momenta which contribute to a pole in $M^{(4)}_{cd}$ generate another pole in the amplitude $M^{(4)}_{ad}$. If the particles were all different we could continue to flip internal propagating particles and we would obtain a closed network with a finite number of diagrams connected by simple flips, as that one discussed in appendix C. In this situation since two particles are identical after two flips the network is completed and we have obtained all the divergent diagrams. Focusing on the situation shown in figure 4.4 in which $M^{(4)}_{cd}$ and $M^{(4)}_{ad}$ diverge simultaneously we compute the residue of the RHS of (4.2.3) with respect to the variable a_3. To this end we write only the divergent part in square brackets of (4.2.3). We keep the two momenta of the d-particles parallel (corresponding to the limit $a_5=a_3$) and we move them simultaneously so that the i particle is nearly on-shell ($p_i^2=m_i^2$). In this way we are close to the pole of the residue. By convention we choose the direction of the momentum p_4 to be the axis with respect to which we measure the angles and we choose counterclockwise to be the positive direction of angles. In this way looking at the first picture in figure 4.5 we have $a_4=1$, $a_1=e^{i\bar{U}^b_{ac}}$, $a_2=e^{-i\bar{U}^a_{bc}}$ and $a_3=a_5=e^{i(\pi-\bar{U}^i_{cd})}$. We remember that $\bar{U}^A_{BC}$ refers to the angle in the triangle Δ_{ABC} between the sides B and C. Substituting such quantities into the divergent part of the residue (4.2.3) we obtain

$$\operatorname*{Res}_{a_5=a_3} M^{(5)}(a_3,a_5)\sim \frac{1}{m_c}\frac{1}{\sin(\bar{U}^i_{cd})}\frac{|\,C^{(3)}_{cd\bar{i}}\,|^2}{p_i^2-m_i^2}-\frac{1}{m_a}\frac{1}{\sin(\bar{U}^j_{ad})}\frac{|\,C^{(3)}_{ad\bar{j}}\,|^2}{p_j^2-m_j^2} \tag{4.2.9}$$

Always referring to the first drawing in figure 4.5 now we move the inclination of $d(p_3)$ and $d(p_5)$ keeping them parallel. Expanding p_j^2 in terms of p_i^2 around the pole $p_i^2=m_i^2$ we obtain

$$p_j^2=m_j^2+\left.\frac{dp_j^2}{dp_i^2}\right|_{p_i^2=m_i^2}(p_i^2-m_i^2)+\ldots=m_j^2+\frac{\Delta_{adj}}{\Delta_{cdi}}(p_i^2-m_i^2)+\ldots \tag{4.2.10}$$

The last equality has been obtained using the formula (B.3.1) on the quadrilateral defined by the sides $a(p_1)$, $b(p_2)$, $i(p_3+p_4)$, $d(p_3)$ and having as diagonal $j(p_1+p_3)$ in the diagram on the top right of figure 4.5. Expressing at this point the pole in terms of p_i^2 we see that (4.2.9) is proportional to

$$\frac{1}{p_i^2-m_i^2}\left[\frac{|\,C^{(3)}_{cd\bar{i}}\,|^2}{\Delta^2_{cdi}}-\frac{|\,C^{(3)}_{ad\bar{j}}\,|^2}{\Delta^2_{adj}}\right]. \tag{4.2.11}$$

Substituting (4.1.6) into (4.2.11) and requiring the quantity in square brackets to

be zero implies the following equality

$$| f_{cd\bar{i}} |^2 = | f_{ad\bar{j}} |^2 . \tag{4.2.12}$$

In fact, this relation follows from the properties already imposed in the cancellation of 2-to-2 off-diagonal processes, as follows. Looking at the three on-shell diagrams of figure 4.5 we note that the following relations hold,

$$f_{ab\bar{c}} f_{cd\bar{i}} f_{\bar{c}\bar{d}i} \underset{\text{type I flip}}{=} f_{ad\bar{j}} f_{jb\bar{i}} f_{\bar{c}\bar{d}i} \underset{\text{type II flip}}{=} f_{ad\bar{j}} f_{\bar{a}\bar{d}j} f_{ab\bar{c}}, \tag{4.2.13}$$

where we used the sign rules satisfied by the different types of flips summarized in figure 4.2. Simplifying the common factor $f_{ab\bar{c}}$ in the first and in the third terms in (4.2.13) and using (4.1.7) we obtain exactly the relation (4.2.12) that is therefore simply a consequence of the flipping rule.

The relation (4.2.12) is consistent with the area rule (4.2.8). This consistency is due to the fact that we are assuming, as part of the simply-laced scattering conditions, that the flipping rule happens between pairs of graphs. If we violated this condition, having an s-, t- and u-channel particle simultaneously on-shell in the quadrilateral defined by $a(p_1)$, $b(p_2)$, $i(p_3+p_4)$, $d(p_3)$ in figure 4.5, not only c and j would contribute to the pole but also another on-shell particle, l say, a bound state of $b(p_2)$ and $d(p_3)$. In this situation an extra contribution $\frac{|C^{(3)}_{bd\bar{l}}|^2}{\Delta^2_{bdl}}$ would be present in the square brackets of (4.2.11), providing another term in the relation (4.2.12) that would become

$$| f_{cd\bar{i}} |^2 = | f_{ad\bar{j}} |^2 + | f_{bd\bar{l}} |^2 . \tag{4.2.14}$$

In this situation, we see that for a given d particle the absolute value of its corresponding f-function depends on the particles with which it couples according with a set of constraints of the form expressed in (4.2.14).

However, though the relation (4.2.12) agrees with the area rule (4.2.8), it is not enough to prove it. At a first glance, it may seem from the expression in (4.2.12) that given a generic particle d, the absolute value of its f-function f_{dij} does not depend on the particles i and j with which it couples. Such a conclusion is too hasty, since the indices $\{c, \bar{i}\}$ and $\{a, \bar{j}\}$ appearing on the LHS and on the RHS of (4.2.12) are not arbitrary but correspond to particular on-shell channels inside the amplitudes $M^{(4)}_{cd}$ and $M^{(4)}_{ad}$. To show that the area rule is universally satisfied by all the models respecting property 4.1 we need to study also the second kind of singularities, happening when the momenta of two particles become collinear; we refer to these as 'collinear singularities'.

Collinear singularities

This second situation can arise only when we have at least three equal particles in the scattering. Indeed suppose we take the limit $a_3 \to a_4$; in this situation the term in front of $M^{(4)}_{cd}(a_3, a_4)$ in equation (4.2.3) becomes infinity but at the same time, if c and d are particles of different types, we also have $M^{(4)}_{cd}(a_3, a_4) \to 0$. This is indeed the limit in which the transmitting and the reflecting processes involving the 2-to-2 scattering of the particles c and d become equal. Since the latter event is

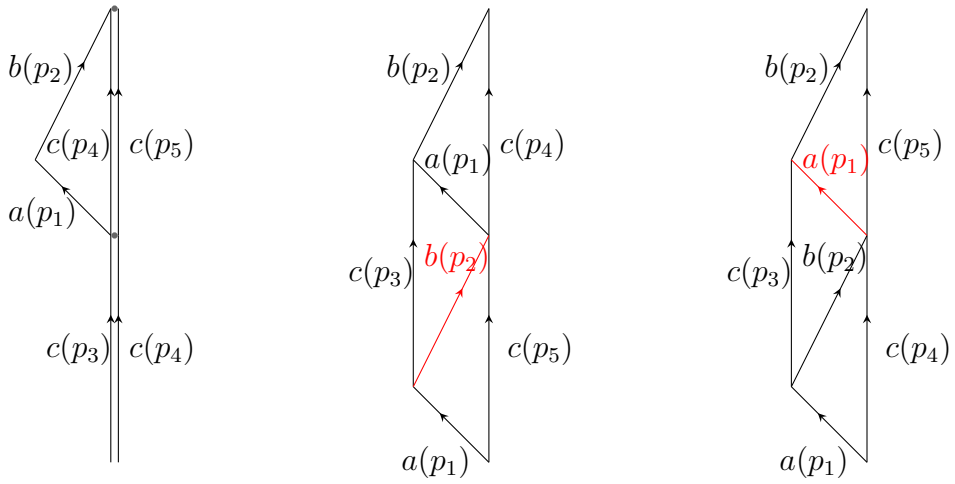

Figure 4.6: Infinite contributions to the residue of the amplitude $a+b+c \to c+c$ when collinear singularities are present. The infinities sum to zero so that in the end the residue is finite.

forbidden in any integrable theory in this limit both the processes need to be zero and collinear singularities are not allowed.

The story is different if the labels c and d are equal. In this case transmission cannot be distinguished from reflection and $M^{(4)}_{cc}(a_3, a_4)$ (we give particles c and d the same label since we are analysing the situation in which they are equal) does not go to zero for $a_3 \to a_4$; so it is possible to have singularities due to collinear momenta. In particular if $d = c$, in the limit $a_3 \to a_4$ the amplitude $M^{(4)}_{cc}(a_4, a_3)$ is nonzero while the term in front of it in equation (4.2.3) goes to infinity. However in this case other poles appear in the amplitudes $M^{(4)}_{bc}$ and $M^{(4)}_{ac}$ that cancel this singularity. A picture of this situation is shown in figure 4.6 where we highlight how the collinear singularity in the first graph is accompanied by two poles due to two on-shell particles propagating in $M^{(4)}_{bc}$ and $M^{(4)}_{ac}$. As before, to evaluate the singular part of the residue, we keep $a_4 = 1$ the direction respect to which we measure the angles following the counterclockwise convention. At this point we choose to move p_3 and p_5 keeping them parallel and with fixed length. So we choose $a_3 = a_5 = e^{i\theta}$. The collinear singularity happens in the limit $\theta \to 0$. Once again we have $a_1 = e^{i\bar{U}^b_{ac}}$, $a_2 = e^{-i\bar{U}^a_{bc}}$. Expanding the red propagators in figure 4.6 with respect to the angle θ around the value $\theta = 0$ we obtain

$$p_b^2(\theta) = m_b^2 - 2m_a m_c \sin(\bar{U}^b_{ac})\theta \quad , \quad p_a^2(\theta) = m_a^2 + 2m_b m_c \sin(\bar{U}^a_{bc})\theta \tag{4.2.15}$$

Now we expand the expression between square brackets in equation (4.2.3) isolating the pole $\frac{1}{\theta}$. After a straightforward calculation we obtain

$$\operatorname*{Res}_{a_5=a_3} M^{(5)}(a_3, a_5) \sim \frac{i}{2m_c\theta}\left[M^{(4)}_{cc}(1,1) + \frac{i}{2m_a^2 \sin^2(\bar{U}^b_{ac})} \mid C^{(3)}_{ab\bar{c}} \mid^2 + \frac{i}{2m_b^2 \sin^2(\bar{U}^a_{bc})} \mid C^{(3)}_{ab\bar{c}} \mid^2\right] \tag{4.2.16}$$

The term $M^{(4)}_{cc}(1,1)$ represents the amplitude for a process $c+c \to c+c$ in which the

momenta of the incoming and outgoing particles are collinear. Then we substitute in this formula the expression for the 3-point coupling in (4.1.6) and we obtain that the residue is equal to zero if in the collinear limit the scattering amplitude for a process of the form $c + c \to c + c$ is given by

$$M_{cc}^{(4)}\Big|_{collinear} = -\frac{i}{4} m_c^2 \mid f_{\bar{a}\bar{b}c} \mid^2 . \tag{4.2.17}$$

Such relations allow the 4-point coupling $C_{cc\bar{c}\bar{c}}^{(4)}$ to be fixed in terms of the 3-point couplings also in those cases in which the procedure described in the end of section 4.1 cannot be applied (i.e. when the 4-point amplitude is diagonal). We note that the absolute value of a function $f_{\bar{a}\bar{b}c}$ containing a particle of type c does not depend on the particles a and b with which it couples, being the LHS of the equality (4.2.17) independent on a and b. In contrast to (4.2.12), the particles a and b are completely arbitrary, being any pair of particles coupling with c. For this reason, we can state that any theory satisfying the simply-laced scattering conditions reported in section 4.1 respects an area rule of the form (4.2.8). Indeed, given the arbitrariness of the interacting particles, from the relation in (4.2.17) we can have only two possible situations: either there exist two decoupled sectors of the theory that do not interact with each other and can have two possible different absolute values of their f-functions, or, if all the particles are connected, there exists only one possible value of $|f_{ijk}|$ that needs to be common to all the 3-point couplings. This implies that the expression in (4.2.17) can consistently be written as

$$M_{cc}^{(4)}\Big|_{collinear} = -\frac{i}{4} m_c^2 \mid f \mid^2 \tag{4.2.18}$$

where $|f|$ is the common value to all the absolute values of the f-functions. The combination of (4.2.18) with the area rule (4.2.8) ensures, in theories satisfying simply-laced scattering conditions, that the residue of the amplitude at the pole $a_5 \to a_3$ is equal to zero, independently of the value of a_3. Therefore the amplitude has no singularities in a_5 and it is a constant in this variable. The entire discussion can be repeated identically for the variable a_3 so that we have

$$\frac{\partial M^{(5)}}{\partial a_3} = \frac{\partial M^{(5)}}{\partial a_5} = 0,$$

and $M^{(5)}$ is constant everywhere.

As a simple check that everything is working correctly, we consider a theory of a single real scalar field of mass m. In this case, the 3-point coupling is given by the relation in (4.1.6) and can be written as

$$C^{(3)} = \frac{\sqrt{3}}{4} m^2 \lambda \tag{4.2.19}$$

where on the right-hand side we have written the value of the area of an equilateral triangle of side m and λ corresponds to the value of the f-function in equation (4.1.6). By a direct calculation of the scattering amplitude for a 2-to-2 collinear

process in this theory we obtain

$$M_{cc}^{(4)}\Big|_{collinear} = (-iC^{(3)})^2\frac{i}{4m^2-m^2} - (-iC^{(3)})^2\frac{i}{m^2} - (-iC^{(3)})^2\frac{i}{m^2} - iC^{(4)}. \quad (4.2.20)$$

Comparing this expression with (4.2.18), where in this case $|f|^2 = \lambda^2$, we find that the value of the 4-point coupling cancelling poles in 5-point events needs to be

$$C^{(4)} = \frac{9}{16}m^2\lambda^2. \quad (4.2.21)$$

The following coupling, $C^{(5)}$, is then fixed by requiring that $M^{(5)}$ is not just a constant but it is zero. It is fixed by using the formula (3.5.7) with $n = 5$, that for this particular case becomes

$$C^{(5)} = \frac{2}{m^2}C^{(4)}C^{(3)} - \frac{1}{m^4}C^{(3)}C^{(3)}C^{(3)},$$

From this expression we read

$$C^{(5)} = \frac{15\sqrt{3}}{64}m^2\lambda^3. \quad (4.2.22)$$

If we write the first few terms of the Lagrangian that we are constructing

$$\mathcal{L} = \frac{1}{2}\partial_\mu\phi\partial^\mu\phi - \frac{m^2}{2}\phi^2 - \frac{1}{3!}\frac{\sqrt{3}}{4}m^2\lambda\phi^3 - \frac{1}{4!}\frac{9}{16}m^2\lambda^2\phi^4 - \frac{1}{5!}\frac{15\sqrt{3}}{64}m^2\lambda^3 + \dots \quad (4.2.23)$$

we note that they are the lower orders in the expansion of the Bullough-Dodd Lagrangian (3.1.11), where the coupling g is defined in terms of λ as $g = \frac{\sqrt{3}}{4}\lambda$. All the other couplings can be obtained by acting iteratively with (3.5.7) and it can be shown that they match with the expansion of (3.1.11).

4.3 No-particle production in 6-point processes

Events involving 6 external particles are relatively simple to analyse once we know that non-diagonal scattering is not allowed in 4- and 5-point processes. In this case, the most general process not trivially equal to zero is given by

$$a(p_1) + b(p_2) + c(p_3) \to a(p_4) + b(p_5) + c(p_6). \quad (4.3.1)$$

Indeed, if there were more than three different particles then any time an internal propagator goes on-shell it would factorise the amplitude into two processes of which at least one is inelastic, generating a zero residue. For the event represented in equation (4.3.1), all the poles also cancel. The reason is that such poles appear always in copies as shown in figure 4.7. The two diagrams in figure 4.7 are equal except for the fact that in the limit $a_4 \to a_1$ (i.e. on the pole) they have two

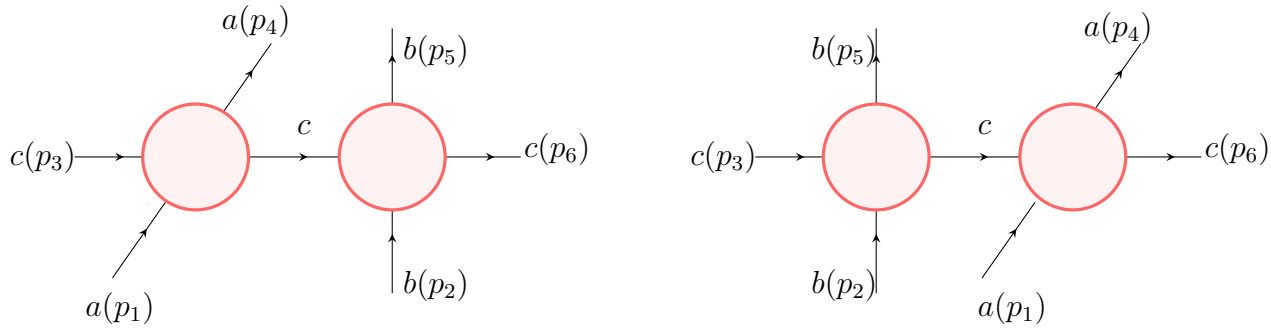

Figure 4.7: Allowed poles in the 6-point amplitude $a+b+c \to a+b+c$. The sum of these two contributions is nonzero only in a subregion of the momentum space where the sets of incoming and outgoing momenta are equal.

propagators with opposite sign, that are given respectively by

$$G_1 = \frac{i}{m_a m_c} \frac{-a_1^2 a_3}{a_1 - a_4} \frac{1}{a_3^2 - a_1^2} \tag{4.3.2}$$

and

$$G_2 = \frac{i}{m_a m_c} \frac{a_1^2 a_3}{a_1 - a_4} \frac{1}{a_3^2 - a_1^2} \tag{4.3.3}$$

This suffices to prove that the sum of the two singularities in the diagrams is equal to zero.

The situation is different if we keep the $i\epsilon$ prescription in the propagators. In this case, each propagator can be written in terms of its principal value and its delta contribution. While the former cancels once it is summed with all the other diagrams (indeed the divergent parts of the principal values of G_1 and G_2 sum to zero while the remaining finite contribution is cancelled by all the other non-divergent diagrams) the latter gives a nonzero result. We can prove this using the distribution formula

$$\lim_{\epsilon \to 0^+} \left(\frac{1}{x + i\epsilon} - \frac{1}{x - i\epsilon} \right) = (-2\pi i)\delta(x). \tag{4.3.4}$$

By a direct sum of the propagators in (4.3.2), (4.3.3) and considering the extra $i\epsilon$ factors in the denominators we obtain

$$\begin{aligned} G_1 + G_2 &= \frac{i}{m_a m_c} a_1^2 a_3 \lim_{\epsilon \to 0^+} \left(\frac{1}{(a_1 - a_4)(a_1^2 - a_3^2) + \frac{i a_1^2 a_3 \epsilon}{m_a m_c}} - \frac{1}{(a_1 - a_4)(a_1^2 - a_3^2) - \frac{i a_1^2 a_3 \epsilon}{m_a m_c}} \right) \\ &= \frac{2\pi}{m_a m_c} \frac{a_1^2 a_3}{|a_1^2 - a_3^2|} \delta(a_1 - a_4) = \frac{\pi}{m_a m_c} \frac{\delta(\theta_1 - \theta_4)}{|\sinh \theta_{13}|} \end{aligned} \tag{4.3.5}$$

where we define θ_{13} the difference between the rapidities of the a- and c-particle, having respectively momenta p_1 and p_3. Using such result by a direct sum of the

two diagrams in figure 4.7 and multiplying by the extra factor

$$(2\pi)^2\delta^{(2)}\Big(\sum_{i=1,2,3}p_i-\sum_{k=4,5,6}p_k\Big)\equiv(2\pi)^2\delta\Big(\sum_{i=1,2,3}p_i^0-\sum_{k=4,5,6}p_k^0\Big)\,\delta\Big(\sum_{i=1,2,3}p_i^1-\sum_{k=4,5,6}p_k^1\Big)$$

coming from the conservation of the total momentum we obtain

$$4\pi^3\,\frac{1}{m_a m_c|\sinh\theta_{13}|}M^{(4)}_{ac}(a_1,a_3)\frac{1}{m_b m_c|\sinh\theta_{23}|}M^{(4)}_{bc}(a_2,a_3)\,\delta(\theta_1-\theta_4)\delta(\theta_2-\theta_5)\delta(\theta_3-\theta_6). \tag{4.3.6}$$

In (4.3.6) we exploited the fact that the additional delta function arising from (4.3.5) constraints the possible space of outgoing momenta to a smaller subregion. In particular we used the following equality

$$\begin{aligned}\delta(\theta_1-\theta_4)\delta^{(2)}\Big(\sum_{i=1,2,3}p_i-\sum_{k=4,5,6}p_k\Big)&=\delta(\theta_1-\theta_4)\delta^{(2)}\big(p_2+p_3-p_5-p_6\big)\\&=\delta(\theta_1-\theta_4)\frac{\delta(\theta_2-\theta_5)\delta(\theta_3-\theta_6)}{m_b m_c|\sinh\theta_{23}|}\end{aligned} \tag{4.3.7}$$

to factorise the 6-point scattering into a product of two 4-point amplitudes. Inserting then the normalisation factor (a multiplicative term $\frac{1}{\sqrt{4\pi}}$ for each external particle) and adding the contribution (4.3.6) to the other two pairs of diagrams similar to the one shown in figure 4.7, but with particles a and b propagating in the middle, we find that the final 6-point S-matrix is given by

$$\begin{aligned}S^{tree}_{abc}(\theta_1,\theta_2,\theta_3)=&\Big[S^{tree}_{ac}(\theta_{13})S^{tree}_{bc}(\theta_{23})+S^{tree}_{ab}(\theta_{12})S^{tree}_{bc}(\theta_{23})+S^{tree}_{ab}(\theta_{12})S^{tree}_{ac}(\theta_{13})\Big]\\&\times\delta(\theta_1-\theta_4)\delta(\theta_2-\theta_5)\delta(\theta_3-\theta_6).\end{aligned} \tag{4.3.8}$$

In the equality above the tree-level part of the 2-to-2 S-matrix is bound to the 4-point amplitude through the relation (3.1.15) which is valid at all the orders in perturbation theory. It is interesting to note how equation (4.3.8) exactly matches the factorisation requirement we expect to see at the tree level. This fact needs to be valid at any order in the coupling if the theory is integrable and therefore must hold order by order in perturbation theory

$$\begin{aligned}S_{abc}(\theta_1,\theta_2,\theta_3)&=S_{ab}(\theta_{12})S_{bc}(\theta_{23})S_{ac}(\theta_{13})\\&=\big(1+S^{tree}_{ab}(\theta_{12})+\dots\big)\big(1+S^{tree}_{bc}(\theta_{23})+\dots\big)\big(1+S^{tree}_{ac}(\theta_{13})+\dots\big).\end{aligned} \tag{4.3.9}$$

The relation in (4.3.8) corresponds to the tree-level order of the expansion (4.3.9), after the disconnected diagrams are discarded.

Summarising, all the non-diagonal 6-point processes are null if we fix the 6-point vertices appropriately through (3.5.7), while the diagonal processes are nonzero only in a small region of the momentum space, exactly when the amplitude is factorised into the product of 2-to-2 interactions.

4.4 Remarks on the tree-level classification

In the previous sections, strictly following the analysis carried out in [1], we have given necessary and sufficient conditions for a theory with a Lagrangian of the form (3.1.12) to be perturbatively integrable, with a purely elastic S-matrix, at the tree level. It has been proved that the theory is completely defined once the mass ratios and the 3-point couplings are known. Once this fundamental data is given, the 4- and the higher-point couplings can be uniquely determined using the equalities in (4.1.13), (3.5.7) and by requiring that a set of tree-level fusing bootstrap relations (4.2.6) is satisfied. The tree-level bootstrap approach is particularly useful to find the 4-point couplings $C^{(4)}_{cccc}$, in which four real equal particles fuse together; indeed such couplings contribute to 4-point elastic processes and the relation (4.1.13) cannot be applied.

Probing the space of tree-level perturbatively integrable theories corresponds to searching for the mass ratios and 3-point couplings from which the entire Lagrangian can be constructed iteratively. This problem can be addressed by two different routes. On the one hand, it is possible to select the possible candidates by searching for what masses and 3-point couplings allow for the cancellation of poles in all 2-to-2 inelastic processes, according to what has been discussed in section 4.1. Subsequently only the models having S-matrices satisfying the relations (4.2.6) are actually integrable models at the tree level. On the other hand, it is possible to address the problem in the opposite direction, by first imposing the tree level bootstrap relations (4.2.6). This second approach is in principle simpler: matching the pole structure of the different S-matrix elements entering the bootstrap corresponds to setting the values of the masses while matching the residues at the poles corresponds to defining the absolute values of the 3-point couplings. To determine the relative signs among the different 3-point couplings we need then to require the cancellation of 4-point inelastic processes from which we obtain a set of relations of the form in (4.1.9).

Although the problem of classifying all perturbatively integrable theories at the tree level is not addressed in this thesis, many of the tools to pursue that goal have been provided. Hints for such a classification can be found in [70, 71] where the first steps were performed for non-perturbative S-matrices of minimal models using a bootstrap approach. Reproducing the classification at the tree level should be simpler than studying the quantum exact S-matrices, since the fact that the RHS of (4.2.6) involves a sum instead of a product (as it happens in (2.4.7)) does not introduce higher-order singularities that often generate inconsistencies. Restricting attention to theories satisfying the simply-laced scattering conditions, it is important to stress that the number of degrees of freedom is further restricted. Once the masses have been fixed, the 3-point couplings (if they are not null) must obey the area rule (4.2.8). The only relevant information is therefore the values of the masses and what 3-point couplings are nonzero. The set of integrable theories with N different particle types and satisfying simply-laced scattering conditions lives in

$$\mathbb{R}^{N-1} \times (\mathbb{Z}_2)^{\frac{N(N+1)(N+2)}{6}} \tag{4.4.1}$$

the product between the space of mass ratios and the 3-point couplings. A group $\mathbb{Z}_2$ is associated with each 3-point coupling: since the absolute value of the coupling is determined by the area of the mass triangle the only relevant information is if the coupling is or it is not zero. The exponent $\frac{N(N+1)(N+2)}{6}$ corresponds then to the number of 3-point couplings in a theory with N types of particles. In the next chapters, we will show how simply-laced and twisted affine Toda field theories belong to this class of models. However it still remains unclear if they are the only integrable models in two dimensions respecting property 4.1, or it is possible to find some integrable theory verifying such conditions that is not an affine Toda theory.

Before moving into the second part of this thesis, which contains a discussion of perturbative aspects of affine Toda field theories, in the next section we show how the bootstrap fusing relations and the factorisation properties at all loops can be derived in perturbation theory from certain constraints on the scattering.

4.5 Loop features

Bootstrap fusing relations and factorization have been largely applied in the past to conjecture exact results for the S-matrices of a variety of quantum field theories. Though these equations, with a small number of extra assumptions, allow us to find non-perturbative S-matrices they have always been taken as a starting genuine axiom, based on integrability properties of the models that are promoted to be preserved at the quantum level. In this section we assume a different perspective showing how such relations appear as residues of particular threshold singularities in loop processes with 5 and 6 external particles, anticipating a topic that will be discussed more rigorously in chapter 7: the Landau poles. The bootstrap and factorization assumptions follow therefore by the absence of non-elastic scattering in perturbation theory. We start by looking at the bootstrap fusing rules.

4.5.1 Pole cancellation and bootstrap relations at loop level

In the present section we describe bootstrap relations at one loop arising from the requirement that, at this loop order, 5-point processes do not present poles since they should be forbidden. The higher loop case can then be obtained straightforwardly as a generalization of these one-loop cancellations.

We consider once again the process (4.2.1) and we take the collinear limit $p_5 \to p_3$ in which the poles appear. At this order in the loop expansion, the singular diagrams are shown in figure 4.8. The first three graphs are exactly analogous to those already seen in the tree-level case. They produce the same expression presented in (4.2.3), with the only difference that the amplitudes in square brackets are now obtained by summing over one-loop Feynman diagrams. The only additional different contribution comes from the last graph in figure 4.8 that will be computed below.

The two blobs appearing in the fourth picture in figure 4.8 contain all the possible tree-level diagrams contributing to the elastic amplitudes $M_{ad}^{(4,0)}$ and $M_{bd}^{(4,0)}$. Compared

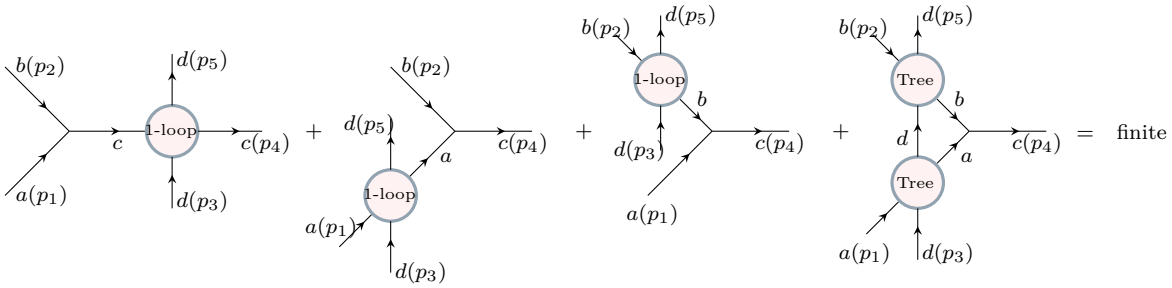

Figure 4.8: The one-loop bootstrap relations are obtained imposing that the sum of the residues of the one-loop singular diagrams contributing to the fusing pole $a + b \to c$ is zero.

to previous notation, where a single superscript index was given in amplitudes to indicate the number of external particles, here we introduce a second index to keep track of the number of loops. Therefore, the expression $M^{(4,0)}$ indicates a 4-point amplitude at 0 loops (i.e. at the tree level). One example of the diagrams appearing in such blobs is shown in figure 4.9 with the corresponding dual description on the RHS. In the collinear limit $p_5 \to p_3$ there is a point in the loop integration region in which the propagators a, b and d connecting the two blobs with the three-point vertex $C_{ab\bar{c}}$ and the two blobs each other are simultaneously on-shell. This brings an order-one pole that needs to be taken into account in the total sum. However, for general kinematics of the d particle, though maintaining the limit $a_5 = a_3$, the on-shell amplitudes $M^{(4,0)}_{ad}$ and $M^{(4,0)}_{bd}$ do not possess any internal on-shell propagators. In other words, all the red particles i and the blue particles j propagating in the two blobs in figure 4.9 are off-shell on the pole position given by having the internal a-, b- and d-propagators on-shell. This is always the case except for a finite discrete number of values of p_3 corresponding to the pole positions of $M^{(0)}_{ad}$ or $M^{(0)}_{bd}$ (or both). Anyway, we suppose to be far away from these positions. The double-blob contribution in the first image in figure 4.9 can therefore be written as

$$D = (-iC_{ab\bar{c}}) \int \frac{d^2l}{(2\pi)^2} \frac{i}{(p_a - l)^2 - m_a^2 + i\epsilon} M^{(4,0)}_{da}(p_3, p_1, p_d + l, p_a - l) \frac{i}{(p_d + l)^2 - m_d^2 + i\epsilon} \times M^{(4,0)}_{db}(p_d + l, p_2, p_5, p_b + l) \frac{i}{(p_b + l)^2 - m_b^2 + i\epsilon} \tag{4.5.1}$$

where we are expanding the loop around some values of the internal a- , b- and d-propagators given by p_a, p_b and p_d. Since the loop integration has two degrees of freedom we can set p_a and p_b on-shell at the position $l = 0$:

$$p_a^2 - m_a^2 = 0 \quad , \quad p_b^2 - m_b^2 = 0. \tag{4.5.2}$$

However for general kinematics of p_5 and p_3 in such a position the momentum p_d is off-shell. In figure 4.10 it is depicted the position $l = 0$ around which we integrate. On the LHS p_3 and p_5 are not parallel and there does not exist a point inside the

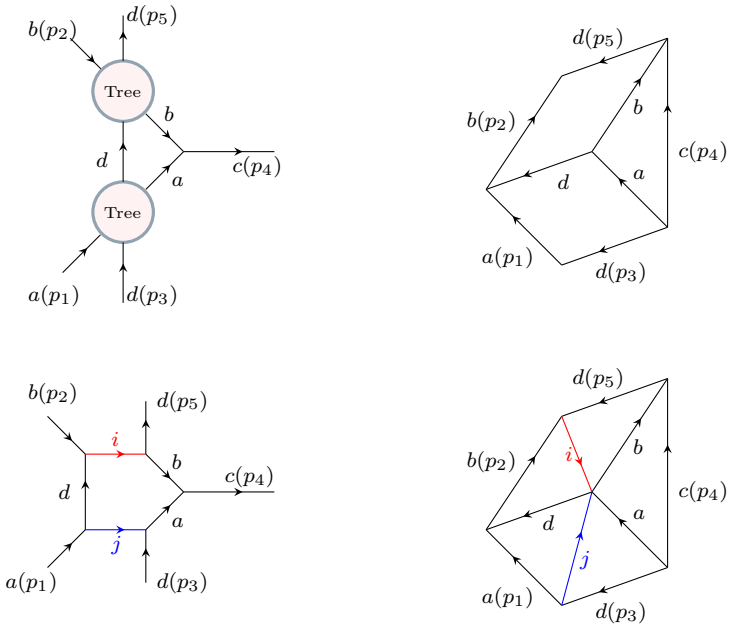

Figure 4.9: Example of Feynman diagrams appearing in the two blobs corresponding to the tree-level amplitudes $M_{ad}^{(4,0)}$, $M_{bd}^{(4,0)}$. On the RHS it is shown their dual geometrical description.

integration region at which the three propagators a, b and d are simultaneously on-shell. In particular for $l = 0$, a and b are on-shell but d is not. On the RHS of figure 4.10 we see how when we take the collinear limit $p_5 \to p_3$ in the position $l = 0$ not only are p_a and p_b on-shell, but also p_d since it becomes equal to the common value $p_d = p_3 = p_5$. Now we write the distance of p_d from its mass-shell condition in terms of the difference $a_5 - a_3$; in this manner, we can express the pole residue in the same way as we did for the other terms in (4.2.3). To determine the quantity $p_d^2 - m_d^2$ in terms of the difference between the two phases a_3 and a_5 we need to combine some relations. First we note that the following equalities hold

$$\begin{aligned} p_d^2 - m_d^2 &= (p_3 + p_1 - p_a)^2 - m_d^2 = \frac{m_a m_d}{a_3 a_1^2}(a_1 - a_a)(a_1^2 - a_3^2) \ , \\ p_d^2 - m_d^2 &= (p_5 + p_b - p_2)^2 - m_d^2 = \frac{m_b m_d}{a_3 a_2^2}(a_b - a_2)(a_2^2 - a_3^2) \ . \end{aligned} \tag{4.5.3}$$

On the RHS of the second line, we have written a_3 instead of a_5 since we are taking the limit $a_5 \to a_3$. Then we use the momentum conservation

$$m_a a_1 + m_b a_2 + m_d a_3 = m_a a_a + m_b a_b + m_d a_5$$

that combined with the two equalities in (4.5.3) leads to the following relation

$$m_d(a_5 - a_3) = m_a(a_1 - a_a) + m_b(a_2 - a_b) = (p_d^2 - m_d^2)\frac{1}{m_d}\left(\frac{a_3 a_1^2}{a_1^2 - a_3^2} - \frac{a_3 a_2^2}{a_2^2 - a_3^2}\right) .$$

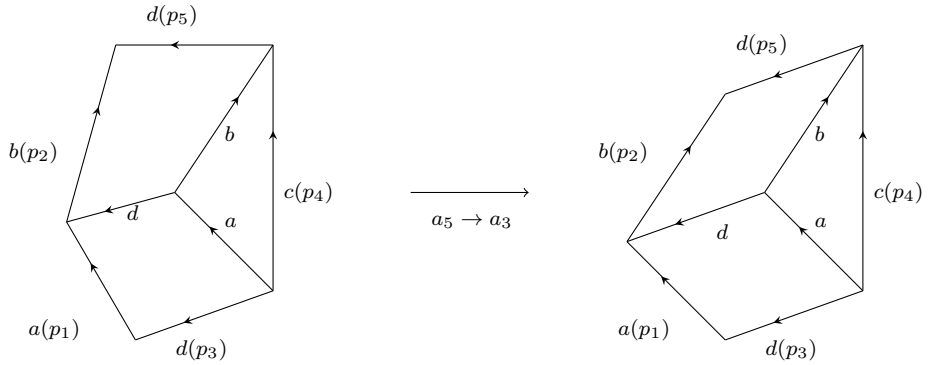

Figure 4.10: Limit $a_5 \to a_3$ shown in the dual Feynman diagram description. Once we fix the values of the a- and b-propagators on-shell on the LHS we highlight that the d internal particle is off-shell. We see how the length of the internal momentum carried by d is shorter than the on-shell value $p_d^2 = m_d^2$. On the RHS in the limit $a_5 \to a_3$ the internal d-propagator goes on-shell and its length becomes equal to the mass m_d generating a first-order pole.

Manipulating a little bit of the expression in brackets on the RHS and writing the a_j variables in terms of the rapidities we obtain the desired result

$$p_d^2 - m_d^2 = 2\frac{m_d^2}{a_3}\frac{\sinh\theta_{13}\sinh\theta_{23}}{\sinh\theta_{21}}(a_5 - a_3) \equiv x(a_5 - a_3). \tag{4.5.4}$$

If we substitute (4.5.2) and (4.5.4) into the loop integral (4.5.1) we obtain that the double-blob contribution around its singular value becomes

$$\begin{aligned} D = (-iC_{ab\bar{c}})\int \frac{d^2l}{(2\pi)^2}\frac{i}{-2p_a\cdot l + l^2 + i\epsilon}\; M_{da}^{(4,0)}(p_3, p_1, p_d + l, p_a - l) \\ \frac{i}{x(a_5 - a_3) + 2p_d\cdot l + l^2 + i\epsilon} M_{db}^{(4,0)}(p_d + l, p_2, p_5, p_b + l)\frac{i}{2p_b\cdot l + l^2 + i\epsilon}. \end{aligned} \tag{4.5.5}$$

At this point we rescale $l = \tilde{l}\,(a_5 - a_3)$ and keep the limit $a_5 \to a_3$ neglecting all the subleading terms which do not carry any additional singularities in this limit

$$\begin{aligned} D = (-iC_{ab\bar{c}})\frac{1}{a_5 - a_3}\int \frac{d^2\tilde{l}}{(2\pi)^2}\frac{i}{-2p_1\cdot\tilde{l} + i\epsilon}\; M_{da}^{(4,0)}(p_3, p_1, p_3, p_1)\frac{i}{x + 2p_3\cdot\tilde{l} + i\epsilon} \\ \times M_{db}^{(4,0)}(p_3, p_2, p_3, p_2)\frac{i}{2p_2\cdot\tilde{l} + i\epsilon}. \end{aligned} \tag{4.5.6}$$

Looking at the RHS image in figure 4.10 we see that p_3 can be expressed in terms

of p_1 and p_2 through the linear combination

$$p_3 = \frac{\Delta_{bd}}{\Delta_{ab}} p_1 - \frac{\Delta_{ad}}{\Delta_{ab}} p_2 \tag{4.5.7}$$

where Δ_{bd}, Δ_{ad} and Δ_{ab} are respectively the areas of the triangles formed by the copies of vectors $(b(p_2), d)$, $(a(p_1), d)$ and $(a(p_1), b(p_2))$. Then we adopt a change of variables which will be largely used also in chapter 7:

$$2p_1 \cdot \tilde{l} = u \quad , \quad 2p_2 \cdot \tilde{l} = v.$$

Keeping into account the Jacobian carried by this new choice of variable

$$d^2\tilde{l} = \frac{du\ dv}{4m_a m_b \sinh\theta_{12}}$$

the loop integral reduces to

$$\begin{aligned} D = (-iC_{ab\bar{c}}) \frac{1}{a_5 - a_3} \frac{1}{4m_a m_b \sinh\theta_{12}} M_{da}^{(4,0)}(p_3, p_1)\ M_{db}^{(4,0)}(p_3, p_2) \\ \times \int \frac{du\ dv}{(2\pi)^2} \frac{i}{-u + i\epsilon}\ \frac{i}{x + \frac{\Delta_{bd}}{\Delta_{abc}} u - \frac{\Delta_{ad}}{\Delta_{abc}} v + i\epsilon}\ \frac{i}{v + i\epsilon}\ . \end{aligned} \tag{4.5.8}$$

The integration can easily be performed using Cauchy's theorem by closing the u-contour on the upper half complex plane and the v-contour on the lower half-plane. The integration result is simply given by $\frac{i}{x}$, so that the result for the double-blob diagram in figure 4.8 can be written as

$$D = \frac{C_{ab\bar{c}}}{x(a_5 - a_3)} \frac{1}{4m_a m_b \sinh\theta_{12}} M_{da}^{(4,0)}(p_3, p_1)\ M_{db}^{(4,0)}(p_3, p_2). \tag{4.5.9}$$

When we substitute the value of x given in (4.5.4) into this last expression the $\sinh\theta_{21}$ in x simplifies with $\sinh\theta_{12}$ in (4.5.9) generating a minus sign. Thus if we sum the four singular contributions depicted in figure 4.8 we obtain

$$\begin{aligned} M_{abd\to cd}^{(5,1)} &= 2a_3\ \frac{C_{ab\bar{c}}}{a_5 - a_3} \\ &\times \Big[\frac{1}{4m_d m_c \sinh\theta_{34}} M_{dc}^{(4,1)}(\theta_{34}) - \frac{1}{4m_d m_a \sinh\theta_{31}} M_{da}^{(4,1)}(\theta_{31}) - \frac{1}{4m_d m_b \sinh\theta_{32}}(\theta_{32}) M_{db}^{(4,1)}(\theta_{32}) \\ &- \frac{1}{4m_d m_a \sinh\theta_{31}} M_{da}^{(4,0)}(\theta_{31})\ \frac{1}{4m_d m_b \sinh\theta_{32}} M_{db}^{(4,0)}(\theta_{32}) \Big]. \end{aligned} \tag{4.5.10}$$

The first three terms on the RHS of (4.5.10) have been obtained in the same way as we did in the tree-level case (4.2.3) with the only difference that amplitudes are given by summing over one-loop diagrams now. Using the relation in (3.1.15) and defining $\theta_{34} \equiv \theta$ the requirement that on the pole $a_5 = a_3$ the singularity disappears becomes

$$S_{dc}^{(1)}(\theta) = S_{da}^{(1)}(\theta - i\bar{U}_{ac}^b) + S_{db}^{(1)}(\theta + i\bar{U}_{bc}^a) + S_{da}^{(0)}(\theta - i\bar{U}_{ac}^b) S_{db}^{(0)}(\theta + i\bar{U}_{bc}^a). \tag{4.5.11}$$

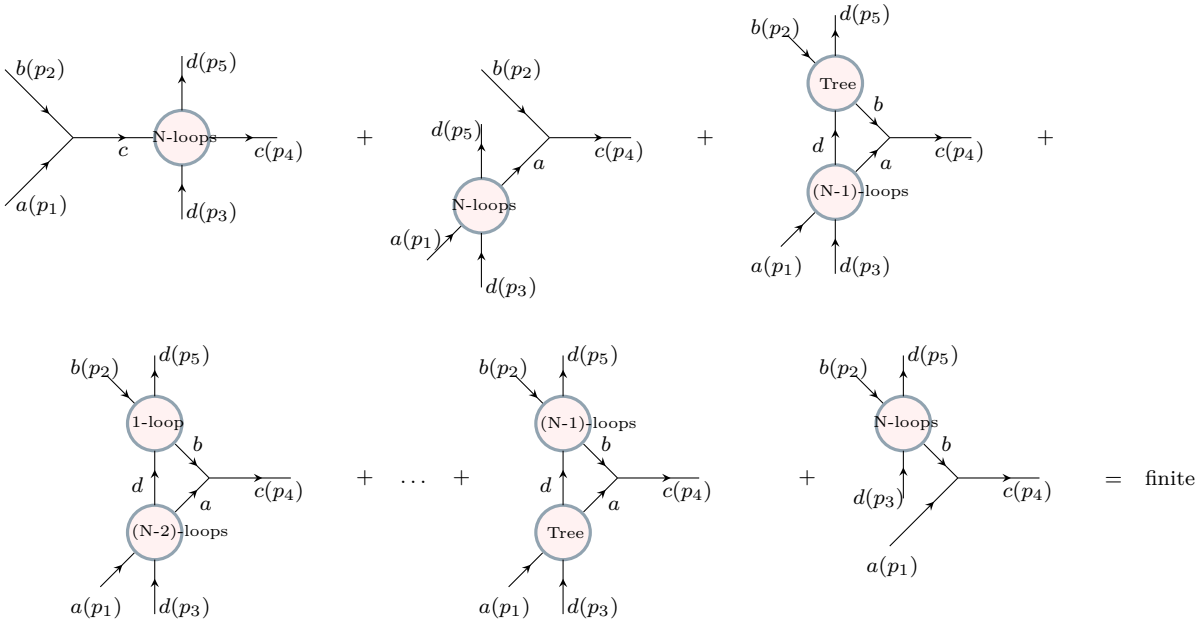

Figure 4.11: List of contributions to the pole in the process $a + b + d \to c + d$. The imposition that the residue is null on the pole position gives the N-loop order bootstrap relation.

This represents the one-loop order of the expansion of the bootstrap relation (2.4.7). Such a relation can be easily generalised at N-loops imposing that at all orders the residue of the pole for the process (4.2.1) is equal to zero. The diagrams contributing to the pole at N loops are shown in figure 4.11 and the imposition that their sum has a zero residue on the pole returns

$$\begin{aligned} S_{dc}^{(N)}(\theta) = S_{da}^{(N)}(\theta - i\bar{U}_{ac}^{b}) + S_{da}^{(N-1)}(\theta - i\bar{U}_{ac}^{b})S_{db}^{(0)}(\theta + i\bar{U}_{bc}^{a}) \\ + S_{da}^{(N-2)}(\theta - i\bar{U}_{ac}^{b})S_{db}^{(1)}(\theta + i\bar{U}_{bc}^{a}) + \ldots + S_{db}^{(N)}(\theta + i\bar{U}_{bc}^{a}), \end{aligned} \tag{4.5.12}$$

where a superscript index is associated to each S-matrix element reporting its loop order. After having taken into account the singular contributions at all the loop orders the imposition of the pole cancellation is written as

$$M_{abd\to cd} \sim \frac{C_{ab\bar{c}}}{a_5 - a_3}\left[S_{dc}(\theta) - S_{da}(\theta - i\bar{U}_{ac}^{b})S_{db}(\theta + i\bar{U}_{bc}^{a})\right] = 0, \tag{4.5.13}$$

which exactly matches the bootstrap relation (2.4.7).

It is still an open problem to verify the full bootstrap equations (4.5.13) in perturbation theory for general purely elastic quantum field theories. Moreover, an important remark is necessary. In the discussion above we implicitly assumed that the 3-point coupling $C_{ab\bar{c}}^{(3)}$, as well as the masses of the propagating particles, remain fixed on their classical values, no matter the loop order we are considering. This claim is false in general. There are examples of quantum theories, such as the non self-dual affine Toda models, where the masses, and therefore the fusing angles (which are $\bar{U}_{ac}^{b}$

and $\bar{U}^a_{bc}$ in (4.5.13)), renormalize in a non-trivial way at the quantum level [57]. We should take into account this fact in (4.5.13). In addition also the 3-point couplings can be modified by quantum corrections. Note that the residue in (4.5.13) is null in two situations: when the bootstrap equation is satisfied, but also when $C_{ab\bar{c}}$ is equal to zero. In particular, the possibility that some 3-point coupling (different from zero at the classical level) cancel after the renormalisation procedure can in principle spoil some of the bootstrap fusing equations. The quantum story is very complicated and a full understanding of it is still lacking.

4.5.2 Loop-level factorisation

Another aspect of integrable theories is the factorisation of their S-matrices. In section 2.2 we reviewed the argument proposed by Parke [21], according to which the presence of two higher spin conserved charges, in addition to energy and momentum, should suffice to have absence of production and factorisation in the scattering. Even though a full perturbative quantum proof of the absence of production is still lacking, in this section we highlight where the factorisation of the S-matrix comes from in perturbation theory. In particular, we point out what contributions, which survive after all the Feynman diagrams are summed, are responsible for splitting a 3-to-3 S-matrix into the product of three 2-to-2 S-matrices. At a given loop order

$$L = m + n + k + 1 \tag{4.5.14}$$

these contributions are reported in figure 4.12, where the blobs represent respectively sums of all the Feynman diagrams with fixed loop numbers m, k and n. As a convention we assume these numbers running on the integers between -1 and $+\infty$, where -1 and 0 inside a blob correspond respectively to have no interactions and tree-level interactions. The two pictures in figure 4.7 in the more general set-up presented here, cover the case $k = 0$, $n = 0$ and $m = -1$.

After having computed the two contributions in figure 4.12 we need to sum over all the integers m, k and $n \in [-1, +\infty]$ satisfying the condition (4.5.14). In this way we obtain the L-loop contribution to the amplitude. We focus on the diagram on the LHS in figure 4.12. As we saw before we can use the two degrees of freedom of the loop integration variable to set the momenta of the particles a and b propagating in the loop on-shell and equal to the external momenta p_1 and p_5. Instead, the momentum of the c-propagator is not free since we have already used our freedom to tune properly the momenta p_a and p_b. For this reason for general external kinematics p_c is off-shell, as depicted on the LHS of figure 4.13. It is only in the collinear limit $a_4 \to a_1$ that also the momentum p_c goes on-shell and becomes equal to the common value $p_c = p_3 = p_6$ as it is shown on the RHS of figure 4.13.

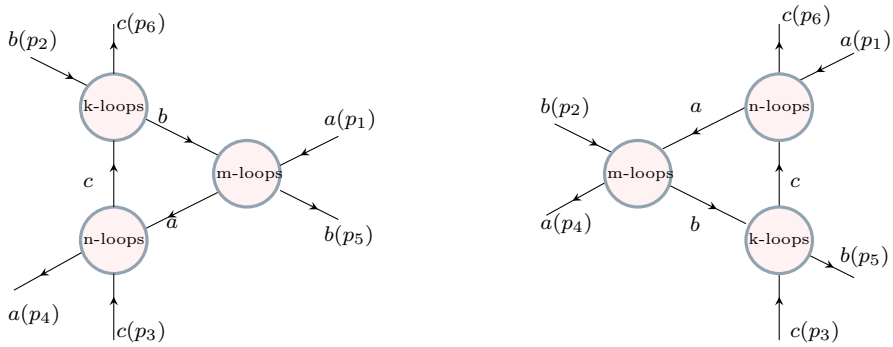

Figure 4.12: Pair of diagrams contributing to the factorisation of the six-point process $a + b + c \to a + b + c$ at the fixed loop-order $L = m + n + k + 1$.

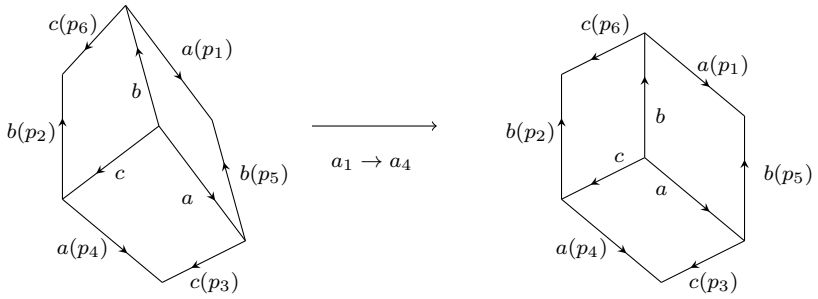

Figure 4.13: Collinear limit of the loop diagram contributing to the factorisation of $a + b + c \to a + b + c$. On the LHS it is shown the point in the integration region in which the internal a and b-propagators are collinear to two external particles. In the limit in which the set of outgoing momenta is equal to the set of the incoming ones also the internal c-propagator becomes on-shell and collinear to the external c-particles.

The integral expanded around the values $p_a = p_1$ and $p_b = p_5$ is given by

$$D_L = \int \frac{d^2l}{(2\pi)^2} \frac{i}{2p_1 \cdot l + l^2 + i\epsilon} M_{ac}^{(4,n)}(p_1 + l, p_3, p_4, p_c + l) \frac{i}{p_c^2 - m_c^2 + 2p_c \cdot l + l^2 + i\epsilon} \times M_{bc}^{(4,k)}(p_2, p_c + l, p_5 + l, p_6) \frac{i}{2p_5 \cdot l + l^2 + i\epsilon} M_{ab}^{(4,m)}(p_1, p_5 + l, p_5, p_1 + l) \tag{4.5.15}$$

The momentum of the c-propagator can then be written in the collinear limit $a_4 \to a_1$

$$p_c^2 - m_c^2 = (p_1 + p_3 - p_4)^2 - m_c^2 \to \frac{m_a m_c}{a_3 a_1^2}(a_1 - a_4)(a_1^2 - a_3^2)$$

We rescale the integration variables multiplying by the displacement from the singular position $a_4 = a_1$

$$l = (a_1 - a_4)\tilde{l},$$

and we consider only the singular value of the integral. Writing p_3 as a linear combination of p_1 and p_2 and using the following change of variables

$$u = 2p_1 \cdot \tilde{l} \quad , \quad v = 2p_2 \cdot \tilde{l}$$

the integral is solved using Cauchy's residue theorem by closing both the u- and the v-contours on the lower half-plane. The final result is

$$D_L = \frac{i}{4m_a m_b \sinh\theta_{12}} M_{ac}^{(4,n)}(p_1, p_3, p_1, p_3) \frac{1}{\frac{m_a m_c}{a_3 a_1^2}(a_1 - a_4)(a_1^2 - a_3^2) + i\epsilon} \times M_{bc}^{(4,k)}(p_2, p_3, p_2, p_3) M_{ab}^{(4,m)}(p_1, p_2, p_1, p_2). \tag{4.5.16}$$

The diagram on the RHS of figure 4.12 can be obtained in the same way with the only difference that now p_c is pointing in the 'opposite direction' (i.e. from the k-loop blob to the n-loop one). Therefore the value of D_R is obtained by substituting a_3 with $-a_3$. Summing the two contributions we obtain

$$\begin{aligned} D_L + D_R =& \frac{i}{4m_a m_b \sinh\theta_{12}} M_{ac}^{(4,n)}(p_1, p_3)\ M_{bc}^{(4,k)}(p_2, p_3)\ M_{ab}^{(4,m)}(p_1, p_2) \\ & \times \lim_{\epsilon \to 0^+} \left[\frac{1}{\frac{m_a m_c}{a_3 a_1^2}(a_1 - a_4)(a_1^2 - a_3^2) + i\epsilon} - \frac{1}{\frac{m_a m_c}{a_3 a_1^2}(a_1 - a_4)(a_1^2 - a_3^2) - i\epsilon} \right] \\ =& \frac{\pi}{4m_a m_b \sinh\theta_{12}} M_{ac}^{(4,n)}(p_1, p_3)\ M_{bc}^{(4,k)}(p_2, p_3)\ M_{ab}^{(4,m)}(p_1, p_2) \frac{1}{m_a m_c \sinh\theta_{13}} \delta(\theta_1 - \theta_4). \end{aligned} \tag{4.5.17}$$

where the distribution formula (4.3.4) has been used. The rest of the computation exactly follows the tree-level case discussed in section 4.3. The delta function $\delta(\theta_1 - \theta_4)$ obtained by sending $i\epsilon$ to zero multiplied by the delta of the overall-energy momentum conservation returns the expression in (4.3.7). Adding finally a normalisation factor $\frac{1}{\sqrt{4\pi}}$ for each external state we get that the contribution arising from the two diagrams

in figure 4.12 is given by

$$\frac{1}{4m_a m_b \sinh\theta_{12}} M_{ab}^{(4,m)}(\theta_{12})\ \frac{1}{4m_b m_c \sinh\theta_{23}} M_{bc}^{(4,k)}(\theta_{23})\ \frac{1}{4m_a m_c \sinh\theta_{13}} M_{ac}^{(4,n)}(\theta_{13}) \times \delta(\theta_1-\theta_4)\delta(\theta_2-\theta_5)\delta(\theta_3-\theta_6) \tag{4.5.18}$$

Summing over all the integers $k, m, n = -1, 0, \ldots L$ satisfying (4.5.14) we obtain the value of the L-loop S-matrix for the process (4.3.1); it is given by

$$S_{abc\to abc}^{(L)} = \sum_{\substack{k,m,n=-1 \\ k+n+m+1=L}}^{L} S_{ab}^{(m)}(\theta_{12}) S_{bc}^{(k)}(\theta_{23}) S_{ac}^{(n)}(\theta_{13}). \tag{4.5.19}$$

The relation in (4.5.19) corresponds to the L-loop order in the expansion of (4.3.9).

Part II

Perturbative Integrability in Affine Toda Field Theories

Chapter 5

Affine Toda models and their underlying geometry

5.1 Definition of the models

From the general considerations discussed in the first part of this thesis, we move on to study a particular class of bosonic quantum field theories: the affine Toda models. In this and the next chapter, we show how all the bootstrap and perturbative requirements are universally satisfied by these models at tree level. These models are a particular class of (1+1)-dimensional quantum field theories describing the interaction of r bosonic scalar fields $\phi = (\phi_1, \ldots, \phi_r) \in \mathbb{R}^r$. Each theory is defined in terms of a set of $r+1$ vectors $\{\alpha'_0 \ldots \alpha'_r\}$, all lying in $\mathbb{R}^r$, whose inner products are encoded in one of the twisted or untwisted affine Dynkin diagrams [72], together with a mass scale m and a coupling g. The Lagrangian is

$$\mathcal{L} = \frac{1}{2}\partial_\mu \phi_a \partial^\mu \phi_a - \frac{m^2}{g^2}\sum_{i=0}^{r} n_i e^{g\cdot\phi_a(\alpha'_i)_a} \tag{5.1.1}$$

where the sum over the repeated indices labelling the components of ϕ and the roots is implicit. Affine Toda theories are associated with Kac-Moody algebras of finite type. The integers n_i appearing in the Lagrangian are characteristic for each algebra. The set $\{\alpha'_i\}_{i=0}^r$ comprises the simple roots of the algebra and the additional root α'_0, necessary to have a stable vacuum, defined by

$$\alpha'_0 = -\sum_{i=1}^{r} n_i \alpha'_i. \tag{5.1.2}$$

In this way, after having imposed $n_0 = 1$, we obtain

$$\sum_{i=0}^{r} n_i \alpha'_i = 0. \tag{5.1.3}$$

The last condition ensures that the Taylor expansion of the potential around $\phi = 0$ does not have a linear term in ϕ and therefore $\phi = 0$ is a stationary point around

which it is possible to perform standard perturbation theory. In that regard, we need to figure out what are the masses and the couplings, in such a way to be able to define the Feynman rules. The potential in the Lagrangian (5.1.1) can be expanded as follows:

$$\begin{aligned} V &\equiv \frac{m^2}{g^2}\sum_{i=0}^{r} n_i e^{g\cdot\phi_a(\alpha'_i)_a} \\ &= \frac{m^2}{g^2}\sum_{i=0}^{r} n_i + \frac{1}{2}M^2_{ab}\phi_a\phi_b + \frac{1}{3!}C^{(3)}_{abc}\phi_a\phi_b\phi_c + \dots \end{aligned} \tag{5.1.4}$$

where the squared of the mass matrix and the couplings are defined in terms of the roots through

$$M^2_{ab} = m^2\sum_{i=0}^{r} n_i(\alpha'_i)_a(\alpha'_i)_b \quad , \quad C^{(3)}_{abc} = m^2 g\sum_{i=0}^{r} n_i(\alpha'_i)_a(\alpha'_i)_b(\alpha'_i)_c \quad , \ \dots \tag{5.1.5}$$

The first step is to diagonalize the mass-squared matrix so to find the masses of the theory: $m_1, \dots, m_r$. Next, after having found the basis making M^2 of the form $M^2 = \text{diag}(m_1^2, \dots, m_r^2)$, we need to express all the couplings in this basis. If these theories are tree-level integrable, the data in (5.1.5) should provide the seeds of integrability and it should be possible to write all the higher point couplings in terms of these fundamental parameters as is done in (3.5.7) and (4.1.13) by imposing absence of production. In the next chapter, we will show how these equations, for the affine Toda theories, emerge from a completely different perspective and are implied by properties of the simple roots $\{\alpha'_i\}_{i=1}^r$. In these cases, the perturbative cancellation of inelastic processes is related to the beautiful geometry of the root systems associated with such models [73, 74]. Aspects of this geometrical structure have been explored in several papers, including [69, 73–79]. In particular, on-shell momentum components with imaginary rapidity corresponding to poles in Feynman diagrams can be seen as projections of higher-dimensional roots, the masses and fusing angles corresponding to bound states of the theory being completely encoded in the root system. Nevertheless, the full role of this geometrical structure in ensuring the absence of production has remained unclear until [1], when a full proof of the tree-level integrability of these theories was given.

In this chapter, a review of the integrability of affine Toda field theories is reported: section 5.2 reviews the derivation of a Lax connection, necessary to prove the classical integrability of these models. After having recalled important geometrical properties of root systems in section 5.3, in section 5.4 (following the argumentation presented in [38]) a correspondence between the spins of the conserved charged and the Lie algebra exponents is made manifest. Through such correspondence in section 5.5 we introduce universal quantum aspects of affine Toda theories reviewing part of the results shown in [73]. The root system properties discussed in the next sections will be relevant also for chapter 6: from them, a universal proof of the tree-level perturbative integrability of affine Toda field theories will be provided, based on the novel results from [1].

5.2 Classical integrability in affine Toda models

To capture all the universal properties making affine Toda models beautiful examples of integrable quantum field theories, some more detail about their underlying mathematical structure is required. To that end, let us consider a semisimple Lie algebra $\mathcal{G}$ and let $\mathcal{H}'$ be a Cartan subalgebra of $\mathcal{G}$, comprising a maximal set of commuting generators $\{H'_a\}_{a=1}^r$. The dimension r of $\mathcal{H}'$ is equal to the rank of the algebra. Diagonalising the adjoint action of this subalgebra on the remaining generators of $\mathcal{G}$ we obtain the following basis in $\mathcal{G}$

$$\{E_{\alpha'}\}_{\alpha'\in\Phi'} \quad , \quad \{H'_a\}_{a=1}^r \tag{5.2.1}$$

where

$$[H'_a, H'_b] = 0 \quad , \quad [H'_a, E_{\alpha'}] = (H'_a, \alpha')E_{\alpha'}. \tag{5.2.2}$$

The index a runs from 1 to r and labels the basis of the Cartan subalgebra while the set of vectors $\{\alpha'\}_{\alpha'\in\Phi'}$ in $\mathcal{H}'$ make up a root system Φ' of $\mathcal{G}$. In (5.2.2) we used the following scalar product

$$(X, Y) = \mathrm{Tr}(\mathrm{ad}_X\ \mathrm{ad}_Y). \tag{5.2.3}$$

The generators $\{H'_a, E_{\alpha'}\}$ of $\mathcal{G}$ can be tuned in such a way to satisfy the following relations:

$$(H'_a, H'^{\dagger}_b) = \delta_{ab}, \tag{5.2.4a}$$
$$(E_{\alpha'}, E_{-\beta'}) = \delta_{\alpha'\beta'}. \tag{5.2.4b}$$

The symbol $\dagger$ represents the hermitian conjugate operation (conjugate transpose) in cases when a matrix representation is chosen for the algebra. More generally the operation $\dagger$ is defined by its action on the abstract elements of the algebra as

$$(X + iY)^{\dagger} = X - iY$$

for any $X, Y \in i\mathcal{T}$ with $\mathcal{T}$ being a compact form of $\mathcal{G}$ (see pp. 1003-1004 of [83]). Given now a generic element $v \in \mathcal{H}'$, it can be written as a vector $\mathbf{v} = (v_1, \ldots, v_r) \in \mathbb{C}^r$ having as components the coefficients of the expansion

$$v = \sum_{a=1}^{r} (v, H'^{\dagger}_a) H'^{\,a} \equiv \sum_{a=1}^{r} v_a H'^{\,a}. \tag{5.2.5}$$

The Lagrangian (5.1.4) can then be written in a form independent of the choice of the basis used to define the root system as

$$\mathcal{L} = \frac{1}{2}(\partial_\mu\phi, \partial^\mu\phi) - \frac{m^2}{g^2}\sum_{i=0}^{r} n_i e^{g\cdot(\phi,\alpha'_i)} \tag{5.2.6}$$

In (5.2.6) the field ϕ and the roots $\{\alpha'_i\}_{i=0}^r$ have to be seen as elements of $\mathcal{H}'$. By expanding the roots and the field on the basis of H'_a, as shown in (5.2.5), with the

further condition ${H'}_a^\dagger = H'_a$, it is immediate to see that the Lagrangian in (5.2.6) is the same as that one in (5.1.1). However, we prefer to relax such a condition here and choose instead

$$ {H'}_a^\dagger = {H'}_{\bar{a}}, \tag{5.2.7} $$

with a and $\bar{a}$ possibly different indices in $\{1, \dots, r\}$. Since ϕ, in some representation, can be written on a basis of hermitian matrices with real coefficients, then of course it has to hold that $\phi^\dagger = \phi$ independently on the basis used to write ϕ. Combined with (5.2.7) this leads to $\phi_a^* = \phi_{\bar{a}}$, which allows us to keep into account also the cases in which antiparticles are present. It will be a matter of the next sections to provide a nice set of $\{H'_a\}_{a=1}^r$ making the squared of the mass matrix in the potential diagonal. By Taylor expanding (5.2.6) on this basis, we will obtain a Lagrangian of the form in (3.1.12) and we will be able to derive the scattering requirements previously found from properties of Lie algebras.

Before moving to the quantum case it is instructive to see why these theories are interesting already at the classical level. Their classical integrability was proven in [38, 80] and relies on the existence of a Lax connection from which an infinite set of conserved charges can be extracted. Below we explain in some detail how this Lax connection can be constructed. First, we should set the following additional properties for the generators:

$$ \begin{aligned} &E_{\alpha'}^\dagger = E_{-\alpha'}, \\ &[E_{\alpha'}, E_{-\alpha'}] = \alpha', \\ &[E_{\alpha'}, E_{\beta'}] = N_{\alpha',\beta'} E_{\alpha'+\beta'}. \end{aligned} \tag{5.2.8} $$

The third equality in (5.2.8) is different from zero only if $\alpha' + \beta'$ is a root, or if $\alpha' + \beta' = 0$ (in this case the second equality holds); $N_{\alpha'\beta'}$ are the structure constants of the algebra. Then the equations of motion derived from the Lagrangian (5.2.6), which are

$$ \partial_\mu \partial^\mu \phi + \frac{m^2}{g} \sum_{i=0}^{r} n_i \alpha'_i e^{g\cdot(\phi,\alpha_i)} = 0, \tag{5.2.9} $$

can be written as the zero curvature condition of a properly chosen two-dimensional vector potential $\mathcal{A}_\mu$. We can define this potential as

$$ \begin{aligned} \mathcal{A}_0 &= \frac{g}{2}\partial_1\phi + \frac{m}{2}\sum_{i=0}^{r}\Big(\lambda c_i E_{\alpha'_i} - \frac{1}{\lambda} c_i^* E_{-\alpha'_i}\Big) e^{\frac{g}{2}(\phi,\alpha'_i)}, \\ \mathcal{A}_1 &= \frac{g}{2}\partial_0\phi + \frac{m}{2}\sum_{i=0}^{r}\Big(\lambda c_i E_{\alpha'_i} + \frac{1}{\lambda} c_i^* E_{-\alpha'_i}\Big) e^{\frac{g}{2}(\phi,\alpha'_i)}, \end{aligned} \tag{5.2.10} $$

where c_i are complex numbers chosen in such a way to satisfy $|c_i|^2 = n_i$, being n_i the same set of numbers appearing in (5.2.6). By using (5.2.2) and (5.2.8), it can be shown that the zero curvature condition

$$ F_{01} = \partial_0 \mathcal{A}_1 - \partial_1 \mathcal{A}_0 + [\mathcal{A}_0, \mathcal{A}_1] = 0, \tag{5.2.11} $$

imposed to be satisfied for any value of the spectral parameter λ, is equivalent to

the equations of motion (5.2.9).

An infinite tower of conserved charges can be defined by making use of the monodromy matrix

$$T(\lambda) \equiv K(-\infty, +\infty; \lambda). \tag{5.2.12}$$

where K is the path ordered exponential evaluated at a fixed time

$$K(a, b; \lambda) \equiv \mathrm{P} \exp\Big(\int_a^b dx_1 \mathcal{A}_1(x_1) \Big).$$

Provided the fields and their spatial derivatives satisfy suitable conditions at $x_1 = \pm\infty$, and making use of the fact that

$$\frac{dK}{dt} = K\mathcal{A}_0(b) - \mathcal{A}_0(a)K$$

then

$$t(\lambda) = \mathrm{Tr}(T(\lambda)) \tag{5.2.13}$$

does not depend on time. The quantity in (5.2.13) is called the transfer matrix and, by performing its expansion in the spectral parameter λ, we can generate an infinite number of conserved charges. This is however not enough to establish that the theory is integrable. The charges generated through (5.2.13) have indeed to commute, which is equivalent to require that values of the transfer matrix evaluated at different points, say $t(\lambda_1)$ and $t(\lambda_2)$, are in involution. The involutary nature of the charges can be checked by proving the so-called fundamental Poisson bracket relation (FPR) [81] between the components $\mathcal{A}_1$ at equal times, which are formulated in terms of a classical r-matrix. The proof for the affine Toda theories, together with an expression for the r-matrix in terms of root system data, is given in [38]. Although we will omit to give a derivation of the r-matrix here, we will return to the derivation of the conserved charges in section 5.5, after some additional tools on Lie algebras will be provided. It is important to mention that the integrability of Toda field theories was studied also in [82], where it was proven that the set of classical conserved charges can be deformed through the coupling and promoted in this way to a quantum set of commuting conserved charges. Even though this is not the definition of quantum integrability adopted in this thesis, which instead relies on the absence of production in scattering processes, these two different setups should ultimately be connected.

5.3 The relevance of the Coxeter geometry

Let Q be the unique element in $\mathcal{H}'$ such that

$$(Q, \alpha_i') = 1 \ \forall \text{ simple root } \alpha_i'. \tag{5.3.1}$$

Then, given a generic root α', written as a linear combination of the simple roots with integer coefficients

$$\alpha' = \sum_{i=1}^{r} m_i \alpha'_i,$$

it holds that

$$[Q, E'_\alpha] = (Q, \alpha') E_{\alpha'} = \mathrm{ht}(\alpha') E_{\alpha'}, \tag{5.3.2}$$

where $\mathrm{ht}(\alpha') = \sum_{i=1}^{r} m_i$ is called the *height* of the root α'. Of course any simple root α'_i satisfies $\mathrm{ht}(\alpha'_i) = 1$. Moreover, if we define $-\alpha'_0$ to be the root with greatest height[1] then $\mathrm{ht}(-\alpha'_0) = h - 1$. The integer h is called the Coxeter number and for untwisted affine Toda theories it is obtained by summing the integers $\{n_0, n_1, \ldots, n_r\}$ defined in (5.1.1). The other heights belong to the sets $E \equiv \{s_i\}_{i=1}^{r}$ and $\tilde{E} \equiv \{-s_i\}_{i=1}^{r}$, where the numbers s_i are positive integers satisfying

$$1 = s_1 \leq s_2 \leq \ldots \leq s_{r-1} \leq s_r = h - 1.$$

The positive sets of integers $E = \{s_i\}_{i=1}^{r}$ are characteristic of each Lie algebra and are called exponents. They always appear in the number r, the rank of the Lie algebra.

Following [75], we can define the element

$$A = \exp\left(\frac{2\pi i}{h} \mathrm{ad}_Q\right), \tag{5.3.3}$$

where h is the Coxeter number introduced above. Such an element acts diagonally on the set of generators $\{H'_a, E_{\alpha'}\}$ used to span the Lie algebra. Indeed, due to (5.3.2), we have

$$A E_{\alpha'} = \omega^s E_{\alpha'} \quad \text{with} \quad \omega = e^{\frac{2\pi i}{h}} \tag{5.3.4}$$

and

$$A H'_a = H'_a. \tag{5.3.5}$$

In (5.3.4) the integer s is an exponent of $\mathcal{G}$, corresponding to the height of α'. It is now possible to define a set of r linearly independent eigenvectors of A, one for each exponent, generating a new Cartan subalgebra $\mathcal{H}$ (different from $\mathcal{H}'$) of $\mathcal{G}$. We label by z_1 and z_{h-1} the two eigenvectors of A with eigenvalues ω and ω^{h-1}, defined by

$$z_1 = \sum_{i=0}^{r} c_i E_{\alpha'_i} \quad \text{and} \quad z_{h-1} = \sum_{i=0}^{r} c_i^* E_{-\alpha'_i} \tag{5.3.6}$$

respectively. The coefficients c_i are the same as those used to define the Lax connection in (5.2.10); they are complex numbers properly tuned so to satisfy $|c_i|^2 = n_i$. Due to this fact, combined with (5.2.8) and (5.1.3), it is not difficult to verify that $[z_1, z_{h-1}] = 0$. The element z_1 in (5.3.6) is a regular element in $\mathcal{G}$ [83], meaning that all the elements commuting with it also commute between one another and form a new Cartan subalgebra $\mathcal{H}$ in $\mathcal{G}$. The other elements comprising the basis of $\mathcal{H}$ can

[1] If (5.1.1) is the Lagrangian of an untwisted affine Toda theory the greatest height root $-\alpha'_0$ exactly matches with the definition given in (5.1.2)

be similarly defined as[2]

$$z_s = \sum_{\mathrm{ht}(\alpha')\in\{s,s-h\}} c_{\alpha'} E_{\alpha'} \quad , \quad z_{h-s} = \sum_{\mathrm{ht}(\alpha')\in\{s,s-h\}} c^*_{\alpha'} E_{-\alpha'}. \tag{5.3.7}$$

The coefficients $c_{\alpha'}$ have to be properly tuned so to ensure that the elements in (5.3.7) commute with z_1 (and therefore, by the fact that z_1 is regular, commute with each other) and satisfy the condition

$$(z^\dagger_{s_1}, z_{s_2}) = h\delta_{s_1 s_2}.$$

Note that, due to the first equality in (5.2.8),

$$z^\dagger_s = z_{h-s}.$$

The fact that the elements in (5.3.7) form a basis for a Cartan subalgebra in $\mathcal{G}$ is a consequence of a lemma in [83] (see discussion at pp. 1012-1013 in [83]). Since the set of $\{z_s\}_{s\in E}$ generates a new Cartan subalgebra $\mathcal{H}$, we can define a new root system in $\mathcal{H}$. By taking a generic root $\alpha \in \mathcal{H}$ we can expand it on the basis of $\{z_s\}_{s\in E}$ as

$$\alpha = \frac{1}{h}\sum_{s\in E}(\alpha, z_{h-s}) z_s \tag{5.3.8}$$

Acting with A on α we get

$$A\alpha = \frac{1}{h}\sum_{s\in E}\omega^s(\alpha, z_{h-s}) z_s$$

From this fact, it should be clear that A is periodic with periodicity h and, for each s, the two real combinations

$$\frac{z_s + z_{h-s}}{2\sqrt{h}} \quad \text{and} \quad \frac{z_s - z_{h-s}}{2i\sqrt{h}} \tag{5.3.9}$$

span a plane in $\mathcal{H}$ on which A acts as a rotation by $\frac{2\pi s}{h}$. As Bertram Kostant [83] noted, the restriction of A to $\mathcal{H}$ is a Coxeter transformation of $\mathcal{H}$. By this, we mean that if we have a (suitably ordered) set of simple roots $\{\alpha_i\}_{i=1}^r$ with respect to $\mathcal{H}$, then the action of A on $\mathcal{H}$ can be written as a product of Weyl reflections, one for each of the simple roots α_i. The details of this construction are given below.

For any root $\alpha \in \mathcal{H}$ we define the corresponding Weyl reflection to be the linear transformation acting as a reflection respect to the hyperplane orthogonal to α:

$$w_\alpha(x) = x - 2\frac{(x,\alpha)}{(\alpha,\alpha)}\alpha. \tag{5.3.10}$$

Such reflections map the root system to itself and the closed group W that they generate is called the Weyl group. For a given choice of simple roots, a Coxeter

[2]The case $s = h/2$ is a bit special; in such a case we can have $z_s = z_{h-s} = z_{h/2}$, if there is a single exponent with value $h/2$, or we can have $z_s = z_{s_1} \neq z_{h-s} = z_{s_2}$ (if there are two separate exponents s_1 and s_2 both equal to $h/2$).

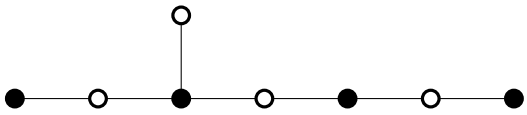

Figure 5.1: E_8 Dynkin diagram.

element of the Weyl group is the product of the Weyl reflections over that set of simple roots. Of course, there are many possible choices depending on the choice of simple roots, but the Coxeter elements that can be constructed starting from these different choices, and the orderings of the reflections in any choice, belong to the same conjugacy class of W. A convenient choice is the so-called Steinberg ordering [84]: split the simple roots into two sets, 'black' and 'white', indicated with the labels $\bullet$ and $\circ$. All the roots inside the same set are mutually orthogonal, and so are not connected on the Dynkin diagram (see the example in figure 5.1). We then write the Coxeter element w as

$$w = w_\bullet w_\circ = \prod_{\alpha\in\bullet} w_\alpha \prod_{\beta\in\circ} w_\beta. \tag{5.3.11}$$

Kostant [83] showed how to define a particular set of r roots $\{\gamma_a\}_{a=1}^r$ from which the entire root system can be generated by the action of a given Coxeter element w. This action produces r closed orbits each with h elements, where h is the Coxeter number of the algebra. A convenient way of writing these roots uses the fundamental weights $\{\lambda_a\}_{a=1}^r$ of the Lie algebra, defined by

$$\frac{2}{(\alpha_a,\alpha_a)}(\lambda_a,\alpha_b) = \delta_{ab}. \tag{5.3.12}$$

The root system can then be generated acting with w on the roots

$$\gamma_a = (1-w^{-1})\lambda_a = \begin{cases} \alpha_a & \text{if } a\in\circ \\ -w^{-1}\alpha_a & \text{if } a\in\bullet \end{cases} \tag{5.3.13}$$

The first equality holds for any Coxeter element, while the second assumes the Steinberg ordering. We define the orbit Γ_a to be the set of roots obtained by acting with the Coxeter element (5.3.11) on the root γ_a (after h steps we come back to the starting root). The relations in (5.3.10), (5.3.11) define the geometrical action of w on the Cartan subalgebra, as a combination of rotations of different subspaces of $\mathcal{H}$.

It is possible to show that the eigenvalues of w are exactly equal to $\{\omega^s\}_{s\in E}$, making possible to identify w with the action of A restricted to $\mathcal{H}$. Then the orthonormal basis diagonalizing w in $\mathcal{H}$ is provided by the set $\{z_s\}_{s\in E}$ in (5.3.7). The projectors onto the different eigenvectors of w, used to expand the root α in (5.3.8), can then be written as [74]

$$P_s = \frac{1}{h} z_s \otimes z_{h-s} = \frac{1}{h}\sum_{p=0}^{h-1} \omega^{-sp} w^p. \tag{5.3.14}$$

While the first expression for the projector, written as a tensor product of z_s and z_{h-s}, makes sense only if it is applied to an element inside $\mathcal{H}$, the second definition

can be extended to the full Lie algebra $\mathcal{G}$. Indeed, making use of the fact that (5.3.3) is the extension of w to the entire of $\mathcal{G}$, we can write

$$P_s = \frac{1}{h}\sum_{p=0}^{h-1}\omega^{-sp}A^p. \tag{5.3.15}$$

If $\{e_\alpha\}$ is the set of generators with respect to the Cartan subalgebra $\mathcal{H}$, satisfying

$$[\alpha, e_\beta] = (\alpha,\beta)e_\alpha,$$

then the action of A on them is easily derived. Defining $P \equiv e^{\frac{2\pi i}{h}Q}$ then $Ae_\beta = Pe_\beta P^{-1}$ and

$$[\alpha, Ae_\beta] = P[P^{-1}\alpha P, e_\beta]P^{-1} = (w^{-1}\alpha,\beta)Pe_\beta P^{-1} = (\alpha, w\beta)Pe_\beta P^{-1}. \tag{5.3.16}$$

From (5.3.16) we see that

$$Ae_\beta = e_{w\beta}. \tag{5.3.17}$$

We can always choose the roots $\{\alpha\}$ to be in $\mathbb{R}^r$ and set the generators so that

$$e_\alpha^\dagger = -e_{-\alpha} \quad , \quad (e_\alpha, e_{-\beta}) = -\delta_{\alpha\beta}. \tag{5.3.18}$$

With these conventions in place then we have

$$[e_\alpha, e_{-\alpha}] = -\alpha \tag{5.3.19a}$$
$$[e_\alpha, e_\beta] = N_{\alpha\beta}\ e_{\alpha+\beta}. \tag{5.3.19b}$$

The reason why we choose a different convention for the new set of generators $\{e_\alpha\}$ compared to (5.2.8) is to have real structure constants $N_{\alpha,\beta}$, a fact that will become useful in the derivation of couplings of affine Toda field theories, as underlined in [74]. An important observation, due to how A is defined in (5.3.3), is that the structure constants of the algebra are connected by

$$N_{\alpha\beta} = N_{w\alpha\ w\beta}. \tag{5.3.20}$$

The check can be done noting that $[Ae_\alpha, Ae_\beta] = P[e_\alpha, e_\beta]P^{-1}$, where the definition of P is the same as that one used in (5.3.16).

Since the Cartan subalgebra $\mathcal{H}'$ was invariant under the action of A (see (5.3.5)), a consistent basis $\{H'_a\}_{a=1}^r$ in $\mathcal{H}'$ is given by [83]

$$H'_a = \frac{i}{\sqrt{h}}\sum_{p=0}^{h-1} e_{w^p\gamma_a} \tag{5.3.21}$$

where $a = 1,\dots,r$ and γ_a are the roots (5.3.13) in $\mathcal{H}$ labelling the orbits. For each orbits Γ_a it holds that $w\Gamma_a = \Gamma_a$ and therefore the elements in (5.3.21) are invariant under the action of the Coxeter element. From the properties in (5.3.18) it is not difficult to prove that also (5.2.4a) is satisfied. Since the elements in (5.3.21) span $\mathcal{H}$ then they have to commute. This implies that any time there are two roots γ and β,

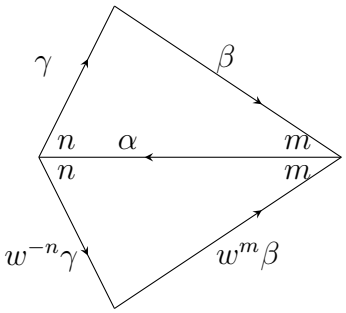

Figure 5.2: Two reflected triangles of roots $\alpha+\gamma+\beta = \alpha + w^{-n}\gamma + w^m\beta = 0$.

belonging to the orbits Γ_c and Γ_b respectively, such that their sum is a root $-\alpha$, then there are exactly two other roots $w^{-n}\gamma$ and $w^m\beta$, for some integers n and m, in the same orbits verifying $N_{w^{-n}\gamma,w^m\beta} = -N_{\gamma,\beta}$. A picture of the two reflected triangles of roots, projected onto the eigenplane of w spanned by real linear combinations of z_1 and z_{h-1} is shown in figure 5.2. In the figure the angles are written in units of $\frac{\pi}{h}$.

Another important fact, of which we do not provide proof here is that the projections of the roots $\{\gamma_a\}_{a=1}^r$ on the eigenplanes of w can be written using complex-number notation as

$$\begin{aligned} P_s(\gamma_a) &= \gamma_a^{(s)} && \text{if } a \in \circ \\ P_s(\gamma_a) &= \gamma_a^{(s)}\ e^{-i\frac{\pi s}{h}} && \text{if } a \in \bullet \end{aligned} \tag{5.3.22}$$

where the phase in (5.3.22) is because there is a $\frac{\pi s}{h}$ angle between the two sets of black and white elements (see figure 5.3). Moreover, the values $\gamma_a^{(s)}$ of the root projections on the different eigenplanes of w are connected to the eigenvectors $\mathbf{q}^{(s)} = (q_1^{(s)}, \dots, q_r^{(s)})$ of the transpose of the Cartan matrix. There are r of such eigenvectors, one for each exponent of the Lie algebra. For a given set of $\mathbf{q}^{(s)}$ satisfying

$$q_a^{(s)} C_{ab}^{[\mathcal{G}]} = 4\sin^2\frac{s\pi}{2h} q_b^{(s)}, \tag{5.3.23}$$

where $C^{[\mathcal{G}]}$ is the Cartan matrix of the Lie algebra $\mathcal{G}$, it holds

$$\gamma_a^{(s)} = \sqrt{2}\frac{\gamma_a^2\ q_a^{(s)}}{|\mathbf{Q}^{(s)}|} \tag{5.3.24}$$

with

$$\mathbf{Q}_s = (|\gamma_1|\ q_1^{(s)}, |\gamma_2|\ q_2^{(s)}, \dots, |\gamma_r|\ q_r^{(s)}). \tag{5.3.25}$$

A proof of this can be derived following for example the lines of [1] and [85].

From the equalities in (5.3.22) we can obtain the projections of all the roots on the different w-eigenplanes by acting with w

$$P_s(w^p\gamma_a) = \omega^{ps} P_s(\gamma_a) \quad , \quad \omega = e^{\frac{2\pi i}{h}}.$$

In table 5.1 we summarize the main ingredients presented in this section, since they

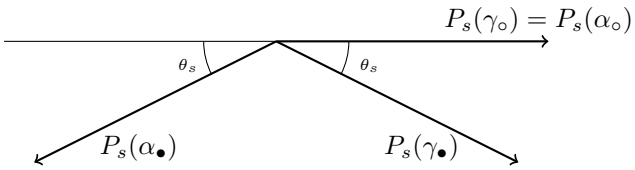

Figure 5.3: Projections of the root $\gamma_\circ = \alpha_\circ$, $\gamma_\bullet = w^{-1}\alpha_\bullet$ and $\alpha_\bullet$ on the eigenplane of w spanned by z_s and z_{h-s}. By $\circ$ and $\bullet$ we respectively mean any element in $\circ$ and $\bullet$ and we defined $\theta_s \equiv \frac{\pi s}{h}$.

$\mathcal{H}' = \text{span}\Big\{H'_a = \frac{i}{\sqrt{h}}\sum_{\alpha\in\Gamma_a} e_\alpha\Big\}_{a=1}^{r}$	$\mathcal{H} = \text{span}\Big\{z_s = \sum_{\text{ht}(\alpha')\in\{s,s-h\}} c_{\alpha'} E_{\alpha'}\Big\}_{s\in E}$
$\{E_{\alpha'}\}_{\alpha'\in\Phi'}$	$\{e_\alpha\}_{\alpha\in\Phi}$
$AE_{\alpha'} = \omega^{\text{ht}(\alpha')} E_{\alpha'}$	$Ae_\alpha = e_{w\alpha}$
$AH'_a = H'_a$	$Az_s = \omega^s z_s$

Table 5.1: Cartan algebras $\mathcal{H}'$ and $\mathcal{H}$ with associated generators.

will be relevant also in the rest of this chapter and in the next one. On the LHS of the table there are the elements used to span the Lie algebra $\mathcal{G}$ having chosen as Cartan subalgebra $\mathcal{H}'$ and associated root system Φ'. Instead on the RHS is the data with respect to the Cartan subalgebra $\mathcal{H}$ and root system Φ. We should stress that the field ϕ, appearing in the Lagrangian (5.2.6), lies in $\mathcal{H}'$.

5.4 Higher spins and Lie algebra exponents

Making use of the definitions for the w-eigenvectors z_1 and z_{h-1} written in (5.3.6), the Lax connection previously defined in (5.2.10) can be rewritten as

$$\begin{aligned}\mathcal{A}_0 &= \frac{g}{2}\partial_1\phi + \frac{m\lambda}{2}e^{\frac{g}{2}\phi}z_1 e^{-\frac{g}{2}\phi} - \frac{m}{2\lambda}e^{-\frac{g}{2}\phi}z_{h-1}e^{\frac{g}{2}\phi},\\ \mathcal{A}_1 &= \frac{g}{2}\partial_0\phi + \frac{m\lambda}{2}e^{\frac{g}{2}\phi}z_1 e^{-\frac{g}{2}\phi} + \frac{m}{2\lambda}e^{-\frac{g}{2}\phi}z_{h-1}e^{\frac{g}{2}\phi}.\end{aligned} \tag{5.4.1}$$

In [38] D. Olive and N. Turok proved in a universal way (not depending on the semisimple Lie algebra $\mathcal{G}$ considered) that a vector potential written in the form (5.4.1) can be gauge transformed into an abelian potential. In the following, we review the results of [38] using the prescriptions defined in the previous section. Under a gauge transformation

$$\mathcal{A}_\mu \to a_\mu = e^G \mathcal{A}_\mu e^{-G} + e^G\partial_\mu(e^{-G})$$

with $G \in \mathcal{G}$ the two-form

$$F_{\mu\nu} = \left[\partial_\mu + \mathcal{A}_\mu, \partial_\nu + \mathcal{A}_\nu\right]$$

transforms as

$$e^G F_{\mu\nu} e^{-G}$$

and (5.2.11) continues to be satisfied. If we find a gauge transformation for which a_μ is abelian then $[a_0, a_1] = 0$ and the zero curvature condition on a_μ reduces to

$$\partial_0 a_1 = \partial_1 a_0,$$

implying that the integral of a_1 on the full spatial line is conserved. The quantity defined by

$$\mathcal{Q}(\lambda) = \int_{-\infty}^{+\infty} dx_1 a_1(x_1; \lambda)$$

becomes therefore a natural generator of the conserved charges.

Using the language of Olive and Turok, we define the loop algebra in the homogeneous grading as the vector space spanned by elements $V \in \mathcal{G}$ times polynomials in λ and $1/\lambda$ that under the action of the Coxeter element behave as

$$A\ V(\lambda) = V(\omega\lambda).$$

The vector potential $\mathcal{A}_\mu$ in (5.4.1) belongs to such a grading[3] and so must a_μ, since the gauge transformation making the vector potential abelian (and for this the reader should consult the paper by Olive and Turok) keeps $\mathcal{A}_\mu$ in the homogeneous grading of the loop algebra. The expansion of a_1 in λ has therefore to be of the following form

$$a_1(\lambda) = \sum_{s \in E \bmod(h)} J^{(s)}(\phi, \partial\phi, \partial^2\phi, \ldots)\lambda^s z_s$$

where the z_s are the eigenvectors of the Coxeter element and the convention $z_{s+h} = z_s$ holds. In the expression above, the $J^{(s)}$ are functions of the fields and their derivatives and correspond to the local densities of the conserved charges. Since the set of $\{z_s\}_{s\in E}$ spans the Cartan subalgebra $\mathcal{H}$, the element a_1 is abelian.

In [38] it was discussed that the abelianization of the vector potential can be performed using two different gauge transformations, generating expansions with positive and negative powers of λ respectively. Here we recall one of them. First of all we apply a gauge transformation on (5.4.1) with $G = g\phi/2$ so to obtain

$$\begin{aligned} \mathcal{A}_0 &= -g\partial_-\phi - \frac{m}{2\lambda} z_{h-1} + \frac{m\lambda}{2} e^{g\phi} z_1 e^{-g\phi} \\ \mathcal{A}_1 &= g\partial_-\phi + \frac{m}{2\lambda} z_{h-1} + \frac{m\lambda}{2} e^{g\phi} z_1 e^{-g\phi}. \end{aligned} \tag{5.4.2}$$

[3] This is easily proved by noting that both ϕ and the element Q used in (5.3.3) to define the Coxeter element belong to $\mathcal{H}'$ and therefore commute.

where the conventions

$$x^{\pm} = x_0 \pm x_1 \quad \text{and} \quad \partial_{\pm} = \frac{1}{2}(\partial_0 \pm \partial_1)$$

have been adopted. Then a further gauge transformation can be found so to transform the spatial component of (5.4.2) into

$$a_1^{(-)} = \frac{m}{2\lambda} z_{h-1} + \sum_{s \geq 1} J^{(-s)}(\phi, \partial_- \phi, \partial_-^2 \phi, \ldots) \lambda^s z_s, \tag{5.4.3}$$

where the sum is performed over the positive integers corresponding to the exponents of the Lie algebra modulo h. A different gauge transformation exists, making the spatial component of (5.4.1) of the form

$$a_1^{(+)} = \frac{m\lambda}{2} z_1 + \sum_{s \geq 1} J^{(s)}(\phi, \partial_+ \phi, \partial_+^2 \phi, \ldots) \frac{1}{\lambda^s} z_{h-s}. \tag{5.4.4}$$

In the class of affine Toda field theories, the expressions for the conserved charges in terms of the Lagrangian fields will assume the following form

$$Q_{\pm(s-1)} = \int_{-\infty}^{+\infty} dx_1 J^{(\pm s)}(\phi, \partial_{\pm} \phi, \partial_{\pm}^2 \phi, \ldots),$$

where the local densities $J^{(\pm s)}$ are the coefficients of the expansion in the spectral parameter of $a_1^{(+)}$ and $a_1^{(-)}$ respectively. The spins of the conserved charges are therefore in correspondence with the exponents of the Lie algebra, a fact that will play a central role in the quantization of such theories. Before moving to the quantum case, it is important to mention that in [38] it was proved that the generators of the integrals of motion can be expressed in the form reported in (5.4.3) and (5.4.4) but an explicit computation of the densities $J^{(\pm s)}$ is not reported in that paper. It would be interesting trying to study such a problem, which at the moment leaves a little hole between the classical and quantum integrability in affine Toda field theories. Filling this hole could hopefully shed light also on related problems, such as providing universal expressions for the densities of local conserved charges in chiral models; in [86] these densities were found for several principal chiral models having as target manifolds certain semisimple Lie algebras. The study performed in [86] was based on a case-by-case analysis and was later extended in [87], where a more universal understanding of the densities of local conserved charges was obtained: among the results of that paper, it was discussed how to connect conserved charges in principal chiral models to conserved charges in affine Toda field theories.

Fortunately in affine Toda field theories, the knowledge of the Lagrangian properties, together with many results derived from the conjectured S-matrices found through the bootstrap philosophy discussed in chapter 2 made it possible to quantize these theories universally [73] without any need to pass through the classical expressions of the conserved currents in terms of the fields. This should not be too surprising if we think that in section 2.5 we derived the values of the masses and eigenvalues of the conserved charges of the E_8 minimal model (up to an overall scale defined for

each $\boldsymbol{\gamma}^{(s)}$) starting from the only set of spins associated to the integrals of motion. The spins of the conserved charges, which are the Lie algebra exponents according to the derivation above, are now provided and can be used to derive the universal quantum properties of these theories. We can therefore consciously jump over the little gap not covered in [38] and explain how to quantise these models.

5.5 Quantum integrability and root projections

In [73] Patrick Dorey claimed that certain universal rules were satisfied for the entire class of affine Toda theories, connecting bootstrap fusing relations satisfied in integrable theories with Coxeter properties of Lie algebras. In this section, we review some of the results conjectured in [73], which form the basis for a universal understanding of quantum aspects of Toda models; instead, we leave to the next chapter a proof of them together with an explanation of their role in ensuring the absence of production in perturbation theory at the tree level.

From section 5.3 we learned that the root system Φ of a rank r Lie algebra $\mathcal{G}$ can be split into r orbits containing h roots each one, being h the periodicity of the Coxeter element. In [73] it was shown how to make a one to one correspondence between the particles of the affine Toda theory and these orbits. Through this correspondence the following fusing rule, early conjectured in [73] and then universally proved in [76] exploiting an idea by M. Freeman [75], can be formulated:

$$C_{ab\bar{c}}^{(3)} \neq 0 \;\; \text{iff} \;\; \exists\, \alpha \in \Gamma_a, \beta \in \Gamma_b \text{ and } \gamma \in \Gamma_c \text{ with } \alpha + \beta = \gamma. \tag{5.5.1}$$

In the expression above Γ_a, Γ_b and Γ_c are the orbits constructed starting applying the Coxeter element w on certain roots γ_a, γ_b and γ_c defined as in (5.3.13). If this property is true, then the bootstrap fusing relations for the different conserved charges, defined in (2.4.6), are obtained by projecting the root triangle $\alpha + \beta = \gamma$ onto the different two-dimensional eigenplanes of the Coxeter element (see figure 5.4). In this way r triangular closing relations are generated, one for each projector; such triangular relations represent conservation laws of charges with different spins, and are responsible for the simplicity of the S-matrix coming out from these integrable theories. For each exponent s it holds that $h-s$ is also an exponent so that each eigenplane of w is spanned by the two real combinations of z_s and z_{h-s} in (5.3.9). Apart from the special case $s = h/2$, which could be associated with a one-dimensional eigenspace of w, in all the other situations there are pairs of projectors P_s and P_{h-s}. Acting with these projectors on the root closure relation $\alpha + \beta = \gamma$ we obtain the two bootstrap fusing relations in (2.4.6). For this reason, from now on we will refer to the eigenplane of w spanned by the two real linear combinations of z_s and z_{h-s} in (5.3.9) as the 'spin-s eigenplane'.

The root triangular relation projected onto the spin-s eigenplane of w (shown in figure 5.4) can be written using the complex number notation (5.3.22) as

$$\gamma_a^{(s)} e^{isU_\alpha} + \gamma_b^{(s)} e^{isU_\beta} = \gamma_c^{(s)} e^{isU_\gamma}$$

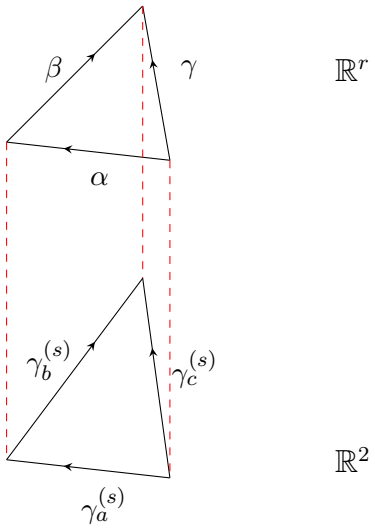

Figure 5.4: Fusing relation $\alpha + \beta = \gamma$ in the root space and its projection $P_s(\alpha) + P_s(\beta) = P_s(\gamma)$.

where U_α, U_β and U_γ are the arguments of the complex vectors that the roots α, β and γ form when they are projected onto the spin-1 eigenplane of w. The relation above can also be written in the probably better form as

$$\gamma_a^{(s)} e^{is(U_\alpha - U_\gamma)} + \gamma_b^{(s)} e^{is(U_\beta - U_\gamma)} = \gamma_c^{(s)} \tag{5.5.2}$$

Comparing this expression with (2.4.6a), the correspondence between root projections and fusing relations should be clear. If α, β and γ are three roots belonging to the orbits Γ_a, Γ_b and Γ_c respectively, then $U_\alpha - U_\gamma = \bar{U}^b_{ac}$ while $U_\beta - U_\gamma = -\bar{U}^a_{bc}$. The mass fusing angles are therefore the angles formed by the roots when they are projected on the real plane spanned by z_1 and z_{h-1}; then the fusing angles of the higher spin mass triangles are the mass fusing angles multiplied by s, the different exponents of the Lie algebra.

The notion of the antiparticle is also naturally taken into account in this language; note that any particle incoming into a vertex, by crossing symmetry can be converted into an outgoing antiparticle (the same property is valid more in general on Feynman diagrams). For example, if $C_{ab\bar{c}} \neq 0$ then there exist three particles, a b and c, with momenta p_a, p_b and p_c respectively, satisfying

$$a + b \to c,$$

with $p_a + p_b = p_c$. However the index $\bar{c}$ in the vertex is responsible not only of the creation of particles of type c, but also of the annihilation of antiparticles of type $\bar{c}$. Another possible fusion is therefore

$$a + b + \bar{c} \to 0,$$

and setting $p_{\bar{c}} = -p_c$ the momentum of the antiparticle, then we get $p_a + p_b + p_{\bar{c}} = 0$.

For this reason, the fusing rule (5.5.1) can equivalently be written as

$$C^{(3)}_{ab\bar{c}} \neq 0 \;\text{ iff }\; \exists\, \alpha \in \Gamma_a, \beta \in \Gamma_b \text{ and } \tilde{\gamma} = -\gamma \in \Gamma_{\bar{c}} \text{ with } \alpha + \beta + \tilde{\gamma} = 0. \qquad (5.5.3)$$

For each orbit Γ_c in correspondence with a certain particle c, it needs to exists an orbit associated to the antiparticle $\bar{c}$ for which it holds $\Gamma_{\bar{c}} = -\Gamma_c$. This fact can also be seen from the point of view of the elements in (5.3.21), which in the next chapter will be used as a basis to expand the Lagrangian field ϕ. For each generator $H'_a = \frac{i}{\sqrt{h}} \sum_{\alpha\in\Gamma_a} e_\alpha$, due to the first property in (5.3.18), we have

$$H'^{\dagger}_a = \frac{i}{\sqrt{h}} \sum_{\alpha\in\Gamma_a} e_{-\alpha} = \frac{i}{\sqrt{h}} \sum_{\alpha\in\Gamma_{\bar{a}}} e_\alpha.$$

Therefore, it makes sense to identify $H'_{\bar{a}} \equiv H'^{\dagger}_a$ and the field components lying along these directions, remembering that $\phi^\dagger = \phi$, will be one complex conjugate of the other. This implies that the orbits Γ_a and $\Gamma_{\bar{a}}$ are associated with two particles a and $\bar{a}$, one the antiparticle of the other. In the special case in which an orbit contains pairs of roots with the opposite sign then it holds that $\Gamma_{\bar{a}} = -\Gamma_a = \Gamma_a$ and the particle a is real.

Simply-laced affine Toda theories are a particular class of the models described in this section in which all the spots in the Dynkin diagram are connected by single links and as a consequence of this the roots have all equal length. If we define the squared length of the roots γ_a in (5.3.13) to be $\gamma_a^2 = \Lambda^2$ then (5.3.24) reduces to

$$\gamma_a^{(s)} = \sqrt{2}\Lambda \frac{q_a^{(s)}}{|\mathbf{q}^{(s)}|}.$$

This means that the vector $\boldsymbol{\gamma}^{(s)} \equiv (\gamma_1^{(s)}, \ldots, \gamma_r^{(s)})$ is the eigenvector of the Cartan matrix (having as eigenvalue $4\sin^2\frac{\pi s}{2h}$) normalized as[4]

$$\boldsymbol{\gamma}^{(s)} = \sqrt{2}\Lambda \frac{\boldsymbol{q}^{(s)}}{|\mathbf{q}^{(s)}|}.$$

In light of this geometrical construction, the results obtained by Zamolodchikov in [19, 20] and reviewed in the end of section 2.5 become more natural.

From the fusing rule (5.5.1) many other interesting properties follow. Among them, in [73] a universal expression for the exact S-matrices of the ADE series of Toda models was found and it was shown that unitarity, crossing symmetry and bootstrap fusing relations were automatically satisfied by these S-matrices, being implied by root system properties. Instead of reviewing such results here, following a historical path, we prefer to postpone them to the next section where we will derive them from perturbation theory providing at the same time a universal proof of the absence of production valid in all the affine Toda models. This will be achieved strictly following the results presented in [1].

[4] More rigorously it is an eigenvector of the transpose of the Cartan matrix as defined in (5.3.23), but since all the roots have the same length then $C^T = C$

Chapter 6

Tree-level integrability in affine Toda field theories

6.1 Universal Lagrangian properties

Many results presented in [73] and reviewed in section 5.5, such as the fusing rule (5.5.1), are valid independently of the existence of a Lagrangian formulation for the integrable theory under consideration. For example, they perfectly apply to the minimal model studied in section 2.5, which does not have a Lagrangian description. In this chapter, we focus more strictly on Lagrangian aspects of affine Toda field theories, where many properties postulated in [73] can be verified and can be subsequently used to prove the tree-level perturbative integrability of these theories, as it was done later in [1]. Some properties of structure constants useful in this chapter are reported in appendix D.

An important observation of Freeman [75] is that is possible to write the potential of a generic untwisted affine Toda field theory in a way that makes many perturbative properties of the model more explicit, as

$$V = \frac{m^2}{g^2}\Big(e^{g\cdot ad_\phi} z_1, z_{h-1}\Big). \tag{6.1.1}$$

The elements z_1, z_{h-1} have been defined in (5.3.6) in terms of the generators $\{E_{\pm\alpha'_i}\}_{i=0}^r$ associated to the Cartan subalgebra $\mathcal{H}'$; it is easy to check that the expression in (6.1.1) is the same as the potential term in (5.2.6) by substituting (5.3.6) into (6.1.1) and using

$$e^{g\cdot ad_\phi} E_{\alpha'} = e^{g\cdot(\phi,\alpha')} E_{\alpha'} \tag{6.1.2}$$

together with (5.2.4b). This is enough to prove that the potential in (6.1.1) is exactly the same as the potential appearing, with a more standard notation, in (5.2.6).

On the other hand, the elements z_1 and z_{h-1} are the eigenvectors of the Coxeter element associated with the root system Φ, composed by the roots $\{\alpha\}$ living in the Cartan subalgebra $\mathcal{H}$ (different from $\mathcal{H}'$). By the fact that the basis in (5.3.21) is orthonormal in $\mathcal{H}'$ (i.e. it satisfies (5.2.4a)) the field can be expanded on this basis

in the following way

$$\phi = \sum_{a=1}^{r} \Big(\phi, H_a'^{\dagger}\Big) H_a' \equiv \sum_{a=1}^{r} \phi_a H_a' \tag{6.1.3}$$

and the kinetic term of the Lagrangian can be written as

$$\frac{1}{2}\Big(\partial_\mu \phi, \partial^\mu \phi\Big) = \frac{1}{2}\partial_\mu \phi_a \partial^\mu \phi_{\bar{a}} \tag{6.1.4}$$

where, as we previously said, we are working with the convention $\phi_{\bar{a}} = \phi_a^*$. Taylor expanding the operator $e^{g \cdot ad_\phi}$ and using the relation in (6.1.3) the potential can be written in the following form

$$V = \sum_{n=0}^{\infty} \frac{1}{n!} C^{(n)}_{a_1 a_2 \ldots a_n} \phi_{a_1} \ldots \phi_{a_n} \tag{6.1.5}$$

with the couplings given by

$$C^{(n)}_{a_1 a_2 \ldots a_n} = m^2 g^{n-2} \Big([H'_{a_1}, [H'_{a_2}, [\ldots [H'_{a_n}, z_1] \ldots]], z_{h-1} \Big). \tag{6.1.6}$$

In order to have a potential formulation making more explicit the properties of the theory, we substitute the explicit form of $\{H'_a\}_{a=1}^r$ (5.3.21) in (6.1.6). After having used the fact that z_1 and z_{h-1} belong to the Cartan subalgebra $\mathcal{H}$ and the properties in (5.3.22) we obtain the following expression for the couplings

$$\begin{aligned} &C^{(n)}_{a_1, a_2, \ldots, a_n} = \\ &- i^n \frac{m^2}{h^{\frac{n}{2}}} g^{n-2} h \; \gamma^{(1)}_{a_1} \gamma^{(1)}_{a_n} \sum_{\alpha_1 \in \Gamma_{a_1} \ldots \alpha_n \in \Gamma_{a_n}} \Big([e_{\alpha_2}, [e_{\alpha_3}, [\ldots [e_{\alpha_{n-1}}, e_{\alpha_n}] \ldots]]], e_{\alpha_1} \Big) e^{i(U_{\alpha_n} - U_{\alpha_1})}. \end{aligned} \tag{6.1.7}$$

The sum runs over the roots inside the different orbits $\Gamma_{a_1}, \ldots, \Gamma_{a_n}$ and $\boldsymbol{\gamma}^{(1)}$ is defined as in (5.3.24). U_{α_1} and U_{α_n} are the angles that the different roots $\alpha_1 \in \Gamma_{a_1}$ and $\alpha_n \in \Gamma_{a_n}$ generate when are projected on the spin-1 eigenplane of the Coxeter element w.

We now proceed to investigate this relation for various values of n so as to find useful expressions for the different couplings of the theory.

6.1.1 Masses

Writing the general formula (6.1.7) in the case $n = 2$ we have

$$C^{(2)}_{ab} = m^2 \gamma^{(1)}_a \gamma^{(1)}_b \sum_{\alpha \in \Gamma_a \beta \in \Gamma_b} \Big(e_\beta, e_\alpha\Big) \; e^{i(U_\beta - U_\alpha)}. \tag{6.1.8}$$

The only terms in the sum different from zero are those corresponding to $\beta = -\alpha$. This is possible only if the particle b is the conjugate of particle a, for which we have $\Gamma_a = -\Gamma_b$. In that case for each root α in the orbit Γ_a there exists exactly one root β such that $U_\beta = U_{-\alpha} = U_\alpha + \pi$. Therefore the exponential in (6.1.8) is equal to -1

for any nonzero term in the sum and there are exactly h terms contributing to the sum (one for each element of the Coxeter orbit). The final result is

$$C^{(2)}_{ab} = m^2 h (\gamma^{(1)}_a)^2 \delta_{\bar{a}b}. \tag{6.1.9}$$

The second-order expansion of the potential associated with such coupling is

$$\frac{1}{2} C^{(2)}_{ab} \phi_a \phi_b = \frac{1}{2} \phi_a \phi^*_a m^2 h (\gamma^{(1)}_a)^2 \tag{6.1.10}$$

from which we can read the values of the masses

$$m_a = m\sqrt{h}\gamma^{(1)}_a. \tag{6.1.11}$$

We note that in the chosen basis the mass-matrix is diagonal, therefore the next orders in the potential expansion exactly correspond to the interaction-couplings of the theory. Comparing the result in (6.1.11) with the formulas in (5.3.22) we see that the masses of the theory are directly connected to the absolute values of root projections onto the $s = 1$ eigenplane of the Coxeter element, a fact which played a role both in the formulation of the fusing rule in [73], and in Freeman's mass formula proof in [75].

6.1.2 3-point couplings

To study other couplings we substitute the expression of the masses (6.1.11) in (6.1.7). Defining

$$\tilde{C}^{(n)}_{\alpha_1,\alpha_2,\ldots,\alpha_n} \equiv e^{i(U_{\alpha_n} - U_{\alpha_1})} \Big([e_{\alpha_2}, [e_{\alpha_3}, [\ldots [e_{\alpha_{n-1}}, e_{\alpha_n}] \ldots]]], e_{\alpha_1} \Big) \tag{6.1.12}$$

we can write the n-point coupling as

$$C^{(n)}_{a_1,a_2,\ldots,a_n} = -i^n \frac{g^{n-2}}{h^{\frac{n}{2}}} m_{a_1} m_{a_n} \sum_{\alpha_1 \in \Gamma_{a_1} \ldots \alpha_n \in \Gamma_{a_n}} \tilde{C}^{(n)}_{\alpha_1,\alpha_2,\ldots,\alpha_n}. \tag{6.1.13}$$

Writing the couplings in this way we see that a given coupling $C^{(n)}_{a_1,a_2,\ldots,a_n}$ is nonzero only if there exist n roots $\alpha_1 \in \Gamma_{a_1}, \ldots, \alpha_n \in \Gamma_{a_n}$ such that $\alpha_1 + \alpha_2 + \ldots + \alpha_n = 0$. These roots form a (possibly non-planar) 'polygon' with n sides whose projection on $s = 1$ plane are the masses of the particles $a_1, a_2, \ldots, a_n$. Moreover the nonzero terms of the sum in (6.1.13) are those for which any partial sum of their roots

$$\begin{aligned} &\alpha_{n-1} + \alpha_n, \\ &\alpha_{n-2} + \alpha_{n-1} + \alpha_n, \\ &\vdots \\ &\alpha_2 + \alpha_3 + \ldots + \alpha_n \end{aligned} \tag{6.1.14}$$

is either a root or zero. This is a simple consequence of the commutation relations in (5.3.19).

Writing the equation (6.1.13) in the case $n = 3$ we obtain

$$C^{(3)}_{abc} = -i^3 \frac{g}{h^{\frac{3}{2}}} m_a m_c \sum_{\alpha\in\Gamma_a,\beta\in\Gamma_b,\gamma\in\Gamma_c} \tilde{C}_{\alpha\beta\gamma}, \tag{6.1.15}$$

While from (6.1.15) is immediate to see that $C^{(3)}_{abc} \neq 0$ requires the existence of three roots $\alpha \in \Gamma_a$, $\beta \in \Gamma_b$ and $\gamma \in \Gamma_c$ summing to zero, the opposite implication cannot be taken for granted and the fusing rule (5.5.1) is still not proven at this point. We proceed to prove it by explicitly computing the coupling.

Suppose we fix the root $\alpha \in \Gamma_a$ and search for all the roots $\gamma \in \Gamma_c$ and $\beta \in \Gamma_b$ such that $\gamma + \beta = -\alpha$. There are exactly two root triangles satisfying this relation composed by $\{\alpha,\ \beta\ ,\ \gamma\}$ and $\{\alpha,\ \beta'\ ,\ \gamma'\}$ (see figure 5.2). Referring to figure 5.2, where $\gamma' = w^{-n}\gamma$ for some integer n, we note that $U_\gamma - U_\alpha = -(U_{\gamma'} - U_\alpha)$. Moreover, as explained in section 5.3, we have $N_{\beta,\gamma} = -N_{\beta',\gamma'}$ and we obtain

$$\tilde{C}_{\alpha\beta\gamma}+\tilde{C}_{\alpha\beta'\gamma'} = e^{i(U_\gamma-U_\alpha)}\Big([e_\beta, e_\gamma], e_\alpha\Big)+e^{i(U_{\gamma'}-U_\alpha)}\Big([e_{\beta'}, e_{\gamma'}], e_\alpha\Big) = -2iN_{\beta,\gamma}\sin(U_\gamma-U_\alpha). \tag{6.1.16}$$

There are exactly h copies of this term connected by the Coxeter element so that the final result for the 3-point coupling is

$$C^{(3)}_{abc} = 2\frac{g}{\sqrt{h}} m_a m_c N_{\beta\gamma}\sin(U_\gamma - U_\alpha) \tag{6.1.17}$$

and the fusing rule (5.5.1) is proved. Since U_α and U_γ are the imaginary values of the rapidities of the fusing particles a and c, this relation can also be written as

$$C^{(3)}_{abc} = f_{abc}\Delta_{abc} \quad \text{with} \quad f_{abc} = 4\frac{g}{\sqrt{h}} N_{\beta\gamma} sign\Big(\sin(U_\gamma - U_\alpha)\Big)\ , \tag{6.1.18}$$

where Δ_{abc} is the area of the fusing triangle composed by the masses of the particles a, b and c, which is the projection of the triangle composed by the roots α, β and γ on the spin-1 eigenplane of the Coxeter element. For simply-laced cases, for which all structure constants have the same absolute value, this gives exactly the area relation for the 3-point couplings. This result was found on a case-by-case basis in [57] and proved in a universal way in [76]. While the proof in the latter paper a little different from that given here, which follows instead the method used in [1], both rely fundamentally on Freeman's re-writing of the potential in the form (6.1.1).

The relation (6.1.18) is of fundamental importance in the pole cancellation of 2-to-2 nonelastic scattering interactions. Indeed we can associate to the f-functions found in chapter 4 the values reported in (6.1.18) where α, β and γ are three arbitrary roots in the orbits Γ_a, Γ_b and Γ_c such that $\alpha + \beta + \gamma = 0$. It is then possible to check that the constraint (4.1.9) directly follows from (D.0.1), implying the absence of singularities in 2-to-2 non-diagonal processes in all the affine Toda theories. Below we verify this in more detail.

The different momenta $p_j = m_j e^{iU_j}$ evaluated on the pole position in figure 4.1 correspond to the root projections onto the spin-1 eigenplane of the Coxeter element, making a correspondence between the imaginary rapidities of the momenta and the

arguments of the projected roots. If a is a particle of the theory corresponding to the orbit Γ_a then on the pole position its rapidity is a purely imaginary number iU_α corresponding to the argument of a projected root $\alpha \in \Gamma_a$ on the spin-1 eigenplane of w. In the computation of the couplings, it is however important to distinguish between particles and antiparticles. In a physical process, by crossing symmetry, we can always convert incoming particles into outgoing antiparticles (and vice versa) leaving the amplitude invariant; the ones can be converted into the others by changing the sign of their momenta and all their quantum numbers in all the Feynman diagrams. This fact is taken into account by the root system where, for a given particle a associated to the orbit Γ_a containing a set of roots $\{\alpha, w\alpha, \dots, w^{h-1}\alpha\}$, we have an antiparticle $\bar{a}$ associated to $-\Gamma_a$ containing the roots $\{-\alpha, -w\alpha, \dots, -w^{h-1}\alpha\}$. If the particle is real then the two orbits Γ_a and $-\Gamma_a$ coincide and both contain the same set of roots. In the process (2.3.1) (in the case $\{a, b\} \neq \{c, d\}$) two particles, a and b, are annihilated and another two, c and d, are created; this means that the Feynman diagrams contributing to the scattering have to contain the pair of indices (a, b), to annihilate the incoming particles, and the pair $(\bar{c}, \bar{d})$, to create the outgoing ones. The associated angles of the projected roots, that enter in the couplings, are U_α and U_β for the incoming states and $U_{-\gamma} = U_\gamma + \pi$, $U_{-\delta} = U_\delta + \pi$ for the two outgoing states.

Suppose that the momenta p_1, p_2, p_3 and p_4, presenting the geometry at the pole shown in figure 4.1, are the projections of some roots $\alpha \in \Gamma_a$, $\beta \in \Gamma_b$, $\gamma \in \Gamma_c$ and $\delta \in \Gamma_d$. Then from figure 4.1, measuring the angles following the counterclockwise convention, the values of signum-functions corresponding to the different channels take the values

$$sign\Big(\sin(U_\beta - U_\alpha)\Big)\ sign\Big(\sin(U_{-\delta} - U_{-\gamma})\Big) = (-1) \times (+1) = -1 \tag{6.1.19a}$$

$$sign\Big(\sin(U_{-\gamma} - U_\alpha)\Big)\ sign\Big(\sin(U_{-\delta} - U_\beta)\Big) = (+1) \times (-1) = -1 \tag{6.1.19b}$$

$$sign\Big(\sin(U_{-\delta} - U_\alpha)\Big)\ sign\Big(\sin(U_{-\gamma} - U_\beta)\Big) = (+1) \times (-1) = -1. \tag{6.1.19c}$$

If now we substitute the values of the f-functions as given in (6.1.18) into the constraint (4.1.9) and use the relations (6.1.19) we end up with the identity (D.0.1). This relation is universally satisfied by the structure constants of any semi-simple Lie algebra and it is the reason for the absence of inelastic scattering in 2-to-2 processes.

Let us also check that the remaining properties of the 3-point couplings are satisfied. First we note that if three roots $\alpha \in \Gamma_a$, $\beta \in \Gamma_b$ and $\gamma \in \Gamma_c$ satisfy $\alpha + \beta + \gamma = 0$ then the following equality holds

$$sign\Big(\sin(U_\alpha - U_\beta)\Big) = sign\Big(\sin(U_\beta - U_\gamma)\Big) = sign\Big(\sin(U_\gamma - U_\alpha)\Big). \tag{6.1.20}$$

This cyclic relation together with property D.1 implies

$$f_{ijk} = f_{jki} = f_{kij}. \tag{6.1.21}$$

If we add to this the fact that both the structure constant $N_{\alpha\beta}$ and $sign\Big(\sin(U_\alpha - U_\beta)\Big)$ are antisymmetric under the exchange $\alpha \leftrightarrow \beta$ we obtain that the 3-point couplings

are symmetric under exchange of any pair of indices. The condition (4.1.7), required to have a real Lagrangian (and therefore a unitary theory) follows from property D.2.

If we specialise now in simply-laced Toda models, we note that the nonzero structure constants of the Lie algebra share the same absolute value

$$|N_{\alpha\beta}|^2 = \frac{\Lambda^2}{2} \tag{6.1.22}$$

where Λ is the normalisation chosen for the root lengths. The relation (6.1.22) follows from (D.0.3) noting that in simply-laced models $\alpha+\beta$ and $\alpha-\beta$ cannot both be roots at the same time, since otherwise we would have $2\Lambda^2 = (\alpha+\beta)^2 + (\alpha-\beta)^2 = 2\alpha^2 + 2\beta^2 = 4\Lambda^2$. This implies that the absolute value of f_{abc}, if not zero, does not depend on the choice of the coupled particles and we can write

$$|f_{abc}| = |f| = 4\frac{g}{\sqrt{h}}\sqrt{\frac{\Lambda^2}{2}}. \tag{6.1.23}$$

Thus all the f-functions in simply-laced theories have the same absolute value, as expected given the general considerations of section 4.2. Indeed in the simply-laced theories, as explained in appendix D, if we have four different roots α, β, γ and δ such that $\alpha+\beta = \gamma+\delta = \epsilon$, where ϵ is another allowed root, then we have that or $\alpha-\gamma$ or $\alpha-\delta$ is a root, but not both. Since the space of momenta producing poles is the projection of the root space, in such theories the cancellation of singularities in 4-point non-diagonal scattering always happens between pairs of diagrams and we never have 3 propagators on-shell simultaneously. On the other hand, we also know, as just remarked, that if $\alpha+\beta$ is a root, $\alpha-\beta$ cannot be a root too. This means that we cannot have more than one on-shell propagating particle at a time in 2-to-2 diagonal scattering. These two conditions satisfied by the simply-laced Toda theories are exactly the simply-laced scattering conditions studied in chapter 4, through which, by imposing the cancellation of poles in inelastic processes, we concluded that $|f_{abc}|$ cannot depend on the choice of indices a, b and c. Thus imposing the absence of particle production in models satisfying property 4.1, and extracting the 3-point couplings of simply-laced affine Toda theories starting from their Lie algebra properties, we find the same area rule.

However simply-laced affine Toda theories are not the only integrable models respecting the simply-laced scattering conditions highlighted in chapter 4. To such theories we should add the twisted theories, obtained by folding the affine extension of certain simply-laced Dynkin diagrams. These models live in a subalgebra of their simply-laced parents and therefore inherit all the properties of the ADE series. We will discuss these cases separately in section 6.3.

We proceed now to the study of higher-point couplings in affine Toda theories.

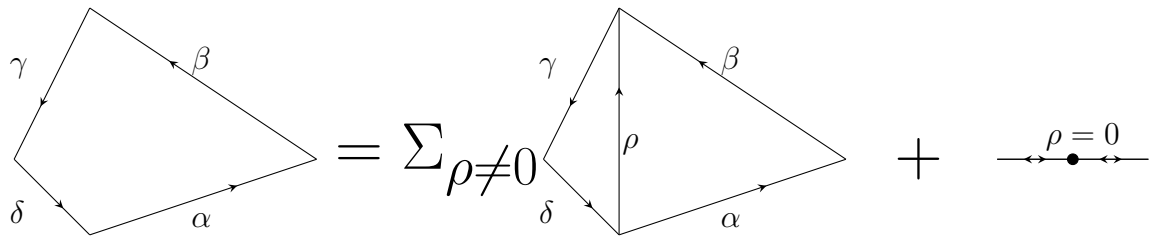

Figure 6.1: Pictorial representation of the 4-point coupling as a sum over roots ρ.

6.1.3 4-point couplings and generalisation

The next step is to compute the 4-point couplings. From (6.1.13) we can write them as

$$C^{(4)}_{abcd} = -\frac{g^2}{h^2} m_a m_d \sum_{\alpha\in\Gamma_a \dots \delta\in\Gamma_d} e^{i(U_\delta - U_\alpha)} \Big([e_\gamma, e_\delta], [e_\alpha, e_\beta] \Big). \tag{6.1.24}$$

By inserting the identity between $[e_\gamma, e_\delta]$ and $[e_\alpha, e_\beta]$, written as

$$I = \frac{1}{h} \sum_{s\in E} z_s \otimes z_{h-s} - \sum_{l=1}^{r} \sum_{\rho\in\Gamma_l} e_\rho \otimes e_{-\rho} \tag{6.1.25}$$

we can split (6.1.24) into two terms

$$C^{(4)}_{abcd} = C^{(4,0)}_{abcd} + C^{(4,1)}_{abcd}. \tag{6.1.26}$$

$C^{(4,0)}_{abcd}$ corresponds to inserting the piece of the identity given by the basis of the Cartan subalgebra. It is reproduced by summing over the configurations $\beta = -\alpha$ and $\gamma = -\delta$ in (6.1.24). $C^{(4,1)}_{abcd}$ is instead obtained by summing over the roots $\alpha + \beta = \rho = -\gamma - \delta$, where ρ is still a root of the system. A geometrical picture is shown in figure 6.1.

We start from the computation of $C^{(4,0)}_{abcd}$ and then we move to $C^{(4,1)}_{abcd}$. Summing over all the roots in the orbits for which we have $\gamma = -\delta$ and $\beta = -\alpha$ we obtain

$$C^{(4,0)}_{abcd} = \frac{g^2}{h^2} m_a m_d \delta_{a\bar{b}} \delta_{c\bar{d}} \sum_{\alpha\in\Gamma_a, \delta\in\Gamma_d} e^{i(U_\delta - U_\alpha)} \Big(\alpha, \delta \Big). \tag{6.1.27}$$

Then we expand the scalar product $\Big(\alpha, \delta\Big)$ on the eigenvectors z_s of the Coxeter element and express the projections in terms of the masses using (6.1.11), (5.3.22). So we find the following result

$$C^{(4,0)}_{abcd} = \frac{g^2}{h^2} \frac{m_a^2 m_d^2}{h m^2} \delta_{a\bar{b}} \delta_{c\bar{d}} \sum_s \sum_{\alpha\in\Gamma_a} e^{iU_\alpha(s-1)} \sum_{\delta\in\Gamma_d} e^{iU_\delta(-s+1)}. \tag{6.1.28}$$

Both the sums over $\alpha \in \Gamma_a$ and $\delta \in \Gamma_d$ constitute closed paths in the complex plane for any s different from one, meaning that $s = 1$ is the only value that returns

nonzero results. Developing for example the second sum we obtain

$$\sum_{\delta\in\Gamma_d} e^{iU_\delta(-s+1)} = h\ \delta_{s1}. \tag{6.1.29}$$

Using this fact the final expression for (6.1.28) is

$$C^{(4,0)}_{abcd} = \frac{g^2}{h}\frac{m_a^2 m_d^2}{m^2}\delta_{a\bar{b}}\delta_{c\bar{d}}. \tag{6.1.30}$$

We compute now $C^{(4,1)}_{abcd}$. To avoid too many indices we omit to indicate the orbits in the sum; it is clear we intend the sum performed over $\alpha\in\Gamma_a$, $\beta\in\Gamma_b$, $\gamma\in\Gamma_c$ and $\delta\in\Gamma_d$, such that $\alpha+\beta=\rho=-\gamma-\delta$. We can write this term in the following form

$$C^{(4,1)}_{abcd} = -\frac{g^2}{h^2}m_a m_d \sum_l \sum_{\rho\in\Gamma_l}\Bigg(\sum_{\substack{\alpha,\ \beta\\ \alpha+\beta=\rho}} e^{i(U_{-\rho}-U_\alpha)}\Big([e_\beta,e_{-\rho}],e_\alpha\Big)\sum_{\substack{\gamma,\ \delta\\ \gamma+\delta=-\rho}} e^{i(U_\delta-U_\rho)}\Big([e_\gamma,e_\delta],e_\rho\Big)\Bigg). \tag{6.1.31}$$

The two sums on the right-hand side of (6.1.31) are evaluated at the same value of ρ and run over all the $\{\alpha,\beta\}$ and $\{\gamma,\delta\}$ in their respective orbits such that $\alpha+\beta=\rho=-\gamma-\delta$, where ρ are roots running in different orbits Γ_l; we have separated the sum over the roots ρ into a sum over orbits l and a sum over the roots inside these orbits. However, it is possible to check that the two sums

$$\sum_{\substack{\gamma,\delta\\ \gamma+\delta=-\rho}} e^{i(U_\delta-U_\rho)}\Big([e_\gamma,e_\delta],e_\rho\Big) \tag{6.1.32}$$

and

$$\sum_{\substack{\alpha,\beta\\ \alpha+\beta=\rho}} e^{i(U_{-\rho}-U_\alpha)}\Big([e_\beta,e_{-\rho}],e_\alpha\Big) \tag{6.1.33}$$

are separately invariant moving ρ inside the orbit Γ_l, so we can choose one of them and substitute it with the average over all the roots ρ in the orbit. The expression in (6.1.31) can therefore be written as

$$C^{(4,1)}_{abcd} = \\ -\frac{g^2}{h^2}m_a m_d\sum_l\Bigg(\frac{1}{h}\sum_{\rho'\in\Gamma_l}\sum_{\alpha+\beta=\rho'} e^{i(U_{-\rho'}-U_\alpha)}\Big([e_\beta,e_{-\rho'}],e_\alpha\Big)\sum_{\rho\in\Gamma_l}\sum_{\gamma+\delta=-\rho} e^{i(U_\delta-U_\rho)}\Big([e_\gamma,e_\delta],e_\rho\Big)\Bigg). \tag{6.1.34}$$

We recognise in this last relation the 3-point couplings that we found in (6.1.15), giving us the result

$$C^{(4,1)}_{abcd} = \sum_l C^{(3)}_{ab\bar{l}}\ \frac{1}{m_l^2}\ C^{(3)}_{lcd} \tag{6.1.35}$$

Combining now (6.1.35) and (6.1.30) we obtain

$$C^{(4)}_{abcd} = \frac{g^2}{h}\frac{m_a^2 m_d^2}{m^2}\delta_{a\bar{b}}\delta_{c\bar{d}} + \sum_l C^{(3)}_{ab\bar{l}}\ \frac{1}{m_l^2}\ C^{(3)}_{lcd}. \tag{6.1.36}$$

This result has been obtained assuming a particular order for the indices a, b, c and d. However, by the symmetry of the coupling, it needs to be valid for any order and we have

$$\begin{aligned}\sum_l C^{(3)}_{ab\bar{l}}\ \frac{1}{m_l^2}\ C^{(3)}_{lcd} + \frac{g^2}{h}\frac{m_a^2 m_d^2}{m^2}\delta_{a\bar{b}}\delta_{c\bar{d}} &= \sum_r C^{(3)}_{ac\bar{r}}\ \frac{1}{m_r^2}\ C^{(3)}_{rbd} + \frac{g^2}{h}\frac{m_a^2 m_d^2}{m^2}\delta_{a\bar{c}}\delta_{b\bar{d}} \\ &= \sum_j C^{(3)}_{ad\bar{j}}\ \frac{1}{m_j^2}\ C^{(3)}_{jbc} + \frac{g^2}{h}\frac{m_a^2 m_b^2}{m^2}\delta_{a\bar{d}}\delta_{c\bar{b}}.\end{aligned} \tag{6.1.37}$$

This relation exactly corresponds to the value that the 4-point coupling must assume to set all the non-diagonal 2-to-2 scattering processes to zero, as shown in (4.1.13). The missing term containing the Kronecker delta functions in (4.1.13) is not in contradiction with (6.1.36) since in the scattering event we assumed the initial and the final particles to be different.

For a generic n-point process we can make a similar decomposition of the coupling into subcouplings. In particular, the number of decompositions depends in a certain sense on the number of possible partitions of the n-sided polygon formed by the roots associated with the n-point coupling considered. For each permutation in which we write the indices of the coupling, we obtain a polygon composed of a particular set of roots. We consider different partitions of such a polygon as the different ways in which we split it into subpolygons, drawing diagonals emerging always from the same vertex. Any time we split the n-gon into two subpolygons drawing a diagonal we obtain one term given by propagators connecting two lower-order couplings and one term corresponding to the null value of the diagonal (in expression (6.1.36) it is given by the Kronecker delta function). The recursion relation obtained in (3.5.7) corresponds to summing three suitable partitions of the coupling so to cancel the values given by the zero-diagonals and leave only the 'propagator-terms'. What we do is to write

$$C^{(n)}_{a_1\dots a_n} = C^{(n)}_{a_1\dots a_n} + C^{(n)}_{a_1\dots a_n} - C^{(n)}_{a_1\dots a_n} \tag{6.1.38}$$

where on the right-hand side the three terms are equal but written in different ways accordingly to their partitions. Referring to figure 6.2 we write all the contributions for the different partitions. They are given by

$$C^{(n)}_{a_1,a_2,\dots,a_n} = \frac{g^2}{h}\frac{m_{a_n}^2}{m^2}\delta_{\bar{a}_n,a_{n-1}} C^{(n-2)}_{a_1,\dots,a_{n-2}} + \sum_l C^{(n-1)}_{a_1,\dots,a_{n-2},l}\frac{1}{m_l^2}C^{(3)}_{\bar{l},a_{n-1},a_n}, \tag{6.1.39}$$

$$C^{(n)}_{a_1,a_2,\dots,a_n} = \frac{g^2}{h}\frac{1}{m^2}C^{(n-3)}_{a_1,\dots,a_{n-3}}C^{(3)}_{a_{n-2},a_{n-1},a_n} + \sum_s C^{(n-2)}_{a_1,\dots,a_{n-3},s}\frac{1}{m_s^2}C^{(4)}_{\bar{s},a_{n-2},a_{n-1},a_n}, \tag{6.1.40}$$

$$\begin{aligned}C^{(n)}_{a_1,a_2,\dots,a_n} = {}& \frac{g^2}{h}\frac{m_{a_n}^2}{m^2}\delta_{\bar{a}_n,a_{n-1}} C^{(n-2)}_{a_1,\dots,a_{n-2}} + \frac{g^2}{h}\frac{1}{m^2}C^{(n-3)}_{a_1,\dots,a_{n-3}}C^{(3)}_{a_{n-2},a_{n-1},a_n} \\ &+ \sum_{l,s} C^{(n-2)}_{a_1,\dots,a_{n-3},s}\frac{1}{m_s^2}C^{(3)}_{\bar{s},a_{n-2},l}\frac{1}{m_l^2}C^{(3)}_{\bar{l},a_{n-1},a_n}.\end{aligned} \tag{6.1.41}$$

Summing the two expressions in (6.1.39), (6.1.40) and then taking the difference

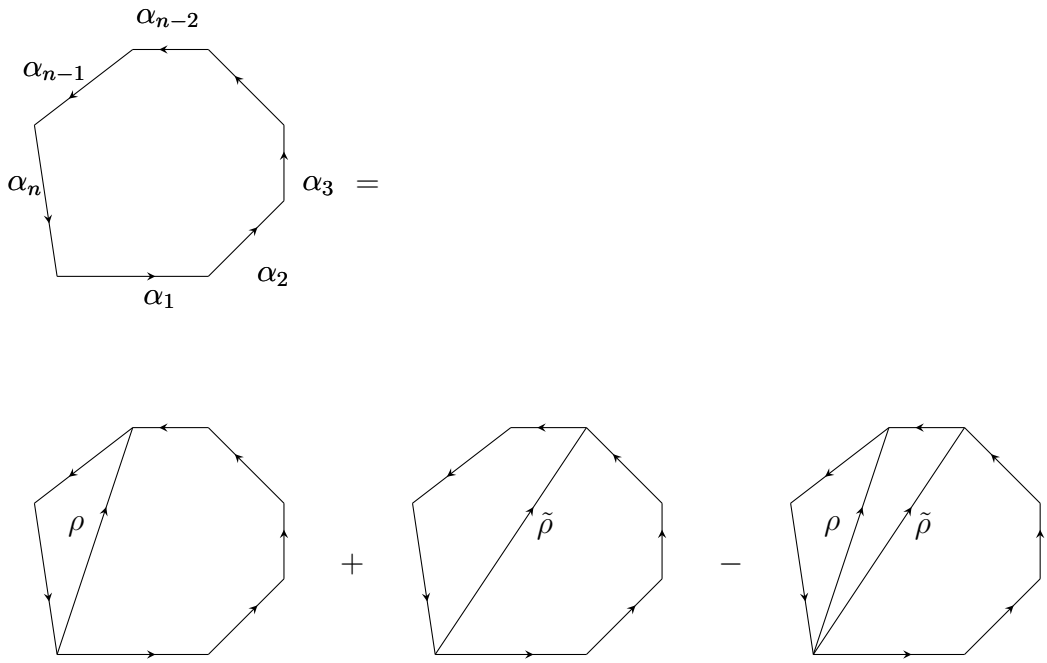

Figure 6.2: Decomposition of a n-point coupling as a sum of different partitions in such a way to obtain the recursion relation (3.5.7).

with (6.1.41) we obtain the following value for the n-point coupling

$$\begin{aligned} C^{(n)}_{a_1,a_2,\ldots,a_n} = &\sum_l C^{(n-1)}_{a_1,\ldots,a_{n-2},l} \frac{1}{m_l^2} C^{(3)}_{\bar{l},a_{n-1},a_n} + \sum_s C^{(n-2)}_{a_1,\ldots,a_{n-3},s} \frac{1}{m_s^2} C^{(4)}_{\bar{s},a_{n-2},a_{n-1},a_n} \\ &- \sum_{l,s} C^{(n-2)}_{a_1,\ldots,a_{n-3},s} \frac{1}{m_s^2} C^{(3)}_{\bar{s},a_{n-2},l} \frac{1}{m_l^2} C^{(3)}_{\bar{l},a_{n-1},a_n}. \end{aligned} \tag{6.1.42}$$

This expression, obtained purely from Lie-algebraic considerations, is the same result as obtained in (3.5.7) by imposing the absence of particle production in the multi-Regge limit in all the untwisted affine Toda models. This is a remarkable fact that emphasizes how the scattering properties of these theories emerge by the Coxeter geometry of their root systems. The idea of formulating a proof of the absence of production in a more natural way is suggestive. It is reasonable to expect that the cancellation between Feynman diagrams at any order of external legs can be formulated in the form of a Gauss's theorem in the space of diagrams. This would make it possible to avoid completely the inductive approach followed in this thesis. Though signals of the existence of a similar construction have been experienced in some examples (see for example appendix C), its universal formulation and connection to the root system geometry are still open.

6.2 From root systems to tree-level S-matrices

To conclude a general proof of tree-level perturbative integrability in affine Toda theories, it remains to check that the bootstrap requirements (4.2.6) are universally

satisfied. As mentioned in the previous part of this thesis, this fact, together with the impossibility of 2-to-2 off-diagonal scattering, imposes the absence of poles in 5-point processes. We will see soon that the constraint (4.2.6) follows directly from root system properties in a geometrical way.

Let us focus on a process of the form in (2.3.1), in the diagonal case in which $d = a$ and $c = b$. Since the process is diagonal the set of outgoing momenta is equal to the set of incoming ones ($p_4 = p_1$, $p_3 = p_2$) and the Mandelstam variables can be written in terms of the rapidity difference $\theta = \theta_1 - \theta_2$ as in (2.3.4). For this particular process, the 4-point coupling (6.1.36) becomes

$$C^{(4)}_{a\bar{a}b\bar{b}} = \frac{g^2}{h}\frac{m_a^2 m_b^2}{m^2} + \sum_l C_{a\bar{a}\bar{l}}\frac{1}{m_l^2}C_{lb\bar{b}}.$$

Since $u = 0$, the sum of the Feynman diagrams coming from the u-channel is cancelled by the second piece of the four-point coupling written above. The amplitude is then given by

$$M_{ab} = -i\sum_i \frac{C^{(3)}_{ab\bar{i}}C^{(3)}_{i\bar{a}\bar{b}}}{s - m_i^2} - i\sum_j \frac{C^{(3)}_{a\bar{b}\bar{j}}C^{(3)}_{j\bar{a}b}}{t - m_j^2} - i\frac{g^2}{h}\frac{m_a^2 m_b^2}{m^2}. \tag{6.2.1}$$

We remark that in this context M_{ab} is a label for the amplitude and is not the mass matrix defined in (5.1.4), (5.1.5). We can write the masses of the propagating particles in terms of the angles formed by the momenta p_1, p_2 on the pole positions $m_i^2 = m_a^2 + m_b^2 + 2m_a m_b \cos U^i_{ab}$, $m_j^2 = m_a^2 + m_b^2 - 2m_a m_b \cos U^j_{ab}$. To find these angles we run over the inequivalent mass triangles in the orbit. We keep the root $\gamma_a \in \Gamma_a$, corresponding to the a-particle, fixed and we move over the roots $\beta = w^{-p}\gamma_b \in \Gamma_b$. Since to each propagating particle there correspond two mass triangles, one the reflection of the other, to find all the inequivalent scattering channels we need to move $w^{-p}\gamma_b$ over half of the orbit. Defining $\tilde{\Gamma}_b$ to be half of the orbit corresponding to the b particle and plugging ((6.1.17), (2.3.4)) into (6.2.1) we can write the s and t channels in the more compact form

$$M_{ab} = \frac{2ig^2}{h} m_a m_b \sum_{\beta\in\tilde{\Gamma}_b} \left(|N_{\gamma_a,\beta}|^2 - |N_{\gamma_a,-\beta}|^2\right)\frac{\sinh^2 iU_{\gamma_a\beta}}{\cosh\theta - \cos U_{\gamma_a\beta}} - i\frac{g^2}{h}\frac{m_a^2 m_b^2}{m^2}.$$

We use the convention of writing the difference between the angles of the root projections on the spin-1 eigenplane of w as $U_{\alpha\beta} = U_\alpha - U_\beta$. Surprisingly, looking at the relation in (D.0.3) we note that the structure constants disappear completely from the formula above, leaving the place for a scalar product between the roots associated with the interacting particles

$$M_{ab} = -\frac{2ig^2}{h} m_a m_b \sum_{\beta\in\tilde{\Gamma}_b} (\gamma_a, \beta)\frac{\sinh^2 iU_{\gamma_a\beta}}{\cosh\theta - \cos U_{\gamma_a\beta}} - i\frac{g^2}{h}\frac{m_a^2 m_b^2}{m^2}. \tag{6.2.2}$$

For the ADE series (i.e. the models constructed from simply-laced affine Dynkin diagrams), only one of $|N_{\gamma_a,\beta}|^2$ and $|N_{\gamma_a,-\beta}|^2$ can be different from zero at a time and indeed the scalar product (γ_a, β) along $\tilde{\Gamma}_b$ can only assume the values $\mp\frac{\Lambda^2}{2}$ corresponding to the propagation of particles in the s/t channels (we remember

that Λ indicates the normalization chosen for the roots; it is convenient to assume $\Lambda = \sqrt{2}$ in simply-laced theories in such a way that the structure constants are phases and the residues for the s/t channels, up to a prefactor, are ± 1). In the case of non simply-laced theories, it is possible that for a given choice of β in $\tilde{\Gamma}_b$ there is a propagating particle both in the s- and in the t-channel at the same time leaving open the possibility for other values of the scalar product (γ_a, β). It is temping to promote the relation in (6.2.2) to the more compact result

$$M_{ab} = -\frac{ig^2}{h} m_a m_b \sinh^2\theta \sum_{\beta\in\Gamma_b} \frac{(\gamma_a,\beta)}{\cosh\theta - \cos U_{\gamma_a\beta}}. \tag{6.2.3}$$

In (6.2.3) we are summing over the roots β in the full orbit Γ_b, and for this reason we have removed the prefactor 2 compared to the expression in (6.2.2) since now we are double counting all the fusing triangles. The other modification has been to remove the surviving piece of the 4-point coupling and promoting the angles at the numerator, corresponding to the poles positions, to be θ dependent , $\sinh iU_{\gamma_a\beta} \to \sinh\theta$.

In order to check that the two expressions in (6.2.2) and (6.2.3) are actually the same we need to study their behaviour in the neighbourhood of all the poles and at $\theta \to \infty$. The verification that the residues of (6.2.2) and (6.2.3) are the same at any singularity $\theta = iU_{\gamma_a\beta}$ is a simple check that we leave to the reader. The only fact that deserves attention is that for any pole, there are two terms in the sum (6.2.3) contributing to it; such terms have to be summed to reproduce the residues of (6.2.2).

We focus on what happens when $\theta \gg 1$. If we write the roots $\beta \in \Gamma_b$ as $\beta = w^{-p}\gamma_b$ with $p = 0, \dots h-1$ then in the limit $\theta \to \infty$ the expression in (6.2.3) becomes

$$\begin{aligned} M_{ab}\Big|_{\theta\gg 1} = -\frac{ig^2}{h} m_a m_b \tanh^2\theta \Big[&\cosh\theta \sum_{p=0}^{h-1} (\gamma_a, w^{-p}\gamma_b) \\ &- \sum_{p=0}^{h-1} (\gamma_a, w^{-p}\gamma_b) \sum_{\substack{q=0\\ q\neq p}}^{h-1} \cos U_{\gamma_a, w^{-q}\gamma_b} + o((\cosh\theta)^{-1}) \Big]. \end{aligned} \tag{6.2.4}$$

Since the sum over all the roots in an orbit is equal to zero, the term proportional to $\cosh\theta$ in the square brackets is zero, avoiding a divergence as $\theta \to \infty$. The coefficient in front of the term of order $(\cosh\theta)^0$ is instead given by

$$\begin{aligned} &\sum_{p=0}^{h-1} (\gamma_a, w^{-p}\gamma_b) \sum_{\substack{q=0\\ q\neq p}}^{h-1} \cos U_{\gamma_a, w^{-q}\gamma_b} = -\sum_{p=0}^{h-1} (\gamma_a, w^{-p}\gamma_b) \cos U_{\gamma_a, w^{-p}\gamma_b} \\ &= -\frac{1}{2} \sum_s \gamma_a^{(s)} \gamma_b^{(s)} \sum_{p=0}^{h-1} \left(e^{i(s+1)(U_{\gamma_a} - U_{w^{-p}\gamma_b})} + e^{i(s-1)(U_{\gamma_a} - U_{w^{-p}\gamma_b})} \right). \end{aligned} \tag{6.2.5}$$

The first equality above has been obtained considering that the sum of $\cos U_{\gamma_a, w^{-q}\gamma_b}$ performed over the entire orbit is equal to zero. The second equality is derived by decomposing the root $w^{-p}\gamma_b$ over the basis of Coxeter eigenvectors and writing the projections using the relation (5.3.22). Finally the remaining sum in the second line

of (6.2.5) generates two Kronecker deltas $h\delta_{s,-1}$ and $h\delta_{s,1}$ leading to

$$\sum_{p=0}^{h-1}(\gamma_a, w^{-p}\gamma_b)\sum_{\substack{q=0\\q\neq p}}^{h-1}\cos U_{\gamma_a,w^{-q}\gamma_b} = -h\gamma_a^{(1)}\gamma_b^{(1)}. \tag{6.2.6}$$

If we substitute the mass expression (6.1.11) into this last relation and plug the result into (6.2.4) we discover that in the large rapidity limit the amplitude reduces to

$$M_{ab}(\theta)\Big|_{\theta\gg 1} = -\frac{ig^2}{h}\frac{m_a^2 m_b^2}{m^2}\tanh^2\theta. \tag{6.2.7}$$

Interestingly the amplitude written in (6.2.3) for $\theta \gg 1$ reproduces exactly the delta term coming from the 4-point coupling and explicitly expressed in (6.2.2), implying the equality between the two expressions in (6.2.2) and (6.2.3).

We may also ask about the behaviour of (6.2.3) in the collinear limit $\theta \ll 1$. In this situation the amplitude is only nonzero if along the orbit Γ_b there is one root β forming a projected angle $U_{\gamma_a,\beta} = 0$ on the spin-1 plane for which at the denominator of (6.2.3) we have a term $\cosh\theta - 1$ going to zero as fast as the $\sinh^2\theta$ term in the numerator. This situation is realised if the roots γ_a and γ_b identifying the orbits have the same colour, $\circ$ or $\bullet$, according to the definition given in section 5.3, i.e. they belong to the same orthogonal root set in the Dynkin diagram. Note that if the roots have opposite colours then the projections of the representatives of their orbits (γ_a and γ_b) on the spin-1 eigenplane of w differ by an angle π/h (as it is shown in figure 5.3 by substituting $s = 1$): in this case, since the Coxeter element on the spin-1 eigenplane acts as a rotation by an angle $2\pi/h$, there is no possibility to have $U_{\gamma_a,\beta} = 0$ for any value of $\beta \in \Gamma_b$. The collinear value of the amplitude is therefore given by

$$\lim_{\theta\to 0} M_{ab}(\theta) = -(\gamma_a,\gamma_b)\frac{ig^2}{h}m_a m_b \lim_{\theta\to 0}\frac{\sinh^2\theta}{\cosh\theta - 1} = -(\gamma_a,\gamma_b)\frac{2ig^2}{h}m_a m_b, \tag{6.2.8}$$

where γ_a and γ_b are the representatives of the orbits Γ_a and Γ_b respectively and have projections $P_1(\gamma_a)$ and $P_1(\gamma_b)$ aligned. Since γ_a and γ_b have the same colour, the only scalar product (γ_a,γ_b) that is different from zero is when the two roots are exactly the same. This implies that in the collinear limit the amplitude is given by

$$M_{ab}(\theta)\Big|_{\theta\ll 1} = -\frac{2ig^2}{h}\gamma_a^2\ m_a^2\delta_{ab}. \tag{6.2.9}$$

In simply-laced models, all the roots have the same length $\gamma_a^2 = \Lambda^2$. In this case, taking into account (6.1.23), the expression in (6.2.9) coincides exactly with the requirement (4.2.18) for the cancellation of 5-point amplitudes in theories satisfying simply-laced scattering conditions. Since simply-laced affine Toda theories belong to this class of models, this concludes the proof of their tree-level integrability.

The constraint (4.2.18) is not valid in non simply-laced theories; indeed it is a requirement for the cancellation of 5-point processes only for theories satisfying property 4.1. Despite that, we can still prove the cancellation of 5-point processes in

non simply-laced models by checking that the tree-level bootstrap relations (4.2.6) are satisfied. This is indeed the requirement for having zero residues in 5-point amplitudes, as discussed in section 4.2.

We can write the tree-level S-matrix elements dividing the amplitude (6.2.3) by the flux and normalisation factor $4m_a m_b \sinh\theta$. We obtain

$$S_{ab}^{tree}(\theta) = -\frac{ig^2}{4h}\sum_{\beta\in\Gamma_b}(\gamma_a,\beta)\frac{\sinh\theta}{\cosh\theta-\cos U_{\gamma_a\beta}}. \tag{6.2.10}$$

In (6.2.10) all the mass dependence has disappeared and the scattering properties are all encoded in the scalar products between γ_a and the different roots β in the orbit Γ_b. From (6.2.10) we see that the building blocks necessary to construct the different S-matrix elements of the theory at the tree level are given by $\frac{\sinh\theta}{\cosh\theta-\cos U_{\gamma_a,\beta}}$, where $U_{\gamma_a,\beta}$ are the different fusing angles formed by the projections of γ_a and β on the spin-1 eigenplane of the Coxeter element. To prove the bootstrap relations in (4.2.6) such building blocks need to be rewritten in a clever way, since at the moment translations of θ and $U_{\gamma_a,\beta}$ do not correspond inside a single building block. To that end we note that the following identity holds

$$\frac{\sinh\theta}{\cosh\theta-\cos U} = \frac{1}{2}\left[\coth\left(\frac{\theta}{2}-i\frac{U}{2}\right)+\coth\left(\frac{\theta}{2}+i\frac{U}{2}\right)\right].$$

Moreover given a generic root β inside the orbit Γ_b for which $(\gamma_a,\beta)\neq 0$, then there exists another root β', whose projection on the spin-1 plane is obtained by reflecting $P_1(\beta)$ with respect to $P_1(\gamma_a)$ and satisfying $(\gamma_a,\beta') = (\gamma_a,\beta)$ (analogously to the situation represented in figure 5.2). If we define $U_{\gamma_a\beta} = U$ then $U_{\gamma_a\beta'} = -U$ and the sum of the associated building blocks can be written as

$$\frac{\sinh\theta}{\cosh\theta-\cos U}+\frac{\sinh\theta}{\cosh\theta-\cos(-U)} = \coth\left(\frac{\theta}{2}-i\frac{U}{2}\right)+\coth\left(\frac{\theta}{2}+i\frac{U}{2}\right)$$

From this fact we see that we can substitute the functions $\frac{\sinh\theta}{\cosh\theta-\cos U}$ in (6.2.10) with either $\coth\left(\frac{\theta}{2}-i\frac{U}{2}\right)$ or $\coth\left(\frac{\theta}{2}+i\frac{U}{2}\right)$. As long as we sum over the entire orbit the choice of sign in front of the fusing angles U it is not important since any time there is a pair of roots whose projections form an angle U then there exists another pair of roots presenting the opposite angle and having the same scalar product. Therefore the S-matrix can be written as

$$S_{ab}^{tree}(\theta) = -\frac{ig^2}{4h}\sum_{\beta\in\Gamma_b}(\gamma_a,\beta)\coth\left(\frac{\theta}{2}\pm i\frac{U_{\gamma_a\beta}}{2}\right), \tag{6.2.11}$$

where the the sign in front of the angles $U_{\gamma_a,\beta}$ can be freely chosen. Using this new building block notation the tree-level bootstrap relations follow directly by the linearity of the scalar product, since now we can match translations of θ with translations of the fusing angles.

Suppose there exists a 3-point coupling $C_{ab\bar{c}}^{(3)}\neq 0$. Then there must be three roots $\alpha\in\Gamma_a$, $\beta\in\Gamma_b$ and $\gamma\in\Gamma_c$ satisfying $\alpha+\beta=\gamma$. Projecting these vectors on the

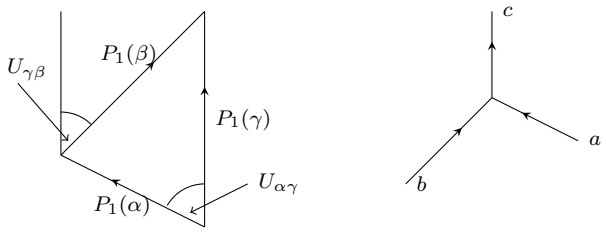

Figure 6.3: The image on the left reports the projections of the roots $\alpha \in \Gamma_a$, $\beta \in \Gamma_b$, $\gamma \in \Gamma_c$ on the momentum plane (spin-1 Coxeter eigenplane) forming the fusing triangle corresponding to the coupling $C^{(3)}_{ab\bar{c}}$. The RHS shows the corresponding fusing process $a + b \to c$.

momentum eigenplane we obtain the mass fusing triangle Δ_{abc}. We refer to figure 6.3 to label the angles of the projected triangle $\bar{U}^b_{ac} = U_{\alpha,\gamma}$ and $\bar{U}^a_{bc} = U_{\gamma,\beta}$. In this manner, using the building block convention (6.2.11) with the choice of plus sign in front of the fusing angles U the bootstrap equality (4.2.6) is verified as follows

$$
\begin{aligned}
&S^{tree}_{da}(\theta - i\bar{U}^b_{ac}) + S^{tree}_{db}(\theta + i\bar{U}^a_{bc}) = S^{tree}_{da}(\theta - iU_{\alpha,\gamma}) + S^{tree}_{db}(\theta + iU_{\gamma,\beta}) = \\
&- \frac{ig^2}{4h}\sum_{p=0}^{h-1}\left[(\alpha, w^{-p}\gamma_d)\coth\left(\frac{\theta}{2} + \frac{i}{2}U_{\alpha w^{-p}\gamma_d} - \frac{i}{2}U_{\alpha\gamma}\right) + (\beta, w^{-p}\gamma_d)\coth\left(\frac{\theta}{2} + \frac{i}{2}U_{\beta w^{-p}\gamma_d} + \frac{i}{2}U_{\gamma\beta}\right)\right] \\
&- \frac{ig^2}{4h}\sum_{p=0}^{h-1}\left[(\alpha, w^{-p}\gamma_d)\coth\left(\frac{\theta}{2} + \frac{i}{2}U_{\gamma w^{-p}\gamma_d}\right) + (\beta, w^{-p}\gamma_d)\coth\left(\frac{\theta}{2} + \frac{i}{2}U_{\gamma w^{-p}\gamma_d}\right)\right] = \\
&- \frac{ig^2}{4h}\sum_{p=0}^{h-1}(\gamma, w^{-p}\gamma_d)\coth\left(\frac{\theta}{2} + \frac{i}{2}U_{\gamma w^{-p}\gamma_d}\right) = S^{tree}_{dc}(\theta).
\end{aligned}
\tag{6.2.12}
$$

A general tree-level proof of the absence of inelastic scattering in all the untwisted affine Toda theories has therefore been completed. It is worth noting that the fusing triangle in figure 6.3 can be reflected with respect to the side corresponding to $P_1(\gamma)$, generating an equivalent mass triangle. The bootstrap relation associated to this new triangle can be proved analogously to what we did in (6.2.12) but using the formula (6.2.11) with the minus sign convention in front of the fusing angles.

The unitarity and crossing equations at the tree level can also be checked starting from the universal expression (6.2.11). If we perform a loop expansion of the S-matrix, as in (4.2.7), then the unitarity equation (2.3.15a) at the tree level reduces to

$$S^{tree}_{ab}(\theta) + S^{tree}_{ab}(-\theta) = 0,$$

which is trivially satisfied by (6.2.10). Crossing symmetry (2.3.15b) is of course true, since it is an intrinsic property of Feynman diagrams, valid order by order in the loop expansion. It is however interesting to see explicitly how it fits into the geometrical

formulation of (6.2.10):

$$\begin{aligned} S_{ab}^{tree}(i\pi-\theta) &= -\frac{ig^2}{4h}\sum_{\beta\in\Gamma_b}(\gamma_a,\beta)\frac{\sinh\theta}{-\cosh\theta-\cos U_{\gamma_a\beta}} \\ &= -\frac{ig^2}{4h}\sum_{\beta\in\Gamma_b}(\gamma_a,-\beta)\frac{\sinh\theta}{\cosh\theta+\cos U_{\gamma_a\beta}} \\ &= -\frac{ig^2}{4h}\sum_{\tilde{\beta}\in-\Gamma_b}(\gamma_a,\tilde{\beta})\frac{\sinh\theta}{\cosh\theta-\cos U_{\gamma_a\tilde{\beta}}} = S_{a\bar{b}}^{tree}(\theta). \end{aligned} \tag{6.2.13}$$

In the last equality we made the substitution $\tilde{\beta}=-\beta$.

6.3 Folding and twisted Coxeter elements

Until this point, we have been working on a semisimple Lie algebra constructed over an untwisted Dynkin diagram. In that case we have a copy of equivalent sets of simple roots $\{\alpha_i\}_{i=1}^r\in\Phi$ and $\{\alpha'_i\}_{i=1}^r\in\Phi'$ associated to two different choices of the Cartan subalgebra, that we have called respectively $\mathcal{H}$ and $\mathcal{H}'$. Root systems associated with twisted Dynkin diagrams can also be included in the previous analysis, as explained in [1] based on considerations from [88]. The Dynkin diagrams of these models can be obtained by 'folding' one and only one of the extended simply-laced diagrams [89].

The idea is the following. Suppose there exists an automorphism σ of a certain extended Dynkin diagram composed by a set of roots $\{\alpha'_i\}_{i=0}^r$ acting as a permutation of the points $\alpha'\to\sigma(\alpha')$. Here σ is a symmetry of the diagram behaving as a linear map over the vector space $\mathcal{H}'$. Therefore we can decompose each vector a in $\mathcal{H}'$ into a component living in the invariant space under the action of σ ($a^{\parallel}$) and into a component perpendicular to such space ($a^{\perp}$)

$$a=a^{\parallel}+a^{\perp}.$$

To obtain the root system associated with the folded diagram starting from the simply-laced one we set all the components $\alpha_i'^{\perp}$ perpendicular to the subspace invariant under the action of σ equal to zero. The new set of roots that is generated in this way lies entirely in the σ-invariant subspace, in other words all the roots in $\{\alpha_i'^{\parallel}\}_{i=0}^r$ are eigenvectors of σ with eigenvalue equal to one. Among them, many roots are equal to each other after the reduction. In particular, all the roots that are connected along a σ-orbit have the same projection on the σ-invariant eigenspace. This implies that the new root system has a smaller number of elements than the one we started with, and now the roots can have in general different lengths since we have removed their projection on the space not invariant under the action of σ.

An equivalent way of seeing this is to look at the vectors defined in (5.3.21) that form an orthonormal basis of $\mathcal{H}'$. Each root in $\mathcal{H}'$ can be written as a linear combination in terms of this basis

$$\alpha'=\sum_{a=1}^{r}\alpha'_aH'_a.$$

A case by case check [57] shows that for twisted Dynkin diagrams the space invariant under the action of σ is generated by a subset of the vectors in (5.3.21). From the point of view of affine Toda field theories, in which ϕ is an element of $\mathcal{H}'$, this corresponds to setting to zero all the field components along the directions H'_a not invariant under the automorphism σ. The root orbits $\tilde{\Gamma}_a \subset \mathcal{H}$ necessary to define the elements H'_a which survive the automorphism define a new root system $\tilde{\Phi}$ which is contained inside the root system Φ associated to the Cartan subalgebra $\mathcal{H}$. The generators associated with the roots in $\tilde{\Phi}$ define a subalgebra in the Lie algebra $\mathcal{G}$ and the action of w in this embedded $\tilde{\Phi}$ is exactly that of a twisted Coxeter element of $\tilde{\Phi}$ [88].

We study now what are the consequences of folding on an affine Toda Lagrangian. Note that we can write the Lagrangian of the model both in terms of the generators associated with the root system Φ, or in terms of the roots in Φ'. If we follow the latter approach, by substituting (5.3.6) in (6.1.1) and using the relation (6.1.2) we find the standard formulation for the Toda potential, as given in the Lagrangian (5.2.6). Then we can apply the folding procedure to the extended set of simple roots, as previously explained. In this way, we reduce the set to $\{\alpha_i'^{\parallel}\}_{i=0}^{r}$, composed by the projections of the roots on the eigenspace invariant under the automorphism σ of the Dynkin diagram. The potential, after the reduction, becomes

$$\frac{m^2}{g^2} \sum_{i=0}^{r} n_i e^{g\cdot(\phi,\alpha_i'^{\parallel})}, \tag{6.3.1}$$

where r is the rank of the starting simply-laced Dynkin diagram. Since many of the $\alpha_i'^{\parallel}$ are equal to each other many terms in (6.3.1) can be summed and we obtain the potential associated with the twisted model. On the other hand, the effect of the reduction is the same as setting to zero all the vectors of the basis (5.3.21) that are not invariant under the action of σ. This corresponds to suppressing all the couplings in (6.1.6) that contain one or more of the vectors H'_a that we set equal to zero. The set of masses and couplings defining the twisted theory is therefore the subset of the masses and couplings of the simply-laced theory that survives the folding. Moreover, the root orbits in Φ defining the set of vectors (5.3.21) invariant under the action of σ form a subalgebra of the initial simply-laced root system. All the scattering properties are then satisfied within this subalgebra. If we consider for example figure 6.2, that corresponds to a pictorial representation of the relation (6.1.42), we note that all the roots ρ and $\tilde{\rho}$ that are expressed as sums of different roots in the σ-invariant subalgebra need to belong themselves to this subalgebra. This implies that for a given set of σ-invariant indices $a_1, \ldots, a_n$ (that means $H'_{a_1}, \ldots, H'_{a_n}$ are invariant under the action of σ) the associated coupling $C^{(n)}_{a_1 \ldots a_n}$ is defined by summing on the RHS of (6.1.42) only over the intermediate indices inside the subalgebra. The relation (3.5.7), together with the other scattering constraints, is therefore completely satisfied internally to such a subalgebra ensuring the perturbative integrability of twisted Toda theories.

At the tree level, the S-matrix elements in the twisted model also come from the ones of the starting simply-laced theory (6.2.10) (or (6.2.11) if we use a different conventions for the tree-level building blocks). Indeed classically the S-matrix ele-

ments of the twisted theory are just the subset of the S-matrix elements of the simply-laced theory having indices invariant under the folding. We can see that by considering a 2-to-2 elastic process presenting external particles in correspondence with two σ-invariant orbits, Γ_a and Γ_b. To find all the particles propagating in the s-channel, corresponding to certain roots γ, we keep fixed $\alpha \in \Gamma_a$ and we move β in Γ_b. In this way, we generate the different bound states as $\gamma = \alpha + \beta$. Since the space invariant under σ is a subalgebra of the starting Lie algebra, all the roots γ generated in this manner will also belong to orbits invariant under σ. A feature of a subalgebra is indeed that any time we commute two elements in it, say e_α and e_β, we obtain another element of the subalgebra, $[e_\alpha, e_\beta] = N_{\alpha,\beta} e_\gamma$. The same argument can be repeated identically for the particles propagating in the t-channel, ensuring that the propagating bound states are all particles contained in the twisted theory. Therefore, the S-matrices of the twisted theory are the subset of the S-matrices of the simply-laced model having indices invariant under the folding.

Note though that this only works at the tree level. Once loops are allowed, it was observed [57] that masses of simply-laced theories renormalize in a uniform way, scaling all with the same multiplicative factor. However, that was not the case for twisted theories. The reason is the following. Consider all the bubble diagrams contributing to the renormalization of the mass of a certain particle c, corresponding to a root, say γ. To find all the bubble diagrams contributing to the mass correction we need to search for the pairs of roots $\{\alpha, \beta\}$ such that $\alpha + \beta = \gamma$. If $\gamma \in \Gamma_c$, where H'_c is an element invariant under the folding, then this does not imply that the roots $\{\alpha, \beta\}$ belong to σ-invariant orbits. Indeed given e_γ in the σ-invariant subalgebra it is in general possible finding generators e_α and e_β outside the subalgebra such that $e_\gamma \sim [e_\alpha, e_\beta]$. The contributions to the mass correction in the starting simply-laced theory are therefore different from the contributions of the twisted theory. In particular, due to the absence of some particles flowing inside the loop, the mass ratios in the twisted theories in general shift in a coupling-dependent way, complicating the picture considerably.

6.3.1 An example: the $A_2^{(2)}$ model from $D_4^{(1)}$

We now illustrate these considerations with a simple example. Let $\alpha'_1, \alpha'_2, \alpha'_3, \alpha'_4$ be the simple roots making up the $D_4^{(1)}$ Dynkin diagram shown in figure 6.4:

$$\alpha'_1 = (\frac{1}{\sqrt{3}}, \frac{1}{\sqrt{6}}, -1, -\frac{1}{\sqrt{2}}) \quad , \quad \alpha'_2 = (\frac{1}{\sqrt{3}}, \frac{1}{\sqrt{6}}, 1, -\frac{1}{\sqrt{2}}),$$
$$\alpha'_3 = (-\frac{2}{\sqrt{3}}, \frac{1}{\sqrt{6}}, 0, -\frac{1}{\sqrt{2}}) \quad , \quad \alpha'_4 = (0, 0, 0, \sqrt{2}),$$

and let α'_0 be the lowest root defined by imposing $\sum_{i=0}^4 n_i \alpha'_i = 0$ with $(n_0, \ldots, n_4) = (1, 1, 1, 1, 2)$. In this case the Coxeter number $h = \sum_{i=0}^4 n_i$ is equal to 6. The affine Toda theory constructed starting from this Dynkin diagram, up to an overall

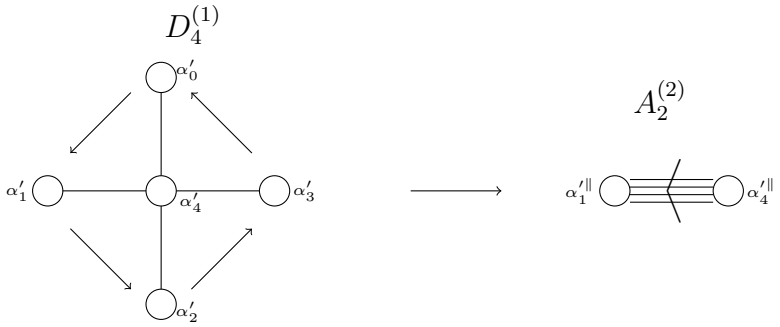

Figure 6.4: Example of $A_2^{(2)}$ Dynkin diagram obtained by folding $D_4^{(1)}$.

multiplicative factor, has a squared mass matrix of the form

$$M^2 = \sum_{i=0}^{4} n_i \alpha_i' \otimes \alpha_i' = diag(2, 2, 2, 6).$$

The diagram automorphism σ defines a linear function by $\sigma\alpha_4' = \alpha_4'$, $\sigma\alpha_1' = \alpha_2'$ and so on for the other roots, as shown by the arrows connecting the different spots on the left-hand side of figure 6.4. The invariant space under the action of σ is spanned by the component $(0, 0, 0, 1)$ along which the root α_4' lies. The reduction procedure necessary to define the new root system associated with $A_2^{(2)}$ starting from the root system of $D_4^{(1)}$ corresponds to projecting the roots onto the direction invariant under sigma, which is $(0, 0, 0, 1)$. If we do this we obtain a new set of roots $\{\alpha_i'^{\parallel}\}_{i=0}^4$, where $\alpha_0'^{\parallel}$, $\alpha_1'^{\parallel}$, $\alpha_2'^{\parallel}$ and $\alpha_3'^{\parallel}$ are all equal to $(0, 0, 0, -\frac{1}{\sqrt{2}})$ and $\alpha_4'^{\parallel} = \alpha_4$. The new Dynkin diagram obtained after the folding is therefore composed by just two roots, that we simply call $\alpha_1'^{\parallel}$ and $\alpha_4'^{\parallel}$ on the right hand side of figure 6.4, having lengths connected by $(\alpha_4'^{\parallel})^2 = 4(\alpha_1'^{\parallel})^2$. The potential of the $D_4^{(1)}$ affine Toda field theory (properly shifted so to have $V = 0$ at $\phi = 0$) is defined as

$$V = \frac{m^2}{g^2}\left(e^{g(\phi,\alpha_0')} + e^{g(\phi,\alpha_1')} + e^{g(\phi,\alpha_2')} + e^{g(\phi,\alpha_3')} + 2e^{g(\phi,\alpha_4')} - 6\right) \tag{6.3.2}$$

and after the folding reduces to

$$V^{\parallel} = \frac{m^2}{g^2}\left(4e^{g(\phi,\alpha_1'^{\parallel})} + 2e^{g(\phi,\alpha_4'^{\parallel})} - 6\right) = \frac{m^2}{g_0^2}\left(2e^{-g_0\phi_4} + e^{2g_0\phi_4} - 3\right), \tag{6.3.3}$$

where in the last equality we set $g \equiv \sqrt{2}g_0$. Up to a redefinition of the mass scale this is exactly the potential of the Bullough–Dodd Lagrangian (3.1.11).

On the other hand, the invariant eigenvector $(0, 0, 0, 1)$ corresponds to the element H_4' in (5.3.21) defined by summing all the generators with roots living in the orbit Γ_4 (the one associated with the central spot of the $D_4^{(1)}$ Dynkin diagram) of the second Cartan subalgebra $\mathcal{H}$. This orbit contains six elements, which form a set of roots for $A_2^{(1)}$. This implies that $A_2^{(1)}$ is a closed subspace of $D_4^{(1)}$ living entirely on the orbit Γ_4. The Bullough–Dodd potential can then be written using Freeman's

formulation (6.1.1) as

$$V^{\parallel} = \sum_{n=0}^{\infty} \frac{1}{n!} C^{(n)} \phi_4^n \tag{6.3.4}$$

with

$$C^{(n)} = m^2 g^{n-2} \Big([\underbrace{H'_4, [H'_4, [\ldots [H'_4}_{n \text{ times}}, z_1] \ldots]], z_{h-1} \Big). \tag{6.3.5}$$

The same analysis holds for any twisted affine Dynkin diagram. In each case, we start from an extended simply-laced diagram and apply the folding procedure. The space invariant under σ is spanned by a subset of the vectors in (5.3.21) and such vectors contain in the sum the generators of a subalgebra of the original simply-laced root system. The Coxeter element w of the initial simply-laced diagram behaves as a twisted Coxeter element defined on this subspace. In the example just presented we started from two equivalent root systems Φ and Φ' both associated with the simply-laced diagram $D_4^{(1)}$; after the folding Φ' reduced to the root systems of $A_2^{(2)}$ and Φ reduced to the root system of $A_2^{(1)}$.

Recalling the results from section 2.5 we should mention that the particle 4 in the $d_4^{(1)}$ affine Toda theory is not 'fundamental' in the sense used by Zamolodchikov [19, 20]. The set of exponents of D_4 is $E = \{1, 3, 3, 5\}$ and the generators $\{e_\alpha\}_{\alpha \in \Gamma_4}$ together with the pair of w-eigenvectors $\{z_1, z_5\}$ close a subalgebra in D_4; this subalgebra is the Lie algebra associated to A_2. Any root $\alpha \in \Gamma_4$ lies entirely on the w-eigenplane spanned by z_1 and z_5 and the masses and fusing angles of the Bullough–Dodd model are contained within this plane. All the roots in Γ_4 have null projections on the spin-3 eigenplane of w so that for the particular spin $\tilde{s} = 3$ we have

$$\gamma_4^{(\tilde{s})} = 0.$$

Applying the bootstrap fusing relations on the particle 4 we never obtain information about the other particles 1, 2 and 3 since we never leave the A_2 subalgebra. In figure 6.5 a pictorial representation of the discussed example is reported.

6.4 From tree- to exact-S-matrices

In section 2.6, reviewing the results from [57], we defined expressions for the S-matrices $S_{ab}(\theta; g)$ obtained by properly adding zeros to the minimal S-matrices of perturbed CFTs, so to obtain $S_{ab}(\theta; 0) = 1$. In [57] it was argued that these are the correct S-matrices arising from the Lagrangians (5.1.1) of affine Toda field theories constructed over simply-laced Dynkin diagrams. We conclude this chapter explaining how to reconstruct the non-perturbative S-matrices of affine Toda field theories starting from the tree-level ones in (6.2.10).

We should first rewrite the root scalar products using the fundamental weights. By using the first equality in (5.3.13) we obtain

$$(\gamma_a, w^{-p}\gamma_b) = ((1 - w^{-1})\lambda_a, w^{-p}\gamma_b) = (\lambda_a, w^{-p}\gamma_b) - (\lambda_a, w^{-p+1}\gamma_b). \tag{6.4.1}$$

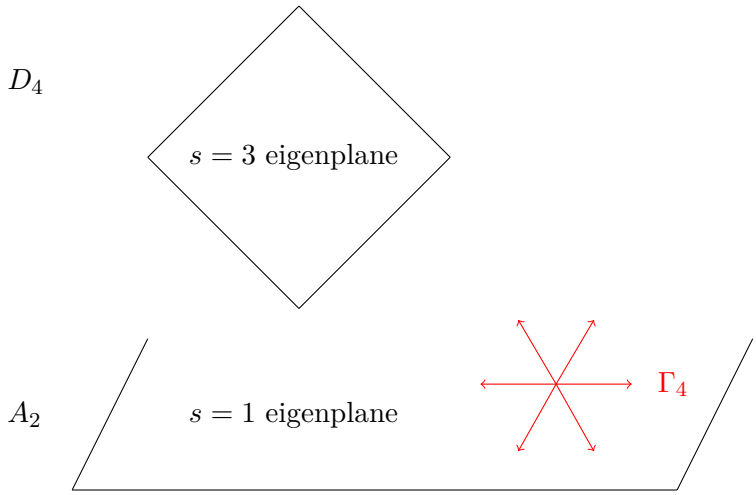

Figure 6.5: The masses and fusing angles of the Bullough–Dodd model are all contained in the spin-1 eigenplane of the Coxeter element of D_4.

If we do so, then the universal expression for the tree-level S-matrix in (6.2.10) can be written as

$$S_{ab}^{tree}(\theta) = \frac{1}{2}\sum_{p=0}^{h-1}(\lambda_a, w^{-p}\gamma_b)\langle 1 + u(\gamma_a, w^{-p}\gamma_b)\rangle_\theta \tag{6.4.2}$$

where we have defined the angles in units of $\frac{\pi}{h}$, $U_{\alpha,\beta} = \frac{\pi}{h}u(\alpha,\beta)$ and the following tree-level building block definition has been used

$$\langle x\rangle_\theta = \frac{ig^2}{2h}\left(-\frac{\sinh\theta}{\cosh\theta - \cos\left(\frac{\pi}{h}(x-1)\right)} + \frac{\sinh\theta}{\cosh\theta - \cos\left(\frac{\pi}{h}(x+1)\right)}\right). \tag{6.4.3}$$

As it happens for the expression in (6.2.10), where we double counted the poles summing over the entire orbits Γ_b, also in (6.4.2) there are pairs of contributions corresponding to equivalent triangles not connected by a Coxeter transformation (an example is shown in figure 5.2). For each value x in the physical strip having a positive coefficient $(\lambda_a, w^{-p}\gamma_b)$ there exists a companion $x' = 2h - x$ with coefficient $(\lambda_a, w^{-p'}\gamma_b) = -(\lambda_a, w^{-p}\gamma_b)$. The sum of the two partners is

$$\frac{1}{2}\Big((\lambda_a, w^{-p}\gamma_b)\langle x\rangle_\theta - (\lambda_a, w^{-p}\gamma_b)\langle 2h - x\rangle_\theta\Big) = (\lambda_a, w^{-p}\gamma_b)\langle x\rangle_\theta$$

where in the last equality we used

$$\langle 2h - x\rangle_\theta = -\langle x\rangle_\theta. \tag{6.4.4}$$

Expressions for the S-matrices of simply-laced affine Toda field theories can be derived from (6.4.2). If we normalize the root length to be $\Lambda^2 = 2$, then from (5.3.12) the scalar products between the fundamental weights and the simple roots can only be zero or one. In (6.2.12) we showed that the tree-level bootstrap relations (4.2.6) follow from the linearity of the scalar products, that allow a single S-matrix element

to be written as a sum of other two S-matrix elements. Similarly the quantum exact bootstrap relations (2.4.7), which relate S-matrices with products of S-matrices, have also to follow from the linearity of the scalar products. The tree-level sum (4.2.6) can be promoted to be the product in (2.4.7) by promoting the coefficients $(\lambda_a, w^{-p}\gamma_b)$ to be the exponents of the building blocks. Since in simply-laced affine Toda theories these coefficients are all integers (having set $\Lambda^2 = 2$), these exponents do not introduce branch cuts and the analytic structure of the S-matrix continues to be consistent. The exact S-matrices can consistently be written as

$$S_{ab}(\theta) = 1 + S_{ab}^{tree}(\theta) + o(g^4) = \prod_{p=0}^{h-1} \Big(1 + \langle 1 + u(\gamma_a, w^{-p}\gamma_b) \rangle_\theta + o(g^4) \Big)^{\frac{1}{2}(\lambda_a, w^{-p}\gamma_b)}, \quad (6.4.5)$$

where the arguments inside the brackets in the product (6.4.5) are the non-perturbative expressions for the building blocks evaluated up to the order g^2. It is reasonable to believe that formula (6.4.5), which has been completely determined starting from perturbation theory, is the order g^2 expansion of the quantum S-matrix

$$S_{ab}(\theta) = \prod_{p=0}^{h-1} \{1 + u(\gamma_a, w^{-p}\gamma_b)\}^{\frac{1}{2}(\lambda_a, w^{-p}\gamma_b)} \quad (6.4.6)$$

in terms of the building blocks (2.6.3). Similarly to what happens at the tree-level, for each brick $\{x\}$ with $0 < x < h$ and associated exponent $(\lambda_a, w^{-p}\gamma_b) > 0$, we find another brick $\{x'\} = \{2h - x\}$ with exponent $(\lambda_a, w^{-p'}\gamma_b) = -(\lambda_a, w^{-p}\gamma_b)$. The product of the two building blocks is obtained by using the properties in (2.6.5):

$$\{x\}^{\frac{1}{2}(\lambda_a, w^{-p}\gamma_b)} \{2h - x\}^{-\frac{1}{2}(\lambda_a, w^{-p}\gamma_b)} = \{x\}^{(\lambda_a, w^{-p}\gamma_b)}.$$

For example, the S-matrix element S_{12} of the $e_8^{(1)}$ affine Toda theory, having $h = 30$, can be written through the universal formula (6.4.6) as

$$S_{12}(\theta) = \{7\}^{1/2}\{13\}^{1/2}\{17\}^{1/2}\{23\}^{1/2}\{37\}^{-1/2}\{43\}^{-1/2}\{47\}^{-1/2}\{53\}^{-1/2},$$

which combining

$$\{7\}^{1/2}\{53\}^{-1/2} = \{7\} \quad , \quad \{13\}^{1/2}\{47\}^{-1/2} = \{13\},$$
$$\{17\}^{1/2}\{43\}^{-1/2} = \{17\} \quad , \quad \{23\}^{1/2}\{37\}^{-1/2} = \{23\}$$

becomes the expression in (2.6.2).

If we compare the values

$$1 + \langle x \rangle_\theta = 1 + \frac{ig^2}{2h} \left(- \frac{\sinh\theta}{\cosh\theta - \cos\left(\frac{\pi}{h}(x-1)\right)} + \frac{\sinh\theta}{\cosh\theta - \cos\left(\frac{\pi}{h}(x+1)\right)} \right),$$

with the expansion of the building blocks (2.6.3) around $B = 0$

$$\{x\}_\theta = 1 + \frac{i\pi B}{h}\left(-\frac{\sinh\theta}{\cosh\theta - \cos\left(\frac{\pi}{h}(x-1)\right)} + \frac{\sinh\theta}{\cosh\theta - \cos\left(\frac{\pi}{h}(x+1)\right)}\right) + o(B^2). \tag{6.4.7}$$

we obtain

$$B = \frac{g^2}{2\pi} + o(g^4).$$

In this way we relate the function B, describing the displacement between poles and zeros in the building blocks (2.6.3), with the coupling g of the Lagrangians of simply-laced affine Toda theories. In section (2.6) we argued that B has to take values between 0 and 2: this was a requirement to preserve the correct signs of the residues associated with bound state particles propagating in the forward and crossed channels. In [57] the following expression for B was proposed

$$B = \frac{g^2}{2\pi}\frac{1}{1 + g^2/4\pi} \tag{6.4.8}$$

matching the expected tree-level result in the limit $g \to 0$ and going to 2 in the limit $g \to \pm\infty$. We recall from section 2.6 that each building block (2.6.3) is invariant under the transformation $B \to 2 - B$, corresponding to swapping the positions of the zeros internally to the building block. This transformation is equivalent to sending $g \to 4\pi/g$, indeed

$$B\left(\frac{4\pi}{g}\right) = 2 - B(g).$$

Therefore, the non-perturbative S-matrices (6.4.6) satisfy the following weak-strong coupling duality

$$S_{ab}(\theta; 4\pi/g) = S_{ab}(\theta; g). \tag{6.4.9}$$

This is very surprising if we think that there is no sign of such a duality in the starting Lagrangian (5.1.1). A similar duality is observed also in $\mathcal{W}$-algebras of affine type as remarked for example in pp. 263-264 of [90]. Although a universal proof of the relation (6.4.8) is missing, its validity has been confirmed at one loop (i.e. at the order g^4) based on a case by case analysis of ADE series of affine Toda models [78]. The simplest example of an affine Toda theory is the sinh-Gordon model having an S-matrix composed of a single building block

$$S_{11}(\theta) = \{1\}_\theta = \frac{(0)(2)}{(B)(2-B)}. \tag{6.4.10}$$

In this case, the Coxeter number h is equal to 2 and $(0) = -(2) = 1$; as a consequence of this fact the S-matrix does not contain any poles in the physical strip. Rearranging the expression in (6.4.10) it can be shown that

$$S_{11}(\theta) = \frac{\sinh\theta - i\sin(\pi B/2)}{\sinh\theta + i\sin(\pi B/2)}. \tag{6.4.11}$$

The S-matrix of this model has a long history and a proposal for it can be found

in [91]. It can also be obtained by analytically continuing $g^2 \to -g^2$ in the B_1-B_1 S-matrix of the sine-Gordon quantum field theory, where B_1 is the lightest breather of the theory and g is the coupling of the sine-Gordon Lagrangian. The S-matrices of the other affine Toda theories are a generalization of this simple example, which has been relevant in the determination of the relation (6.4.8).

Another possible universal expression for the tree-level S-matrix is obtained by substituting (6.4.1) into (6.2.11). If we do so we end up with

$$S_{ab}^{tree}(\theta) = \frac{ig^2}{4h}\sum_{p=0}^{h-1}(\lambda_a, w^{-p}\gamma_b)\Big(-\coth\Big(\frac{\theta}{2} \pm \frac{i\pi}{2h}u(\gamma_a, w^{-p}\gamma_b)\Big) + \coth\Big(\frac{\theta}{2} \pm \frac{i\pi}{2h}u(\gamma_a, w^{-(p+1)}\gamma_b)\Big)\Big). \tag{6.4.12}$$

Equation (6.4.12) corresponds to the tree-level expansion of a universal formula obtained the first time in [73, 74]; in those papers, a general expression for the S-matrices of simply-laced affine Toda theories was formulated in terms of 'half building blocks', through which it was verified that the unitarity, crossing and bootstrap properties were universally satisfied. However, we prefer here not to introduce additional expressions for the building blocks and keep as the only definition the one reported in equation (2.6.3). With this prescription for the building blocks the non-perturbative S-matrix is given in (6.4.6); this prescription is the same as used in [92] manipulating results previously obtained in [73]. While the S-matrices of simply-laced affine Toda theories found their universal formulation in [73, 74], many previous papers, in which a case by case study was performed, were of great importance in figuring out the exact S-matrices of these models. Among them we mention [57, 70, 91, 93–96].

We should stress that the ADE series of affine Toda models represent a class that behaves well at the quantum level: at one loop they preserve all the mass ratios [57] suggesting that the geometrical structure obtained from the bootstrap is maintained at quantum level in perturbation theory. In these cases the tree-level S-matrices obtained in (6.2.10) can consistently be promoted to the non-perturbative expressions (6.4.6), which passed many perturbative checks [69, 78, 79, 97, 98]. The situation becomes more complicated for models constructed from non simply-laced Dynkin diagrams [99–103] where the masses renormalize in a coupling dependent way spoiling the natural geometrical connection between S-matrices and Coxeter geometry. A geometrical formulation for the non-perturbative S-matrices of these more complicated theories was proposed in [103], though it is much more convoluted than the formulation of simply-laced theories.

Chapter 7

Loop-level integrability in affine Toda field theories

7.1 Higher-order poles in bootstrapped S-matrices

In chapter 2 we noted that sometimes the elementary building blocks $(x)_\theta$ of certain bootstrapped S-matrices appear with multiplicity higher than one. This was the case for the minimal S-matrix element S_{13} in (2.5.17) where $(11)^2$ and $(19)^2$ were two blocks contributing to poles of order two, located at the rapidity values $i\frac{11}{30}\pi$ and $i\frac{19}{30}\pi$ respectively. Also in affine Toda field theories, where the elementary building blocks assume the brick structure in (2.6.3), these higher-order poles can in general be present. If we look at figure 2.16, containing some of the S-matrix elements of the $e_8^{(1)}$ affine Toda model, we note that most of the poles are of higher order and correspond to the positions in which two or more bricks touch each other. In this chapter, we focus on the mechanism under which these higher-order poles are generated in perturbation theory in simply-laced affine Toda theories, i.e. models having an underlying Lie algebra belonging to the ADE series. We assume the squared length common to all the roots to be $\Lambda^2 = 2$.

The non-perturbative S-matrices associated with these theories are written in (6.4.6) in terms of the roots and weights of their underlying root systems. As already remarked in the previous section, for a given S-matrix element S_{ab} the building blocks $\{x\}$ (written in units of π/h) always appear in copies with opposite exponents as

$$\{x\}^{\frac{1}{2}N_{ab}(x)}\{2h-x\}^{-\frac{1}{2}N_{ab}(x)} = \{x\}^{N_{ab}(x)}.$$

In the end S_{ab} takes the form (2.6.4), with all the x belonging to the interval $[1, h-1]$ and all the $N_{ab}(x)$ being positive integers. Combining (6.4.7) with (6.4.8) we see that each building block $\{x\}$, for small values of g, can be Taylor expanded, presenting at leading order in the Lagrangian coupling two simple poles

$$\{x\}_\theta = 1 + \frac{ig^2}{2h}\left(-\frac{1}{\theta - \frac{i\pi}{h}(x-1)} + \frac{1}{\theta - \frac{i\pi}{h}(x+1)} + \dots\right) + o(g^4)\ . \tag{7.1.1}$$

The ellipses in the brackets above are finite at the pole positions $\theta = \frac{i\pi}{h}(x \pm 1)$, while in $o(g^4)$ (which includes powers of the coupling g equal and higher than four) are contained both finite and 1^{st}-order poles at $\theta = \frac{i\pi}{h}(x \pm 1)$.

Our purpose here is to analyze the leading order singularities arising in the S-matrices due to the presence of these building blocks. By leading order singularities we mean that we perform the Laurent expansion of the S-matrix around a pole position and at each order in the pole expansion we consider only the leading order in g^2. In other words, if we have a pole of order P sitting at the position $\theta = i\theta_0$ we can write the S-matrix around the pole as

$$S_{ab}(\theta) = \sum_{p=0}^{P} \frac{1}{(\theta - i\theta_0)^p} \left(\frac{g^2}{2h}\right)^p \left(a_p + b_p g^2 + o(g^4)\right) + o(\theta - i\theta_0). \tag{7.1.2}$$

For each coefficient of the Laurent series, we are interested in finding the leading order terms in the coupling expansion, which are $a_0,\ a_1, \ldots, a_P$. It is straightforward to obtain such coefficients from the bootstrapped result (2.6.4). A P^{th}-order pole in $\theta = \frac{i\pi}{h}x$, with $P = M + N$, arises from terms in the S-matrix of the form

$$\{x-1\}^M \{x+1\}^N \sim \left(1 + \frac{ig^2}{2h}\frac{1}{\theta - \frac{i\pi}{h}x}\right)^M \left(1 - \frac{ig^2}{2h}\frac{1}{\theta - \frac{i\pi}{h}x}\right)^N , \tag{7.1.3}$$

where in (7.1.3) we substituted the terms of the building block expansion (7.1.1) which are singular at $\theta = \frac{i\pi}{h}x$. Each term obtained in the expression above corresponds to a leading order coefficient of the Laurent expansion written in (7.1.2). Other quantities are present due to the complete expansion of the brick (7.1.1), but these are subleading terms in g^2. Note that the difference between multiplicities of neighbouring bricks is a scalar product between roots, as written in (6.4.1). Therefore the quantity $N_{ab}(x+1) - N_{ab}(x-1)$, in simply-laced Toda models, can only take values in $\{-1, 0, +1\}$. The leading order contributions to the Laurent expansion around the pole $i\theta_0$ can then be written as

$$S_{ab}(\theta) \sim \sum_{n=0}^{N} \binom{N}{n} \left(\frac{g^2}{2h}\right)^{2n} \frac{1}{(\theta - i\theta_0)^{2n}} + \nu \sum_{n=0}^{N} \binom{N}{n} \left(\frac{g^2}{2h}\right)^{2n+1} \frac{1}{(\theta - i\theta_0)^{2n+1}} . \tag{7.1.4}$$

The coefficient ν is equal to zero if two bricks, both of multiplicity N, touch each other generating an even pole of order $P = 2N$. Instead, we have $\nu = +i/-i$ when there is a jump from a brick of multiplicity $N + 1/N$ on the left to a brick of multiplicity $N/N + 1$ on the right. These second types of poles are called odd-order singularities since $P = 2N + 1$. The different situations are illustrated in figure 7.1.

In this chapter we try to highlight the origin of the formula (7.1.4) using perturbation theory. The $n = 0$ contributions in (7.1.4) are naturally interpreted as the identity (i.e. free propagators), in the first sum, and a bound state particle propagating at the tree level in the forward/crossed channel ($\nu = +i/-i$), in the second sum. From $n = 1$ onwards, loop contributions start. Such higher-order singularities emerging by imposing the closure of the bootstrap fusing relations can be explained in perturbation theory in terms of the Coleman-Thun mechanism [39]: they are anomalous

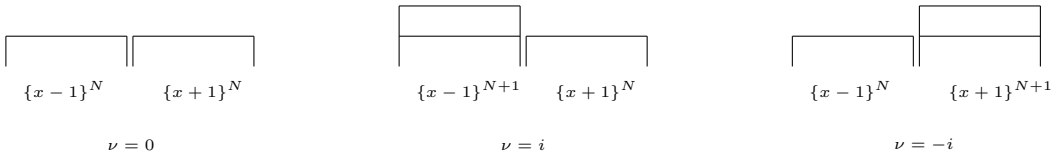

Figure 7.1: Higher order singularities at $\theta = i\frac{\pi x}{h}$. From left to right are reported a $2N$-order pole and respectively a forward/crossed channel pole of order $2N+1$. All the situations are encoded in equation (7.1.4) substituting the corresponding values of ν.

thresholds coming from Feynman diagrams in which all the internal propagators, within the integration loops, can go simultaneously on-shell for particular choices of the external kinematics. In the next sections the analysis will be carried out for second- and third-order poles (which is $P = 2$ and $P = 3$ in (7.1.2)) in diagonal scattering processes. In all the cases the coefficient a_p of each term of the Laurent expansion (7.1.2) are computed, displaying perfectly agreement with the bootstrap formula (7.1.4). In [69] the authors studied poles of order $P = 2$ and $P = 3$ finding in both cases the coefficient a_P of the maximal singularity in (7.1.2). While the results found matched the bootstrap expectations, the underlying mechanism that led to the answer was not completely clear, particularly for $P = 3$. In that case, the Feynman diagrams contributing to the pole generated a collection of complicated numbers which, only after the sum, miraculously collapsed to the correct residue expected from the bootstrap. We will highlight better the reason why this happens following the argumentation of [2, 3]. Other aspects of higher-order singularities are also covered in this chapter, although the computation of all the leading coefficients a_p of the Laurent expansion at arbitrary P has not yet been achieved, due to the huge number of singular Feynman diagrams arising at higher loops. However we do see some sign of how a general proof may be achieved.

Before moving on to study these poles by computing loop diagrams in perturbation theory, we should mention some properties of the 3-point couplings characterising simply-laced affine Toda models. Having set the squared of the root length to be $\Lambda^2 = 2$, the relation (6.1.23) requires

$$f_{abc} = 4\frac{g}{\sqrt{h}}\sigma_{abc} \quad \text{with} \quad |\sigma_{abc}| = 1.$$

In the expression above σ_{abc} is a phase of unit modulus, connected to the structure constants and to the orientation of the projected root triangle through (6.1.18), by which we get

$$\sigma_{abc} = N_{\alpha,\beta} sign\Big(\sin(U_\alpha - U_\beta)\Big),$$

with $\alpha \in \Gamma_a$ and $\beta \in \Gamma_b$. If all the particles of the model are real then the structure constants have to be real, indeed in this case each orbit contains pairs of opposite

roots; for any root $\alpha \in \Gamma_a$ then $-\alpha = w^{h/2}\alpha \in \Gamma_a$ and it holds that

$$N_{-\alpha,-\beta} = N_{w^{h/2}\alpha,w^{h/2}\beta} = N_{\alpha,\beta},$$

where in the last equality we used (5.3.20). By property D.2 it follows that $N^*_{\alpha,\beta} = N_{\alpha,\beta}$. In the case in which some particles are complex, the structure constants associated with the orbits of such particles could in principle be complex phases. However, we can always tune the generators $\{e_\alpha\}_{\alpha\in\Phi}$ so that equations (5.3.18) and (5.3.19) are satisfied and the structure constants are real. An explicit expression for them in terms of scalar products between roots and fundamental weights was derived in [74]. For this reason is not restrictive to assume all the σ_{abc} to be real so that the values of the 3-point couplings, if they are nonzero, can be written as

$$C^{(3)}_{abc} = f_{abc}\Delta_{abc} \quad \text{with} \quad f_{abc} = \pm 4\frac{g}{\sqrt{h}}. \tag{7.1.5}$$

Despite it being possible to swap the signs of some 3-point couplings by transforming e_{Γ_a} into $-e_{\Gamma_a}$ (by which we mean that the transformation has to be performed on each generator e_α with $\alpha \in \Gamma_a$), not all the f_{abc} have arbitrary sign: remember that the constraint (D.0.1) on structure constants has to be satisfied. This constraint is responsible for the equality (4.1.9), which is necessary to avoid poles in 2-to-2 inelastic scattering processes. Since in this chapter we focus on the ADE series of affine Toda field theories the simply-laced scattering conditions 4.1 are satisfied and the pole cancellations in 4-point processes happen between pairs of singular diagrams. One of the three terms in (4.1.9) is therefore always absent. The flipping rule for the cancellation of tree-level non-diagonal processes also enters in loop diagrams and is of great importance to find all the loop diagrams contributing to the higher-order poles.

7.2 Landau poles and cuts

In this section, we review the mechanism responsible for the generation of higher-order poles in perturbation theory following the approach used in [2]. This method, compared with the technique used in [69], is beneficial in the fact that makes evident how the loops, on the pole position, factorise into particular products of singular tree-level diagrams. This makes it possible to use the tree-level techniques studied in [1] to obtain loop results. We work directly in the momentum space instead of using Feynman parameters since this is particularly convenient in two dimensions. To each order p in (7.1.2) we are only interested in finding the leading order in the g^2 expansion, which corresponds to finding Feynman diagrams with the maximum number of internal on-shell momenta and carrying the minimum power of g. We will show that such a situation occurs if the only vertices entering into the diagrams are 3-point couplings.

Let us consider a loop process involving the diagonal scattering of two particles, a and b. Since there are two degrees of freedom for each loop, we can always tune the

loop variables so that two momenta inside each loop are on-shell. Therefore we set $2L$ momenta satisfying the mass-shell condition

$$q_j^2 - m_j^2 = 0 \tag{7.2.1}$$

where $j = 1, \ldots, 2L$ and L is the total number of loops. Then we expand the loop integrals around the values where these $2L$ momenta are on-shell

$$Q_j = q_j + \sum_{i=1}^{L} \lambda_{ji}^{(Q)} l_i \equiv q_j + k_j^{(Q)}. \tag{7.2.2}$$

The vectors $l_1, \ldots, l_L$ are the L loop integration variables. This permits the corresponding propagators to be written in the following form

$$\frac{1}{Q_j^2 - m_j^2 + i\epsilon} = \frac{1}{2q_j \cdot k_j^{(Q)} + (k_j^{(Q)})^2 + i\epsilon}. \tag{7.2.3}$$

All the loop integration variables are contained in the vectors $k_j^{(Q)}$. If we define I to be the total number of propagators then the remaining $I - 2L$ momenta (those that are not expanded around their on-shell values) are given by

$$P_j = p_j + \sum_{i=1}^{L} \lambda_{ji}^{(P)} l_i \equiv p_j + k_j^{(P)}. \tag{7.2.4}$$

The remaining set of momenta p_j around which the loops are expanded are frozen, since we have already used all the loop freedom to set the momenta q_j on-shell in (7.2.1). Differently from q_j the values p_j are generally off-shell and could go on-shell only at a particular value of the external kinematics in certain diagrams. Suppose we define $p_a^{(0)}$ and $p_b^{(0)}$ to be the values of the incoming momenta corresponding to the pole position

$$s_0 = \left(p_a^{(0)} + p_b^{(0)}\right)^2 \tag{7.2.5}$$

at which not only the momenta q_j in (7.2.1) are mass-shell but also the remaining vectors p_j in (7.2.4), then we can expand p_j around s_0

$$p_j^2 - m_j^2 = \left.\frac{dp_j^2}{ds}\right|_{s=s_0} (s - s_0) + \frac{1}{2} \left.\frac{d^2 p_j^2}{ds^2}\right|_{s=s_0} (s - s_0)^2 + \ldots \tag{7.2.6}$$

Therefore up to extra multiplicative factors, irrelevant to the purpose of the discussion, the Feynman diagram in the neighborhood of s_0 can be written as

$$I = \int \prod_{i=1}^{L} \frac{d^2 l_i}{(2\pi)^2} \prod_{j=1}^{2L} \frac{1}{2q_j \cdot k_j^{(Q)} + (k_j^{(Q)})^2 + i\epsilon} \prod_{j=1}^{I-2L} \frac{1}{\left.\frac{dp_j^2}{ds}\right|_{s=s_0} (s - s_0) + \frac{1}{2} \left.\frac{d^2 p_j^2}{ds^2}\right|_{s=s_0} (s - s_0)^2 + \ldots + 2p_j \cdot k_j^{(P)} + (k_j^{(P)})^2 + i\epsilon}. \tag{7.2.7}$$

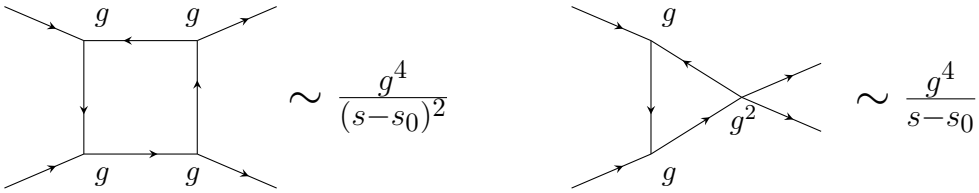

Figure 7.2: Examples of diagrams contributing to the coefficients a_2 and b_1 in equation (7.1.2).

Redefining the integration variables in the following manner

$$l_i = (s - s_0)\tilde{l}_i \ , \tag{7.2.8}$$

we can isolate the singular part of the diagram at $s = s_0$:

$$I = \frac{1}{(s-s_0)^{I-2L}} \int \prod_{i=1}^{L} \frac{d^2\tilde{l}_i}{(2\pi)^2} \prod_{j=1}^{2L} \frac{1}{2q_j \cdot \tilde{k}_j^{(Q)} + (\tilde{k}_j^{(Q)})^2(s-s_0) + i\epsilon} \prod_{j=1}^{I-2L} \frac{1}{\frac{dp_j^2}{ds}\Big|_{s=s_0} + 2p_j \cdot \tilde{k}_j^{(P)} + (\tilde{k}_j^{(P)})^2(s-s_0) + \frac{1}{2}\frac{d^2p_j^2}{ds^2}\Big|_{s=s_0}(s-s_0) + \ldots + i\epsilon} . \tag{7.2.9}$$

The order of the pole is defined by $p = I - 2L$ where, as already specified, I is the total number of propagators flowing in the diagram and L is the total number of loops. For fixed L, this order is maximal when the number I of singular propagators is maximal, which corresponds to having all vertices with three legs. For example, a one-loop diagram with four 3-point vertices and four propagators can contribute to a second-order pole since $I - 2L = 4 - 2 = 2$. On the other hand, a one-loop diagram with two 3-point vertices and one 4-point vertex contains only three propagators: in this case, $I - 2L = 3 - 2 = 1$ and the order of the pole is one. Despite the order of the pole being different in these two diagrams, by the fact that in affine Toda theories a vertex of order n contributes as $C^{(n)} \sim g^{n-2}$, they both contain a power of the coupling g^4. The two diagrams are depicted in figure 7.2.

For a fixed power of g, the leading coefficients a_p in (7.1.2) are obtained by summing over the maximal singular contributions of Feynman diagrams containing only 3-point vertices and with all the internal propagators simultaneously on-shell. They can be evaluated through (7.2.9) by omitting all the subleading contributions in $s - s_0$. If we do so the formula (7.2.9) becomes

$$I = \frac{1}{(s-s_0)^{I-2L}} \int \prod_{i=1}^{L} \frac{d^2\tilde{l}_i}{(2\pi)^2} \prod_{j=1}^{2L} \frac{1}{2q_j \cdot \tilde{k}_j^{(Q)} + i\epsilon} \prod_{j=1}^{I-2L} \frac{1}{\frac{dp_j^2}{ds}\Big|_{s=s_0} + 2p_j \cdot \tilde{k}_j^{(P)} + i\epsilon} . \tag{7.2.10}$$

For example the box on the LHS of figure 7.2 contributes to the coefficient a_2 through (7.2.10). On the other hand, by using (7.2.9), we can perform an expansion

of the box diagram around the pole and obtain its contribution at the order $(s-s_0)^{-1}$, which together with the triangular diagram in figure 7.2 contributes to the coefficient b_1.

Evaluating the coefficients b_p through Feynman diagrams is in principle possible, though it is complicated since the number of diagrams that need to be computed is in general very large. In [98] the coefficient b_1 was evaluated in the case $P = 2$ in the affine Toda models of type $A_r^{(1)}$; in [2], by exploiting general tree-level integrability properties of simply-laced models, this coefficient is computed for all the ADE series of affine Toda theories at poles of arbitrary even order $P = 2N$. Incredibly all the results display perfect agreement with the universal bootstrapped S-matrix formula (6.4.6).

We return now to the main problem of this chapter: the evaluation of the leading order coefficients a_p in (7.1.2). To this purpose the integral (7.2.10) has to be computed. We observe that all the denominators in the propagators of (7.2.10) are linear functions of the loop variables, therefore the integration is simple. It can be performed by closing a contour in the complex plane and using Cauchy's theorem. Depending on the choice of variables adopted when we perform the integral the number of poles in the integration contour can change and the same result can be written as sums over different residues. Each one of these sums is a sum over different products of tree-level diagrams where each propagator with respect to which we take the residue is cut. We show this explicitly in section 7.2.1 with an example.

After the computation we need to multiply by the following remaining factors, which have been omitted in (7.2.10):

$$\begin{aligned} &\text{For each vertex:} && -iC^{(3)}_{abc} \\ &\text{For each propagator:} && i \\ &\text{A total multiplicative factor:} && \frac{1}{4m_a m_b \sinh i\theta_0} = \frac{1}{8i\Delta_{ab}} \end{aligned} \tag{7.2.11}$$

The last term comes by expressing the overall energy-momentum conservation delta function $(2\pi)^2\delta^{(2)}(p_a^{in}+p_b^{in}-p_a^{out}-p_b^{out})$ in terms of the rapidities on the pole position and inserting the usual normalization factor $\frac{1}{\sqrt{4\pi}}$ for each external particle. Δ_{ab} is the area of the triangle formed by the vectors p_a, p_b on the pole position. Finally, we need to express $s - s_0$ in terms of the rapidity at the pole

$$s - s_0 = 2m_a m_b\Big(\cosh\theta - \cosh i\theta_0\Big) = 4i\Delta_{ab}(\theta - i\theta_0) \tag{7.2.12}$$

where in the last equality we have expanded $\cosh\theta$ around $\theta = i\theta_0$ and used $\Delta_{ab} = \frac{1}{2}m_a m_b \sin\theta_0$.

Once we understand what residues to take the difficult part in the evaluation of the integral (7.2.10) is to compute the derivatives of the squared momenta on the pole position, which are the terms on the RHS of (7.2.6). We have already mentioned that the rapidity values at which poles can appear are purely imaginary numbers, so Feynman diagrams at $l_1 = l_2 = \ldots = l_L = 0$ (the point in which all loop propagators are singular simultaneously) are represented as planar geometrical figures in which

the internal segments have lengths equal to the masses of the propagating particles. Then evaluating the derivatives of the momenta squared amounts to a geometrical problem, similar to the one already addressed in chapter 4 in the context of tree-level scattering.

To compute the loop diagrams it is often useful to write the oriented area of the triangle identified by a pair of vectors A, B in $\mathbb{R}^2$ as the determinant

$$\Big\langle AB \Big\rangle \equiv \frac{1}{2} \begin{vmatrix} A_x & B_x \\ A_y & B_y \end{vmatrix} . \tag{7.2.13}$$

In different situations, it will be necessary to write vectors in a non-orthogonal basis. To do this the following identity can be used

$$\Big\langle AB \Big\rangle \, D + \Big\langle BD \Big\rangle \, A + \Big\langle DA \Big\rangle \, B = 0 \tag{7.2.14}$$

on any triplet of vectors A, B and D in $\mathbb{R}^2$. Doing the vector product with a fourth element C we obtain the Plücker relation connecting areas of different triangles

$$\Big\langle AB \Big\rangle \Big\langle CD \Big\rangle + \Big\langle BD \Big\rangle \Big\langle CA \Big\rangle + \Big\langle DA \Big\rangle \Big\langle CB \Big\rangle = 0. \tag{7.2.15}$$

In the next section, we show an example of Feynman diagram in which the Coleman-Thun mechanism [39] for the generation of Landau singularities is manifest. The example is simple and already known [69] but it contains some subtleties that are characteristic of also more difficult cases and it is good to explain them here following the lines of [2, 3].

7.2.1 An example: the box integral

Let us consider the box diagram in figure 7.3. The RHS shows the on-shell description of the diagram, which is the point where the loop integration variable l is equal to zero and all the internal propagators B, C, B' and C' are simultaneously on-shell. With a small abuse of notation, we define with the letters B, C, B', C' both the on-shell vectors and the particle labels. As explained previously, since the loop carries two degrees of freedom we can set two momenta, say B and C, on-shell and expand the integral around their on-shell values, which means that at $l = 0$ we have

$$B^2 - m_B^2 = 0 \quad , \quad C^2 - m_C^2 = 0. \tag{7.2.16}$$

Having used all the loop freedom to set the values of B and C, for a general choice of the external kinematics B' and C' are off-shell at $l = 0$, and their propagators diverge only at the special point $s = s_0$ where the box diagram is singular. If we expand the vectors B' and C' around s_0 we obtain

$$\begin{aligned} B'^2 - m_{B'}^2 &= \frac{dB'^2}{ds}\Big|_{B,C} (s - s_0) + \dots \\ C'^2 - m_{C'}^2 &= \frac{dC'^2}{ds}\Big|_{B,C} (s - s_0) + \dots \end{aligned} \tag{7.2.17}$$

Figure 7.3: Box diagram on the left and its on-shell dual description on the right.

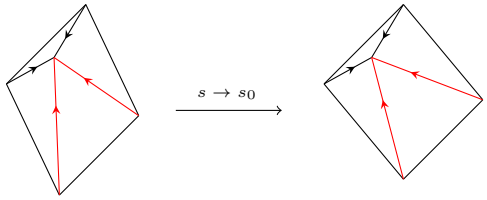

Figure 7.4: Loop expansion around the on-shell values $B^2 = m_B^2$ and $C^2 = m_C^2$. The remaining momenta B' and C' (drawn in red in the figure) are not on-shell for general external kinematics (on the LHS) and go on-shell only on the pole position $s = s_0$ (on the RHS).

where inside ... higher powers of $(s - s_0)$ are contained. The subscript letters B and C in the derivatives indicate that we are differentiating B'^2 and C'^2 with respect to s keeping the lengths of B and C fixed at their on-shell values. The situation is shown in figure 7.4 where on the LHS we see that near the pole position only B and C are on-shell (the black internal momenta) while the red momenta B' and C' are off-shell; indeed their lengths do not correspond to the values of their masses. We perform the integral in this position $s \sim s_0$ but at $s \neq s_0$, and in the end, we take the limit $s \to s_0$ (RHS part of figure 7.4) at which the Feynman diagram becomes singular. Expanding the loop around the values in (7.2.16), (7.2.17) and rescaling the loop variable $l = (s - s_0)\tilde{l}$ we obtain

$$I_\square = \frac{1}{(s-s_0)^2} \int \frac{d^2\tilde{l}}{(2\pi)^2} \frac{1}{2B\cdot\tilde{l} + i\epsilon} \frac{1}{2C\cdot\tilde{l} + i\epsilon} \frac{1}{\frac{dB'^2}{ds}\Big|_{B,C} + 2B'\cdot\tilde{l} + i\epsilon} \frac{1}{\frac{dC'^2}{ds}\Big|_{B,C} + 2C'\cdot\tilde{l} + i\epsilon}, \tag{7.2.18}$$

that is a particular case of the general formula (7.2.10). The residue at the pole is isolated in the integral expression above and can be easily computed using Cauchy's theorem. With the purpose of using the scalar products $2B\cdot\tilde{l}$ and $2C\cdot\tilde{l}$ as integration variables we express all the momenta in (7.2.18) as linear combinations of B and C. This is easily done by using (7.2.14):

$$B' = -\frac{\Delta_{B'C}}{\Delta_{BC}} B - \frac{\Delta_{B'B}}{\Delta_{BC}} C \quad , \quad C' = -\frac{\Delta_{C'C}}{\Delta_{BC}} B - \frac{\Delta_{C'B}}{\Delta_{BC}} C. \tag{7.2.19}$$

In these expressions we have labeled by Δ_{XY} the area of the triangle having as sides two vectors X and Y, which means, referring to definition (7.2.13), $\Delta_{XY} = \sqrt{\langle XY\rangle^2}$. We point out that all the coefficients of the linear combinations in (7.2.19) are negative numbers. This is pictorially understood if we look at the right-hand side part of figure 7.3. There we see that both B' and C' belong to the section of the plane spanned by positive linear combinations of the vectors $-B$ and $-C$, since the oriented lines identifying their directions are contained in the angle formed between the arrows of B and C. If we write the integral (7.2.18) in terms of the integration variables

$$u = 2B\cdot\tilde{l} \quad , \quad v = 2C\cdot\tilde{l}$$

we obtain

$$I_{\square} = \frac{1}{(s-s_0)^2}\frac{1}{(2\pi)^2 8i\Delta_{BC}}\int du\,dv\,\underbrace{\frac{1}{u+i\epsilon}}_{B}\,\underbrace{\frac{1}{v+i\epsilon}}_{C}$$
$$\underbrace{\frac{1}{\left.\frac{dB'^2}{ds}\right|_{B,C} - \frac{\Delta_{B'C}}{\Delta_{BC}}u - \frac{\Delta_{B'B}}{\Delta_{BC}}v + i\epsilon}}_{B'}\,\underbrace{\frac{1}{\left.\frac{dC'^2}{ds}\right|_{B,C} - \frac{\Delta_{C'C}}{\Delta_{BC}}u - \frac{\Delta_{C'B}}{\Delta_{BC}}v + i\epsilon}}_{C'}, \tag{7.2.20}$$

where the factor in front of the integral comes from the Jacobian associated to the change of variables

$$d^2\tilde{l} = \frac{1}{8i\Delta_{BC}}du\,dv.$$

Each of the terms in the integral (7.2.20) corresponds to a particular propagator whose particle label is indicated under it. The different ways in which we can close the u/v-contours in the complex plane to write the result as sums over different residues correspond to different possible decompositions of the loop as sums over products of tree-level graphs. Let us consider the simplest situation in which we close both the u- and v-contours in the lower half complex plane with a semicircle of infinite radius. Using the residue theorem the result is simply given by

$$I_{\square} = \frac{i}{(s-s_0)^2}\frac{1}{8\Delta_{BC}}\underbrace{\frac{1}{\left.\frac{dB'^2}{ds}\right|_{B,C}}}_{B'}\underbrace{\frac{1}{\left.\frac{dC'^2}{ds}\right|_{B,C}}}_{C'}. \tag{7.2.21}$$

The propagators corresponding to the B- and C-particles have been removed in taking the residues, since they had simple poles in the lower half plane. On the other hand, the propagators corresponding to B' and C' survived since their poles were not contained in the integration contour. Such surviving propagators are evaluated at fixed on-shell lengths of the external momenta and fixed on-shell lengths of B and C. This means that the loop integral has been reduced to a tree-level diagram in which B and C play the role of external on-shell momenta. The quantities $\frac{1}{\frac{dB'^2}{ds}(s-s_0)}$ and $\frac{1}{\frac{dC'^2}{ds}(s-s_0)}$ correspond to the values of the B'- and C'-propagators respectively near the pole position. A pictorial representation of the cut is represented in the

first equality in figure 7.5.

At this point the problem amounts to finding the derivatives of B'^2 and C'^2 respect to the Mandelstam variable s. We focus on the triangle Δ_{bC}, having as sides p_b, C and B' and on the triangle Δ_{ab} having as sides the external particles p_a, p_b. The values of B'^2 and s are given by

$$B'^2 = m_b^2 + m_C^2 - 2m_b m_C \cos \bar{U}_{bC} \quad , \quad s = m_a^2 + m_b^2 - 2m_a m_b \cos \bar{U}_{ab} \tag{7.2.22}$$

where we indicate by $\bar{U}_{XY}$ the angle between sides X and Y. Since the momenta p_a, B and C defining the thin triangle Δ_{aBC} are on-shell, the angle $\bar{U}_{aC}$ is fixed along the limit $s \to s_0$ and

$$d\bar{U}_{bC} = d\bar{U}_{ab}.$$

Thanks to this fact the derivative of B'^2 respect to s can be written as

$$\frac{dB'^2}{ds} = \frac{\frac{dB'^2}{d\bar{U}_{bC}}}{\frac{ds}{d\bar{U}_{ab}}} = \frac{\Delta_{bC}}{\Delta_{ab}}.$$

The last equality in the relation above has been obtained by using the expressions in (7.2.22). Similarly, it is possible to show that

$$\frac{dC'^2}{ds} = -\frac{\Delta_{bB}}{\Delta_{ab}}.$$

By plugging the values of such derivatives into (7.2.21), multiplying by the remaining factors (7.2.11), (7.2.12) and using the area rule (7.1.5) we obtain

$$D_\square = \frac{1}{(\theta - \theta_0)^2} \frac{1}{4^5} \frac{\Delta_{B'C'}}{\Delta_{ab}} f_{Ba\bar{C}} f_{Cb\bar{B}'} f_{B'\bar{a}\bar{C}'} f_{C'\bar{b}\bar{B}}. \tag{7.2.23}$$

By substituting the values of the f-functions defined in (7.1.5) inside (7.2.23) we obtain the residue of the diagram at the pole. This value is given up to an overall sign which is not completely specified from (7.1.5). We postpone this sign problem to the next section where we will study the full network of Feynman diagrams contributing to the threshold singularity. Let us instead consider here what happens if we choose a different integration contour when we use Cauchy's theorem. We perform the integral (7.2.20) in two steps. First we integrate the u-variable closing the u-contour with a semicircle in the lower half complex plane: in this way we obtain

$$I_\square = \frac{1}{(s-s_0)^2} \frac{2\pi i}{(2\pi)^2 8 i \Delta_{BC}} \int dv \underbrace{\frac{1}{v + i\epsilon}}_{C} \underbrace{\frac{1}{\frac{dB'^2}{ds}\Big|_{B,C} - \frac{\Delta_{B'B}}{\Delta_{BC}} v + i\epsilon}}_{B'} \underbrace{\frac{1}{\frac{dC'^2}{ds}\Big|_{B,C} - \frac{\Delta_{C'B}}{\Delta_{BC}} v + i\epsilon}}_{C'}. \tag{7.2.24}$$

The B-propagator has disappeared from the integral, i.e. it has been cut. At this point instead of closing also the v-path in the region below the real axis (generating only one residue) we close the path in the upper half complex plane where both the 'propagators' B' and C' in (7.2.24) have simple poles. The final result is a sum of

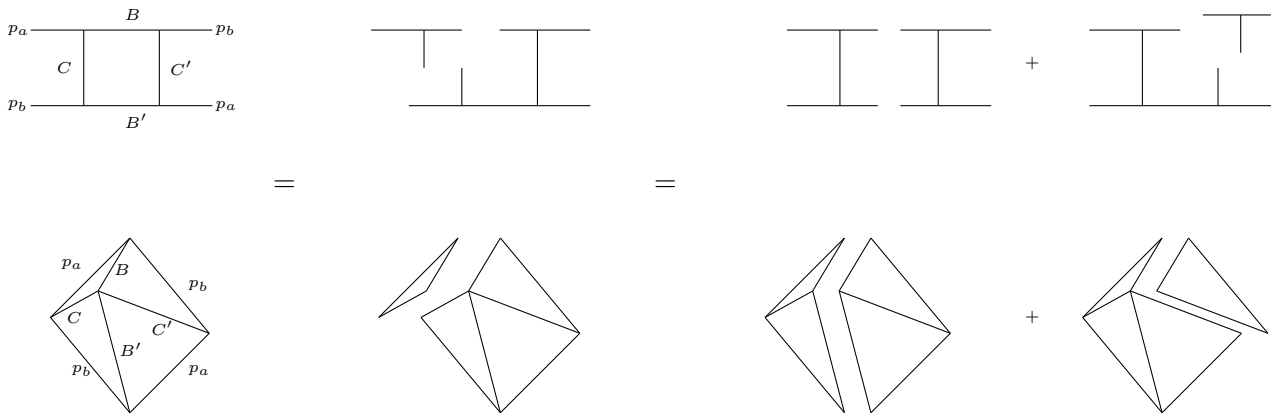

Figure 7.5: Box integral on the pole written as different sums over tree-level diagrams. In the first line Feynman diagrams are reported and in the second line their on-shell dual description is shown.

two residues, one for each propagator presenting a pole in the region enclosed in the integration path:

$$I_{\square} = \frac{1}{(s-s_0)^2}\frac{i}{8}\Bigg[\frac{1}{\Delta_{BB'}}\underbrace{\frac{1}{\frac{\Delta_{BC}}{\Delta_{B'B}}\frac{dB'^2}{ds}\Big|_{B,C}}}_{C}\underbrace{\frac{1}{\frac{dC'^2}{ds}\Big|_{B,C}-\frac{\Delta_{C'B}}{\Delta_{B'B}}\frac{dB'^2}{ds}\Big|_{B,C}}}_{C'}+ \\ \frac{1}{\Delta_{C'B}}\underbrace{\frac{1}{\frac{\Delta_{BC}}{\Delta_{C'B}}\frac{dC'^2}{ds}\Big|_{B,C}}}_{C}\underbrace{\frac{1}{\frac{dB'^2}{ds}\Big|_{B,C}-\frac{\Delta_{B'B}}{\Delta_{C'B}}\frac{dC'^2}{ds}\Big|_{B,C}}}_{B'}\Bigg]. \tag{7.2.25}$$

The factor $\frac{1}{\Delta_{XY}}$ in front of each term in the sum above is a Jacobian depending on which variables have been used in the integration; it can be used as a pointer indicating which propagators X, Y have been cut. In the first term for example we read $\frac{1}{\Delta_{BB'}}$ indicating that the propagators B and B' have been cut, indeed we take the residues with respect to their poles, and such propagators disappear in the final result. The remaining particles C and C' are evaluated close to their on-shell values making the diagram singular.

Making use of (B.3.1) it is not difficult to check that each combination of derivatives in the denominators of (7.2.25) can be written in a simpler form and the result for the singular diagram is given by

$$I_{\square} = \frac{1}{(s-s_0)^2}\frac{i}{8}\left[\frac{1}{\Delta_{BB'}}\frac{1}{\frac{dC^2}{ds}\Big|_{B,B'}}\frac{1}{\frac{dC'^2}{ds}\Big|_{B,B'}}+\frac{1}{\Delta_{C'B}}\frac{1}{\frac{dC^2}{ds}\Big|_{C',B}}\frac{1}{\frac{dB'^2}{ds}\Big|_{C',B}}\right].$$

In the first term the particles B and B' are on-shell and the derivatives are performed at fixed values $p_a^2 = m_a^2$, $p_b^2 = m_b^2$, $B^2 = m_B^2$, $B'^2 = m_{B'}^2$. In the second term the

vectors having fixed lengths are instead p_a, p_b, C' and B. Multiplying by the usual vertex and flux factors (7.2.11) and writing the pole in terms of the rapidity difference as in (7.2.12) we obtain

$$D_{\square} = \frac{1}{(\theta-\theta_0)^2}\frac{1}{4^5} f_{Ba\bar{C}} f_{Cb\bar{B}'} f_{B'\bar{a}\bar{C}'} f_{C'\bar{b}\bar{B}} \left[\frac{\Delta_{B'C}}{\Delta_{ab}} + \frac{\Delta_{B'B}}{\Delta_{ab}}\right]. \tag{7.2.26}$$

To verify that the two results in (7.2.26) and (7.2.23) are the same we just write the triangle areas in terms of vector products and note that

$$\big\langle CB'\big\rangle + \big\langle B'B\big\rangle = \big\langle (C-B)B'\big\rangle = \big\langle p_a B'\big\rangle.$$

The box integral near to the Landau pole can be written both as a single term, $D(B,C)$, given by cutting the internal propagators B, C and multiplying by the Jacobian factor $\frac{1}{8i\Delta_{BC}}$, or as a sum over two terms. Each one of these two terms, $D(B,B')$ and $D(B,C')$, corresponds to a particular cut. A pictorial representation of the two different ways of writing the singularity is shown in figure 7.5.

In summary, we have seen that the anomalous threshold singularity of the box integral can be written as different sums over residues. To each residue a Feynman diagram decomposition is associated, in which propagators having poles in the integration contour disappear, i.e. they are cut. In this manner, the diagram behaves as a tree-level graph with more external on-shell particles. The different ways in which the loop can be broken into sums of these atoms (we refer sometimes to the full diagram as a molecule, and to its residue decompositions as atoms) are dictated by the on-shell description of the diagram. In the case considered the choice of B and C to define the integration variables is a bit special. The triangle defined by these two vectors is the 'thinnest' among the triangles reported on the RHS of figure 7.3 and all the other momenta (B' and C') are linear combinations of B and C having negative coefficients. The complete result is therefore obtained by cutting B and C. We report below some of the different sums over cuts through which the box integral can be written

$$D_{\square} = D(B,C) = D(B,B') + D(B,C') = D(B',C) + D(C',C). \tag{7.2.27}$$

The first equality in the expression above is given by closing both the u and v contours in (7.2.20) in the lower half-plane. In this way, we obtain a single term generated by cutting the propagators associated with momenta B and C, i.e. the special vectors with respect to which all the other momenta are negative linear combinations. The second equality in (7.2.27) corresponds to closing the u-contour in (7.2.20) in the lower half-plane (there is a single pole in the integration path due to the B-propagator) and the v-contour in the upper half-plane. Since now there are two poles in the integration v-contour we have a sum over two different cuts, associated with B' and C'. On the other hand on the RHS of the third equality in (7.2.27) we have performed before the integration over v, closing the integration path in the lower half complex plane. The v-contour encloses a single pole of the propagator associated with the particle C, and therefore we obtain a single residue corresponding to the cut of the C-propagator. Then closing the u-contour in the

upper half-plane we obtain a sum over two residues, one corresponding to cutting the B'-propagator and the other corresponding to cutting the C'-propagator.

In the following sections, we will study networks of Feynman diagrams contributing to some higher-order singularities. In this context, it is important to understand how to decompose each diagram of the network in a clever way, so as to make manifest the simplifications. We will show how special decompositions of diagrams connected by flipping internal propagators sum to zero and the total result is given by only a few surviving cuts. We proceed to study this phenomenon for 2^{nd}-order poles and then we move to 3^{rd}-order poles.

7.3 Second-order poles

Second-order poles in the bootstrapped S-matrix appear when two building blocks, both of multiplicity equal to one, touch each other and a product of the form $\{x-1\}\{x+1\}$ is present. These are even order singularities with $N=1$ and $\nu=0$, for which the formula (7.1.4) becomes

$$S_{ab}(\theta) \sim 1 + \left(\frac{g^2}{2h}\right)^2 \frac{1}{(\theta - i\theta_0)^2}. \tag{7.3.1}$$

The singular part of the S-matrix can be explained in terms of threshold singularities and was computed for the first time using perturbation theory in a paper by Braden, Corrigan, Dorey and Sasaki [69]. What is not clear from that paper is the reason why Feynman diagrams connected by flipping internal propagators, that normally cancel at the tree level in 4-point non-diagonal processes, do not sum to zero at loop level. In this section we show that this fact is related to how the loop diagrams are cut and we write explicitly the surviving cuts contributing to the final result.

There are in total four Feynman diagrams contributing to the pole connected by flips of type II, according to the convention discussed in section 4.1. The full network of Feynman diagrams, together with their on-shell dual description, is reproduced in figure 7.6. The external shape of each on-shell diagram entering the network is always the same, representing the external particles; it is a parallelogram having as sides the masses of the asymptotic incoming and outgoing states. Internally the parallelogram is filled with triangles, representing 3-point vertices, having as sides the masses of the propagators. An internal empty gap is necessary for the diagrams number (2) and (4) on the RHS of figure 7.6 to represent propagators that cross each other. Starting from any diagram of the network we can generate all the others by flipping internal propagators. For example, to pass from diagram (1) to diagram (2) in figure 7.6 we apply a flip on the RHS part of diagram (1): the positions of the vectors B and B' are exchanged and C' is flipped into C. As explained in section 4.1 this is a flip of type II and does not change the product of the 3-point couplings entering the diagram. The same type of flip connects also the remaining diagrams of the network to one another. After each flip, the product of the 3-point coupling

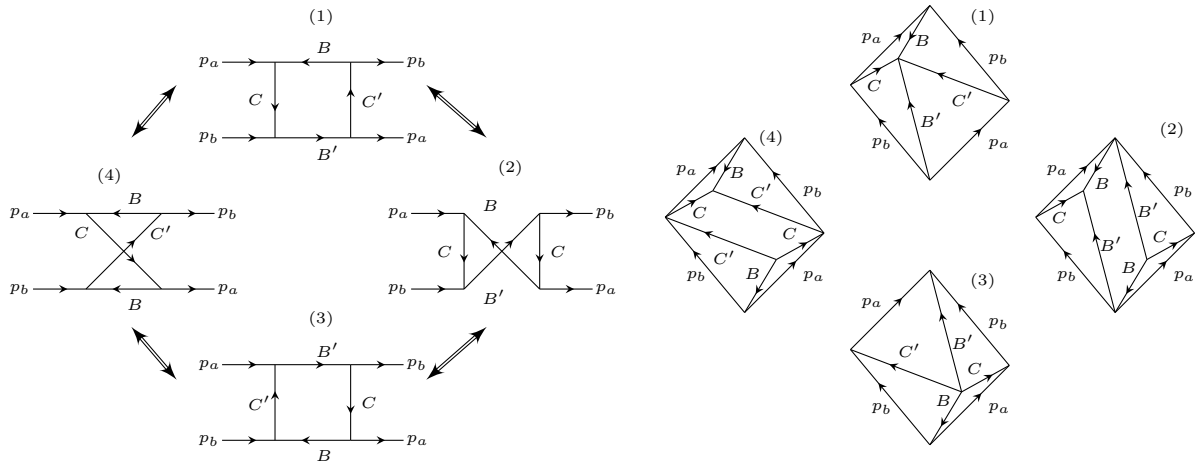

Figure 7.6: Network of Feynman diagrams (on the left) and their on-shell description (on the right) contributing to a second-order pole.

does not change sign and we have

$$f_{Ba\bar{C}}f_{Cb\bar{B}'}f_{B'\bar{a}\bar{C}'}f_{C'\bar{b}\bar{B}} \underbrace{=}_{(1)\to(2)} |f_{Ba\bar{C}}|^2|f_{Cb\bar{B}'}|^2 \underbrace{=}_{(2)\to(3)} f_{Bb\bar{C}'}f_{C'a\bar{B}'}f_{B'\bar{b}\bar{C}}f_{C\bar{a}\bar{B}}$$
$$\underbrace{=}_{(3)\to(4)} |f_{Ba\bar{C}}|^2|f_{Bb\bar{C}'}|^2 = \left(\frac{4g}{\sqrt{h}}\right)^4.$$

Since diagrams (2) and (4) contain products of 3-point couplings that are necessarily positive, being the absolute values squared of certain numbers, the product of the f-functions has positive sign and it is given by $\left(\frac{4g}{\sqrt{h}}\right)^4$. Using this fact combined with (7.2.26) the first diagram of the network in 7.6 can be written as

$$D^{(1)} = \frac{1}{(\theta-\theta_0)^2}\left(\frac{g^2}{2h}\right)^2\left[\frac{\Delta_{B'C}}{\Delta_{ab}} + \frac{\Delta_{B'B}}{\Delta_{ab}}\right], \tag{7.3.2}$$

where, as already explained in the previous section, the two pieces in the sum (7.3.2) represent two different cuts of the box.

The values associated with the other diagrams are straightforwardly obtained in the same way. Diagram number (3) is similar to diagram number (1); in this case we write its numerical value summing the cuts $D^{(4)}(C,B')$ and $D^{(4)}(C,C')$. It is given by

$$D^{(4)} = \frac{1}{(\theta-\theta_0)^2}\left(\frac{g^2}{2h}\right)^2\left[\frac{\Delta_{C'B}}{\Delta_{ab}} + \frac{\Delta_{C'C}}{\Delta_{ab}}\right].$$

The remaining diagrams (2) and (4) are also simple; their integrals are

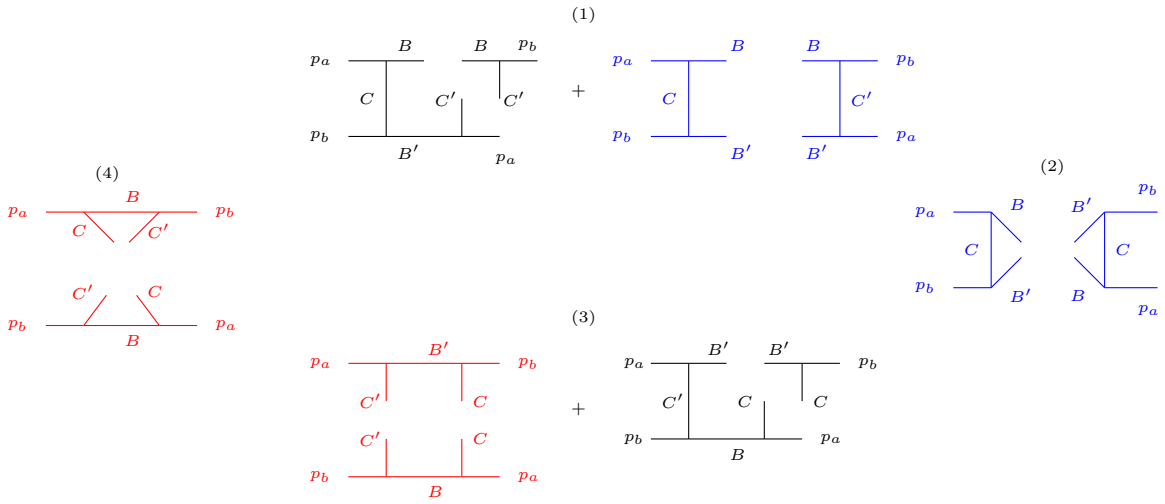

Figure 7.7: Feynman diagrams decomposition into sums of products of tree-level graphs.

$$I^{(2)} = \frac{1}{(s-s_0)^2}\frac{1}{(2\pi)^2 8i\Delta_{BB'}}\int dudv \underbrace{\frac{1}{u+i\epsilon}}_{B}\underbrace{\frac{1}{v+i\epsilon}}_{B'}\underbrace{\frac{1}{\left(\frac{dC^2}{ds}\Big|_{B,B'} - \frac{\Delta_{CB'}}{\Delta_{BB'}}u - \frac{\Delta_{CB}}{\Delta_{BB'}}v + i\epsilon\right)^2}}_{C},$$

$$I^{(4)} = \frac{1}{(s-s_0)^2}\frac{1}{(2\pi)^2 8i\Delta_{CC'}}\int dudv \underbrace{\frac{1}{u+i\epsilon}}_{C}\underbrace{\frac{1}{v+i\epsilon}}_{C'}\underbrace{\frac{1}{\left(\frac{dB^2}{ds}\Big|_{C,C'} - \frac{\Delta_{BC'}}{\Delta_{CC'}}u - \frac{\Delta_{BC}}{\Delta_{CC'}}v + i\epsilon\right)^2}}_{B}.$$

Each one of the two results is given by a single cut, which is $D^{(2)}(B,B')$ in the case of diagram number (2) and $D^{(4)}(C,C')$ in the case of diagram number (4):

$$D^{(2)} = \frac{1}{(\theta-\theta_0)^2}\left(\frac{g^2}{2h}\right)^2\left(\frac{-\Delta_{BB'}}{\Delta_{ab}}\right),$$
$$D^{(4)} = \frac{1}{(\theta-\theta_0)^2}\left(\frac{g^2}{2h}\right)^2\left(\frac{-\Delta_{CC'}}{\Delta_{ab}}\right).$$

The full network of diagrams and its on-shell description, both cut into tree-level graphs, are depicted in figures 7.7 and 7.8 respectively. In figure 7.8 we plot with the same colour loop decompositions that differ by a single 4-point non-elastic tree-level diagram in which one propagator is flipped. For example, looking at the blue cuts, we see that on RHS there are two tree-level diagrams in which a particle propagating in the t-channel and a particle propagating in the u-channel are simultaneously on-shell. These tree-level graphs cancel in the sum to forbid poles in non-elastic scattering at the tree level. The effect is that only two among the six different cuts in figure 7.8

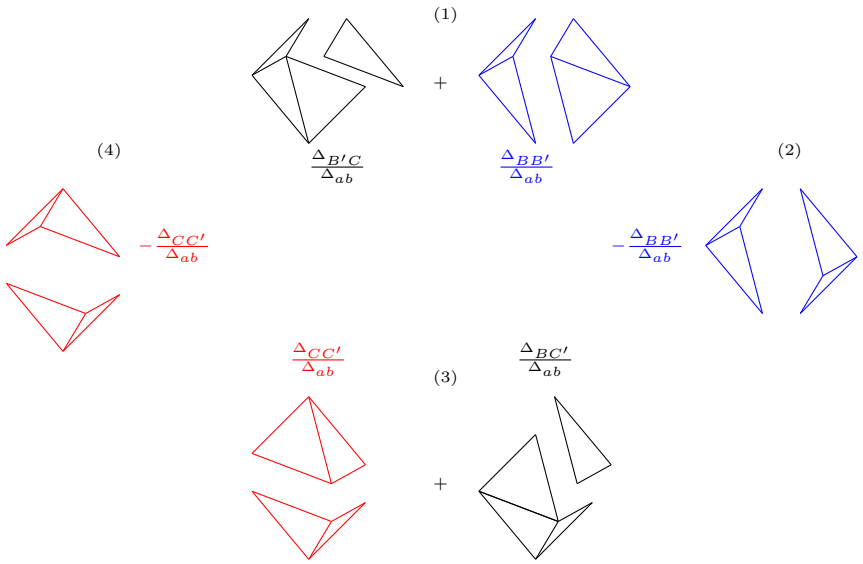

Figure 7.8: On-shell decomposition of diagrams into the product of tree-level graphs. The numerical values of the diagrams are reported omitting an overall factor $\frac{1}{(\theta-\theta_0)^2}\left(\frac{g^2}{2h}\right)^2$.

contribute to the final result; they are the two black atoms having values

$$D^{(1)}(B,C') = \frac{1}{(\theta-\theta_0)^2}\left(\frac{g^2}{2h}\right)^2 \frac{\Delta_{B'C}}{\Delta_{ab}} \quad \text{and} \quad D^{(3)}(B',C) = \frac{1}{(\theta-\theta_0)^2}\left(\frac{g^2}{2h}\right)^2 \frac{\Delta_{BC'}}{\Delta_{ab}}. \tag{7.3.3}$$

A general property is that given a point inside a parallelogram the sum of the areas of the two triangles on the opposite sides of the point is equal to half the area of the parallelogram. In our case we have $\Delta_{B'C} + \Delta_{BC'} = \Delta_{BC} + \Delta_{B'C'} = \Delta_{ab}$. Therefore summing the surviving contributions in (7.3.3) we obtain

$$D^{(1)}(B,C') + D^{(3)}(B',C) = \frac{1}{(\theta-\theta_0)^2}\left(\frac{g^2}{2h}\right)^2, \tag{7.3.4}$$

that exactly matches the leading order part of the second order singularity in the bootstrapped S-matrix.

This result has been achieved noting that some atoms in the network differ from each other by the presence of a pair of 4-point tree-level non-elastic diagrams connected by flipping an internal propagator. Such atoms simplify in the final sum so that only two cuts among the four initial diagrams are relevant and contain the information necessary to obtain the S-matrix at the pole position. The problem of evaluating all the Feynman diagrams at their threshold singularity reduces therefore to a decomposition problem, in which the only relevant thing is to understand how the loop needs to be cut. Then, without evaluating every single cut, we know what are the cuts cancelling in the sum and we reproduce the final result by evaluating only the surviving terms.

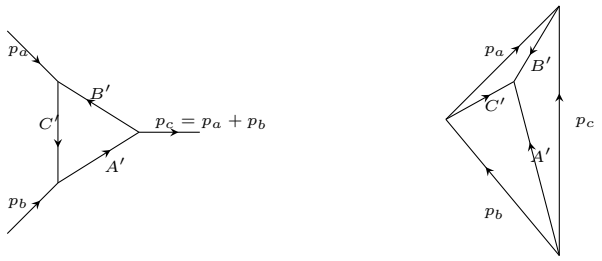

Figure 7.9: Triangle diagram (on the left) and its on-shell representation (on the right).

7.4 Third-order poles

We now focus on the origin of third-order poles, restricting our analysis to the forward channel since poles in the crossed channel can be obtained by sending $\theta \to i\pi - \theta$ through crossing symmetry. A general S-matrix, presenting two building blocks of the following structure $\{x-1\}^2\{x+1\}$, will be considered. The Laurent expansion of the bootstrapped S-matrix around the pole $\theta = i\theta_0 = i\frac{\pi x}{h}$ has a leading order expansion in g given by

$$S_{ab}(\theta) \sim 1 + i\Big(\frac{g^2}{2h}\Big)\frac{1}{(\theta - i\theta_0)} + \Big(\frac{g^2}{2h}\Big)^2\frac{1}{(\theta - i\theta_0)^2} + i\Big(\frac{g^2}{2h}\Big)^3\frac{1}{(\theta - i\theta_0)^3}, \qquad (7.4.1)$$

where the relation above is obtained by substituting $N = 1$ and $\nu = i$ in (7.1.4). It would be interesting to understand how the different terms in (7.4.1) are generated in perturbation theory. The identity is of course the non-interacting part of the S-matrix while the contribution $i\big(\frac{g^2}{2h}\big)\frac{1}{(\theta - i\theta_0)}$ comes from a tree-level diagram in which an intermediate bound state is propagating. Since a detailed study of tree-level scattering has already been performed in the previous chapter, we focus here only on the last two contributions in (7.4.1), having poles of order two and three respectively.

7.4.1 Vertex corrections contributing to third-order singularities

Before moving into the study of the S-matrix we focus on possible singular vertex corrections. Such corrections are due to diagrams of the form shown in figure 7.9, when along the loop integration there exists a point in which all the internal propagators are on-shell. We focus first on the problem of determining the sign of the product of the 3-point couplings appearing in the diagram.

Consider the forbidden process $a + b \to A + \bar{B}$, with different incoming and outgoing states. The event is well reproduced on the RHS of figure 7.9, where p_c and C' correspond to a copy of particles propagating respectively in the forward and crossed channels. Since the two channels are connected by a flip of type III, according to the conventions used in section 4.1, the product of the couplings entering the two

different channels changes sign after the flip. We have

$$f_{B'a\bar{C}'}f_{C'b\bar{A}'} = -f_{ab\bar{c}}f_{\bar{A}'cB'}.$$

Multiplying both the right and the left hand sides of the expression above by $f_{A'\bar{c}\bar{B}'} = f^*_{\bar{A}'cB'}$ we obtain

$$f_{B'a\bar{C}'}f_{C'b\bar{A}'}f_{A'\bar{c}\bar{B}'} = -\left(\frac{4g}{\sqrt{h}}\right)^2 f_{ab\bar{c}}. \tag{7.4.2}$$

This is a universal formula connecting the product of the f-functions entering the tiling of a 3-point coupling $C^{(3)}_{abc}$ to the f-function f_{abc} of the coupling.

The pole residue at $(p^{(0)}_a + p^{(0)}_b)^2 = m^2_c \equiv s_0$ can be derived by parametrising the internal loop momenta in the following way

$$\begin{aligned}
&(A'+l)^2 - m^2_{A'} + i\epsilon = 2A'\cdot l + l^2 + i\epsilon \\
&(B'+l)^2 - m^2_{B'} + i\epsilon = 2B'\cdot l + l^2 + i\epsilon \\
&(C'+l)^2 - m^2_{C'} + i\epsilon = \frac{dC'^2}{ds}\Big|_{A',B'}(s-s_0) + 2C'\cdot l + l^2 + i\epsilon
\end{aligned} \tag{7.4.3}$$

where we have chosen A' and B' to be the on-shell vectors around which to expand the integral. Using the relation in (7.2.10) we obtain

$$I_{\triangle'} = \frac{1}{s-s_0}\int \frac{d^2\tilde{l}}{(2\pi)^2}\frac{1}{2\tilde{l}\cdot A' + i\epsilon}\,\frac{1}{2\tilde{l}\cdot B' + i\epsilon}\,\frac{1}{\frac{dC'^2}{ds}\Big|_{A',B'} + 2C'\cdot\tilde{l} + i\epsilon}\,. \tag{7.4.4}$$

We adopt the usual choice of integration variables

$$u = 2\tilde{l}\cdot A' \quad , \quad v = 2\tilde{l}\cdot B'. \tag{7.4.5}$$

The relation in (7.2.14) allows to express C' as a linear combination of A' and B' leading to the following expression for the integral

$$I_{\triangle'} = \frac{1}{s-s_0}\frac{1}{(2\pi)^2 8i\Delta_{A'B'}}\int dudv \frac{1}{u+i\epsilon}\,\frac{1}{v+i\epsilon}\,\frac{1}{\frac{dC'^2}{ds}\Big|_{A',B'} - \frac{\Delta_{C'B'}}{\Delta_{A'B'}}u - \frac{\Delta_{C'A'}}{\Delta_{A'B'}}v + i\epsilon}. \tag{7.4.6}$$

As in the box case, the integral can be easily computed by closing both the u and the v contours in the lower half-plane. Using Cauchy's residue theorem the result is

$$I_{\triangle'} = \frac{i}{8\Delta_{A'B'}}\frac{1}{\frac{dC'^2}{ds}\Big|_{A',B'}}\frac{1}{s-s_0} = \frac{i}{8}\frac{\Delta_{ab}}{\Delta_{B'C'}\Delta_{A'C'}}\frac{1}{s-s_0}. \tag{7.4.7}$$

The last equality has been obtained by performing the derivative of C'^2 with respect to s keeping the lengths of A' and B' fixed at their mass-shell values.

After having inserted the extra vertex and propagator factors (first two lines in

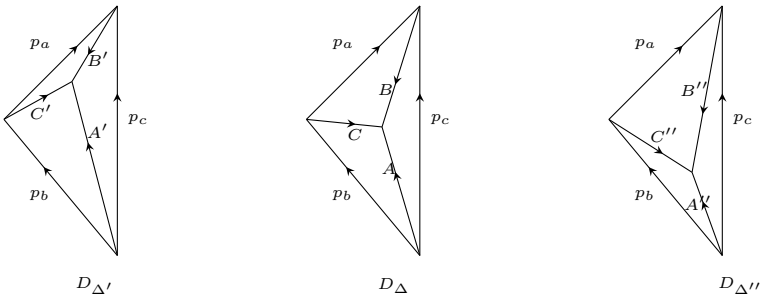

Figure 7.10: Three types of vertex corrections contributing to a third-order pole.

(7.2.11)) we obtain that the final value of the Feynman diagram is

$$D_{\triangle'} = \frac{i}{8}\frac{\Delta_{ab}\Delta_{A'B'}}{s-s_0} f_{A'\bar{c}\bar{B}'} f_{B'a\bar{C}'} f_{C'b\bar{A}'} = -\frac{g^2}{2h} f_{ab\bar{c}} \frac{\Delta_{A'B'}}{\theta - i\theta_0} \tag{7.4.8}$$

where in the second equality above we used (7.4.2) and we expressed $s - s_0$ in terms of θ.

In all the cases analysed exactly three vertex corrections are found. This is a fact noted in [69] that still requires an explanation in terms of root system properties. The three different vertex corrections are reported in figure 7.10 following an increasing order with respect to the angle formed between p_a and the internal propagators C', C and C''. It has been observed that their constituents always satisfy the following universal relations

$$\begin{aligned} \Delta_{B'C'} + \Delta_{BC} + \Delta_{B''C''} &= \Delta_{ab} \\ \Delta_{A'C'} + \Delta_{AC} + \Delta_{A''C''} &= \Delta_{ab} \\ \Delta_{A'B'} + \Delta_{AB} + \Delta_{A''B''} &= \Delta_{ab}. \end{aligned} \tag{7.4.9}$$

It is still unexplained how these identities are satisfied, though it is reasonable to believe that they follow from universal properties of the Coxeter geometry associated with root systems. Summing the three vertex corrections and combining (7.4.8) with the third line in (7.4.9) we obtain the universal formula for the leading order singularity of the vertex contributing to a third-order pole in the S-matrix. It is given by

$$D_{\triangle'} + D_{\triangle} + D_{\triangle''} = -\frac{g^2}{2h}\frac{f_{ab\bar{c}}\Delta_{ab}}{\theta - i\theta_0} = -\frac{g^2}{2h}\frac{C_{ab\bar{c}}}{\theta - i\theta_0}. \tag{7.4.10}$$

7.4.2 One-loop contributions

We show how to use the vertex correction (7.4.10) to compute the leading order expansion of the S-matrix around the pole position. We compute one loop contributions first, which are responsible for the coefficient of order $(\theta - i\theta_0)^{-2}$ in the Laurent expansion around the third-order pole in (7.4.1). To each vertex correction $D_{\triangle'}$, $D_{\triangle}$ and $D_{\triangle''}$ three singular Feynman diagrams are associated, connected by flipping

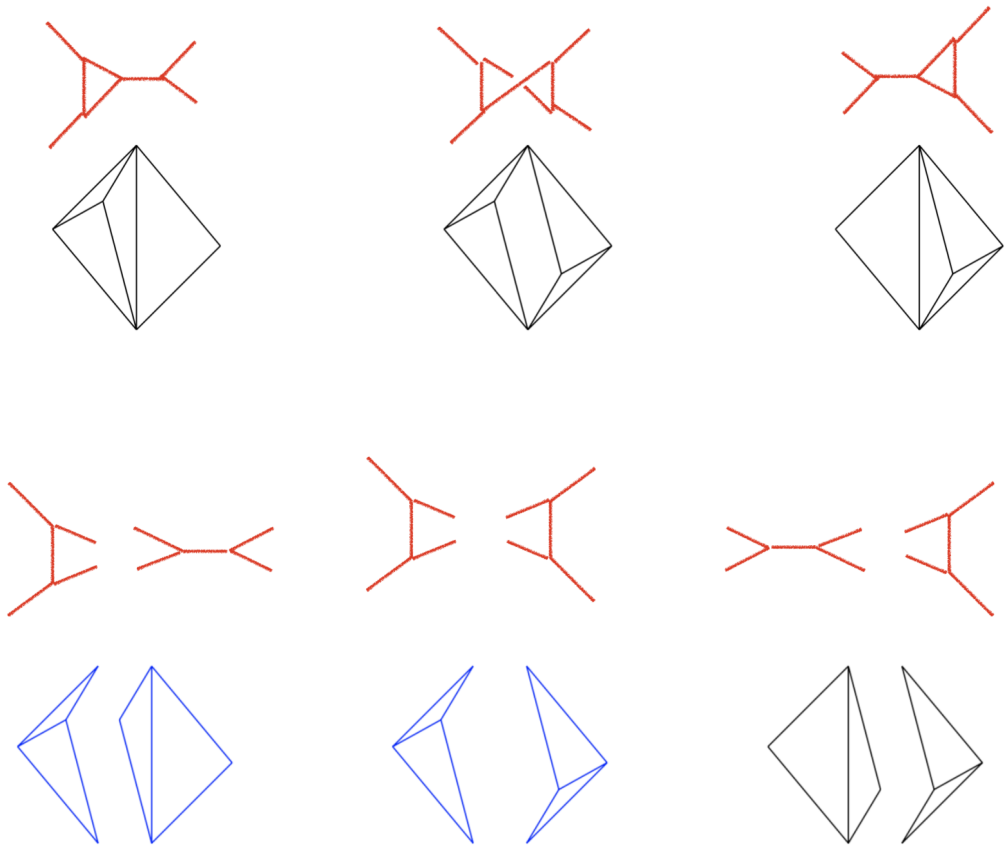

Figure 7.11: Part of the one loop network of Feynman diagrams contributing to the coefficient a_2 (according to the notation in (7.1.2)) of the Laurent expansion around a third-order pole. In the second line cut diagrams are shown. Diagrams of the same colour cancel in the sum since they differ by a pair of flipped 4-point tree-level graphs.

internal propagators. We show in figure 7.11 the three diagrams associated with the vertex correction $D_{\triangle'}$. We start by considering a one-particle reducible Feynman diagram having on the LHS a vertex correction of type $D_{\triangle'}$ and in which a bound state is propagating on its on-shell value. Both $D_{\triangle'}$ and the propagating bound state carries a pole of order one so that their product generates an order two singularity, matching the order $\frac{1}{(\theta-\theta_0)^2}$ we intend to analyse. Among the three different diagrams, two cancel in the sum (the blue ones in figure 7.11). Indeed when we compute the loop integral they split into tree-level graphs two of which differ by flipping one internal propagator. The sum of the three graphs in figure 7.11 is therefore simply given by a single one-particle reducible graph presenting in order a 3-point vertex $(-iC_{ab\bar{c}})$, an on-shell bound state propagator $\frac{i}{s-s_0}$ and the one loop vertex correction $D_{\triangle'}$. Since we need to repeat the same analysis for Feynman diagrams obtained by

flipping one-particle reducible graphs containing $D_{\triangle}$ and $D_{\triangle''}$ the final result for the second-order coefficient of the Laurent expansion is proportional to

$$(-iC_{ab\bar{c}})\frac{i}{s-s_0}(D_{\triangle'}+D_{\triangle}+D_{\triangle''}).$$

By adding the flux factor as written in the third line of (7.2.11), using (7.4.10) and expressing the pole in terms of the rapidity difference we obtain

$$\frac{1}{32\Delta_{ab}^2}\frac{g^2}{2h}\frac{|C_{ab\bar{c}}|^2}{(\theta-i\theta_0)^2}=\left(\frac{g^2}{2h}\right)^2\frac{1}{(\theta-i\theta_0)^2}. \tag{7.4.11}$$

This expression exactly matches the order $(\theta-i\theta_0)^{-2}$ of the S-matrix expansion around the third-order pole obtained using the bootstrap.

7.4.3 Two-loop contributions

The maximal singular leading order term of the S-matrix on the pole position comes from a two-loop computation. The complete network of Feynman diagrams, together with their values, contributing to such a result was found for the first time in [69]. However, in that paper, the authors limited themselves to giving the final answer, and did not explain the simplification structure underlying the network. In this section we show how the result comes entirely by summing proper cuts located at the boundary of the network while the bulk part simplifies. Using the flipping move discussed in section 4.1 we also explain how to obtain the correct sign of each Feynman diagram.

The network of singular diagrams is well represented in the PhD thesis of Patrick Dorey [104], from which figure 7.12 is extracted and has a disk topology. Indeed, after six vertical steps along the first column, the diagrams repeat periodically. The diagrams in the first two columns, together with the three isolated graphs $D^{(-2)}$, $D^{(-1)}$ and $D^{(0)}$, are planar. The diagrams $D^{(13)},\dots,D^{(23)}$ in the centre of the disk are instead non-planar and gaps are added in their tilings to represent propagators that cross. Moreover, graphs in the network connected by a line are related by a flip. Always following the convention of section 4.1, the first and the second column are connected by a flip of type I, while in all the other situations (both moving from the second to the third column, from the third to the fourth column and from the fourth column to the central diagram $D^{(23)}$) the flip entering in play is of type II.

Among the different graphs, the one-particle reducible ones are particularly simple to be computed. These diagrams are obtained by glueing vertex corrections on the opposite sides of an on-shell bound state propagator. They are reported in the first column (containing diagrams $D^{(1)}\dots D^{(6)}$) and in the isolated part of the network, comprising $D^{(-2)}$, $D^{(-1)}$ and $D^{(0)}$. In total there are 9 one-particle reducible diagrams of this type, 3×3 since there are three types of vertex corrections, as shown in figure

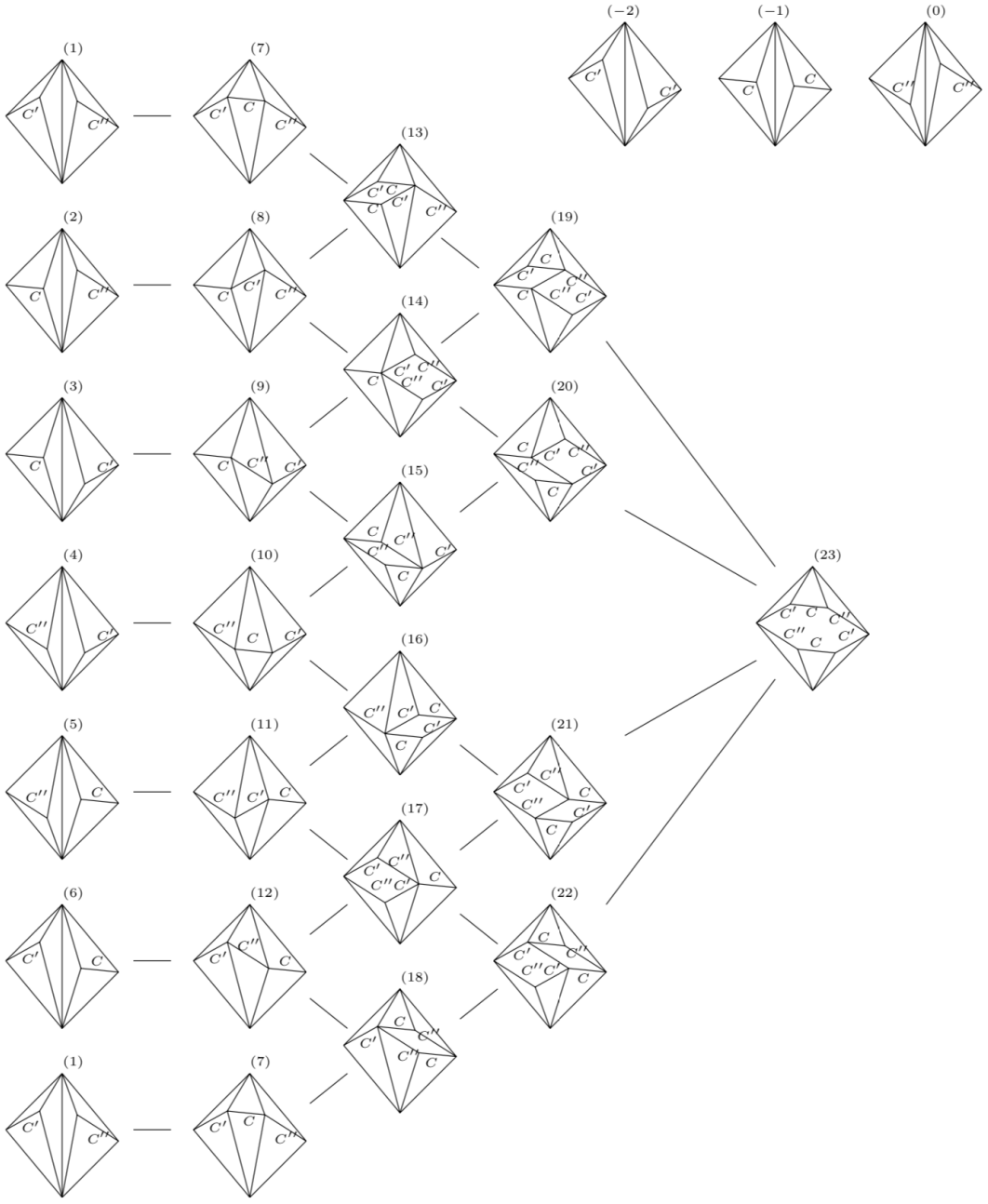

Figure 7.12: Network of Feynman diagrams (copied from [104]) contributing to the a_3 coefficient (see (7.1.2)) of a 3^{rd}-order pole.

7.10. Summing over all the one-particle reducible two-loop diagrams we obtain

$$\begin{aligned} S_{ab}^{(1pr)}(\theta) &= \frac{1}{8i\Delta_{ab}}(D_{\triangle'}+D_{\triangle}+D_{\triangle''})\frac{i}{s-s_0}(D_{\triangle'}+D_{\triangle}+D_{\triangle''}) \\ &= -i\Big(\frac{g^2}{2h}\Big)^3\frac{1}{(\theta-i\theta_0)^3}, \end{aligned} \tag{7.4.12}$$

where in the last equality we used relations (7.2.12), (7.4.10) together with the area rule (7.1.5). The result in (7.4.12) is universal, valid whatever simply-laced Toda model we are considering. However, as remarked in [69], it carries a minus sign compared to the result expected from the expansion of the bootstrapped S-matrix (7.4.1). We will show now how the remaining diagrams $D^{(7)}$, $D^{(8)}$, ..., $D^{(23)}$ conspire to reproduce exactly $2\times i\Big(\frac{g^2}{2h}\Big)^3\frac{1}{(\theta-i\theta_0)^3}$ in such a way that summing this new term to (7.4.12) we obtain exactly the expected coefficient present in (7.4.1) in front of $\frac{1}{(\theta-i\theta_0)^3}$.

The contributions necessary to restore the bootstrapped result come from cuts of the double-box diagrams $D^{(7)}, D^{(8)}, \ldots, D^{(12)}$. We explain what cuts we need first; then we show why these cuts are the correct ones. For all these diagrams we can decide to remove respectively the top left and the top right vertices or the bottom left and the bottom right vertices. The important thing is that once we choose what vertices to remove, those that sit at the top or the bottom of the graph, we need to maintain the same choice for all the diagrams in the second column of the network 7.12.

We decide to locate the cuts at the top of the diagrams, as it is shown in figure 7.13 where the graph $D^{(8)}$ is considered. The cut is associated with a particular residue that is picked up when we compute the integral. The result is given by

$$\begin{aligned} I^{(8)} &\rightsquigarrow \frac{i}{8\Delta_{BC}}\frac{i}{8\Delta_{A''C''}}\frac{1}{\frac{dA^2}{ds}}\frac{1}{\frac{dB''^2}{ds}}\frac{1}{\frac{dC'^2}{ds}}\frac{1}{(s-s_0)^3} \\ &= \frac{i}{8\Delta_{BC}}\frac{i}{8\Delta_{A''C''}}\frac{\Delta_{ab}}{\Delta_{AC}}\frac{\Delta_{ab}}{\Delta_{B''C''}}\Big(\frac{-\Delta_{ab}}{\Delta_{BA''}}\Big)\frac{1}{(s-s_0)^3}. \end{aligned} \tag{7.4.13}$$

The two factors $\frac{i}{8\Delta_{BC}}$ and $\frac{i}{8\Delta_{A''C''}}$ are the Jacobian determinants (multiplied by imaginary units coming from the Cauchy's theorem) of the choice of variables adopted to perform the integration. The integration variables are $2B\cdot l = u_l$, $2C\cdot l = v_l$ for the box on the LHS part of the diagram and $2A''\cdot k = u_k$, $2C''\cdot k = v_k$ for the box on the RHS. Then there are the propagators that have not been cut; close to the pole they are given by $\frac{1}{A^2-m_A^2} = \frac{1}{\frac{dA^2}{ds}(s-s_0)}$, $\frac{1}{B''^2-m_{B''}^2} = \frac{1}{\frac{dB''^2}{ds}(s-s_0)}$, $\frac{1}{C'^2-m_{C'}^2} = \frac{1}{\frac{dC'^2}{ds}(s-s_0)}$. The derivatives in the denominators are performed in the last equality of (7.4.13) keeping fixed the lengths of the momenta associated with the cut propagators. At this point we still need to multiply the expression in (7.4.13) by the remaining quantities in (7.2.11), and write the pole in terms of the rapidity. To this end we compute the product of the f-functions entering the 3-point vertices of the diagrams $D^{(7)}, \ldots, D^{(12)}$.

The flip used to pass from the double-vertex graphs $(D^{(1)}, \ldots, D^{(6)})$ in the first column to the double-box diagrams in the second column $(D^{(7)}, \ldots, D^{(12)})$ of figure

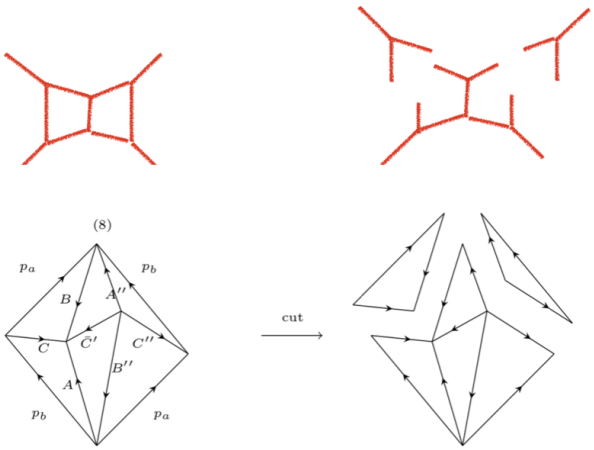

Figure 7.13: Example of a cut contributing to the final result.

7.12 is of type I and does not change the sign of the product of the 3-point couplings. Therefore, if we use relation (7.4.2), the product of the f-functions entering the different graphs in the second column of the network is always given by

$$\left[-\left(\frac{4g}{\sqrt{h}}\right)^2 f_{ab\bar{c}}\right]\left[-\left(\frac{4g}{\sqrt{h}}\right)^2 f_{\bar{a}\bar{b}c}\right] = \left(\frac{4g}{\sqrt{h}}\right)^6. \tag{7.4.14}$$

Using this fact and multiplying the expression (7.4.13) by the remaining terms in (7.2.11) the cut of the diagram $D^{(8)}$ can be written in terms of the rapidity difference as

$$D^{(8)} \rightsquigarrow i\left(\frac{g}{\sqrt{2h}}\right)^6 \frac{\Delta_{AB''}}{\Delta_{ab}} \frac{1}{(\theta - i\theta_0)^3}. \tag{7.4.15}$$

The result for the cut is proportional to the area $\Delta_{AB''}$ of the triangle in the central bottom part of the graph. At this point, we note that $D^{(8)}$ admits a related diagram, $D^{(11)}$, which is exactly $D^{(8)}$ rotated by an angle π. If we decide to cut such a diagram in the same way, i.e. we remove the top left and the top right vertices, the associated cut is given by

$$D^{(11)} \rightsquigarrow i\left(\frac{g}{\sqrt{2h}}\right)^6 \frac{\Delta_{BA''}}{\Delta_{ab}} \frac{1}{(\theta - i\theta_0)^3}.$$

Noting that $\Delta_{AB''} + \Delta_{BA''} = \Delta_{AB} + \Delta_{A''B''}$ the sum of these two cuts is

$$i\left(\frac{g}{\sqrt{2h}}\right)^6 \frac{1}{\Delta_{ab}} \frac{1}{(\theta - i\theta_0)^3} (\Delta_{AB} + \Delta_{A''B''}).$$

The same analysis can be repeated for the copy of diagrams $D^{(7)}$ and $D^{(10)}$, which again are related by a rotation of a π angle. In this situation, we obtain that the sum is proportional to $\Delta_{A'B'} + \Delta_{A''B''}$. Finally summing the results obtained by cutting the 3-point vertices on the top of diagrams $D^{(9)}$ and $D^{(12)}$ generates $\Delta_{AB} + \Delta_{A'B'}$.

The sum of the 6 cuts of the diagrams in the second column is therefore given by

$$\begin{aligned}\sum_{n=7}^{12} D^{(n)} \rightsquigarrow & i\Big(\frac{g}{\sqrt{2h}}\Big)^6 \frac{1}{\Delta_{ab}} \frac{1}{(\theta - i\theta_0)^3} 2(\Delta_{AB} + \Delta_{A'B'} + \Delta_{A''B''}) \\ = & 2i\Big(\frac{g}{\sqrt{2h}}\Big)^6 \frac{1}{(\theta - i\theta_0)^3} \ ,\end{aligned} \tag{7.4.16}$$

where in the last equality the third identity in (7.4.9) has been used. This result summed to (7.4.12) generates the expected answer predicted by the bootstrapped S-matrix.

The relations we obtained, both the formula in (7.4.12) and the contribution in (7.4.16) are universal; they do not depend on the particular simply-laced Toda theory we are considering and their sum returns the correct bootstrapped result. Two questions arise at this point. First of all, we did not explain why the cuts that we considered for the double-box integrals should reproduce exactly the right answer. Secondly, we still need to explain why we are not considering the non-planar graphs present in the centre of the network. In the remaining part of this section, we answer these questions.

Let us consider the computation of the graph $D^{(8)}$ in more detail. Looking at figure 7.13 we see that such a Feynman diagram is composed of two boxes, one on the RHS comprising the momenta $\bar{C}'$, B'', C'' and A'', the other one on the LHS comprising the momenta C, A, $\bar{C}'$ and B. In the on-shell diagram in figure 7.13 we have reversed the direction of the C'-vector compared to the vertex correction in figure 7.10 to make the loop integration more smooth; this is consistent if at the same time we change the particle label C' with its antiparticle $\bar{C}'$ as we did in 7.13. Each momentum carries then a loop integration variable, say l for the momenta flowing in the LHS box and k for the momenta flowing in the RHS one, with $\bar{C}'$ containing both l and k since it belongs to both the boxes. If all the LHS momenta are translated by l with propagators $\frac{1}{(C+l)^2-m_C^2+i\epsilon}$, $\frac{1}{(A+l)^2-m_A^2+i\epsilon}$, $\frac{1}{(B+l)^2-m_B^2+i\epsilon}$ and similarly the RHS propagators are translated by k, then $\bar{C}'$ is translated by the quantity $l+k$. The double-box integral can then be performed by computing one at a time the single-box integrals, before the one on the RHS and then the one on the LHS of the graph. If we integrate first the loop variable k we note that both B'' and $\bar{C}'$ can be written as negative linear combinations of A'' and C'', therefore the box on the RHS can be broken cutting the propagators associated with the particles A'' and C'': the integration generates a single residue as explained in the previous section. Similarly, on the LHS box, we see that the two vectors with respect to which all the others are negative linear combinations are A and C. Indeed both $\bar{C}'$ and B can be written as linear combinations of them with negative coefficients. Integrating over l we can write the sum over residues of the LHS box equivalently as a single cut (A, C) or as a sum of two cuts (B, C) and (B, C') exactly as we did in the expression (7.2.27). In this case, we obtain

$$D^{(8)} = D^{(8)}(A, C, A'', C'') = D^{(8)}(B, C, A'', C'') + D^{(8)}(C', C, A'', C'') \tag{7.4.17}$$

In the first equality, we have written the complete result for the double box integral

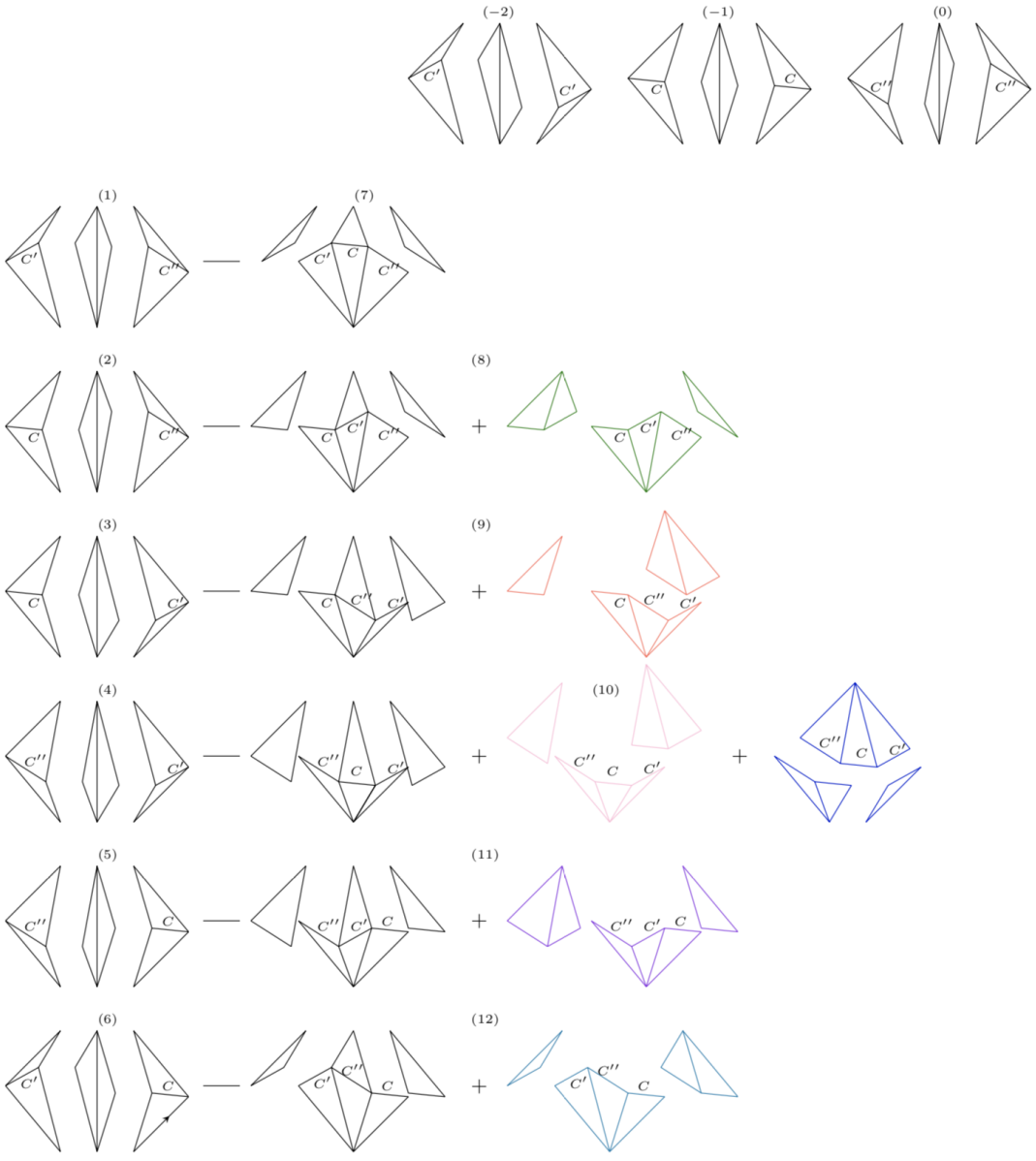

Figure 7.14: Atoms contributing to the third-order pole coefficient of the S-matrix (in black) and additional coloured terms coming from Cauchy's residue theorem cancelling the internal part of the network.

corresponding to the diagram $D^{(8)}$. It corresponds to a single tree-level diagram obtained by cutting the propagators A, C, A'' and C''. However, similarly to what happens in the one-loop case, it is possible to write the result as a sum over different cuts, corresponding to different choices of residues when we use Cauchy's theorem. In this respect $D^{(8)}(B, C, A'', C'')$ returns the desired cut contributing to (7.4.16) while the remaining atom $D^{(8)}(C', C, A'', C'')$ (the green shape in figure 7.14) will cancel out with some bulk contribution of the network, as it will be shown in one moment. In figure 7.14 all the cuts associated with the boundary of the network are reported. The black pieces are the desired cuts contributing to the final result expected from the bootstrapped S-matrix while the coloured cuts cancel out with the bulk part of the network. The cancellation mechanism inside the bulk is shown in figure 7.15. Apart from the diagram number (7), which entirely contributes to the boundary and generates a zero remainder, all the other diagrams $D^{(8)}, \dots, D^{(12)}$ are split into more pieces, some contributing to the bootstrapped answer, the others cancelling the diagrams $D^{(13)}, \dots, D^{(23)}$ in the central part of the network. The cancellation mechanism happens in different sectors, which we depicted with different colours in figure 7.15. There are in total nine pairs of cut diagrams composed of graphs differing by a single flipped four-point tree-level diagram. If we look for example at the green cuts associated with the diagrams $D^{(8)}$ and $D^{(13)}$ in figure 7.15 we see they are equal but for a singular tree-level graph that is flipped passing from $D^{(8)}$ to $D^{(13)}$. Since the sum of such a pair of tree-level diagrams is zero, the sum of the two green atoms is null. In addition to these pairs of canceling atoms there are also six blue cuts coming from diagrams $D^{(10)}, D^{(15)}, D^{(16)}, D^{(20)}, D^{(21)}, D^{(23)}$ that are equal with respect to their 3- and 4-point part but present different 5-point tree-level diagrams. All these 5-point terms contribute to the singular part of a 5-point scattering process and therefore they generate a zero amplitude after the sum as explained in appendix C. This is a mere consequence of the tree-level perturbative integrability of the model, which forbids production processes at the tree level.

Despite the result being expected from the bootstrap, it is surprising. The pole structure of the bootstrapped S-matrix emerges in perturbation theory from an underlying simplification which is explained using only the tree-level properties of the model. How the different atoms of the internal parts of the network simplify against each other is reminiscent of the divergence theorem: only a subset of the original Feynman diagrams reproduces the expected answer through contributions entirely located at the boundary. How the loops need to be cut to observe such simplification is however still an empirical fact and in some cases not immediately evident from the on-shell structure of the Feynman diagrams. The most difficult situations are found when the loop is split into more than two atoms, as happens for diagrams $D^{(10)}$, $D^{(16)}$ and $D^{(21)}$. In all this, a fundamental role is played by the fusing angles associated with the on-shell geometry of the Feynman diagrams that determine which cuts are allowed and which are forbidden. These angles are determined by the root system underlying the theory and it is reasonable to believe that a deeper understanding of what is observed, which is based on a case by case study of different models, can be found from general properties of the Coxeter geometry. However, finding a proof is still an open problem.

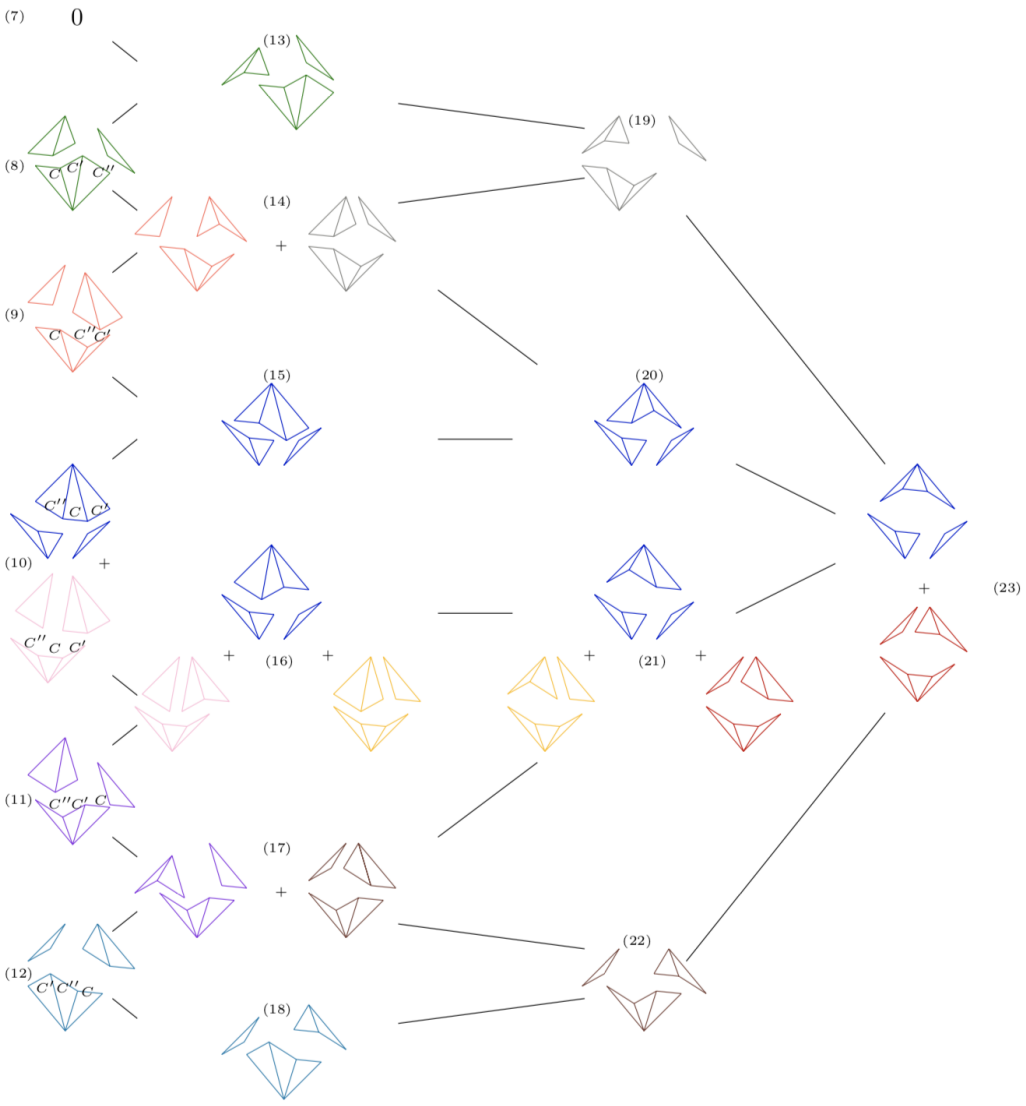

Figure 7.15: Cancellation mechanism in the bulk part of the Feynman diagram network. Atoms of the same colour are equal but for singular tree-level diagrams contributing to non-allowed processes therefore they sum to zero.

In the remaining part of the chapter other universal properties of the Landau poles are revealed by relying on observations made using such a cutting procedure.

7.5 Universal features of higher-order singularities

We present general features of higher-order singularities starting by reviewing some empirical properties of the geometry of the tiled parallelograms, as first discovered in [69]. We show the relevance of these properties in the computation of certain Laurent coefficients of the S-matrix expansion, following results that will be published in [3].

In the region of purely imaginary rapidities, we can always associate to a n-point scattering process a dual n-gon having as sides the masses of the interacting particles. Following [69], we identify the *depth* of such a polygon with the number of elementary triangles necessary to tile it completely. With elementary triangles we mean that they have unit depth, i.e. they cannot be tiled into smaller constituents. For example, the parallelogram corresponding to the second-order pole in figure 7.6 has a depth equal to 4 since it can be tiled in four elementary triangles. Similarly, the fusing triangle in figure 7.10 has a depth 3 since it can be tiled in three smaller vertices having unit depth. From how it is defined it is clear that the depth is an additive quantity and any figure composed by $\mathcal{N}$ constituents has a depth equal to

$$d = \sum_{i=1}^{\mathcal{N}} d_i \tag{7.5.1}$$

where d_i is the depth of each constituent. This is the same definition introduced in [69]. If all the constituents we are looking at are elementary triangles then all of them have unit depth and $d = \mathcal{N}$. Instead, if one of the constituents, say j in the sum, is not elementary, which means it can be further tiled in smaller pieces, the total depth is obtained counting such term d_j times; in other words, it contributes to the sum with all its sub-pieces.

Under some circumstances, it may be interesting to look not at the complete tilings of a polygon but only at some of its partial tilings. An example is provided by figure 7.11 where to compute the second-order coefficient of the Laurent expansion of the S-matrix around a third-order singularity we had to tile only partially the parallelogram, contrarily to what happens in the network 7.12 where the full tiles need to be taken into account. This example easily generalises as follows: to any polygon of depth d a set of partial-depths are associated, defined as the set of integer numbers ranging from 1 to d. We introduce here the concept of partial depth, originally absent in [69], to explain the different coefficients a_p of the Laurent expansion (7.1.2). A parallelogram of depth $d = 2P$ is associated with any pole of order P of the S-matrix. Then the coefficient a_P in (7.1.2) is generated by summing Feynman diagrams corresponding to complete tilings of the parallelogram. All the

lower order coefficients a_p are instead obtained by summing over tilings of partial-depth $2p$. This is exactly what we did to obtain the coefficients a_2 and a_3 of the expansion around the third-order pole: we summed over tilings of depth 4 and 6 respectively (see figures 7.11 and 7.12). This is not surprising if we think that we are summing over Feynman diagrams with only 3-point vertices (remember that all the diagrams with higher-point vertices contribute to the sub-leading coefficients of the Laurent expansion). If we label the number of vertices by V , the number of loops by L and the number of propagators by I the topology of such diagrams imposes the relation $V = 2I - 4L$ which is exactly equal to $2p$, two times the order of the pole as shown in (7.2.10). Since the number of vertices is exactly equal to the number of constituents composing the tiling, and therefore to the partial (total) depth considered, this agrees with our previous claim that the partial (total) depths of the tilings contributing to the different coefficients a_p are equal to $2p$.

We distinguish now two different situations depending on the order P of the maximal singular contribution: it can be even or odd.

Even-order poles. If the maximal singular contribution at the pole is even, say $P = 2N$ (i.e. the bootstrapped S-matrix contains two bricks of the form $\{x-1\}^N\{x+1\}^N$), then the parallelogram corresponding to the process has a depth $4N$ and there exist N copies of the network 7.6 in which the internal constituents can further be tiled. This is an empirical fact first observed in [69] that was applied in [2] to compute the a_2 coefficient of the S-matrix expansion. The derivation is the following. Each of the N copies of the network is composed of tilings of partial depth 4 and can be computed separately. It carries a contribution (7.3.4) so that the result given by the sum over all the N copies is simply N times the result of a single network

$$S_{ab}(\theta) = 1 + N\left(\frac{g^2}{2h}\right)^2 \frac{1}{(\theta - i\theta_0)^2} + \dots \tag{7.5.2}$$

This result is in agreement with what we observe in the bootstrapped S-matrix (7.1.4) where the a_2 coefficient of the expansion around the $2N^{\text{th}}$-order pole is the binomial factor $\binom{N}{1}$. An example of pair of networks contributing to the second-order coefficient around a 4^{th}-order pole is shown in figure 7.16.

In the image we see that the two networks, at this depth level, are disjoint and are not connected by any flip. Each one contributes separately to the final result. This is no longer the case if we start searching for the tilings with a depth higher than 4, which in this case can be 6 or 8. The latter case corresponds to the search for Feynman diagrams contributing to the a_4 coefficient at the pole. The number of such diagrams is huge. The graphs containing two vertices of depth 3 in figure 7.16 contribute with 9 Feynman diagrams (3×3 since each vertex of depth 3 counts 3 possible corrections of the form in 7.10) while the graphs containing a depth-four parallelogram contribute with 4 diagrams (those coming from the second-order pole network). In total there are 62 diagrams contributing to the a_4 coefficient to which we should add all the graphs obtained by them through the flipping move. The fact that such a big number of diagrams should reproduce the simple result that we observe in the bootstrapped S-matrix suggests that probably, as it happens for

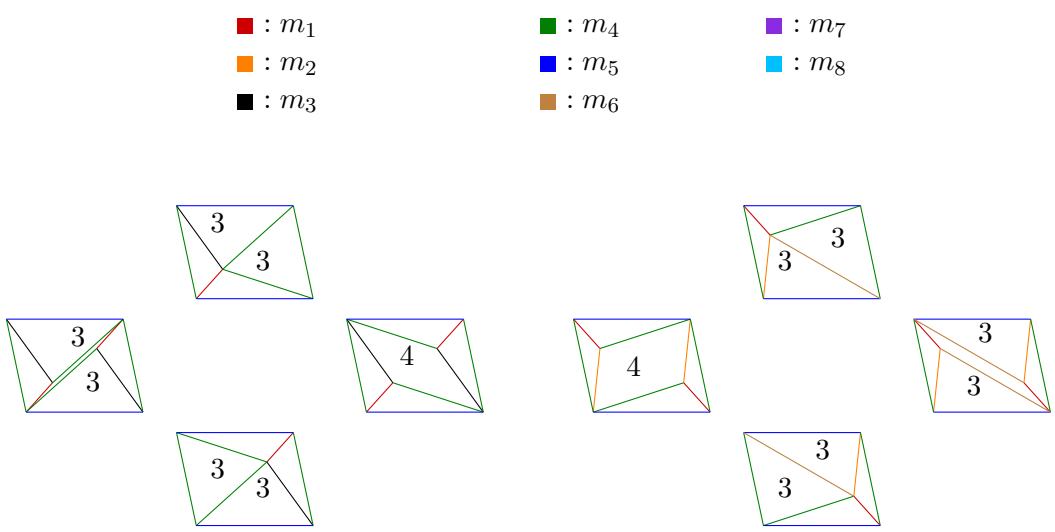

Figure 7.16: Pair of networks contributing to the a_2 coefficient (see (7.1.2)) of the Laurent expansion of the S-matrix around a 4^{th}-order pole. The example has been taken from the $e_8^{(1)}$ affine Toda model and its masses are reported with different colours following the order $m_1 < m_2 < \cdots < m_8$. Inside the different tiles (apart from those with unitary depth) their depth is reported.

third-order poles, the computation is reproduced by only a small number of cuts. It would be very interesting to investigate the space of Feynman diagrams contributing to such a simple result. On the other hand, there exist also Feynman diagrams with partial depth equal to six. These are two-loop diagrams contributing to the a_3 coefficient of the Laurent expansion around the pole. We expect a zero result for this number. Indeed it is evident from the expression (7.1.4) that all the odd-order coefficients of the expansion around a generic even-order singularity are zero. Once again we do not have a motivation for why this happens, but it is probably due to an underlying simplification that can be obtained by cutting the different diagrams inside a network. A universal explanation, based on diagrammatic computations, of the absence of all the odd-order terms in the expansion (7.1.4) around a generic even-order pole would be very interesting.

Odd-order poles. If P in (7.1.2) is odd, then we have an odd-order singularity in the S-matrix. In this case, the parallelogram associated with the diagonal process can be split into two triangles each one of depth P. In the known examples coming from affine Toda field theories, P can be any odd number from 1 up to and including 11.

Based on empirical observations we note that to each triangle of depth $P = 2N + 1$ we can associate N triplets of vertex corrections of the form in figure 7.10, so that the triangle can be tiled exactly in $3N$ ways, as it was remarked in [69]. Then the relations (7.4.9) are applied separately over each one of the N different triplets of triangles $(\Delta^{(1)}, \Delta^{(2)}, \Delta^{(3)}), \ldots, (\Delta^{(3N-2)}, \Delta^{(3N-1)}, \Delta^{(3N)})$. If we associate respectively the label Δ_a, Δ_b and Δ_c to the triangles constructed over the sides p_a, p_b and p_c

then we have

$$\sum_{i=1}^{3}\Delta_a^{(3n-3+i)}=\sum_{i=1}^{3}\Delta_b^{(3n-3+i)}=\sum_{i=1}^{3}\Delta_c^{(3n-3+i)}=\Delta_{ab}. \tag{7.5.3}$$

for each triplet $n=1,\dots,N$. This equality, pointed out in [3], is stronger than the one noted in [69] in which the authors noticed that the sum over all the triangles composing the $3N$ different tilings respect

$$\sum_{i=1}^{3N}\Delta_a^{(i)}=\sum_{i=1}^{3N}\Delta_b^{(i)}=\sum_{i=1}^{3N}\Delta_c^{(i)}=N\Delta_{ab}.$$

The same sign rule (7.4.2) is applied to each one of the $3N$ different tilings. Labelling by $(f_a^{(i)},f_b^{(i)},f_c^{(i)})$ the three f-functions entering the 3-point couplings constructed over the sides a, b and c in the i-th tiling, with $i=1,\dots,3N$, we have

$$f_a^{(i)}f_b^{(i)}f_c^{(i)}=-\left(\frac{4g}{\sqrt{h}}\right)^2 f_{ab\bar{c}}. \tag{7.5.4}$$

It is easy at this point to explain the origin of the coefficient $a_2=\binom{N}{1}$ in the S-matrix expansion (7.1.4). It comes by simply performing N times, one for each triplet of vertex corrections, the computation reproduced in section 7.4.2, so that the final result is simply given multiplying by N the result in (7.4.11) [3].

As happens for even-order singularities, also in this case to study the higher-order coefficients of the Laurent expansion $a_3,a_4,\dots$ we need to keep into account depths of higher order. The N triplets of vertex corrections, that are disconnected at one loop, by considering nested tilings start to become connected by flipping internal propagators. We show an example of vertex corrections contributing to a 5^{th}-order pole in the next subsection.

We conclude this discussion of the properties of higher-order poles by noting that the relation (7.5.4) can be iterated, a fact that was already known in [69]. We have already explained that a triangle of total depth $2N+1$ can be tiled in three sub triangles exactly in $3N$ ways. Then the triangles composing each one of these $3N$ tilings can be further tiled in triangles and so on. By looking to more and more nested tilings we end up with a configuration composed of $2N+1$ pieces. By iterating relation (7.5.4), the product of all the f-functions composing these maximal depth tilings is given by

$$\prod_{j=1}^{2N+1}f_j^{(k)}=(-1)^N\left(\frac{4g}{\sqrt{h}}\right)^{2N}f_{ab\bar{c}} \tag{7.5.5}$$

where $k=1,\dots,M$ labels the different tilings. The number M of possible different tilings grows rapidly with N.

7.5.1 Two-loop vertex corrections and fifth-order poles

In this subsection the leading order singularity of a 3-point vertex having a depth equal to 5 is computed and used to derive the one-particle reducible part of the

S-matrix on a 5^{th}-order pole. Also in this case the results obtained are universal, valid in any simply-laced affine Toda model. The triangle in question can be divided in three sub-triangles in exactly 6 different ways. We identify two triplets of tilings at one loop, $[(1,\bullet),(2,\bullet),(3,\bullet)]$ and $[(4,\bullet),(5,\bullet),(6,\bullet)]$, satisfying separately the relation (7.5.3) (with $N=2$):

$$\Delta_c^{(1,\bullet)}+\Delta_c^{(2,\bullet)}+\Delta_c^{(3,\bullet)}=\Delta_{ab}\quad\text{and}\quad\Delta_c^{(4,\bullet)}+\Delta_c^{(5,\bullet)}+\Delta_c^{(6,\bullet)}=\Delta_{ab}. \tag{7.5.6}$$

We used the subscript letter c to indicate that we are summing, within the same triplet, all the triangles constructed on the side c. The same relation is valid summing the triangles constructed respectively on the a- and on the b-side as we pointed out in (7.5.3).

Each one of these six different tilings is composed of two triangles having a depth equal to 1 and one triangle having a depth equal to 3; the latter can therefore be tiled in three different ways. The total depth, given by summing all the elementary constituents of a single tiling is then 5. To take into account such a nested level of tiles we use a second index, which is absent in (7.5.6) and substituted with a bullet. Since for a given one-loop tiling we identify 3 additional nested tilings such a second index takes values in $\{1,2,3\}$. Then the pairs of numbers (j,k), running respectively from 1 to 6 and from 1 to 3, label the complete tiling. For example, the pair $(1,2)$ indicates the tiling number one at the depth level 3, and among the three different possibilities to further divide one of its constituents we choose the sub-tiling number two. We did not identify a preferred order to arrange these tilings; we follow the enumeration shown in figure 7.17. There, apart from the non-planar diagrams $(7,1)$, $(7,2)$ and $(7,3)$[1], the tilings are arranged in two blocks of 9 diagrams each. The six different rows label the main tiling, while the three columns provide a label for the nested tilings. We then use the convention of labelling by $\Delta_c^{(j,\bullet)}$ the triangle constructed over the side c in the one-loop configuration j while we label by $\Delta_c^{(j,k)}$ the triangle constructed over the side c in the nested tiling (j,k). To give an example, $\Delta_c^{(3,\bullet)}$ corresponds to the triangle $\Delta_{ce''m''}$ reported in any of the configurations $(3,1)$, $(3,2)$ and $(3,3)$ in figure 7.17 while $\Delta_c^{(3,1)}$ corresponds to $\Delta_{cd''o}$ that is one of the components of the configuration $(3,1)$.

The two blocks of diagrams

$$\{(1,1),(1,2),(1,3),(2,1),(2,2),(2,3),(3,1),(3,2),(3,3)\}$$

and

$$\{(4,1),(4,2),(4,3),(5,1),(5,2),(5,3),(6,1),(6,2),(6,3)\}$$

in figure 7.17 are connected by flipping internal propagators. Starting from a generic diagram of the first block we can generate a diagram of the second block acting with a finite number of flips. In figure 7.17 we identified with the same symbol diagrams connected by flips. Sometimes a single type I flip is enough to connect the two diagrams in the different blocks; an example is provided by the tilings $(1,1)$

[1]Note though that the example considered in figure 7.17 is degenerate. The momenta o and f are parallel and this fact makes the diagram $(7,1)$ null.

and $(5,1)$. According to the convention previously explained the little triangle Δ_{aih} common to both the tilings, can be equivalently labelled by $\Delta_a^{(1,1)}$ or $\Delta_a^{(5,\bullet)}$. In some other situations, we need two flips of type II to connect the pair of diagrams. This second case is represented by the pair of graphs $(2,3)$ and $(5,3)$. To pass from the first diagram to the second one we need to pass through an intermediate non-planar diagram $(7,2)$ acting with two flips of type II: $(2,3) \to (7,2) \to (5,3)$.

For each diagram in figure 7.17 we write its cut decomposition under it, representing with different colours the cuts that cancel in pairs. The values of the non-cancelling black atoms are reported under the diagrams, omitting an overall multiplicative factor. We compute their sum one row at a time

$$\begin{aligned} &\sum_{i=1}^{3} D^{(1,i)} = \Delta_c^{(1,\bullet)} \quad , \quad \sum_{i=1}^{3} D^{(2,i)} = \Delta_c^{(2,\bullet)}, \\ &\sum_{i=1}^{3} D^{(4,i)} = \Delta_c^{(4,\bullet)} \quad , \quad \sum_{i=1}^{3} D^{(5,i)} = \Delta_c^{(5,\bullet)}. \end{aligned} \tag{7.5.7}$$

We also notice that

$$D^{(3,3)} + D^{(6,3)} = \frac{\Delta_{jm''n} + \Delta_{jmv}}{\Delta_{aj}} \, \Delta_{cjx} = \Delta_{cjx}, \tag{7.5.8}$$

which implies

$$D^{(3,3)} + D^{(6,3)} = \Delta_c^{(3,3)} = \Delta_c^{(6,3)}. \tag{7.5.9}$$

The sum of (7.5.7) and (7.5.9) is easily performed noting that $\Delta_c^{(4,\bullet)} = \Delta_c^{(3,1)}$ and $\Delta_c^{(5,\bullet)} = \Delta_c^{(3,2)}$, so that

$$(7.5.7)+(7.5.9) = \Delta_c^{(1,\bullet)}+\Delta_c^{(2,\bullet)}+\Delta_c^{(3,3)}+\Delta_c^{(4,\bullet)}+\Delta_c^{(5,\bullet)} = \Delta_c^{(1,\bullet)}+\Delta_c^{(2,\bullet)}+\Delta_c^{(3,\bullet)} = \Delta_{ab},$$

where in the second equality we used

$$\Delta_c^{(3,1)} + \Delta_c^{(3,2)} + \Delta_c^{(3,3)} = \Delta_c^{(3,\bullet)}.$$

After introducing the proper overall multiplicative factor taking into account (7.5.5), we obtain the value of the two-loop vertex correction at the pole

$$D_{vertex} = i\Big(\frac{g^2}{2h}\Big)^2 \frac{f_{ab\bar{c}}}{(\theta - i\theta_0)^2}\Delta_{ab} = i\Big(\frac{g^2}{2h}\Big)^2 \frac{C_{ab\bar{c}}}{(\theta - i\theta_0)^2}. \tag{7.5.10}$$

Differently from the one-loop vertex correction found in (7.4.10), the residue of (7.5.10) is purely imaginary. This implies that the one-particle reducible part of the S-matrix on the 5^{th}-order pole acquires a different sign compared to the 3^{rd}-order pole S-matrix (7.4.12). In the present case we have

$$S_{ab}^{(1pr)}(\theta) = \frac{1}{8i\Delta_{ab}} D_{vertex} \frac{i}{s - s_0} D_{vertex} = i\Big(\frac{g^2}{2h}\Big)^5 \frac{1}{(\theta - i\theta_0)^5}, \tag{7.5.11}$$

that exactly matches the Laurent coefficient of order $(\theta - i\theta_0)^{-5}$ expected from the bootstrapped relation (7.1.4) for $N = 2$ and $\nu = i$. Surprisingly the one-particle

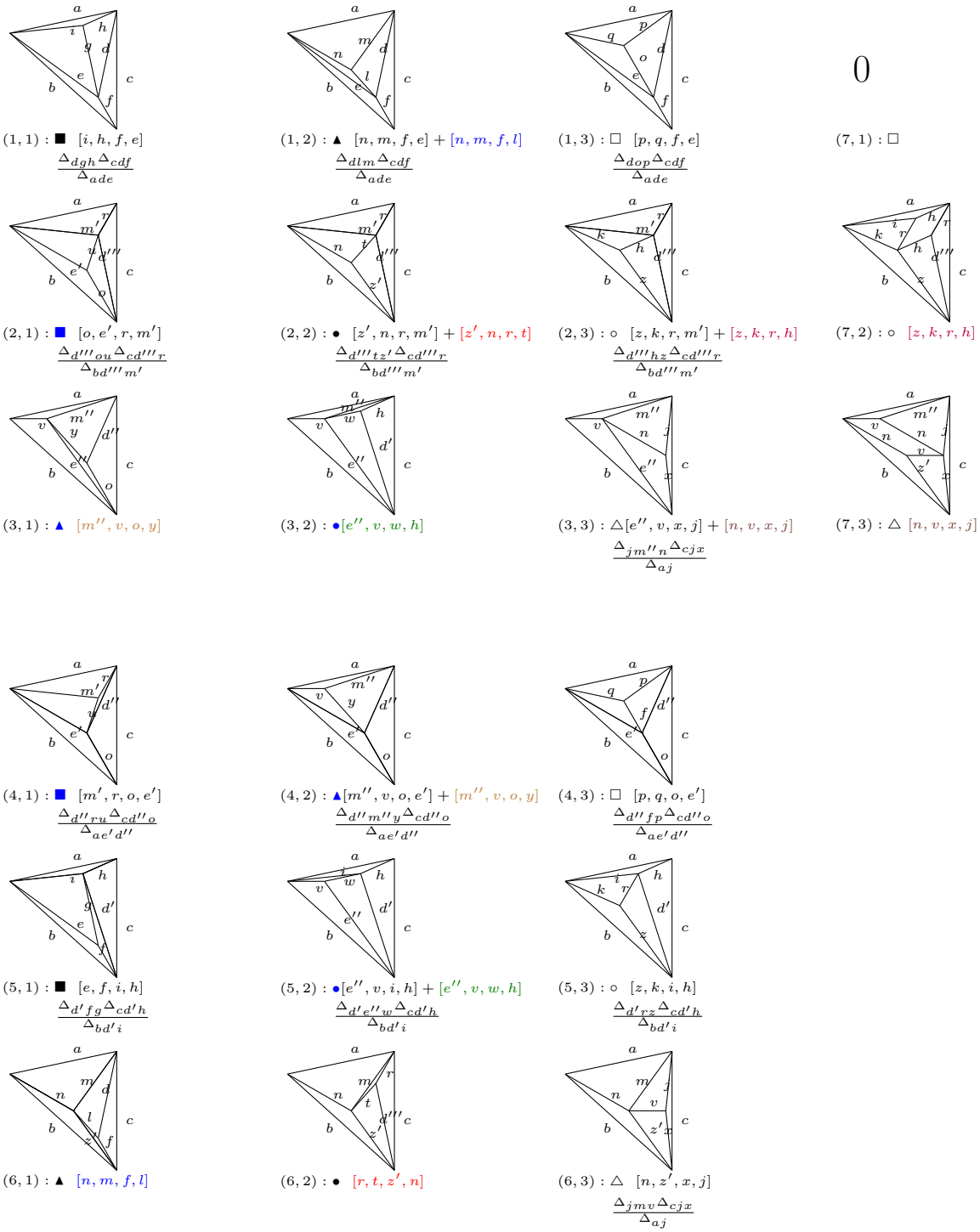

Figure 7.17: Two-loop vertex corrections. Graphs with the same symbol (△, ○, □, ▲, ●, ■, ▲, ●, ■) are connected by flipping one diagonal. Under each graph the cut propagators are reported together with the values of the non-canceling contributions written omitting the overall factor $i\left(\frac{g^2}{2h}\right)^2 \frac{f_{ab\bar{c}}}{(\theta - i\theta_0)^2}$.

reducible diagrams reproduce the result expected from the bootstrap. In total there are $21 \times 21 = 441$ such diagrams, since there are in general 21 different tilings of the vertex, as reported in figure 7.17. Analogously to what happened for the 3^{rd}-order pole, we can then start applying flips on each of the one-particle reducible diagrams to generate a network of Feynman diagrams contributing to the 5^{th}-order pole. The boundary of the 3^{rd}-order pole network was composed of 9 one-particle reducible diagrams (6 on the boundary of the disk plus the 3 separate diagrams $D^{(-2)}$, $D^{(-1)}$ and $D^{(0)}$ in figure 7.12); similarly here we may have a boundary composed by 441 different diagrams. The internal part of the network contains therefore a tremendous amount of graphs. Remarkably, all the irreducible graphs internal to the network have to cancel between one another to reproduce the bootstrapped result. The simplification should work in a similar way to what happens in figure 7.15, but with a much bigger network. Finding the full network of singular diagrams and showing that the particle-irreducible graphs of this network cancel between each other would provide an important step forward in the understanding of the quantum integrability of affine Toda models.

Chapter 8

Conclusions

One of the main motivations for the work carried out in this thesis was to provide a better understanding of integrability in perturbation theory. While the axiomatic bootstrap machinery allowed in the past decades to conjecture analytical results for the S-matrices of a variety of (1+1)-dimensional integrable models, its connection with Feynman diagram computations is often still ill-understood, as is the underlying mechanism responsible for the cancellation of all non-elastic processes. An indication that the bootstrap cannot be the end of the story comes from the fact that classically integrable theories, having a Lax formulation of their equations of motion allowing for the existence of an infinite tower of conserved charges, often are ruined at the quantum level. Examples are provided by non simply-laced affine Toda models: though is believed these theories are still integrable at quantum level [105], the masses of the particles, fundamental to establishing the fusing angles entering the bootstrap relations, renormalise in a bad way. This was observed already at one loop [57] and makes the bootstrap construction much more convoluted [100]. Poles in the S-matrices become coupling dependent and feeding the bootstrap with the classical data simply leads to a wrong answer for the S-matrix elements. It is therefore natural to ask if there is any connection between the axiomatic approach proposed by Alexander and Alexei Zamolodchikov in [18] and the more standard Feynman diagrammatic formulation of scattering amplitudes. In particular, it would be important to discover a systematic approach to seeing if a theory is integrable in perturbation theory and when loops modify its classical integrability.

As the first step in that direction, a systematic study of the absence of production in bosonic massive quantum field theories with polynomial-like potentials has been performed. By imposing the absence of off-diagonal processes at the tree level in perturbation theory many constraints emerge on the mass spectrum and Lagrangian couplings. Defining all the possible sets of masses and couplings satisfying these constraints would correspond to classifying all the bosonic quantum field theories with purely elastic S-matrices and polynomial-like potentials. Although we did not pursue that goal, we checked the validity of these constraints for the class of affine Toda quantum field theories proving in this way their tree-level perturbative integrability. The proof has been formulated in such a way to be as rigorous as possible and combine many results coming from different papers. Most importantly

on-shell diagrams, contributing to singularities in amplitudes, are projections of certain higher-dimensional polytopes composed of roots of the root system. The cancellation of poles in non-elastic processes can then be proved by exploiting the properties of the roots. To verify that all the non-elastic amplitudes are null an important role has been played by the recursive approach [37], through which it is shown how higher-order couplings can be recursively generated from the masses and 3-point couplings. The same equation found in [37] by requiring the absence of production at the tree level arises in all the affine Toda field theories by making use of different Lie algebra properties.

At the tree level, no relevant distinction is made between simply- and non-simply-laced affine Toda theories: in both cases the classical masses and fusing angles are encoded in the underlying root systems leading to universal expressions for the tree-level S-matrix elements. However, if we derive exact S-matrices from the tree-level ones by promoting sums over building blocks to products of them, the non simply-laced affine Toda theories generate inconsistencies. Indeed the powers to which the building blocks are raised can in general be non-integer numbers, introducing unexpected branch cuts in the S-matrices. The derivation of the quantum S-matrices in non simply-laced cases is then further complicated by the fact that at the loop level the mass ratios become coupling-dependent and a direct connection between on-shell momenta and root projections is lost. Formulas for the exact S-matrices of these theories have been proposed [100, 101, 103], but much of the elegance of their simply-laced partners is lost. In contrast, for the ADE series of Toda theories, it was verified that the mass ratios do not renormalize at one loop [57]. Therefore these theories provide beautiful examples for studying perturbative quantum aspects of integrable models.

A loop investigation of the higher-order poles arising in the bootstrapped S-matrices of simply-laced affine Toda field theories has been performed. For each imaginary value of the rapidity at which a higher-order pole is expected collections of singular Feynman diagrams can be found and organised inside networks [69]: these diagrams contain propagators inside loops that are all simultaneously on-shell, generating in this way Landau singularities [39]. The number of Feynman diagrams contributing to such singular values grows incredibly fast with the order of pole considered, which is proportional to the number of loops. Not all the Feynman diagrams entering the networks contribute to the results; many of them cancel each other out in a way that can be traced back to the tree-level properties of the model. The only relevant terms come from some particular cuts of the diagrams located at the boundary of the networks, whose sum reproduces the expected value of the bootstrapped S-matrix at the singularities. Differently from [69], where only the maximal singular contributions of the S-matrix elements were studied, we performed the full Laurent expansion of the bootstrapped S-matrices on the higher-order poles. Each coefficient of the expansion can therefore be compared with perturbative calculations. While the coefficients a_2 and a_3 in equation (7.1.2) have been reproduced by networks of singular diagrams lying on one- and two-dimensional surfaces respectively, it is reasonable to expect higher dimensional networks for the coefficient a_n with $n > 3$. The coefficients a_n, for $n > 3$, are reproduced in perturbation theory by Feynman diagrams with

more than two loops and the computation can become very challenging. However, simplifications are expected for all the coefficients. An example has been shown in computing the one-particle reducible diagrams contributing to a_4: surprisingly these diagrams reproduce the expected result, meaning that all the one-particle irreducible graphs, probably lying on the internal part of some higher-dimensional network, have to cancel between one another. If on one hand more and more difficult networks are generated by increasing the number of loops, on the other hand, we can keep the number of loops fixed and study the lower order coefficients a_n in (7.1.2) for arbitrary P. As a first case, it would be interesting to derive a_3 in perturbation theory by summing over two-loop diagrams for arbitrary P. Indeed the network 7.12 studied in this thesis corresponds to the case $P = 3$, while two-loop networks contributing to the coefficient a_3 for arbitrary P have not been studied yet. If we search for singular one-loop diagrams contributing to a_2 for P arbitrary we find always the same network repeated with higher multiplicities; something similar should happen also for a_3. An important difference is that a_3 has to be null every time the order P of the pole is even: this is important to have a matching with the bootstrapped result in (7.1.4). We should also remark that despite the obtained results being universal and independent of the particular simply-laced theory studied, we based on a case by case analysis. More work is necessary to connect the obtained results to root-system properties of the underlying Lie algebras in a universal way as it has been done for the tree-level case. A possible approach to the problem would be to reconstruct loop amplitudes starting from tree-level results. This would be possible following an approach similar to that one used in [106, 107] and assuming as starting point the universal expressions for the tree-level S-matrices of affine Toda theories given in equation (6.4.2) in terms of the tree-level building blocks (6.4.3).

The tree-level perturbative integrability discussed in chapters 3 and 4 also leads to different open problems. For example, it would be interesting to classify all Lagrangians showing purely elastic S-matrices at the tree level, employing the tree-level bootstrap relations and flipping rule discussed in this thesis. While we proved that all the affine Toda theories satisfy the constraints of pure elasticity, we did not verify that these are the only such theories. The discussion can be generalized as well to Lagrangians containing massive fields other than scalar ones, for which integrable examples are known [108, 109], or having derivatives in the potential. By imposing the absence of production, it may be possible to find all deformations preserving integrability at the tree level, rediscovering within this class the deformations presented in [110, 111], whose Lagrangians are in most cases known [112].

Other deformations that can be studied by imposing the absence of production at tree level are boundaries and defects [113, 114]: if properly defined, these impurities can be introduced in integrable theories so to preserve a subset of the conserved charges of the undeformed theory. In the context of affine Toda field theories, boundaries and defect potentials have been found in [115] and [116] respectively by imposing the survival of some conserved charges at the classical level. Approaching the same problem from a different perspective, it would be interesting to study integrability-preserving boundaries and defects by imposing the absence of production on the impurity. The boundary and defect data necessary for the absence of production

should be encoded in the root systems and it would be desirable to write the boundary and defect potentials provided in [115, 116] in a way that makes the absence of production more explicit. For example, a geometrical construction of the boundary- and defect-couplings may be obtained by writing the field in a clever basis; the Freeman construction [75] can be a possible approach to the problem. Finding quantitative expressions for Landau singularities present in the conjectured boundary reflection factors is also possible in principle. The prosaic origin of such singularities has already been highlighted in [117] for certain integrable models and it would be interesting to derive exact expressions for the residues at the poles by performing perturbative computations as discussed for example in [118]. A perturbative study of these impurities is further motivated by the fact that boundary and defect potentials that are classically integrable can generate anomalies at the quantum level that destroy the conservation laws [119, 120].

Appendix A

Double covering the complex plane

Property A.1. *Given a fourth-order polynomial in z*

$$R(z) = az^4 + bz^3 + cz^2 + dz + e$$

such that the roots of $R(z) = 0$ are all unequal and the coefficients a and b are not zero simultaneously, then there exists a map

$$z = \frac{\alpha z' + \beta}{z' + \delta} \tag{A.0.1}$$

making

$$R'(z') \equiv \frac{(z' + \delta)^4}{(\beta - \alpha\delta)^2} R(z) \tag{A.0.2}$$

of the form

$$R'(z') = 4z'^3 - g_2 z' - g_3. \tag{A.0.3}$$

Proof. By writing (A.0.1) as $z = \alpha + \frac{\beta - \alpha\delta}{z' + \delta}$ then (A.0.2) can be Taylor expanded around $z = \alpha$ as

$$\begin{aligned} R'(z') = \frac{R(\alpha)}{(\beta - \alpha\delta)^2}(z' + \delta)^4 + \frac{R^{(1)}(\alpha)}{\beta - \alpha\delta}(z' + \delta)^3 + \frac{R^{(2)}(\alpha)}{2!}(z' + \delta)^2 \\ + \frac{R^{(3)}(\alpha)}{3!}(\beta - \alpha\delta)(z' + \delta) + \frac{R^{(4)}(\alpha)}{4!}(\beta - \alpha\delta)^2, \end{aligned} \tag{A.0.4}$$

where it has been defined $R^{(n)}(\alpha) \equiv \frac{d^n R}{dz^n}\Big|_{z=\alpha}$. At this point it is possible to properly tune the parameters α, β and γ in such a way to convert R' in the form (A.0.3). By choosing α to be one of the four roots of the polynomial R we obtain $R(\alpha) = 0$; in this way, the coefficient of the fourth power in z' in (A.0.4) is made to vanish. Subsequently, if it is set

$$\delta = -\frac{R^{(2)}(\alpha)}{24} \quad \text{and} \quad \beta = -\frac{R^{(2)}(\alpha)}{24}\left(\alpha - \frac{6R^{(1)}(\alpha)}{R^{(2)}(\alpha)}\right) \tag{A.0.5}$$

$R'(z')$ is reduced to be a third-order polynomial of type (A.0.3). □

From property A.1 it follows that any rational function F in the variables z and $\sqrt{R(z)}$, where R is a generic polynomial of order four presenting different roots, can be written as a rational function f in z' and $\sqrt{R'(z')}$

$$F(z, \sqrt{R(z)}) = F\Big(\frac{\alpha z' + \beta}{z' + \delta}, \frac{(\beta - \alpha\delta)}{(z' + \delta)^2}\sqrt{R'(z')}\Big) \equiv f(z', \sqrt{R'(z')}). \tag{A.0.6}$$

The initial function F is not single valued on $\mathbb{C}$, indeed for each point z there are two possible values of $\sqrt{R(z)}$ defined over two different Riemann sheets. However after the conversion (A.0.6) it is easy to map such a double cover of the complex plane to a torus. This is achieved by using the parametrization $z' = \wp(x)$, where the symbol $\wp$ represents the Weierstrass elliptic function. To each value z' on the complex plane there are two different points x_1 and x_2 on a torus such that $\wp(x_1) = \wp(x_2) = z'$. Moreover, the lattice Ω associated to $\wp$ is completely defined by a pair of numbers g_2 and g_3 in terms of which $\wp$ satisfies the following differential equation

$$(\wp(x)')^2 = 4\wp(x)^3 - g_2\wp(x) - g_3.$$

Then the values of the derivative of $\wp$ at the points x_1 and x_2 are one the opposite of the other and correspond to the two branches of solutions of $\sqrt{R'(z')}$. The starting double valued function F can therefore be mapped into a single-valued periodic meromorphic function

$$f(\wp(x), \wp(x)')$$

defined on a torus. This implies that if $F(z, \sqrt{R(z)})$ does not have any poles on either of its Riemann sheets, then $f(\wp(x), \wp(x)')$ has to be bounded on the torus, and by Liouville's theorem it must be a constant not depending on x.

Appendix B

The Cayley-Menger determinant

This appendix is extracted from [1] and collects some elementary geometrical properties of simplices; such properties are used in the thesis both to prove the absence of singularities in inelastic processes and to compute values of Landau poles.

B.1 The basic formula

Let $\mathbf{x}^0$, $\mathbf{x}^1$, ..., $\mathbf{x}^n$ be $n+1$ points in $\mathbb{R}^n$, and set $X_{ij} = \|\mathbf{x}^i - \mathbf{x}^j\|^2$ for $0 \leq i, j \leq n$. Let v_n be the n-dimensional simplex with vertices $\mathbf{x}^0$, $\mathbf{x}^1$, ..., $\mathbf{x}^n$. Then a classic result from distance geometry states that $\mathrm{vol}(v_n)^2$, the square of the volume of v_n, is given by the Cayley-Menger determinant:

$$\mathrm{vol}(v_n)^2 = \frac{(-1)^{n+1}}{(n!)^2 2^n} \begin{vmatrix} 0 & X_{01} & X_{02} & \cdots & X_{0n} & 1 \\ X_{10} & 0 & X_{12} & \cdots & X_{1n} & 1 \\ X_{20} & X_{21} & 0 & \cdots & X_{2n} & 1 \\ \vdots & \vdots & \vdots & \ddots & \vdots & \vdots \\ X_{n0} & X_{n1} & X_{n2} & \cdots & 0 & 1 \\ 1 & 1 & 1 & \cdots & 1 & 0 \end{vmatrix} . \tag{B.1.1}$$

B.2 A generalisation

Now let $\mathbf{x}^0$, $\mathbf{x}^1$, ..., $\mathbf{x}^{n+1}$ be $n+2$ points in $\mathbb{R}^n$, and set $X_{ij} = \|\mathbf{x}^i - \mathbf{x}^j\|^2$ for $0 \leq i, j \leq n+1$. Let v_n be the simplex with vertices $\mathbf{x}^0$, $\mathbf{x}^1$, ..., $\mathbf{x}^n$, and v_{n+1} the simplex with vertices $\mathbf{x}^0$, $\mathbf{x}^1$, ..., $\mathbf{x}^{n-1}$, $\mathbf{x}^{n+1}$. Note that v_n and v_{n+1} have as a

common face the $n-1$ dimensional simplex with vertices $\mathbf{x}^0$, $\mathbf{x}^1$, …, $\mathbf{x}^{n-1}$. Then

$$\mathrm{vol}(v_n)\mathrm{vol}(v_{n+1}) = \frac{\varepsilon\,(-1)^{n+1}}{(n!)^2 2^n} \begin{vmatrix} 0 & X_{01} & \cdots & X_{0,n-1} & X_{0n} & 1 \\ X_{10} & 0 & \cdots & X_{1,n-1} & X_{1n} & 1 \\ \vdots & \vdots & \ddots & \vdots & \vdots & \vdots \\ X_{n-1,0} & X_{n-1,1} & \cdots & 0 & X_{n-1,n} & 1 \\ X_{n+1,0} & X_{n+1,1} & \cdots & X_{n+1,n-1} & X_{n+1,n} & 1 \\ 1 & 1 & \cdots & 1 & 1 & 0 \end{vmatrix} \tag{B.2.1}$$

where $\varepsilon = +1/-1$ according to whether $\mathbf{x}^n$ and $\mathbf{x}^{n+1}$ lie on the same / opposite sides of the codimension one hyperplane occupied by the common face. In the special case where $\mathbf{x}^{n+1} = \mathbf{x}^n$, we have $\varepsilon = +1$, $v_{n+1} = v_n$, $X_{n+1,i} = X_{n,i}$ for $i = 1, \ldots, n$ and $X_{n+1,n} = 0$, and this reduces to the Cayley-Menger determinant.

To prove this result, we first set $\mathbf{x}^0 = \mathbf{0}$. Then *RHS*, the right-hand side of the above formula, is equal to $\frac{\varepsilon(-1)^{n+1}}{(n!)^2 2^n}\, D$, where $D =$

$$\begin{vmatrix} 0 & \|\mathbf{x}^1\|^2 & \|\mathbf{x}^2\|^2 & \cdots & \|\mathbf{x}^n\|^2 & 1 \\ \|\mathbf{x}^1\|^2 & 0 & \|\mathbf{x}^1\|^2 - 2\mathbf{x}^1\cdot\mathbf{x}^2 + \|\mathbf{x}^2\|^2 & \cdots & \|\mathbf{x}^1\|^2 - 2\mathbf{x}^1\cdot\mathbf{x}^n + \|\mathbf{x}^n\|^2 & 1 \\ \|\mathbf{x}^2\|^2 & \|\mathbf{x}^2\|^2 - 2\mathbf{x}^2\cdot\mathbf{x}^1 + \|\mathbf{x}^1\|^2 & 0 & \cdots & \|\mathbf{x}^2\|^2 - 2\mathbf{x}^2\cdot\mathbf{x}^n + \|\mathbf{x}^n\|^2 & 1 \\ \vdots & \vdots & \vdots & \ddots & \vdots & \vdots \\ \|\mathbf{x}^{n+1}\|^2 & \|\mathbf{x}^{n+1}\|^2 - 2\mathbf{x}^{n+1}\cdot\mathbf{x}^1 + \|\mathbf{x}^1\|^2 & \|\mathbf{x}^{n+1}\|^2 - 2\mathbf{x}^{n+1}\cdot\mathbf{x}^2 + \|\mathbf{x}^2\|^2 & \cdots & \|\mathbf{x}^{n+1}\|^2 - 2\mathbf{x}^{n+1}\cdot\mathbf{x}^n + \|\mathbf{x}^n\|^2 & 1 \\ 1 & 1 & 1 & \cdots & 1 & 0 \end{vmatrix}.$$

Subtracting the first row from every other row and the first column from every other column except for the last ones,

$$D = \begin{vmatrix} 0 & \|\mathbf{x}^1\|^2 & \|\mathbf{x}^2\|^2 & \cdots & \|\mathbf{x}^n\|^2 & 1 \\ \|\mathbf{x}^1\|^2 & -2\|\mathbf{x}^1\|^2 & -2\mathbf{x}^1\cdot\mathbf{x}^2 & \cdots & -2\mathbf{x}^1\cdot\mathbf{x}^n & 0 \\ \|\mathbf{x}^2\|^2 & -2\mathbf{x}^2\cdot\mathbf{x}^1 & -2\|\mathbf{x}^2\|^2 & \cdots & -2\mathbf{x}^2\cdot\mathbf{x}^n & 0 \\ \vdots & \vdots & \vdots & \ddots & \vdots & \vdots \\ \|\mathbf{x}^{n+1}\|^2 & -2\mathbf{x}^{n+1}\cdot\mathbf{x}^1 & -2\mathbf{x}^{n+1}\cdot\mathbf{x}^2 & \cdots & -2\mathbf{x}^{n+1}\cdot\mathbf{x}^n & 0 \\ 1 & 0 & 0 & \cdots & 0 & 0 \end{vmatrix}.$$

Expanding by the last row and column,

$$D = -\begin{vmatrix} -2\mathbf{x}^1\cdot\mathbf{x}^1 & -2\mathbf{x}^1\cdot\mathbf{x}^2 & \cdots & -2\mathbf{x}^1\cdot\mathbf{x}^n \\ -2\mathbf{x}^2\cdot\mathbf{x}^1 & -2\mathbf{x}^2\cdot\mathbf{x}^2 & \cdots & -2\mathbf{x}^2\cdot\mathbf{x}^n \\ \vdots & \vdots & \ddots & \vdots \\ -2\mathbf{x}^{n+1}\cdot\mathbf{x}^1 & -2\mathbf{x}^{n+1}\cdot\mathbf{x}^2 & \cdots & -2\mathbf{x}^{n+1}\cdot\mathbf{x}^n \end{vmatrix} = -(-2)^n \begin{vmatrix} \mathbf{x}^1\cdot\mathbf{x}^1 & \mathbf{x}^1\cdot\mathbf{x}^2 & \cdots & \mathbf{x}^1\cdot\mathbf{x}^n \\ \mathbf{x}^2\cdot\mathbf{x}^1 & \mathbf{x}^2\cdot\mathbf{x}^2 & \cdots & \mathbf{x}^2\cdot\mathbf{x}^n \\ \vdots & \vdots & \ddots & \vdots \\ \mathbf{x}^{n+1}\cdot\mathbf{x}^1 & \mathbf{x}^{n+1}\cdot\mathbf{x}^2 & \cdots & \mathbf{x}^{n+1}\cdot\mathbf{x}^n \end{vmatrix}.$$

Now without loss of generality we choose coordinates so that $\mathbf{x}^1 = (x_1^1, 0, 0, \ldots)$, $\mathbf{x}^2 = (x_1^2, x_2^2, 0, \ldots)$, …, $\mathbf{x}^n = (x_1^n, x_2^n, \ldots x_n^n)$, $\mathbf{x}^{n+1} = (x_1^{n+1}, x_2^{n+1}, \ldots x_n^{n+1})$. Notice that in

these coordinates the hyperplane inhabited by the common face is $\mathrm{span}(\mathbf{e}_1,\ldots,\mathbf{e}_{n-1})$, and so $\varepsilon = \mathrm{sign}(x_n^n x_n^{n+1})$. Then

$$RHS = \frac{\varepsilon(-1)^{n+1}}{(n!)^2 2^n} D = \frac{\varepsilon}{(n!)^2} \begin{vmatrix} x_1^1 x_1^1 & x_1^1 x_1^2 & \cdots & x_1^1 x_1^n \\ x_1^2 x_1^1 & x_1^2 x_1^2 + x_2^2 x_2^2 & \cdots & x_1^2 x_1^n + x_2^2 x_2^n \\ \vdots & \vdots & \ddots & \vdots \\ x_1^{n+1} x_1^1 & x_1^{n+1} x_1^2 + x_2^{n+1} x_2^2 & \cdots & x_1^{n+1} x_1^n + x_2^{n+1} x_2^n + \ldots \end{vmatrix}$$

$$= \frac{\varepsilon\, x_1^1}{(n!)^2} \begin{vmatrix} x_1^1 & x_1^1 x_1^2 & \cdots & x_1^1 x_1^n \\ x_1^2 & x_1^2 x_1^2 + x_2^2 x_2^2 & \cdots & x_1^2 x_1^n + x_2^2 x_2^n \\ \vdots & \vdots & \ddots & \vdots \\ x_1^{n+1} & x_1^{n+1} x_1^2 + x_2^{n+1} x_2^2 & \cdots & x_1^{n+1} x_1^n + x_2^{n+1} x_2^n + \ldots \end{vmatrix}.$$

Subtracting x_1^2 times the first column from the second, x_1^3 times the first column from the third, and so on, and then expanding by the first row,

$$RHS = \frac{\varepsilon\, x_1^1}{(n!)^2} \begin{vmatrix} x_1^1 & 0 & \cdots & 0 \\ x_1^2 & x_2^2 x_2^2 & \cdots & x_2^2 x_2^n \\ \vdots & \vdots & \ddots & \vdots \\ x_1^{n+1} & x_2^{n+1} x_2^2 & \cdots & x_2^{n+1} x_2^n + \ldots \end{vmatrix} = \frac{\varepsilon\,(x_1^1)^2}{(n!)^2} \begin{vmatrix} x_2^2 x_2^2 & \cdots & x_2^2 x_2^n \\ \vdots & \ddots & \vdots \\ x_2^{n+1} x_2^2 & \cdots & x_2^{n+1} x_2^n + \ldots \end{vmatrix}.$$

Now we repeat the procedure until, as final step, we obtain

$$RHS = \frac{\varepsilon\,(x_1^1)^2 (x_2^2)^2 \ldots (x_{n-2}^{n-2})^2}{(n!)^2} \begin{vmatrix} x_{n-1}^{n-1} x_{n-1}^{n-1} & x_{n-1}^{n-1} x_{n-1}^n \\ x_{n-1}^{n+1} x_{n-1}^{n-1} & x_{n-1}^{n+1} x_{n-1}^n + x_n^{n+1} x_n^n \end{vmatrix}$$

$$= \frac{\varepsilon\,(x_1^1)^2 (x_2^2)^2 \ldots (x_{n-1}^{n-1})^2 x_n^n x_n^{n+1}}{(n!)^2}.$$

Since $x_n^n x_n^{n+1} = \varepsilon |x_n^n x_n^{n+1}|$, this is equal to $\mathrm{vol}(v_n)\mathrm{vol}(v_{n+1})$, as required.

B.3 An application

Let $\mathbf{x}^i$, $i = 0, 1, 2, 3$, be vectors identifying four points on a plane. Embedding the plane in $\mathbb{R}^3$, the Cayley-Menger determinant for the volume of the simplex with these four vertices must vanish:

$$0 = \begin{vmatrix} 0 & X_{01} & X_{02} & X_{03} & 1 \\ X_{10} & 0 & X_{12} & X_{13} & 1 \\ X_{20} & X_{21} & 0 & X_{23} & 1 \\ X_{30} & X_{31} & X_{32} & 0 & 1 \\ 1 & 1 & 1 & 1 & 0 \end{vmatrix}$$

Differentiating the above equation,

$$0 = d\begin{vmatrix} 0 & X_{01} & X_{02} & X_{03} & 1 \\ X_{10} & 0 & X_{12} & X_{13} & 1 \\ X_{20} & X_{21} & 0 & X_{23} & 1 \\ X_{30} & X_{31} & X_{32} & 0 & 1 \\ 1 & 1 & 1 & 1 & 0 \end{vmatrix} = \begin{vmatrix} 0 & dX_{01} & dX_{02} & dX_{03} & 0 \\ X_{10} & 0 & X_{12} & X_{13} & 1 \\ X_{20} & X_{21} & 0 & X_{23} & 1 \\ X_{30} & X_{31} & X_{32} & 0 & 1 \\ 1 & 1 & 1 & 1 & 0 \end{vmatrix} + \begin{vmatrix} 0 & X_{01} & X_{02} & X_{03} & 1 \\ dX_{10} & 0 & dX_{12} & dX_{13} & 0 \\ X_{20} & X_{21} & 0 & X_{23} & 1 \\ X_{30} & X_{31} & X_{32} & 0 & 1 \\ 1 & 1 & 1 & 1 & 0 \end{vmatrix}$$
$$+ \begin{vmatrix} 0 & X_{01} & X_{02} & X_{03} & 1 \\ X_{10} & 0 & X_{12} & X_{13} & 1 \\ dX_{20} & dX_{21} & 0 & dX_{23} & 0 \\ X_{30} & X_{31} & X_{32} & 0 & 1 \\ 1 & 1 & 1 & 1 & 0 \end{vmatrix} + \begin{vmatrix} 0 & X_{01} & X_{02} & X_{03} & 1 \\ X_{10} & 0 & X_{12} & X_{13} & 1 \\ X_{20} & X_{21} & 0 & X_{23} & 1 \\ dX_{30} & dX_{31} & dX_{32} & 0 & 0 \\ 1 & 1 & 1 & 1 & 0 \end{vmatrix}.$$

Expanding this expression row by row and using the fact that the determinant of a matrix is equal to that of its transpose we obtain

$$0 = -2\,dX_{01}\begin{vmatrix} X_{10} & X_{12} & X_{13} & 1 \\ X_{20} & 0 & X_{23} & 1 \\ X_{30} & X_{32} & 0 & 1 \\ 1 & 1 & 1 & 0 \end{vmatrix} + 2\,dX_{02}\begin{vmatrix} X_{10} & 0 & X_{13} & 1 \\ X_{20} & X_{21} & X_{23} & 1 \\ X_{30} & X_{31} & 0 & 1 \\ 1 & 1 & 1 & 0 \end{vmatrix} - 2\,dX_{03}\begin{vmatrix} X_{10} & 0 & X_{12} & 1 \\ X_{20} & X_{21} & 0 & 1 \\ X_{30} & X_{31} & X_{32} & 1 \\ 1 & 1 & 1 & 0 \end{vmatrix}$$
$$-2\,dX_{12}\begin{vmatrix} 0 & X_{01} & X_{03} & 1 \\ X_{20} & X_{21} & X_{23} & 1 \\ X_{30} & X_{31} & 0 & 1 \\ 1 & 1 & 1 & 0 \end{vmatrix} + 2\,dX_{13}\begin{vmatrix} 0 & X_{01} & X_{02} & 1 \\ X_{20} & X_{21} & 0 & 1 \\ X_{30} & X_{31} & X_{32} & 1 \\ 1 & 1 & 1 & 0 \end{vmatrix} - 2\,dX_{23}\begin{vmatrix} 0 & X_{01} & X_{02} & 1 \\ X_{10} & 0 & X_{12} & 1 \\ X_{30} & X_{31} & X_{32} & 1 \\ 1 & 1 & 1 & 0 \end{vmatrix}$$

Swapping some judiciously-chosen rows and columns within the determinants and using the generalised Cayley-Menger determinant (B.2.1) we obtain

$$\begin{aligned} &\varepsilon_{01}(2,3)\Delta_{230}\Delta_{231}\,dX_{01} + \varepsilon_{02}(1,3)\Delta_{130}\Delta_{132}\,dX_{02} + \\ &\varepsilon_{03}(1,2)\Delta_{120}\Delta_{123}\,dX_{03} + \varepsilon_{12}(0,3)\Delta_{031}\Delta_{032}\,dX_{12} + \\ &\varepsilon_{13}(0,2)\Delta_{021}\Delta_{023}\,dX_{13} + \varepsilon_{23}(0,1)\Delta_{012}\Delta_{013}\,dX_{23} = 0. \end{aligned} \tag{B.3.1}$$

where $\varepsilon_{ij}(m,n) = +1/-1$ according to whether $\mathbf{x}^i$ and $\mathbf{x}^j$ lie on the same / opposite sides of the line connecting $\mathbf{x}^m$ and $\mathbf{x}^n$.

Let the lengths of the sides of the quadrilateral, defined by the ordered vertices $\mathbf{x}^i$ $(i = 0, 1, 2, 3)$, be fixed, so to move only its diagonals. This is equivalent to requiring $dX_{01} = dX_{12} = dX_{23} = dX_{30} = 0$. In this case the relation (B.3.1) becomes

$$\frac{dX_{13}}{dX_{02}} = -\frac{\varepsilon_{02}(1,3)}{\varepsilon_{13}(0,2)}\frac{\Delta_{130}\Delta_{132}}{\Delta_{021}\Delta_{023}} \tag{B.3.2}$$

If the quadrilateral is convex then $\varepsilon_{02}(1,3) = \varepsilon_{13}(0,2) < 0$ giving relation (4.1.3). Instead, if the quadrilateral is concave, then either $\varepsilon_{02}(1,3) = -\varepsilon_{13}(0,2) = 1$ or $\varepsilon_{02}(1,3) = -\varepsilon_{13}(0,2) = -1$. In both cases the RHS of (B.3.2) is positive and (4.1.4) holds.

It is important to note that in relation (B.3.1) triangles are defined by the names

of their vertices while in the rest of the thesis triangles are defined by the labels of their sides.

Appendix C

Cancelling second-order poles in 5-point amplitudes

In this appendix, the cancellation mechanism of second-order singularities associated with 5-point processes at the tree level is shown for a theory satisfying 'simply-laced scattering conditions'. We focus on a creation event of the form

$$A + B \to G + F + D, \tag{C.0.1}$$

where, with a bit of abuse of notation, we label by A, B, G, F and D both the momenta and the types of the interacting particles. In the analysed case, for a particular choice of the external kinematics, we assume there are in total six Feynman diagrams presenting a double pole. They are connected by flipping the internal propagators and are represented in figure C.1 on the vertices of a hexagon. Each side of the hexagon corresponds to one flip, in which one propagator remains fixed while the other one is modified. After a finite number of flips, the path of diagrams closes generating in this particular case a hexagon. The corresponding on-shell diagrams are reported in figure C.2.

We study the diagrams in the neighbourhood of the second-order singularity, where the propagators are affected by small variations with respect to their mass-shell condition. Looking for example at the diagram $D^{(1)}$ in figure C.1 (and at its on-shell description in figure C.2) its internal propagating momenta respect

$$|L^2 - m_L^2| \ll 1 \quad , \quad |E^2 - m_E^2| \ll 1. \tag{C.0.2}$$

The same is valid for the propagators entering in the other diagrams of the network. Using the parametrization (4.1.6) for the couplings, the first diagram can be written as

$$D^{(1)} = F^{(1)} \frac{\Delta_{ADL}\Delta_{BEL}\Delta_{EFG}}{(L^2 - m_L^2)\,(E^2 - m_E^2)} \tag{C.0.3}$$

where we have defined

$$F^{(1)} = f_{A\bar{D}\bar{L}} f_{LB\bar{E}} f_{E\bar{G}\bar{F}}.$$

The diagram $D^{(2)}$ in C.2 is connected to the first one by a flip of type III. For this reason, the product of the f-terms entering into the 3-point vertices of the second

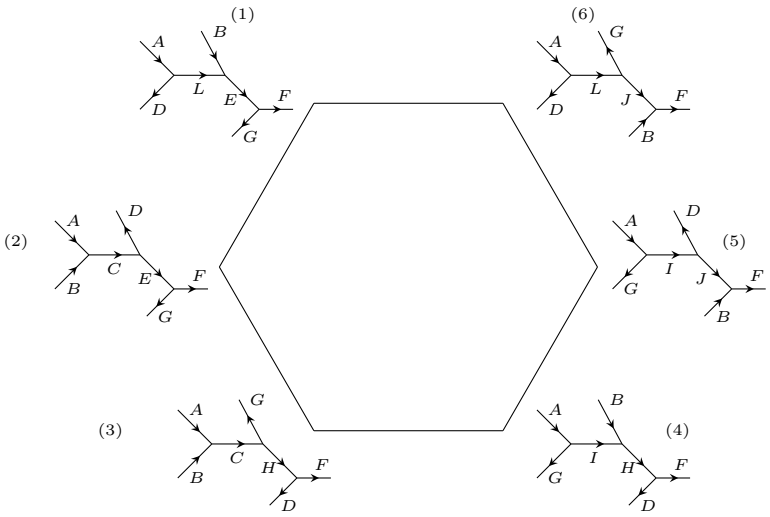

Figure C.1: Example of a network of singular Feynman diagrams in a non-allowed 5-point process.

diagram is $F^{(2)} = -F^{(1)}$, as explained in section 4.1, and we obtain

$$D^{(2)} = -F^{(1)} \frac{\Delta_{ABC}\Delta_{CDE}\Delta_{EFG}}{(E^2 - m_E^2)\ (C^2 - m_C^2)}. \tag{C.0.4}$$

Once we set the lengths of the external sides (those associated with the masses of the incoming and outgoing particles) we only have two remaining degrees of freedom to define the shape of the pentagon associated with the 5-point process (C.0.1). This means that the quantity $(C^2 - m_C^2)$ can be written as a function of $(E^2 - m_E^2)$ and $(L^2 - m_L^2)$. Since the propagators differ by small variations with respect to their on-shell condition we can use the relation in (B.3.1). Focusing on the polygon defined by the sides $\{E, D, A, B\}$ in the first diagram in C.2, having as diagonals C and L, we derive

$$C^2 - m_C^2 = \frac{\Delta_{ABC}}{\Delta_{BEL}}(E^2 - m_E^2) + \frac{\Delta_{ABC}\Delta_{CDE}}{\Delta_{BEL}\Delta_{ADL}}(L^2 - m_L^2). \tag{C.0.5}$$

Therefore

$$D^{(1)} + D^{(2)} = \frac{F^{(1)}\ \Delta_{EFG}}{(L^2 - m_L^2)\ (E^2 - m_E^2)\ (C^2 - m_C^2)}\Big[(C^2 - m_C^2)\ \Delta_{ADL}\Delta_{BEL} - (L^2 - m_L^2)\Delta_{ABC}\Delta_{CDE}\Big] = F^{(1)} \frac{\Delta_{ADL}\Delta_{ABC}\Delta_{EFG}}{(L^2 - m_L^2)(C^2 - m_C^2)}. \tag{C.0.6}$$

An interesting fact is that the sum of two diagrams connected by one flip is not zero, instead, it behaves as a new Feynman diagram-like object, with three areas at the numerator and the two terms $(L^2 - m_L^2)$ and $(C^2 - m_C^2)$ at the denominator. Indeed

the propagator $\frac{1}{E^2-m_E^2}$, common to $D^{(1)}$ and $D^{(2)}$, has disappeared and the sum of the two diagrams connected by the flip contains only two propagators. Let see what happens if we go forward summing also the diagram number (3). In this case, the diagram $D^{(3)}$ is connected to $D^{(2)}$ by a type-I flip, therefore the sign of the diagram does not change and we have $F^{(3)} = F^{(2)} = -F^{(1)}$. We can write

$$D^{(3)} = -F^{(1)} \frac{\Delta_{ABC}\Delta_{CGH}\Delta_{DFH}}{(C^2 - m_C^2)\ (H^2 - m_H^2)}. \tag{C.0.7}$$

Adding also this diagram to the sum it holds

$$\begin{aligned} D^{(1)} + D^{(2)} + D^{(3)} = & \frac{F^{(1)}\ \Delta_{ABC}}{(L^2 - m_L^2)(C^2 - m_C^2)(H^2 - m_H^2)} \\ & \times \Big[(H^2 - m_H^2)\ \Delta_{ADL}\Delta_{EFG} - (L^2 - m_L^2)\Delta_{CGH}\Delta_{DFH})\Big]. \end{aligned} \tag{C.0.8}$$

Using again the relation in (B.3.1) before on the polygon defined by sides $\{F, D, C, G\}$ and then on that one with sides $\{E, D, A, B\}$ we come to the identity

$$H^2 - m_H^2 = -\frac{\Delta_{DFH}\Delta_{BG}}{\Delta_{ABC}\Delta_{EFG}}(C^2 - m_C^2) + \frac{\Delta_{CGH}\Delta_{DFH}}{\Delta_{EFG}\Delta_{ADL}}(L^2 - m_L^2).$$

Substituting such expression in (C.0.8) we obtain

$$D^{(1)} + D^{(2)} + D^{(3)} = -F^{(1)} \frac{\Delta_{ADL}\Delta_{DFH}\Delta_{BG}}{(L^2 - m_L^2)(H^2 - m_H^2)}. \tag{C.0.9}$$

Once again the common propagator is disappeared and we obtain that the sum of $D^{(1)}$, $D^{(2)}$ and $D^{(3)}$ is a new 'Feynman diagram' not present in the initial network. Repeating these steps we find that the sum of the diagrams $D^{(1)}, \ldots, D^{(5)}$ in figure C.2 is a new diagram whose propagators are L and J. Such a diagram is exactly equal to $-D^{(6)}$ and the sum of all the diagrams in the network, close to the double pole, is equal to zero.

Another way to see that the sum of all the graphs is null on the 2^{nd}-order pole is to parametrise the propagators around the pole. A good choice for the parametrisation is the following

$$L^2 - m_L^2 = (x + a_1)\ \delta \quad , \quad E^2 - m_E^2 = (x + a_2)\ \delta \tag{C.0.10}$$

where a_1 and a_2 are two real numbers such that

$$a_1 - a_2 = \Delta_{ADL}\Delta_{BLE}\Delta_{EFG} \tag{C.0.11}$$

and δ is a parameter going to zero. What we are trying to do is keeping the limit on the double pole $\delta \to 0$. In doing this we can go close to the pole in different ways depending on the value of x. For example we can take $x \sim -a_1$; in this case in the limit $\delta \to 0$ the propagator $\frac{1}{L^2-m_L^2}$ diverges much faster than the propagator $\frac{1}{E^2-m_E^2}$. Any value of x corresponds to a particular direction we are following to go to the double pole.

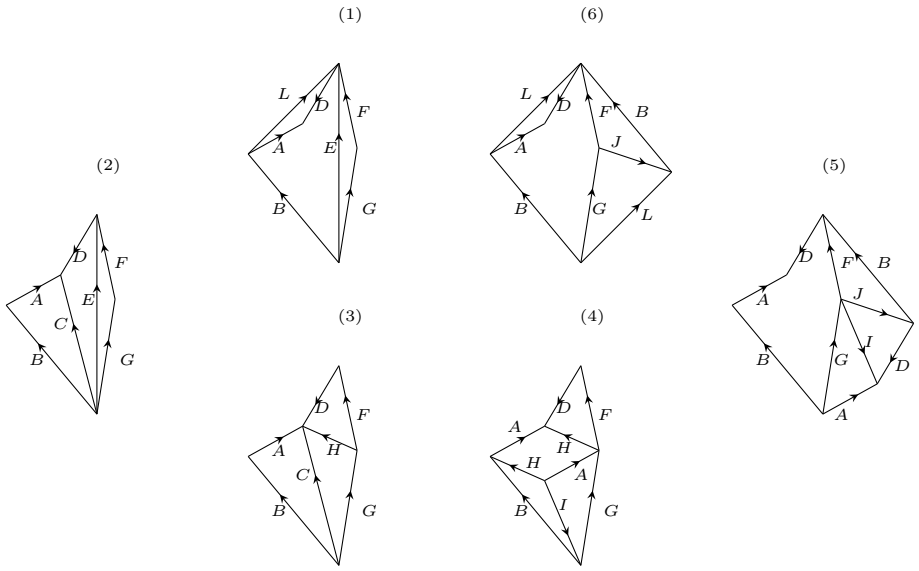

Figure C.2: On-shell representation of the singular Feynman diagrams in a non-allowed 5-point process.

The reason why we adopt the parametrisation in (C.0.10) will become clear in one moment. For now, we see that the diagram $D^{(1)}$ in figure C.2 can be written as

$$D^{(1)} = \frac{a_1 - a_2}{\delta^2 (x + a_1)(x + a_2)} \tag{C.0.12}$$

Using the relation in (C.0.5) we have

$$C^2 - m_C^2 = \delta\ (x + a_2)d + \delta\ (x + a_1)b \tag{C.0.13}$$

where we have defined

$$d = \frac{\Delta_{ABC}}{\Delta_{BEL}} \quad , \quad b = \frac{\Delta_{ABC}\Delta_{CDE}}{\Delta_{BEL}\Delta_{ADL}} = \frac{\Delta_{ABC}\Delta_{CDE}\Delta_{EFG}}{a_1 - a_2}. \tag{C.0.14}$$

If we write the second Feynman diagram in terms of these new parameters we obtain

$$\begin{aligned} D^{(2)} &= \frac{-b(a_1 - a_2)}{\delta^2 (x + a_2)\Big[(x + a_1)b + (x + a_2)d\Big]} \\ &= \frac{-b(a_1 - a_2)}{\delta^2 (x + a_2)(b + d)\Big[x + \frac{a_1 b + a_2 d}{b + d}\Big]} \end{aligned} \tag{C.0.15}$$

Now if we define

$$a_3 = \frac{a_1 b + a_2 d}{b + d} \tag{C.0.16}$$

we obtain

$$D^{(2)} = \frac{a_2 - a_3}{\delta^2 (x + a_2)(x + a_3)}. \tag{C.0.17}$$

When the expression in (C.0.17) has a pole for $x \sim -a_2$ (which means the propagating particle E goes on-shell much faster than the particle C) the expression in (C.0.12) has also a pole. This is because the propagator corresponding to the E particle is present in both diagrams. More interesting is that while the diagram $D^{(2)}$ for $x \to -a_2$ has residue equal to -1 the diagram $D^{(1)}$ has residue equal to 1. What we are observing is a mere consequence of the fact that when E goes on-shell the diagrams $D^{(1)}$ and $D^{(2)}$ present as residues two on-shell four-point graphs whose sum is non-singular. We are simply moving the poles of the propagators into the poles of the variable x regulating the direction that we are following to get close to the double pole position. After having repeated the previous steps for the other diagrams we obtain that around the double pole the tree-level 5-point amplitude is given by

$$\begin{aligned} M_5 &= \frac{1}{\delta^2}\left[\frac{a_1-a_2}{(x+a_1)(x+a_2)}+\frac{a_2-a_3}{(x+a_2)(x+a_3)}+\ldots+\frac{a_N-a_1}{(x+a_N)(x+a_1)}\right] \\ &= \frac{1}{\delta^2}\left[-\frac{1}{x+a_1}+\frac{1}{x+a_2}-\frac{1}{x+a_2}+\frac{1}{x+a_3}+\ldots-\frac{1}{x+a_N}+\frac{1}{x+a_1}\right]=0, \end{aligned} \tag{C.0.18}$$

where in this specific example $N = 6$. This is a telescoping sum and has an interesting consequence: when we sum more diagrams we care only about the value of the first one and of the last one. The coefficients a_j parametrise the space of Feynman diagrams.

Heuristically we can define a density function

$$\rho_x(a) = -\frac{1}{(x+a)^2} \tag{C.0.19}$$

defined on the space of the Feynman diagrams. If we integrate over the closed path given by the hexagon in figure C.2 we obtain zero,

$$\int_C da\ \rho_x(a) = 0 \tag{C.0.20}$$

independently by the value of x. On the other hand, if we integrate only on a connected part of the path we obtain

$$\int_{a_i}^{a_j} da\ \rho_x(a) = \frac{a_i-a_j}{(x+a_i)(x+a_j)} \tag{C.0.21}$$

This has the same structure as a Feynman diagram but now i and j are not consecutive in general. Therefore what we have written is a new Feynman diagram-like object not present in the initial network. In other words, the sum of Feynman diagrams along the path is still Feynman diagram-like object that combines different propagators. This reflects exactly the same result that we have found in (C.0.9) acting directly on the propagators. The sum over the Feynman diagrams of the entire network is then equal to zero since we are integrating over the entire closed path.

Appendix D

Some properties of structure constants

In this appendix some simple properties of the structure constants that have interesting consequences on the couplings of the corresponding Toda theory are derived. For a more detailed discussion we invite the interested reader to look at the chapter 4 of [121].

Property D.1. *If α, β and γ are three roots satisfying $\alpha+\beta+\gamma=0$ then $N_{\alpha\beta}=N_{\beta\gamma}=N_{\gamma\alpha}$*

Proof. Using the relations in (5.3.18) and (5.3.19b) we obtain

$$N_{\alpha\beta}=-\Big([e_\alpha,e_\beta],e_\gamma\Big)=-\Big(e_\alpha,[e_\beta,e_\gamma]\Big)=N_{\beta\gamma}$$

The rest of the equalities are proved by cyclicity. □

Property D.2. $N^*_{\alpha\beta}=N_{-\alpha,-\beta}$

Proof. Combining again (5.3.18) and (5.3.19b) we obtain

$$N^*_{\alpha\beta}e_{-\alpha-\beta}=-(N_{\alpha,\beta}\ e_{\alpha+\beta})^\dagger=-[e_\alpha,e_\beta]^\dagger=-[e_{-\beta},e_{-\alpha}]=N_{-\alpha,-\beta}\ e_{-\alpha-\beta}$$

□

Property D.3. *Given four roots α, β, γ, δ (with $\alpha\neq\gamma$, $\alpha\neq\delta$) such that $\alpha+\beta=\gamma+\delta=\epsilon$ where ϵ is another root, then*

$$N_{\alpha,\beta}N_{-\gamma,-\delta}-N_{\alpha,-\gamma}N_{\beta,-\delta}+N_{\alpha,-\delta}N_{\beta,-\gamma}=0 \tag{D.0.1}$$

and at least one of the following conditions (or both) are satisfied

- *$\gamma-\alpha=\beta-\delta=\rho$, with ρ root*
- *$\delta-\alpha=\beta-\gamma=\tilde{\rho}$, with $\tilde{\rho}$ root*

Proof. Since $\alpha+\beta$ and $\gamma+\delta$ correspond to the same root ϵ the two structure constants corresponding to $\{\alpha,\beta\}$ and $\{\gamma,\delta\}$ are nonzero and we can write their product in the following way

$$N_{\alpha,\beta}N_{-\gamma,-\delta} = -\Big([e_\alpha,e_\beta]\ ,[e_{-\gamma},e_{-\delta}]\Big) = -\Big(e_\alpha\ ,[e_\beta,[e_{-\gamma},e_{-\delta}]\ ]\Big) \tag{D.0.2}$$

where (5.3.18) and (5.3.19b) have been used. At this point we use the Jacobi identity and obtain

$$\begin{aligned} N_{\alpha,\beta}N_{-\gamma,-\delta} &= \Big(e_\alpha\ ,[e_{-\gamma},[e_{-\delta},e_\beta]\ ]\Big) + \Big(e_\alpha\ ,[e_{-\delta},[e_\beta,e_{-\gamma}]\ ]\Big) \\ &= \Big([e_\alpha,e_{-\gamma}],[e_{-\delta},e_\beta]\ ]\Big) + \Big([e_\alpha,e_{-\delta}],[e_\beta,e_{-\gamma}]\ ]\Big) \\ &= N_{\alpha,-\gamma}N_{-\delta,\beta}(e_{-\rho},e_\rho) + N_{\alpha,-\delta}N_{\beta,-\gamma}(e_{-\tilde\rho},e_{\tilde\rho}) \end{aligned}$$

From this fact using the convention in (5.3.18) and the antisymmetry of the structure constants we obtain (D.0.1).

It is clear that if $\gamma-\alpha$ $(=\beta-\delta)$ or $\delta-\alpha$ $(=\beta-\gamma)$ is not a root we have that $N_{\alpha,-\gamma}$ or $N_{\alpha,-\delta}$ respectively is equal to zero. However since the equality in (D.0.1) always holds and we know that the first term in the sum is nonzero then also the second or the third term in the sum (or both) need to be different from zero, that means that at least one of $\gamma-\alpha$ and $\delta-\alpha$ is a root. □

This fact is of fundamental importance in the cancellation of 2-to-2 non-diagonal processes in affine Toda models. We highlight that in simply-laced theories $\alpha-\gamma$ and $\alpha-\delta$ cannot both be roots at the same time. Indeed in this case, setting the root length equal to $\sqrt{2}$, and assuming that $\alpha-\gamma$ is a root, the equalities $(\alpha+\beta)^2=2$ and $(\alpha-\gamma)^2=2$ imply $(\alpha,\beta)=-1$ and $(\alpha,\gamma)=1$. Hence $(\alpha,\delta)=(\alpha,\alpha+\beta-\gamma)=2-1-1=0$ and so $(\alpha-\delta)^2=4$, and $\alpha-\delta$ is not a root.

Property D.4. *The ratios of the structure constants of any semisimple Lie algebra take specific values. In particular if the long roots of $\mathcal{G}$ are normalised to length $\sqrt{2}$ we have the following possibilities: if there are three roots α, β and γ satisfying $\alpha+\beta+\gamma=0$ we can have*

- $|N_{\alpha,\beta}|=1$ *if* $|\alpha|=|\beta|=|\gamma|=\sqrt{2}$ *or there is one root of length* $\sqrt{2}$ *and the other two are shorter and with the same length.*
- $|N_{\alpha,\beta}|=\frac{1}{\sqrt{2}}$ *if* $|\alpha|=|\beta|=|\gamma|=1$.
- $|N_{\alpha,\beta}|=\frac{2}{\sqrt{3}}$ *if* $|\alpha|=|\beta|=|\gamma|=\sqrt{\frac{2}{3}}$.

while in all the other cases $|N_{\alpha,\beta}|=0$.

Proof. We can write the absolute value of the structure constant corresponding to two roots α, β in the following form

$$\begin{aligned} |N_{\alpha\beta}|^2 &= \Big(N_{\alpha\beta}\ e_{\alpha+\beta}\ ,\ N^*_{\alpha\beta}\ e^\dagger_{\alpha+\beta}\Big) = \Big([e_\alpha,e_\beta]\ ,\ [e_{-\beta},e_{-\alpha}]\Big) = \Big([[e_\alpha,e_\beta]\ ,e_{-\beta}]\ ,\ e_{-\alpha}\Big) \\ &= -([[e_{-\beta},e_\alpha]\ ,e_\beta]\ ,\ e_{-\alpha}) - ([[e_\beta,e_{-\beta}]\ ,e_\alpha]\ ,\ e_{-\alpha}) = N_{-\beta,\alpha}N_{\alpha-\beta,\beta} - (\beta\ ,\ \alpha) \end{aligned}$$

Combining properties D.1 and D.2 we have

$$N_{\alpha-\beta,\beta} = N_{\beta,-\alpha} = N^*_{-\beta,\alpha}$$

and therefore we obtain

$$|N_{\alpha,\beta}|^2 = |N_{-\beta,\alpha}|^2 - (\beta\ ,\ \alpha). \tag{D.0.3}$$

All the absolute values of the structure constants can be obtained from this equality. We focus on the case in which $|\alpha| = |\beta| < |\gamma| = \sqrt{2}$; the other situations can be studied similarly. By the fact that α, β and γ close a triangle and $\alpha^2 = \beta^2$ the following relation holds

$$\alpha^2 = \gamma^2 + \beta^2 + 2(\gamma,\beta) \to 2(\gamma,\beta) = -\gamma^2. \tag{D.0.4}$$

We observe that the vector $\gamma - \beta$ cannot be a root since

$$(\gamma-\beta)^2 = 2\gamma^2 + \beta^2 > 4 \tag{D.0.5}$$

which is bigger of the maximal allowed length. Therefore from the expression in (D.0.3) we obtain

$$|N_{\gamma,\beta}| = -(\gamma,\beta) = \frac{\gamma^2}{2} = 1 \tag{D.0.6}$$

All the other situations can be analogously studied. □

Bibliography

[1] P. Dorey and D. Polvara, "Tree level integrability in 2d quantum field theories and affine Toda models," JHEP **02** (2022), 199 doi:10.1007/JHEP02(2022)199 [arXiv:2111.02210 [hep-th]].

[2] P. Dorey and D. Polvara, In preparation

[3] P. Dorey and D. Polvara, In preparation

[4] E. Ising,"Beitrag zur Theorie des Ferromagnetismus," Z. Physik **31** (1925) 253. doi.org/10.1007/BF02980577

[5] L. Onsager, "Crystal statistics. 1. A Two-dimensional model with an order disorder transition," Phys. Rev. **65** (1944), 117-149 doi:10.1103/PhysRev.65.117

[6] A. M. Polyakov, "Conformal symmetry of critical fluctuations," JETP Lett. **12** (1970), 381-383 jetpletters.ru/ps/1737/article26381.shtml

[7] A. M. Polyakov, "Nonhamiltonian approach to conformal quantum field theory," Zh. Eksp. Teor. Fiz. **66** (1974), 23-42 http://www.jetp.ras.ru/cgi-bin/dn/e_039_01_0010.pdf

[8] V. G. Kac (1979) "Contravariant form for infinite-dimensional Lie algebras and superalgebras". Lecture Notes in Physics **94** (1979), 441-445 doi.org/10.1007/3-540-09238-2_102

[9] A. A. Belavin, A. M. Polyakov and A. B. Zamolodchikov, "Infinite Conformal Symmetry in Two-Dimensional Quantum Field Theory," Nucl. Phys. B **241** (1984), 333-380 doi:10.1016/0550-3213(84)90052-X

[10] D. Friedan, Z. a. Qiu and S. H. Shenker, "Conformal Invariance, Unitarity and Two-Dimensional Critical Exponents," Phys. Rev. Lett. **52** (1984), 1575-1578 doi:10.1103/PhysRevLett.52.1575

[11] D. A. Huse, "Exact exponents for infinitely many new multicritical points," Phys. Rev. B **30** (1984), 3908-3915 doi:10.1103/PhysRevB.30.3908

[12] A. B. Zamolodchikov, "Infinite Additional Symmetries in Two-Dimensional Conformal Quantum Field Theory," Theor. Math. Phys. **65** (1985), 1205-1213 doi:10.1007/BF01036128

[13] D. Friedan, Z. a. Qiu and S. H. Shenker, "Superconformal Invariance in Two-Dimensions and the Tricritical Ising Model," Phys. Lett. B **151** (1985), 37-43 doi:10.1016/0370-2693(85)90819-6

[14] V. G. Knizhnik and A. B. Zamolodchikov, "Current Algebra and Wess-Zumino Model in Two-Dimensions," Nucl. Phys. B **247** (1984), 83-103 doi:10.1016/0550-3213(84)90374-2

[15] P. Goddard, A. Kent and D. I. Olive, "Virasoro Algebras and Coset Space Models," Phys. Lett. B **152** (1985), 88-92 doi:10.1016/0370-2693(85)91145-1

[16] P. Goddard, A. Kent and D. I. Olive, "Unitary Representations of the Virasoro and Supervirasoro Algebras," Commun. Math. Phys. **103** (1986), 105-119 doi:10.1007/BF01464283

[17] R. J. Eden, P. V. Landshoff, D. I. Olive and J. C. Polkinghorne, "The analytic S-matrix," Cambridge at the University Press (1966)

[18] A. B. Zamolodchikov and A. B. Zamolodchikov, "Factorized s Matrices in Two-Dimensions as the Exact Solutions of Certain Relativistic Quantum Field Models," Annals Phys. **120** (1979) 253. doi:10.1016/0003-4916(79)90391-9.

[19] A. B. Zamolodchikov, "Integrals of Motion and S Matrix of the (Scaled) T=T(c) Ising Model with Magnetic Field," Int. J. Mod. Phys. A **4** (1989), 4235 doi:10.1142/S0217751X8900176X

[20] A. B. Zamolodchikov, "Integrable field theory from conformal field theory," Adv. Stud. Pure Math. **19** (1989), 641-674 doi.org/10.1016/B978-0-12-385342-4.50022-6

[21] S. J. Parke, "Absence of Particle Production and Factorization of the S Matrix in (1+1)-dimensional Models," Nucl. Phys. B **174** (1980) 166. doi:10.1016/0550-3213(80)90196-0.

[22] A. B. Zamolodchikov, "Thermodynamic Bethe Ansatz in Relativistic Models. Scaling Three State Potts and Lee-yang Models," Nucl. Phys. B **342** (1990), 695-720 doi:10.1016/0550-3213(90)90333-9

[23] T. R. Klassen and E. Melzer, "Purely Elastic Scattering Theories and their Ultraviolet Limits," Nucl. Phys. B **338** (1990) 485. doi:10.1016/0550-3213(90)90643-R.

[24] V. A. Fateev and A. B. Zamolodchikov, "Conformal field theory and purely elastic S matrices," Int. J. Mod. Phys. A **5** (1990), 1025-1048 doi:10.1142/S0217751X90000477

[25] G. Sotkov and C. J. Zhu, "Bootstrap Fusions and Tricritical Potts Model Away From Criticality," Phys. Lett. B **229** (1989), 391-397 doi:10.1016/0370-2693(89)90425-5

[26] R. Rattazzi, V. S. Rychkov, E. Tonni and A. Vichi, "Bounding scalar operator dimensions in 4D CFT," JHEP **12** (2008), 031 doi:10.1088/1126-6708/2008/12/031 [arXiv:0807.0004 [hep-th]].

[27] S. El-Showk, M. F. Paulos, D. Poland, S. Rychkov, D. Simmons-Duffin and A. Vichi, "Solving the 3D Ising Model with the Conformal Bootstrap," Phys. Rev. D **86** (2012), 025022 doi:10.1103/PhysRevD.86.025022 [arXiv:1203.6064 [hep-th]].

[28] S. El-Showk, M. F. Paulos, D. Poland, S. Rychkov, D. Simmons-Duffin and A. Vichi, "Solving the 3d Ising Model with the Conformal Bootstrap II. c-Minimization and Precise Critical Exponents," J. Stat. Phys. **157** (2014), 869 doi:10.1007/s10955-014-1042-7 [arXiv:1403.4545 [hep-th]].

[29] F. Kos, D. Poland and D. Simmons-Duffin, "Bootstrapping Mixed Correlators in the 3D Ising Model," JHEP **11** (2014), 109 doi:10.1007/JHEP11(2014)109 [arXiv:1406.4858 [hep-th]].

[30] F. Kos, D. Poland, D. Simmons-Duffin and A. Vichi, "Precision Islands in the Ising and $O(N)$ Models," JHEP **08** (2016), 036 doi:10.1007/JHEP08(2016)036 [arXiv:1603.04436 [hep-th]].

[31] M. F. Paulos, J. Penedones, J. Toledo, B. C. van Rees and P. Vieira, "The S-matrix bootstrap II: two dimensional amplitudes," JHEP **11** (2017), 143 doi:10.1007/JHEP11(2017)143 [arXiv:1607.06110 [hep-th]].

[32] A. Guerrieri, J. Penedones and P. Vieira, "Where Is String Theory in the Space of Scattering Amplitudes?," Phys. Rev. Lett. **127** (2021) no.8, 081601 doi:10.1103/PhysRevLett.127.081601 [arXiv:2102.02847 [hep-th]].

[33] M. Kruczenski, J. Penedones and B. C. van Rees, "Snowmass White Paper: S-matrix Bootstrap," [arXiv:2203.02421 [hep-th]].

[34] K. Costello and M. Yamazaki, "Gauge Theory And Integrability, III," [arXiv:1908.02289 [hep-th]].

[35] B. Hoare, "Integrable deformations of sigma models," J. Phys. A **55** (2022) no.9, 093001 doi:10.1088/1751-8121/ac4a1e [arXiv:2109.14284 [hep-th]].

[36] P. Dorey, "Exact S matrices," hep-th/9810026.

[37] B. Gabai, D. Mazáč, A. Shieber, P. Vieira and Y. Zhou, "No Particle Production in Two Dimensions: Recursion Relations and Multi-Regge Limit," JHEP **1902** (2019) 094 doi:10.1007/JHEP02(2019)094 [arXiv:1803.03578 [hep-th]].

[38] D. I. Olive and N. Turok, "Local Conserved Densities and Zero Curvature Conditions for Toda Lattice Field Theories," Nucl. Phys. B **257** (1985) 277. doi:10.1016/0550-3213(85)90347-5.

[39] S. R. Coleman and H. J. Thun, "On the Prosaic Origin of the Double Poles in the Sine-Gordon S Matrix," Commun. Math. Phys. **61** (1978), 31 doi:10.1007/BF01609466

[40] D. Bombardelli, "S-matrices and integrability," J. Phys. A **49** (2016) no.32, 323003 doi:10.1088/1751-8113/49/32/323003 [arXiv:1606.02949 [hep-th]].

[41] P. Fendley and H. Saleur, "Massless integrable quantum field theories and massless scattering in (1+1)-dimensions," [arXiv:hep-th/9310058 [hep-th]].

[42] A. Sfondrini, "Towards integrability for AdS_3/CFT_2," J. Phys. A **48** (2015) no.2, 023001 doi:10.1088/1751-8113/48/2/023001 [arXiv:1406.2971 [hep-th]].

[43] L. D. Faddeev, "Quantum completely integral models of field theory," Sov. Sci. Rev. C **1** (1980), 107-155

[44] D. Bernard and A. Leclair, "Quantum group symmetries and nonlocal currents in 2-D QFT," Commun. Math. Phys. **142** (1991), 99-138 doi:10.1007/BF02099173

[45] M. Luscher, "Quantum Nonlocal Charges and Absence of Particle Production in the Two-Dimensional Nonlinear Sigma Model," Nucl. Phys. B **135** (1978), 1-19 doi:10.1016/0550-3213(78)90211-0

[46] F. Loebbert, "Lectures on Yangian Symmetry," J. Phys. A **49** (2016) no.32, 323002 doi:10.1088/1751-8113/49/32/323002 [arXiv:1606.02947 [hep-th]].

[47] A. M. Polyakov, "Hidden Symmetry of the Two-Dimensional Chiral Fields," Phys. Lett. B **72** (1977), 224-226 doi:10.1016/0370-2693(77)90707-9

[48] R. Shankar and E. Witten, "The S Matrix of the Supersymmetric Nonlinear Sigma Model," Phys. Rev. D **17** (1978), 2134 doi:10.1103/PhysRevD.17.2134

[49] Coldea, Radu, et al. "Quantum criticality in an Ising chain: experimental evidence for emergent E_8 symmetry." Science 327.5962 (2010): 177-180. doi: 10.1126/science.1180085

[50] M. Karowski, "On the Bound State Problem in (1+1)-dimensional Field Theories," Nucl. Phys. B **153** (1979), 244-252 doi:10.1016/0550-3213(79)90600-X

[51] A. B. Zamolodchikov, "Irreversibility of the Flux of the Renormalization Group in a 2D Field Theory," JETP Lett. **43** (1986), 730-732

[52] J. L. Cardy and G. Mussardo, "S Matrix of the Yang-Lee Edge Singularity in Two-Dimensions," Phys. Lett. B **225** (1989), 275-278 doi:10.1016/0370-2693(89)90818-6

[53] S. J. van Tongeren, "Introduction to the thermodynamic Bethe ansatz," J. Phys. A **49** (2016) no.32, 323005 doi:10.1088/1751-8113/49/32/323005 [arXiv:1606.02951 [hep-th]].

[54] G. Mussardo, "Off critical statistical models: Factorized scattering theories and bootstrap program," Phys. Rept. **218** (1992), 215-379 doi:10.1016/0370-1573(92)90047-4

[55] T. Eguchi and S. K. Yang, "Deformations of Conformal Field Theories and Soliton Equations," Phys. Lett. B **224** (1989), 373-378 doi:10.1016/0370-2693(89)91463-9

[56] T. J. Hollowood and P. Mansfield, "Rational Conformal Field Theories At, and Away From, Criticality as Toda Field Theories," Phys. Lett. B **226** (1989), 73 doi:10.1016/0370-2693(89)90291-8

[57] H. W. Braden, E. Corrigan, P. E. Dorey and R. Sasaki, "Affine Toda Field Theory and Exact S Matrices," Nucl. Phys. B **338** (1990) 689. doi:10.1016/0550-3213(90)90648-W.

[58] C. J. Goebel, "On the Sine-Gordon S Matrix," Prog. Theor. Phys. Suppl. **86** (1986), 261-273 doi:10.1143/PTPS.86.261

[59] I. Arefeva and V. Korepin, "Scattering in two-dimensional model with Lagrangian (1/gamma) ((d(mu)u)**2/2 + m**2 cos(u-1))," Pisma Zh. Eksp. Teor. Fiz. **20** (1974), 680

[60] C. Kalousios, C. Vergu and A. Volovich, "Factorized Tree-level Scattering in AdS(4) x CP**3," JHEP **09** (2009), 049 doi:10.1088/1126-6708/2009/09/049 [arXiv:0905.4702 [hep-th]].

[61] B. Hoare, N. Levine and A. A. Tseytlin, "On the massless tree-level S-matrix in 2d sigma models," J. Phys. A **52** (2019) no.14, 144005 doi:10.1088/1751-8121/ab0b79 [arXiv:1812.02549 [hep-th]].

[62] C. R. Nappi, "Some Properties of an Analog of the Nonlinear σ Model," Phys. Rev. D **21** (1980), 418 doi:10.1103/PhysRevD.21.418

[63] S. P. Khastgir, "Affine Toda field theory from tree unitarity," Eur. Phys. J. C **33** (2004) 137 doi:10.1140/epjc/s2003-01523-7 [hep-th/0308032].

[64] C. Bercini and D. Trancanelli, "Supersymmetric integrable theories without particle production," Phys. Rev. D **97** (2018) no.10, 105013 doi:10.1103/PhysRevD.97.105013 [arXiv:1803.03612 [hep-th]].

[65] L. Wulff, "Integrability of the superstring in $AdS_3\times S^2\times S^2\times T^3$," J. Phys. A **50** (2017) no.23, 23LT01 doi:10.1088/1751-8121/aa70b5 [arXiv:1702.08788 [hep-th]].

[66] L. Wulff, "Classifying integrable symmetric space strings via factorized scattering," JHEP **02** (2018), 106 doi:10.1007/JHEP02(2018)106 [arXiv:1711.00296 [hep-th]].

[67] Gareth. A. Jones, David Singerman, "Complex Functions" (Cambridge University Press, 1987), Chapter 4.

[68] G. Mittag-Leffler, An Introduction to the Theory of Elliptic Functions. Annals of Mathematics, 24(4), second series (1923), 271. doi:10.2307/1967677

[69] H. W. Braden, E. Corrigan, P. E. Dorey and R. Sasaki, "Multiple poles and other features of affine Toda field theory," Nucl. Phys. B **356** (1991) 469. doi:10.1016/0550-3213(91)90317-Q

[70] P. Christe and G. Mussardo, "Elastic S Matrices in (1+1)-Dimensions and Toda Field Theories," Int. J. Mod. Phys. A **5** (1990) 4581. doi:10.1142/S0217751X90001938.

[71] A. Koubek, G. Mussardo and R. Tateo, "Bootstrap trees and consistent S matrices," Int. J. Mod. Phys. A **7** (1992), 3435-3446 doi:10.1142/S0217751X92001526

[72] V. G. Kac, "Infinite-dimensional Lie algebras", third ed., Cambridge University Press, Cambridge, 1990.

[73] P. Dorey, "Root systems and purely elastic S matrices," Nucl. Phys. B **358** (1991) 654. doi:10.1016/0550-3213(91)90428-Z.

[74] P. Dorey, "Root systems and purely elastic S matrices. 2.," Nucl. Phys. B **374** (1992) 741 doi:10.1016/0550-3213(92)90407-3 [hep-th/9110058].

[75] M. D. Freeman, "On the mass spectrum of affine Toda field theory," Phys. Lett. B **261** (1991) 57. doi:10.1016/0370-2693(91)91324-O

[76] A. Fring, H. C. Liao and D. I. Olive, "The Mass spectrum and coupling in affine Toda theories," Phys. Lett. B **266** (1991) 82 doi:10.1016/0370-2693(91)90747-E

[77] A. Fring, "Couplings in affine Toda field theories," hep-th/9212107.

[78] H. W. Braden and R. Sasaki, "The S matrix coupling dependence for a, d and e affine toda field theory," Phys. Lett. B **255** (1991) 343. doi:10.1016/0370-2693(91)90777-N

[79] H. W. Braden and R. Sasaki, "Affine Toda perturbation theory," Nucl. Phys. B **379** (1992) 377. doi:10.1016/0550-3213(92)90601-7

[80] A. V. Mikhailov, M. A. Olshanetsky and A. M. Perelomov, "Two-Dimensional Generalized Toda Lattice," Commun. Math. Phys. **79** (1981) 473. doi:10.1007/BF01209308.

[81] L. Faddeev, "In Recent advances in field theory and statistical mechanics", Les Houches Summer School Proc., Vol. 39 (North-Holland, Amsterdam, 1984)

[82] B. Feigin and E. Frenkel, "Integrals of motion and quantum groups," Lect. Notes Math. **1620** (1996), 349-418 doi:10.1007/BFb0094794 [arXiv:hep-th/9310022 [hep-th]].

[83] B. Kostant, "The Principal Three-Dimensional Subgroup and the Betti Numbers of a Complex Simple Lie Group," Am. J. Math. **81** (1959) 973 https://www.jstor.org/stable/2372999.

[84] R. Steinberg, "Finite reflection groups," Transactions of the American Mathematical Society **91** (1959) 493.

[85] E. Corrigan, "Recent developments in affine Toda quantum field theory," [arXiv:hep-th/9412213 [hep-th]].

[86] J. M. Evans, M. Hassan, N. J. MacKay and A. J. Mountain, "Local conserved charges in principal chiral models," Nucl. Phys. B **561** (1999), 385-412 doi:10.1016/S0550-3213(99)00489-7 [arXiv:hep-th/9902008 [hep-th]].

[87] J. M. Evans, "Integrable sigma models and Drinfeld-Sokolov hierarchies," Nucl. Phys. B **608** (2001), 591-609 doi:10.1016/S0550-3213(01)00157-2 [arXiv:hep-th/0101231 [hep-th].

[88] P. Dorey, "Hidden geometrical structures in integrable models," Proceedings of the conference 'Integrable Quantum Field Theories,' Como, 1992 [arXiv:hep-th/9212143 [hep-th]].

[89] D. I. Olive and N. Turok, "The Symmetries of Dynkin Diagrams and the Reduction of Toda Field Equations," Nucl. Phys. B **215** (1983), 470-494 doi:10.1016/0550-3213(83)90256-0

[90] E. Frenkel and D. Ben-Zvi, "Vertex algebras and algebraic curves, second ed.", American Mathematical Society **No. 88** (2004).

[91] A. E. Arinshtein, V. A. Fateev and A. B. Zamolodchikov, "Quantum s Matrix of the (1+1)-Dimensional Todd Chain," Phys. Lett. **87B** (1979) 389. doi:10.1016/0370-2693(79)90561-6.

[92] A. Fring and D. I. Olive, "The Fusing rule and the scattering matrix of affine Toda theory," Nucl. Phys. B **379** (1992), 429-447 doi:10.1016/0550-3213(92)90602-8

[93] P. G. O. Freund, T. R. Klassen and E. Melzer, "S Matrices for Perturbations of Certain Conformal Field Theories," Phys. Lett. B **229** (1989) 243. doi:10.1016/0370-2693(89)91165-9.

[94] P. Christe and G. Mussardo, "Integrable Systems Away from Criticality: The Toda Field Theory and S Matrix of the Tricritical Ising Model," Nucl. Phys. B **330** (1990) 465. doi:10.1016/0550-3213(90)90119-X.

[95] C. Destri and H. J. de Vega, "The Exact S Matrix of the Affine $E(8)$ Toda Field Theory," Phys. Lett. B **233** (1989) 336. doi:10.1016/0370-2693(89)91319-1.

[96] H. W. Braden, E. Corrigan, P. E. Dorey and R. Sasaki, "Extended Toda Field Theory and Exact S Matrices," Phys. Lett. B **227** (1989) 411. doi:10.1016/0370-2693(89)90952-0.

[97] R. Sasaki and F. P. Zen, "The affine Toda S matrices versus perturbation theory," Int. J. Mod. Phys. A **8** (1993), 115-134 doi:10.1142/S0217751X93000059

[98] H. W. Braden, H. S. Cho, J. D. Kim, I. G. Koh and R. Sasaki, "Singularity analysis in A(n) affine Toda theories," Prog. Theor. Phys. **88** (1992), 1205-1212 doi:10.1143/PTP.88.1205 [arXiv:hep-th/9207025].

[99] G. W. Delius, M. T. Grisaru and D. Zanon, "Exact S matrices for the non simply-laced affine Toda theories a(2)(2n-1)," Phys. Lett. B **277** (1992) 414 doi:10.1016/0370-2693(92)91804-I [hep-th/9112007].

[100] G. W. Delius, M. T. Grisaru and D. Zanon, "Exact S matrices for non simply-laced affine Toda theories," Nucl. Phys. B **382** (1992) 365 doi:10.1016/0550-3213(92)90190-M [hep-th/9201067].

[101] E. Corrigan, P. E. Dorey and R. Sasaki, "On a generalized bootstrap principle," Nucl. Phys. B **408** (1993), 579 doi:10.1016/0550-3213(93)90381-X [arXiv:hep-th/9304065 [hep-th]].

[102] P. Dorey, "A Remark on the coupling dependence in affine Toda field theories," Phys. Lett. B **312** (1993), 291 doi:10.1016/0370-2693(93)91083-Y [arXiv:hep-th/9304149 [hep-th]].

[103] T. Oota, "q deformed Coxeter element in non simply-laced affine Toda field theories," Nucl. Phys. B **504** (1997), 738-752 doi:10.1016/S0550-3213(97)00555-5 [hep-th/9706054].

[104] P. Dorey, "The exact s-matrices of affine toda field theories," Doctoral thesis, Durham University.

[105] G. W. Delius, M. T. Grisaru and D. Zanon, "Quantum conserved currents in affine Toda theories," Nucl. Phys. B **385** (1992), 307-328 doi:10.1016/0550-3213(92)90103-I [arXiv:hep-th/9202069 [hep-th]].

[106] L. Bianchi, V. Forini and B. Hoare, "Two-dimensional S-matrices from unitarity cuts," JHEP **07** (2013), 088 doi:10.1007/JHEP07(2013)088 [arXiv:1304.1798 [hep-th]].

[107] L. Bianchi and B. Hoare, "$AdS_3 \times S^3 \times M^4$ string S-matrices from unitarity cuts," JHEP **08** (2014), 097 doi:10.1007/JHEP08(2014)097 [arXiv:1405.7947 [hep-th]].

[108] G. W. Delius, M. T. Grisaru, S. Penati and D. Zanon, "The Exact S matrices of affine Toda theories based on Lie superalgebras," Phys. Lett. B **256** (1991) 164. doi:10.1016/0370-2693(91)90668-G.

[109] G. W. Delius, M. T. Grisaru, S. Penati and D. Zanon, "Exact S matrix and perturbative calculations in affine Toda theories based on Lie superalgebras," Nucl. Phys. B **359** (1991) 125. doi:10.1016/0550-3213(91)90295-9.

[110] F. A. Smirnov and A. B. Zamolodchikov, "On space of integrable quantum field theories," Nucl. Phys. B **915** (2017), 363-383 doi:10.1016/j.nuclphysb.2016.12.014 [arXiv:1608.05499 [hep-th]].

[111] A. Cavaglià, S. Negro, I. M. Szécsényi and R. Tateo, "$T\bar{T}$-deformed 2D Quantum Field Theories," JHEP **10** (2016), 112 doi:10.1007/JHEP10(2016)112 [arXiv:1608.05534 [hep-th]].

[112] G. Bonelli, N. Doroud and M. Zhu, "$T\bar{T}$-deformations in closed form," JHEP **06** (2018), 149 doi:10.1007/JHEP06(2018)149 [arXiv:1804.10967 [hep-th]].

[113] S. Ghoshal and A. B. Zamolodchikov, "Boundary S matrix and boundary state in two-dimensional integrable quantum field theory," Int. J. Mod. Phys. A **9** (1994), 3841-3886 [erratum: Int. J. Mod. Phys. A **9** (1994), 4353] doi:10.1142/S0217751X94001552 [arXiv:hep-th/9306002 [hep-th]].

[114] G. Delfino, G. Mussardo and P. Simonetti, "Scattering theory and correlation functions in statistical models with a line of defect," Nucl. Phys. B **432** (1994), 518-550 doi:10.1016/0550-3213(94)90032-9 [arXiv:hep-th/9409076 [hep-th]].

[115] P. Bowcock, E. Corrigan, P. E. Dorey and R. H. Rietdijk, "Classically integrable boundary conditions for affine Toda field theories," Nucl. Phys. B **445** (1995) 469 doi:10.1016/0550-3213(95)00153-J [hep-th/9501098].

[116] P. Bowcock, E. Corrigan and C. Zambon, "Affine Toda field theories with defects," JHEP **0401** (2004) 056 doi:10.1088/1126-6708/2004/01/056 [hep-th/0401020].

[117] P. Dorey, R. Tateo and G. Watts, "Generalizations of the Coleman-Thun mechanism and boundary reflection factors," Phys. Lett. B **448** (1999), 249-256 doi:10.1016/S0370-2693(99)00004-0 [arXiv:hep-th/9810098 [hep-th]].

[118] Z. Bajnok, G. Bohm and G. Takacs, "On perturbative quantum field theory with boundary," Nucl. Phys. B **682** (2004), 585-617 doi:10.1016/j.nuclphysb.2004.01.018 [arXiv:hep-th/0309119 [hep-th]].

[119] S. Penati, A. Refolli and D. Zanon, "Classical versus quantum symmetries for Toda theories with a nontrivial boundary perturbation," Nucl. Phys. B **470** (1996) 396 doi:10.1016/0550-3213(96)00163-0 [hep-th/9512174].

[120] S. Penati and D. Polvara, "Quantum anomalies in $A_r^{(1)}$ Toda theories with defects," JHEP **1906** (2019) 062 doi:10.1007/JHEP06(2019)062 [arXiv:1902.10690 [hep-th]].

[121] R. Carter, "Simple groups of Lie type" (Wiley, New York, 1972)